CHALMERS
UNIVERSITY OF TECHNOLOGY

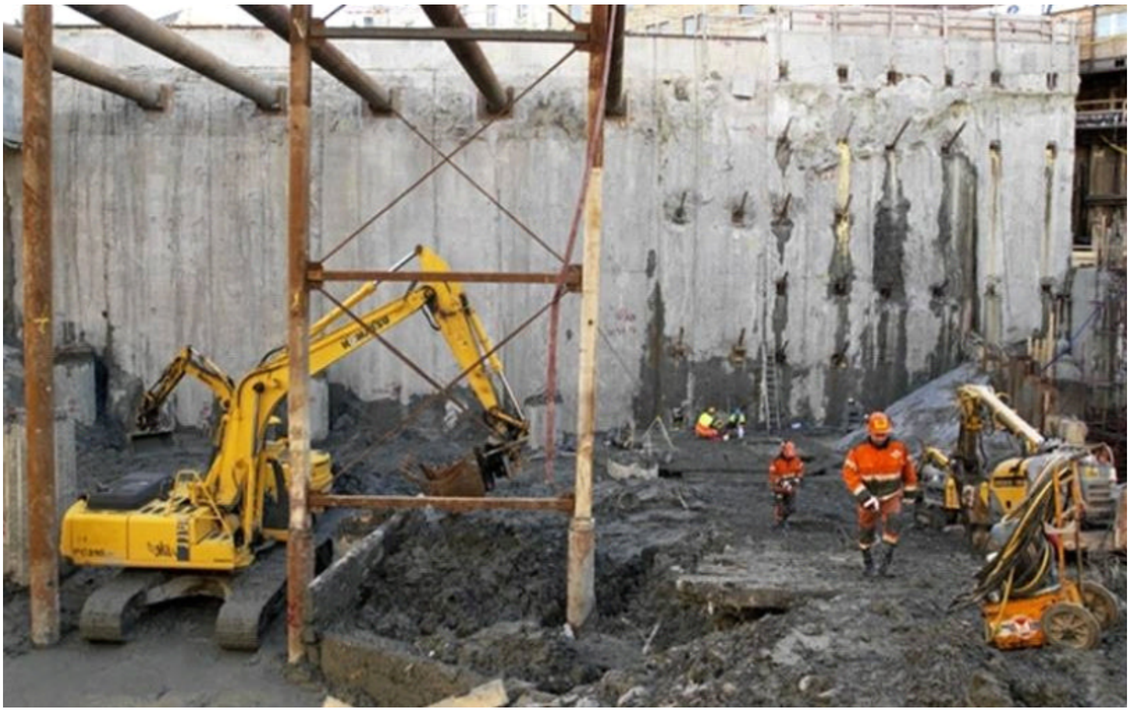

Sensitivity analysis of numerical models for diaphragm walls with cross-walls in soft soils

Master's thesis in Master Programme Infrastructure and Environmental Engineering

ROBIN BORGH

Department of Architecture and Civil Engineering
CHALMERS UNIVERSITY OF TECHNOLOGY
Gothenburg, Sweden 2018

Master's thesis

Sensitivity analysis of numerical models for diaphragm walls with cross-walls in soft soils

ROBIN BORGH

Department of Architecture and Civil Engineering
Division of Division Geology and Geotechnics
Chalmers University of Technology
Gothenburg, Sweden 2018

Sensitivity analysis of numerical models for diaphragm walls with cross-walls in soft soils
ROBIN BORGH

© ROBIN BORGH, 2018.

Academic supervisor:
Senior Lecturer Mats Karlsson
Department of Architecture and Civil Engineering,
Division of Geology and Geotechnics

Industrial supervisor:
Geotechnical Engineer Jorge Yannie
NCC Sweden
Engineering and Sustainable development

Industrial supervisor:
Leading Geotechnical Specialist Tara Wood
NCC Sweden
Engineering and Sustainable development

Examiner:
Professor Minna Karstunen
Department of Architecture and Civil Engineering,
Division of Geology and Geotechnics

Master's Thesis
Department of Architecture and Civil Engineering
Division of Geology and Geotechnics
Chalmers University of Technology
SE-412 96 Gothenburg
Telephone +46 31 772 1000

Cover: Picture from the construction of the Lilla Bommen tunnel part (Alén et al., 2006).

Typeset in LaTeX
Gothenburg, Sweden 2018

Sensitivity analysis of numerical models for diaphragm walls with cross-walls in soft soils
ROBIN BORGH
Department of Architecture and Civil Engineering
Division of Geology and Geotechnics
Chalmers University of Technology

Abstract

This master thesis presents a sensitivity analysis of parameters used in modelling a deep excavation in soft soil. The main purpose is to understand the impact of different parameters while modeling for the deep excavation of a new railway station in the West Link project, Gothenburg, Sweden.

One of the challenges in this project is to predict how the usage of an international proven construction method will preform in the specific soft soil properties of the Gothenburg clay, and how to best model it. The thesis presents the experience of similar projects conducted with similar conditions and how the support structure of diaphragm wall and cross-walls is used and installed.

In order to create a model representing these particular circumstances, the Lilla Bommen section of the Göta Tunnel project is modelled as a reference model using the PLAXIS 2D program with two different material models representing the clay behavior. The chosen material models are the Hardening soil model using small strain and the NGI ADP-model.

One of the difficulties in modelling the excavation, supported by the diaphragm wall and cross-wall, was to simulate the 3D effects of the perpendicular cross-wall in a 2D model, where the out-of-plane spacing and the interface between the structure and soil of cross-wall is unable to recreated. However, this was solved by converting the lateral support of the cross-wall into imaginary steels truss and having the cross-wall parallel to the diaphragm wall instead.

The comparison between the material models showed that the NGI-ADP-model had greater displacements than the Hardening Soil small strain model. The sensitivity analysis of the parameter study also showed some interesting results of what parameters have the larger impact. The interface strength R_{inter} is hard to estimate due to several reasons but had an affect on the bending moment and lateral deformations of the diaphragm wall. The stiffness parameters of the Hardening Soil model were hard to study separately since they are depended on each other. In the NGI-ADP-model the ratio of un-/reloading shear stress modulus and active plane strain shear strength G_{ur}/S_u^A showed to have notable impact on the heave at the excavation bottom.

Keywords: Soft soil, diaphragm walls, cross-walls, Hardening soil model, small strain stiffness, NGI-ADP.

Acknowledgements

This thesis have been written at the Department of Infrastructure and Environmental Engineering at Chalmers University of Technology and in collaboration with NCC Engineering and Sustainable development department. After a long and quite periodic journey, I would like express my gratitude to the people who have been involved and helped me trough the process.

First of all, special thanks to Jorge Yannie for your support and interest in helping me with this master thesis. Especially in the moments of doubt, when you optimistically encouraged me to carry on. Also a particular acknowledgment to Tara Wood for her limitless geotechnical expertise and inputs. I would also like to thanks Mats Karlsson for assisting me trough this long journey, for your advises that I now in hindsight wish I would had listened more carefully to. They all warned me about the difficulties of start working full time and write the master thesis as a side project, and I learn the hard way that they were indeed correct.

Finally I would also thank all my friends and colleagues who encouraged me to finally finish this report.

Robin Borgh, Gothenburg, 2018

"True knowledge exists in knowing that you know nothing. And in knowing that you know nothing, that makes you the smartest of all."

Socrates (469-399 BC)

Contents

List of Figures

List of Tables

Notations

Roman upper case letters

E_0	Small strain Young's modulus	kN/m^2
E_{50}	Secant stiffness Young's modulus	kN/m^2
E_{oed}	Tangent stiffness Young's modulus	kN/m^2
E_{ur}	Unloading/reloading stiffness Young's modulus	kN/m^2
G	Shear modulus	-
G_0	Initial shear modulus ratio	-
G_{ur}	Unloading/reloading shear modulus ratio	-
K_0	Coefficient of lateral earth pressure at rest	-
K_0^{nc}	K_0-value for normal consolidation	-
R_f	Failure ratio q_f/q_a (default R_f= 0.9)	-
R_{inter}	Interface strength	-

Roman lower case letters

c'	Effective cohesion	kN/m^2
c_u, s_u	Undrained shear strength	kN/m^2
m	Power of stress-level dependency of stiffness	$-$
p^{ref}	Reference stress for stiffness	kN/m^2
p'	Mean effective stress	$-$
q	Deviatoric stress	kN/m^2
s'	Stress invariant	$-$
s_u	Undrained shear strength	kN/m^2
t	Stress invariant	$-$

Greek lower case letters

γ	Shear strain	%
ν	Poission's ratio	-
ν_{ur}	Poission's ratio for un/re-loading (default = 0.2)	-
$\sigma_{tension}$	Tensile strength (default $\sigma_{tension}$= 0 stress units)	kN/m^2
σ_v, σ_1	Vertical stress	kN/m^2
σ_h, σ_3	Horizontal stress	kN/m^2
ϕ	Friction angle	$\circ$
ψ	Angle of dilatancy	$\circ$
τ	Shear stress	kN/m^2
τ_f	Shear stress at failure	kN/m^2

Abbreviations

ADP	NGI-ADP
CIRIA	Construction Industry Research and Information Association
CRS	Constant Rate of Strain
CSL	Critical State Line
CW	Cross-wall
DSS	Direct Simple Shear
DW	Diaphragm wall
FE	Finite element (model)
HS	Hardening Soil
HSs	Hardening Soil small strain
LBT	Lilla Bommen Tunnel
MC	Mohr-Coulomb
OCR	Over Consolidation Ratio
POP	Pre Overconsolidation Pressure
SBUF	Svenska Byggbranschens Utvecklingsfond
SPW	Sheet Pile Wall

1
Introduction

1.1 Background

In the upcoming construction of the West Link railway tunnel in Gothenburg, new challenges have emerged since only a few similar projects of this size have been constructed in Sweden. Especially with the peculiar geotechnical conditions of the soft clay in the Gothenburg region.

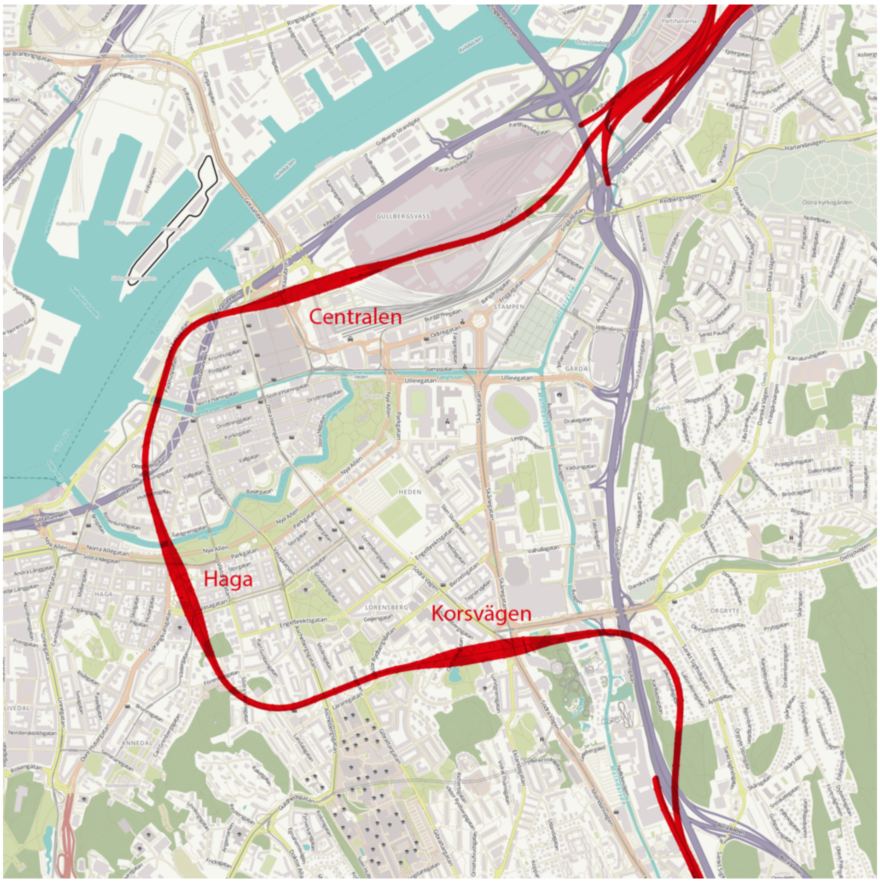

Figure 1.1: The West Link and the three underground transit stations Centralen, Haga and Korsvägen (OpenStreetMaps, 2015)

Large infrastructure projects like this located within a dense urban area could have a significant impact on nearby buildings and the environment, which results in high requirements from the Swedish authorities. This require a stable, robust and secure geotechnical construction to minimize the negative effects for its surroundings, but also to facilitate the works during the construction phase. One of the many solutions, which the West Link project will use, are diaphragm walls in combination with cross-walls for the deep and wide excavation of the transit underground station at Centralen. This method is widely used in international projects for deep excavations in limited urban areas (Long, 2001).

However, this construction method have not been commonly used in Sweden, leastwise not as a permanent part in the construction design. The main reason for this have been higher technical demands from the Swedish authorities compared to international equivalents and therefore not economically beneficial.

The higher technical demand for using diaphragm walls in Sweden was more or less a consequence of applying existing standards for concrete constructions and without considering the purpose for the specific solution. Recently an investigation of these regulations were conducted and resulted in changing the regulations for this method and therefore becoming a economical beneficial solution.

The practical knowledge and field experience for this method, with the specific Gothenburg soil conditions, is therefore quite limited. For that reason it is vital for the West Link project to have reliable models to predict the effects of using excavation methods such as the diaphragm walls in soft clay.

Numerical calculations have been used for a long time, however the material models predicting the soil behavior are constantly improved and new models are developed. Due to the complex behavior of soil properties and various soil types, the material models are focusing on different aspects which makes it applicable and suitable for different types of output, but also need different parameters as input data.

1.2 Aim and objectives

The aim of this thesis is to investigate the use of diaphragm walls in combination with cross-walls for deep excavations in soft clay. This will be conducted by numerical modelling of a case study, using two different material models, and present the result in a sensitivity analysis.

The objectives are as follows:

- Explain the use and function of diaphragm walls, and in combination with cross-walls.
- Investigate the experiences of using diaphragm walls and cross-walls in Sweden, but also in other projects with similar conditions.
- Explain two numerical material models in commercial usage for a numerical analysis of deep excavations in soft soil.
- Model a deep excavation using diaphragm walls and cross-walls in a numerical analysis.
- Compare the differences in using the two different material models.
- Conduct a sensitivity analysis of the parameters used in the two models.
- Validate the theoretical results with real results from similar conditions.

1.3 Methodology

Initially a literature study will be conducted to explain the key aspects related to the method of using diaphragm walls and cross-walls. It will answer some of the objectives regarding the diaphragm walls, cross-walls, previous experiences and the relevant geotechnical and numerical theory.

Secondly a case study will be study from one of the previous experiences in Sweden, in this case the Göta Tunnel. A model will be created by gathering as much information as possible from old drawings, field tests etc. with a type section that approximately will represent the the Göta tunnel.

Finally a sensitivity analysis will be conducted as the result for the discussion and conclusion, see the illustrated implementation in Figure 1.2.

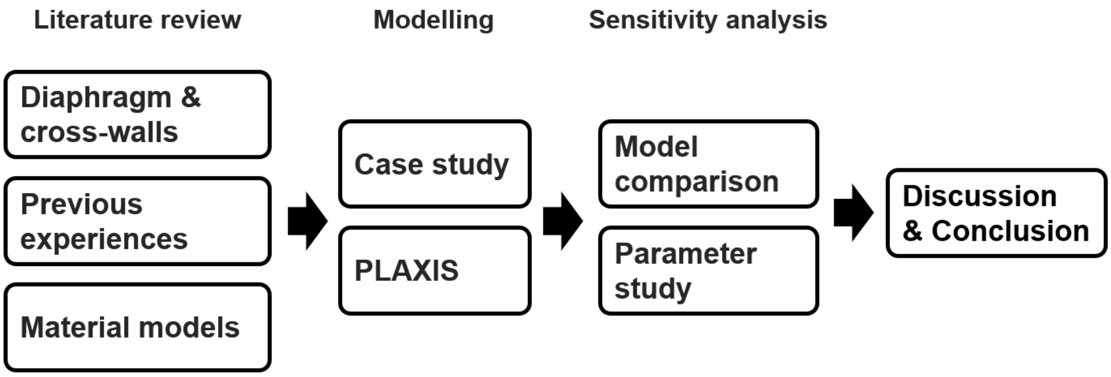

Figure 1.2: Methodology in this Thesis.

1.4 Limits

- This thesis is intended for readers with elementary geotechnical knowledge at university studies, for more information and theory see reference literature and articles.
- Model used are commercial available only.
- Only 2D-modelling in the numerical analysis.
- Validation by back-calculations of real measurements was initially outlined but had to be dismissed due to lack of time and relevant data.
- Limited evaluation and calibration of parameter values. Given values from nearby field test were compared with simulated lab tests of the assumed parameters for the model.

2

Literature review

This section will briefly explain some necessary technical terms, construction methods, experiences and relevant geotechnical theory used in this thesis. However, it is only a limited review since focus will be within the modelling. For further details see the referred literature and articles.

2.1 Deep excavations and support structures

The depth of a deep excavation can vary according to different definitions. This thesis will use the same definition stated in the book "Deep Excavations: a practice manual" by Puller (2003) who refers to a CIRIA Report on trenching practice. The report make a approximate division between shallow and deep excavation at a depth of 6 m.

Several types of earth retaining wall systems can be used to support deep excavations based on different criteria such as size of excavation, ground conditions, groundwater level, limits in displacements, cost, etc (Ergun, 2008). The most commonly used support structures for excavations are listed below, most of them are often combined with some of the other methods.

- Braced walls, soldier pile and lagging walls.
- Sheet-piling or sheet pile walls.
- Jet grout and deep mixed walls.
- Pile walls (contiguous and secant).
- Diaphragm walls and cross-walls.
- Cofferdams and caissons (watertight retaining systems).

2.2 Diaphragm walls

This thesis will focus on the use of diaphragm walls as an earth pressure retaining system. The concept is quite simple; a reinforced concrete wall is founded in a narrow trench upheld by a support slurry, see Figure 2.1. The method is well used internationally and often for deep excavations used for basements and infrastructure projects within urban areas (Alén et al., 2006). The advantage of diaphragm walls is that it achieves a stiff and sealed structure and minimizes the effect of its surroundings in terms of noise, deformation, lowering of groundwater and activities interruptions. The last two factors, are very important within a urban area considering a social-economical perspective. However, the usage of this technique in Sweden have been quite limited due to high requirements from the Swedish authorities which only allowed the method to be used as temporal construction method. This regulation made it difficult for the diaphragm wall method to be beneficial. Since 2007 it was approved as permanent part of the structure after an extensive research investigation conducted by the Swedish Transport Administration and the Development Fund of the Swedish Construction Industry, short in Swedish SBUF (Alén et al., 2006).

2.2.1 Construction method

Figure 2.1 and following explanations describe the installation of a diaphragm wall according to Keller (2017) and Lager and Persson (2005). The procedure are more or less the same for all type of projects and ground conditions. During the construction of diaphragm walls each element are divided into panels with a thickness around 0,5-1,5 m and length up to 10 m. The depth of a panel can range between a few meters and in some extreme cases down to 120 meters (Alén et al., 2006).

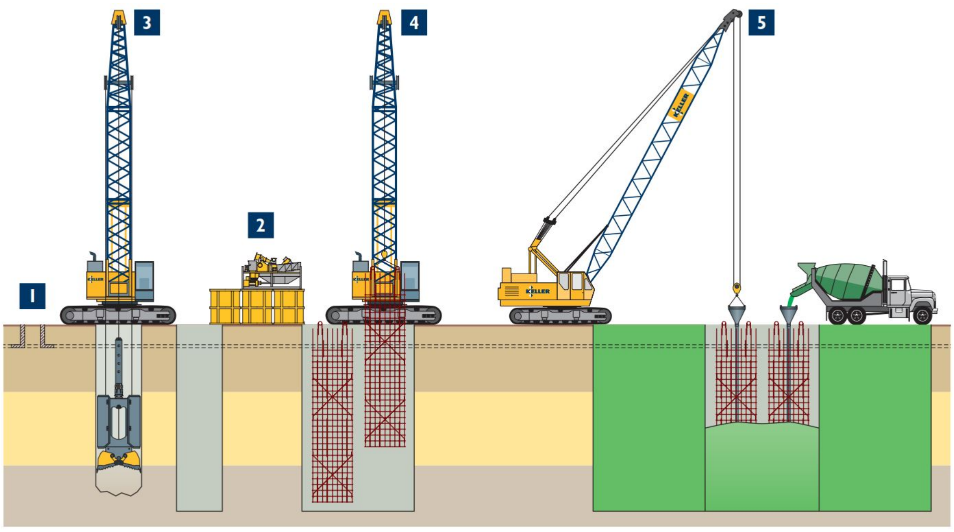

Figure 2.1: Installation steps of diaphragm walls (Keller, 2017).

Step 1. Guide walls

Initially guide walls are constructed by reinforced concrete to stabilize the upper part of the diaphragm wall. They reflect the geometry of the diaphragm walls and ensure their verticality. The guide walls also enables required level of support slurry needed for stabilizing the open trench.

Step 2. Preparation of supporting slurry

Diaphragm walls are stabilized by using the hydrostatic pressure developed by a support slurry, usually based on bentonites or specific polymers.

Step 3. Excavation of panels

Depending on the soil properties different special excavators are used such as rope grabs or trench cutters with special shovels adapted for the specific soil. The excavation need to be executed carefully since the trench walls act as the concrete formwork.

Step 4. Installation of reinforcement cages

The reinforcement are positioned by cranes in the trench and can consist of several reinforcements cages. However, it is important to ensure necessary spacing for the concrete to flow trough the reinforcement.

Step 5. Concreting of panels

As soon as the reinforcements are in place the concrete process starts. While filling the trench with concrete, it replaces the support slurry due to higher density. The displaced support slurry get pumped into special storage for reuse in the next panel excavation. To ensure water tightness between adjacent panels, special designed seals are used for the joints between the panels.

2.2.2 Cross-walls

Cross-walls are an additional support to the diaphragm walls and constructed in the same way but perpendicular to the diaphragm walls. They are generally located under the excavation bottom. According to Hsieh et al. (2008) cross-walls are often used in urban areas to reduce diaphragm wall displacements and associated ground movements. It also provide additional lateral support to prevent inward displacements of diaphragm walls during the excavation.

One major advantage of using cross-walls in deep excavations is the possibility of being constructed at same time as the diaphragm walls and with the same construction method. By using cross-walls instead of struts near the excavation bottom more work space becomes available. See Figure 2.2 from (Wu et al., 2014) for a schematic overview.

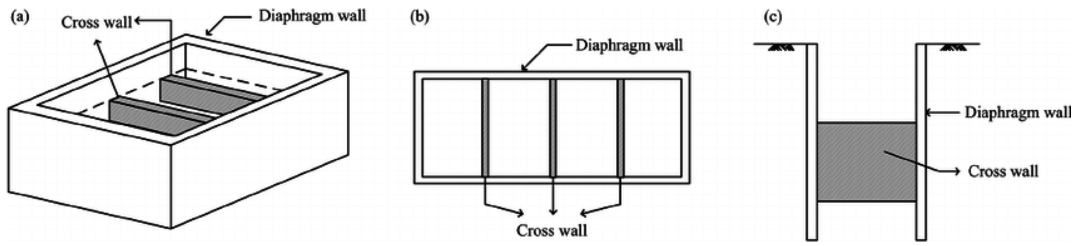

Figure 2.2: Example of cross-walls in 3D-, plan- and profile-view. Adapted from (Wu et al., 2014).

2.2.3 Cut-and-cover method

The cut-and-cover method is a simple construction method commonly used for excavation of tunnels. Initially a support structure, such as diaphragm walls, is installed and during the excavation process additional lateral support of struts and cross-walls is added as well (Li et al., 2014). There are two basic procedures in using the cut-and-cover method, 1) a conventional Bottom-up construction or 2) a Top-down construction. Figure 2.3 illustrate the outline of them both.

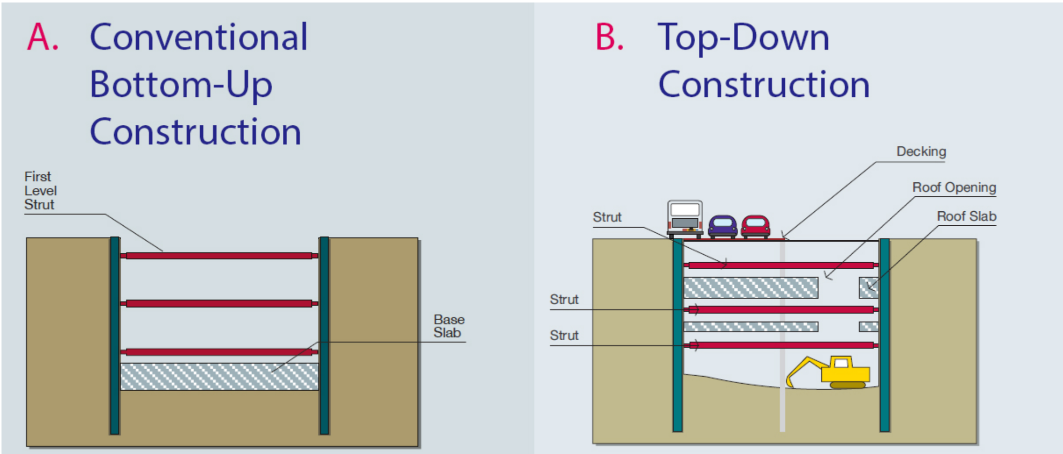

Figure 2.3: Illustration of conventional Bottom-up and Top-down construction (RailSystem, 2015).

The major difference between them is that in the bottom up construction, the final tunnel structure is independent from the support structure while the Top-down construction integrate the support structure with the final tunnel structure.

2.3 Previous experiences of diaphragm and cross-walls

This section will present experiences of using diaphragm walls and cross-walls in three different projects with similar conditions. All of them are included in the extensive "Database for retaining wall and ground movements due to deep excavations" by Long (2001) and two of them provides considerable inputs to the SBUF report mentioned earlier (Alén et al., 2006). In addition, works from Professor Kjell Karlsrud at the Norwegian Geotechnical Institute, NGI, are a central source for the presented experiences.

For more information of the following projects go to the referred reports and articles, since this section will briefly explain the conditions and state the evaluated advantages and disadvantages of diaphragm walls, cross-walls and analytic modelling of these.

2.3.1 The Studenterlunden tunnel, Oslo, Norway

The first project is a deep excavation for a subway and railway tunnel in Studenterlunden Park in central Oslo, see excavation overview in Figure 2.4 from Karlsrud (1983).

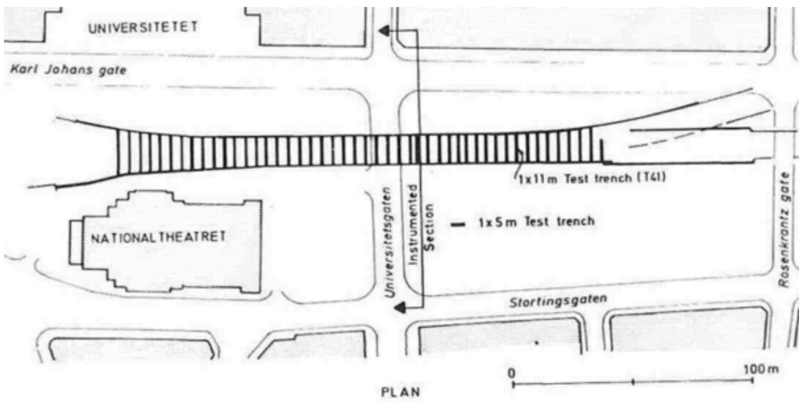

Figure 2.4: Excavation overview at Studenterlunden (Karlsrud, 1983).

This project was one of the first using the combination of diaphragm walls with cross-walls in soft soil during the early 1970s (Karlsrud and Andresen, 2008). The excavation was 240 m long and the ground conditions for the construction site consisted of fill and weathered clay crust with underlying soft normally consolidated clay. Figure 2.5 shows the installation of the reinforcement cage in the diaphragm wall and a small part of the excavation where diaphragm walls are supported by struts.

Figure 2.5: Construction of Studenterlunden in Oslo, Norway (Rude, 1972) (Rude, 1975).

The excavation depth reached down to 15 m and had a width of 11 m, see Figure 2.6 from Karlsrud (1983) which also illustrate the construction sequence of Studenterlunden. The longitudinal diaphragm wall were first established and extended down to 21 m below the surface, then the cross-walls were installed at the same depth with a spacing of 4.5 m. The excavation was done using a top-down construction method.

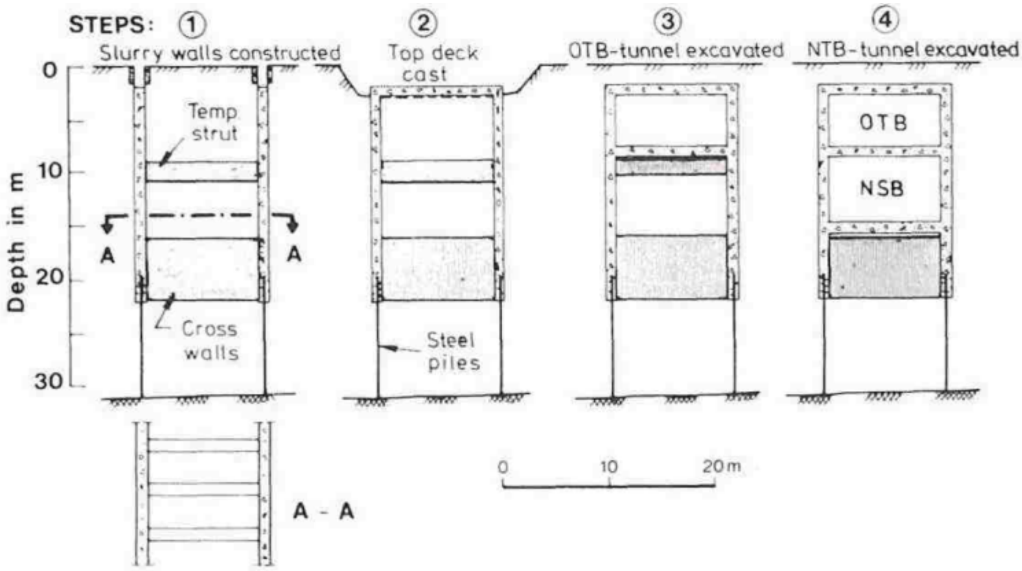

Figure 2.6: Construction sequence of Studenterlunden using the top-down method (Karlsrud, 1983).

In order to analyze the effects of the cross-walls, a similar project executed a few years earlier at Kongensgt, was closely monitored and modelled with FEM-analysis. Figure 2.7 display the comparison between the the measured displacements and the results from two FEM-analyses assuming different preconditions. For further reading see (Karlsrud, 1983).

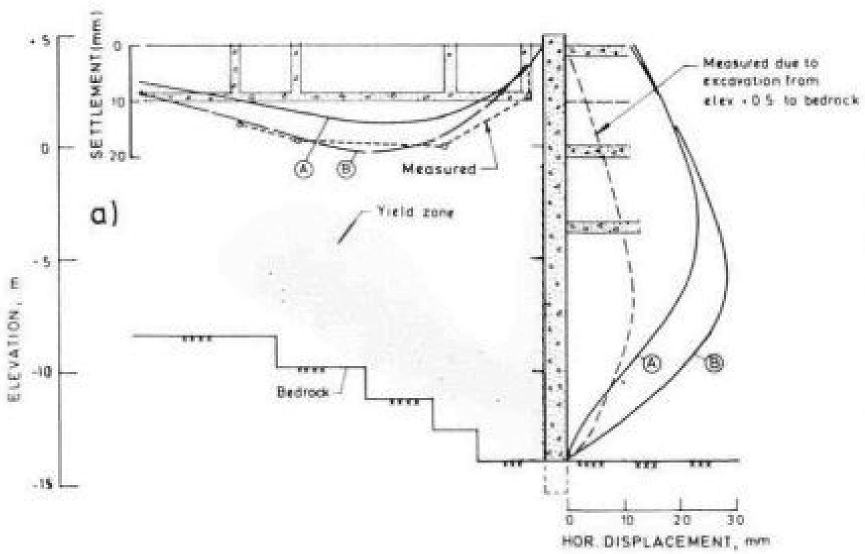

Figure 2.7: Horizontal displacements and settlements at Kongensgt (Karlsrud, 1983).

Experiences from Studentlunden tunnel project

- Except for higher stiffness and strength of a diaphragm wall compared to other flexible earth retaining systems, the designing methods were in principal the same. However, one must be careful adopting common empirical experiences based on the performance observed from other methods, such as sheet pile walls, and use analytical or numerical methods instead. This can be done by using finite element method to include the interaction between soil-wall and support system, making use of the stress-strain characteristics of different media (Karlsrud, 1983).

- The use of cross-walls made it difficult to create a 2D FEM-model and account for its impact (Karlsrud, 1983).

- The cross walls used in Studentenlunden had the dual benefit of improving bottom heave stability and also served as pre-installed bottom struts which had a substantial impact on minimizing lateral displacements during the excavation (Karlsrud and Andresen, 2008).

- Due to relatively high construction costs, diaphragm walls are presumably only economically feasible as a permanent part of the structure (Karlsrud, 1983).

2.3.2 The Göta tunnel project, Lilla Bommen

Between the years 2001-2006 a large tunnel was constructed in central Gothenburg between Järntorget and Lilla Bommen to improve the traffic situation in the city centre (Kullingsjö, 2007). The main part of the tunnel goes trough bedrock but at each end it cuts trough deep soft soil deposits and a deep excavations were needed. In the eastern end, at Lilla Bommen, it included a 230 meter long and 8 to 16 meter deep cut-and-cover excavation, see Figure 2.8. It was supported by temporary diaphragm walls, cross-walls under the excavation bottom and struts at ground surface level, a cut-and-cover with bottom up approach (Karlsrud et al., 2006).

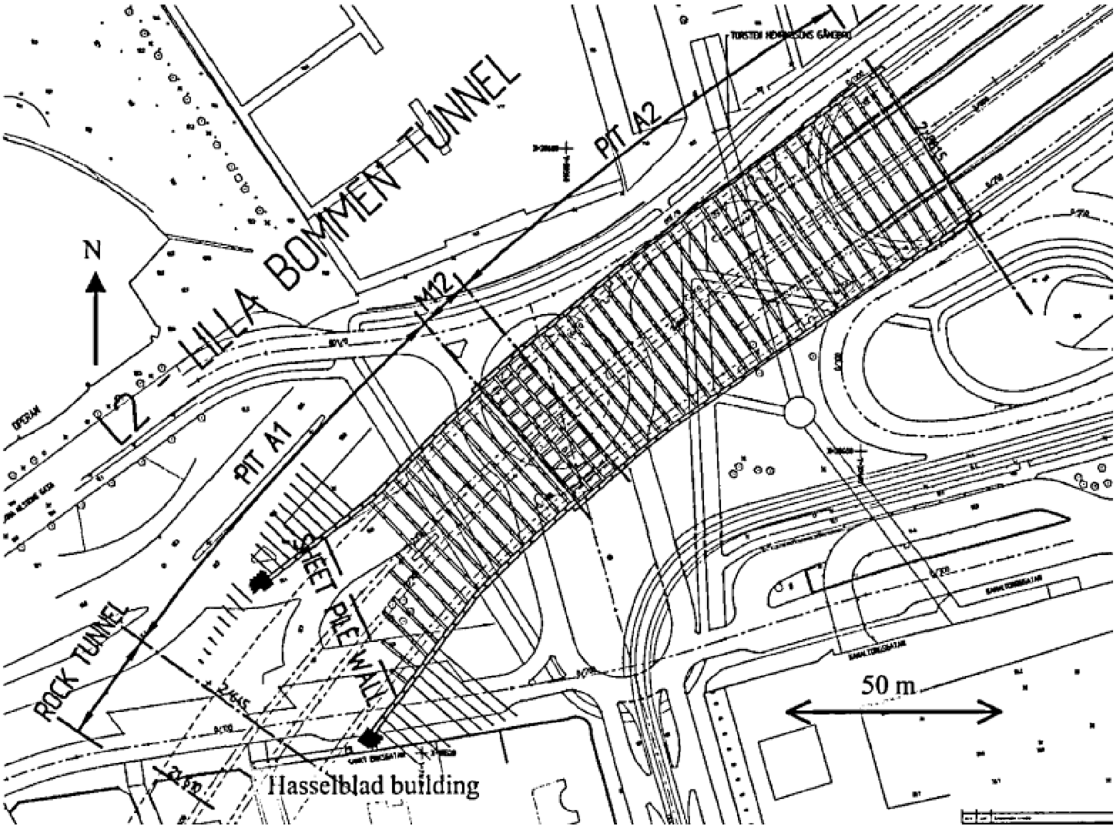

Figure 2.8: Plan view of Lilla Bommen tunnel (Karlsrud et al., 2006).

The design concept was a further development of the previous mentioned tunnel-project in Oslo. The very soft clay in combination with large depths to the bedrock made it challenging to prevent bottom heave. The calculation of the design was based on both conventional limit equilibrium analysis and FEM-analysis. Figure 2.9 illustrate a typical cross section in Lilla Bommen to the left and to the right a modelled cross-section used in a FE-program PLAXIS. Figure 2.10 shows the tunnel during the construction, using the cut and cover "bottom up" method (Karlsrud et al., 2006).

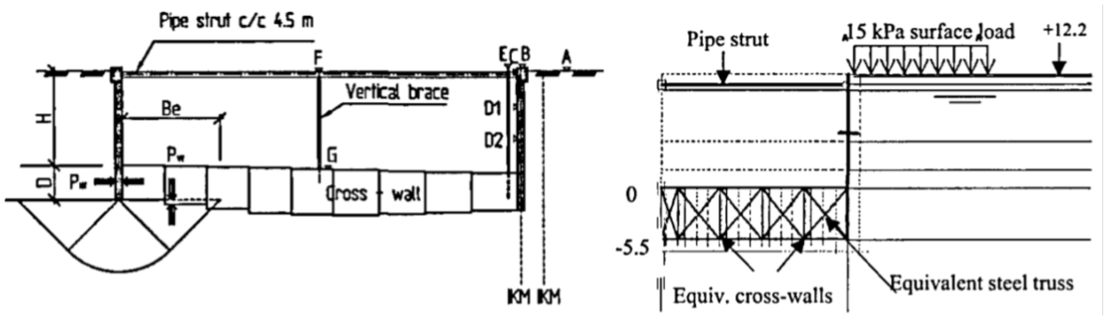

Figure 2.9: Lilla Bommen; design cross-section and PLAXIS model cross-section (Karlsrud et al., 2006).

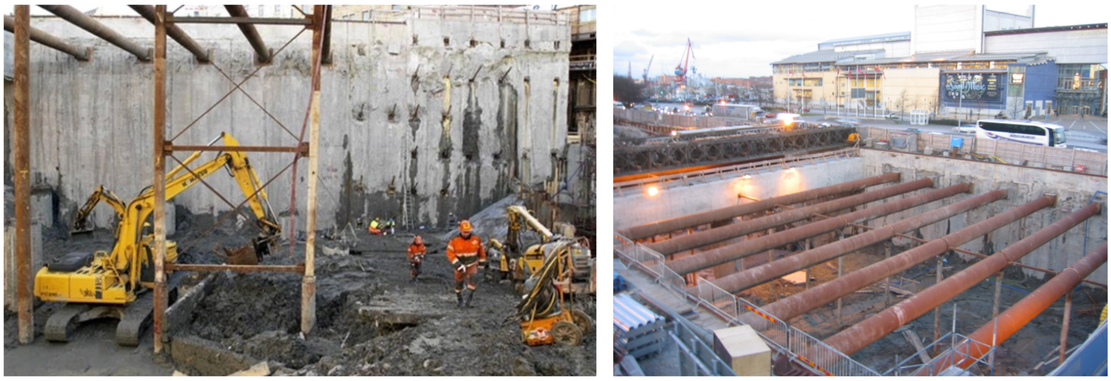

Figure 2.10: Construction of Lilla Bommen tunnel, using the cut-and-cover "bottom up" method (Trafikverket, 2016).

Experiences from the Göta tunnel project

- The combination of diaphragm walls and cross walls in the Lilla Bommen tunnel improved bottom heave stability in the soft clay and reduced displacements to acceptable limits for nearby buildings (Karlsrud et al., 2006).
- Comparison between the predicted and observed soil behaviour were substantially on the safe side. This implicated that a shorter panel depth of the cross walls could have been used or opening up larger parts of the pit, enabling more work space for the construction of the tunnel (Karlsrud et al., 2006).
- The concept of diaphragm walls with cross-walls showed to be successful with maximum lateral displacements after final excavation of only 15 to 30 mm (Karlsrud et al., 2006)

2.3.3 UPIB-building, Taipei city, Taiwan

A case study conducted by Ou et al. (2010) investigate the construction of a tall building in the center of Taipei city, Taiwan, called the UPIB-building. It is a 30-story building with a seven-level basement within a dense urban area. The excavation depth of this construction was 32.5 m below surface level and retained by diaphragm walls down to a depth of 57.5 m. The thickness of the diaphragm walls was 1.5 m and supported by cross walls and buttress walls, illustrated in Figure 2.11.

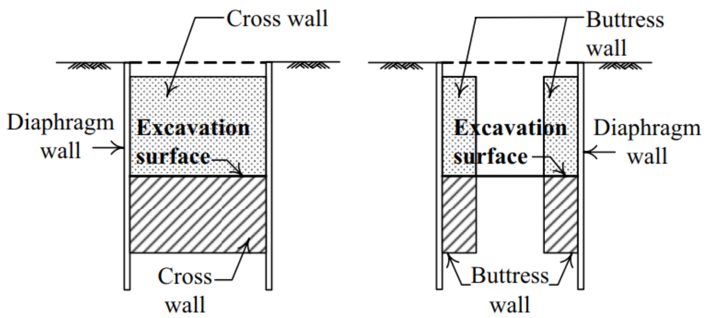

Figure 2.11: Cross-wall and buttress-wall used in the construction of UPIB. (Ou et al., 2010)

A numerical analysis was conducted using a simplified small strain soil model described in Ou et al. (2010) to investigate the effect of installation of cross-walls in reducing diaphragm wall deflection and ground movement. In Figure 2.12 a comparison is displayed between the observed movements and analyzed movements in the diaphragm walls at the final excavation stage, with and without using cross-walls.

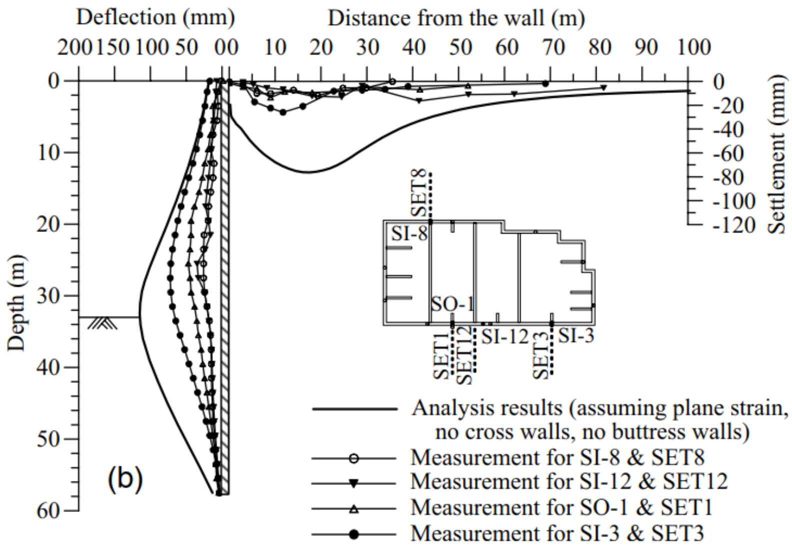

Figure 2.12: UPIB-building, Taipei city, Taiwan (Ou et al., 2010).

Experiences from the UPIB-building project

- Compared to the numerical analysis, the effect of using cross-walls reduced the maximum wall deflection in the diaphragm walls and ground settlements by about 75 % and 82 %, respectively (Ou et al., 2010).
- Wall deflection and ground settlement increased with the increasing depth and distance from the cross-wall (Ou et al., 2010).
- Wall deflection and ground settlement near corners in the excavation showed to be very small, due to the arching effect (Ou et al., 2010).

2.3.4 Summarized experiences from the SBUF-report

The SBUF-report acted as decision basis for the approval of using diaphragm walls, including cross-walls, and presented some of its advantages and disadvantages, SBUF "Slitsmurar som permantenta konstruktioner" (Alén et al., 2006).

Advantages:

- Diaphragm walls have a high stiffness which enables deeper excavations than conventional retaining systems.
- Installation of diaphragm walls reduce noise and vibrations compared to other methods.
- By using diaphragm walls in deep excavation it enables more work space by reducing other additional supporting structures, e.g. struts.
- The cross-walls can be constructed at the same time as the diaphragm walls, before the excavation starts.

Disadvantages:

- Limited practical experiences of using diaphragm walls in Sweden.
- Require heavy and space consuming machines during the installation.
- Some installations difficulties can occur in transition zones between soils and bedrock.

2.4 Laboratory soil tests

In order to retrieve data from soil samples, different lab tests will be used in this study and evaluate the soil behavior.

2.4.1 Undrained triaxial test

A triaxial test is used for measuring the soil behaviour under shear loading. It is preformed by applying axial(vertical) σ_1 and radial(horizontal) σ_3 stress on a cylindrical undisturbed soil sample in a triaxial apparatus (Knappett and Craig, 2012). This can be preformed under drained or undrained conditions, where the later will be used in this study.

The outputs from the test are used to determinate the strength and strain parameters of the soil, namely the friction angle ϕ, effective cohesion c', and stiffness parameters. The data can be plotted using different stress relations. A typical international practice is to use stress invariations of deviatoric stress q and mean effective stress p', see Figure 2.13 and Equations in 2.1.

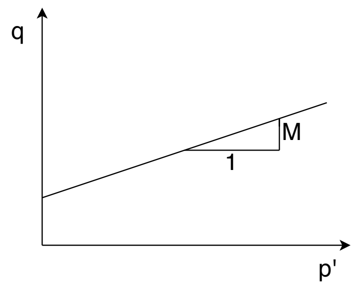

Figure 2.13: $p' - q$ plots, adapted from (Knappett and Craig, 2012).

$$q = \sigma_1 - \sigma_3, \quad p' = \frac{\sigma_1' + 2\sigma_3'}{3} \tag{2.1}$$

The critical state line in p'-q space is determine using Equation 2.2, and for the case of having a effective cohesion c', this is transformed in p'-q using Equation 2.3.

$$M = \frac{q}{p'} = \frac{6sin\phi'}{3 - sin\phi'} \quad sin\phi' = \frac{3M}{6 + M} \tag{2.2}$$

$$c'_{mc} = c'_c \frac{6cos\phi}{3 - sin\phi} \quad c'_{me} = c'_e \frac{6cos\phi}{3 + sin\phi} \tag{2.3}$$

2.4.2 Oedometer and CRS tests

These tests determine the behaviour of soil by simulating one-dimensional consolidation or swelling. The soil sample is placed in a metallic ring between two porous stone material which allow drainage in a submerged environment. The oedometer test then apply incremental cumulative loading while the CRS test apply a constant rate of strain (Knappett and Craig, 2012).

The stress history of the soil can be defined by the maximum effective vertical stress of the past, pre-consolidation pressure σ'_p, and the in-situ vertical effective vertical stress σ'_v. The relation between them is called the overconsolidation ratio OCR, see Equation 2.4 (Knappett and Craig, 2012).

$$OCR = \frac{\sigma'_p}{\sigma'_v} \tag{2.4}$$

It is also possible to specify the initial stress state by using the pre-overburden pressure POP as an alternative to describe the overconsolidation ratio, see Equation 2.5 (Brinkgreve, 2017*a*).

$$POP = \mid \sigma'_p - \sigma'_v \mid = \Delta\sigma_{POP} \tag{2.5}$$

Figure 2.14 clarify the stress terms together with the soil overconsolidated ratio OCR and pre-overconsolidation pressure POP.

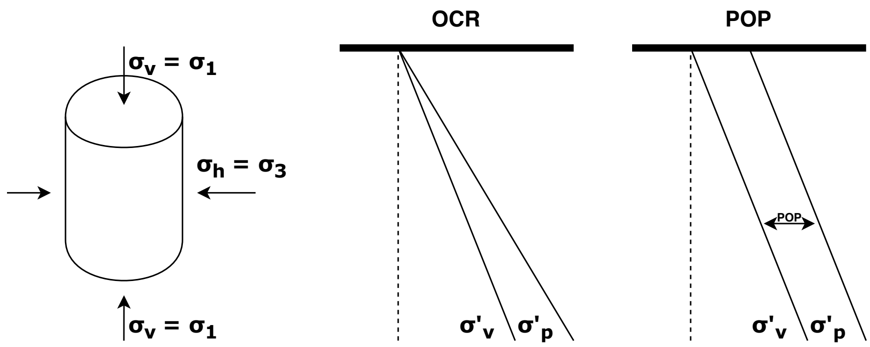

Figure 2.14: Vertical and horizontal stresses, overconsolidated ratio OCR and pre-overconsolidation pressure POP.

2.5 Material models

In the pursuit of describing the behaviour of soils several different models have been developed. These models are constitutive relations between stress and strain and their complexity varies between different type of soils due to soil composition and mechanical behaviour. The following models are briefly described to explain the basis for their use in this thesis, for more detailed explanations it is recommended to read the references.

2.5.1 Linear Elastic model

The first and most simplified model describing soil behavior is the elastic model based on Hooke's law, which only assumes elastic deformations and that all strains return to the origin after unloading, see Figure 2.15.

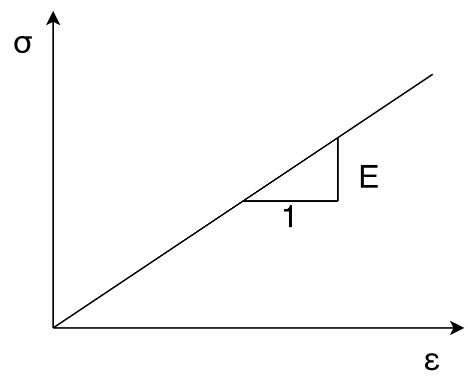

Figure 2.15: Stress and strain relation according to Hooke's law.

The parameters used for this model are the elasticity modulus E and Poisson's ratio ν which can be retrieved from triaxial tests. From these two parameters it is possible to calculate two other important parameters, shear modulus G and bulk modulus K according to Equation 2.6 and 2.7 (Wood, 2004).

$$G = \frac{E}{2(1+\nu)} \tag{2.6}$$

$$K = \frac{E}{3(1-2\nu)} \tag{2.7}$$

The shear modulus state the relation between shear stress and strain while the bulk modulus describe volume changes due to isotropic pressure. Changes in strain $\delta\varepsilon$, which occur at stress changes in the mean effective stress p' and the deviatoric stress q is formulated by Wood (2004) as:

$$\begin{pmatrix} \delta p' \\ \delta q \end{pmatrix} = \begin{pmatrix} K & 0 \\ 0 & 3G \end{pmatrix} \begin{pmatrix} \delta \varepsilon_p \\ \delta \varepsilon_q \end{pmatrix} \tag{2.8}$$

Nevertheless, the assumption of a total linear-elastic behaviour does not comply with the reality since soil behaviour is not elastic at higher strain conditions. The linear assumption is only valid at small strains where the plastic deformations are negligible.

2.5.2 Mohr-Coulomb model (MC)

This model is a linear elastic perfectly-plastic model where the material yielding is assumed to have a perfectly plastic behaviour (Brinkgreve, 2017*b*), see Figure 2.16. When the stress level exceeds the elastic stress interval irreversible plastic deformations take form. Both elastic and plastic deformations consist of shear strain and volume change due to stress changes.

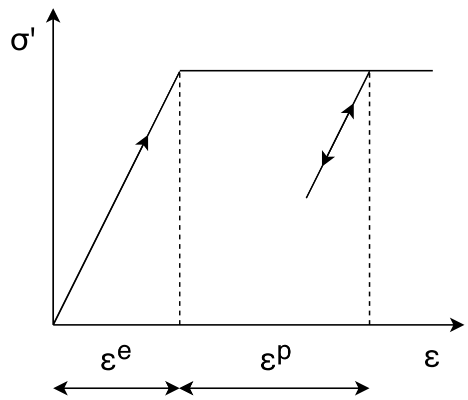

Figure 2.16: Linear elastic perfectly-plastic model, adapted from (Brinkgreve, 2017*b*)

The MC-model represents a 'first order' approximation of soil behaviour and it is recommended to use this as an estimate of a problem. The stiffness of a soil layer can be set to a mean value or increase linearly with depth. This simplification makes the computations faster to give an initial estimation of the deformations (Brinkgreve, 2017*b*).

The MC-model use the same elastic parameters as in LE-model:

E	Young's modulus	kN/m^2
ν	Poisson's ratio	$-$
G	Shear modules	kN/m^2
K	Bulk modulus	$\circ$

The plastic deformations adds some new parameters from the Mohr-Coulomb failure criterion, presented in Equation 2.9 (Knappett and Craig, 2012):

τ_f	Soil shear stress	kN/m^2
c	Cohesion	kN/m^2
ϕ'	Friction angle	$\circ$
ψ	Dilatancy angle	$\circ$

$$\tau_f = c' + \sigma' \cdot tan(\phi') \tag{2.9}$$

The relationship is visualized in Figure 2.17 where the size of the Mohr circles change with different stress combinations from various stress paths. Triaxial tests are often used to retrieve these parameters.

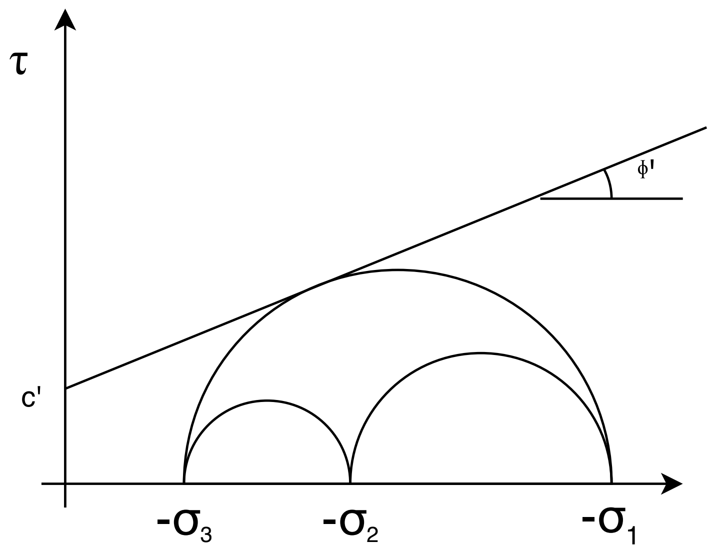

Figure 2.17: Illustration of Mohr-Coulomb failure criterion, adapted from (Brinkgreve, 2017*b*).

Dilatancy is the volume change observed in soil materials when its subjected to shear deformations. Unlike most other materials, such as steel and plastics, some soils tend to expand in volume as they are sheared (Wood, 2004). In Figure 2.18, the volume change (c) is is illustrated for both loose (a) and dense (b) packed soils. The dilatancy angle ψ is defined as the angle of the displacements (Knappett and Craig, 2012). However, the MC-model idealize a constant dilation rate when the soil is sheared which is unrealistic (Karstunen, 2016).

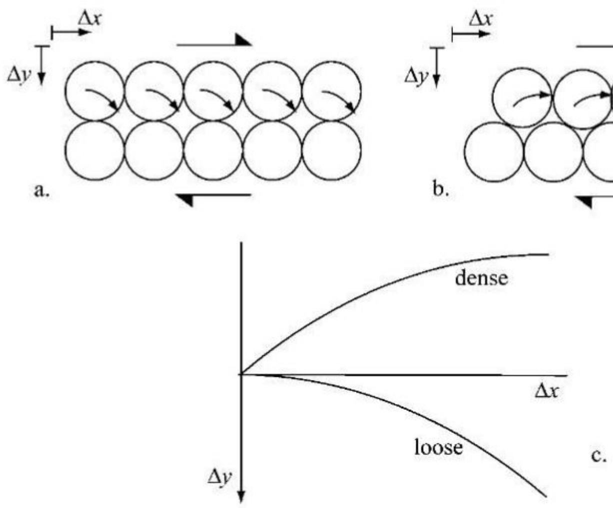

Figure 2.18: Illustration of volume change due to dilatancy ψ, (Brinkgreve, 2017*b*).

While using the MC-model it is also important to be aware of the difference between the modeled stress path in undrained conditions compared (a) to the real stress path (b), illustrated in Figure 2.19. For this reason, the MC-models risk to overestimate the undrained shear strength.

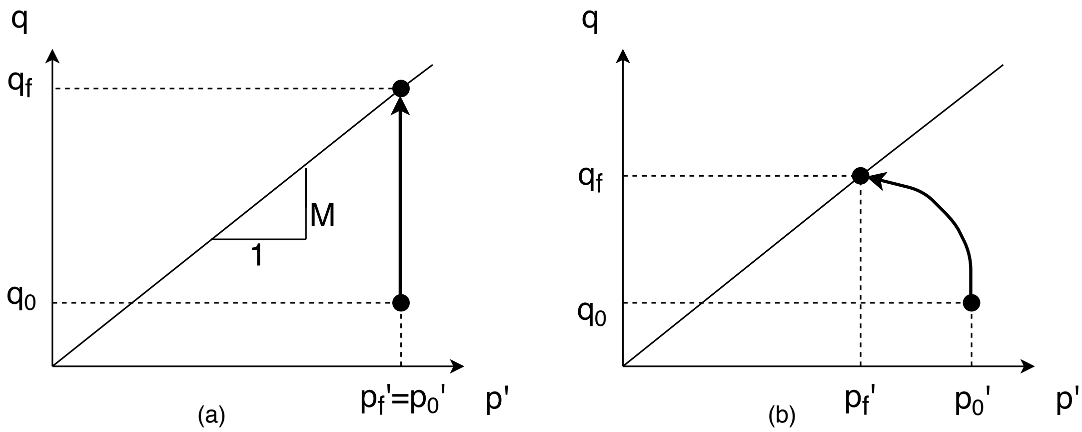

Figure 2.19: Stress paths of undrained (a) and real (b) conditions, based on figures from (Brinkgreve, 2017*b*).

2.5.3 Hardening Soil model (HS)

The HS-model simulate the behaviour of different types of soils and is a more advanced model compared to the MC-model. The soil behavior is described more accurately by simulating plastic straining of deviatoric loading, compression and elastic un-/reloading. The main input parameters of the model are E_{50}, E_{ur} and E_{oed} and can be evaluated from triaxial and oedometer tests, shown in Figure 2.20. The model also include input from soil dialatancy and a yield cap (Brinkgreve, 2017*b*).

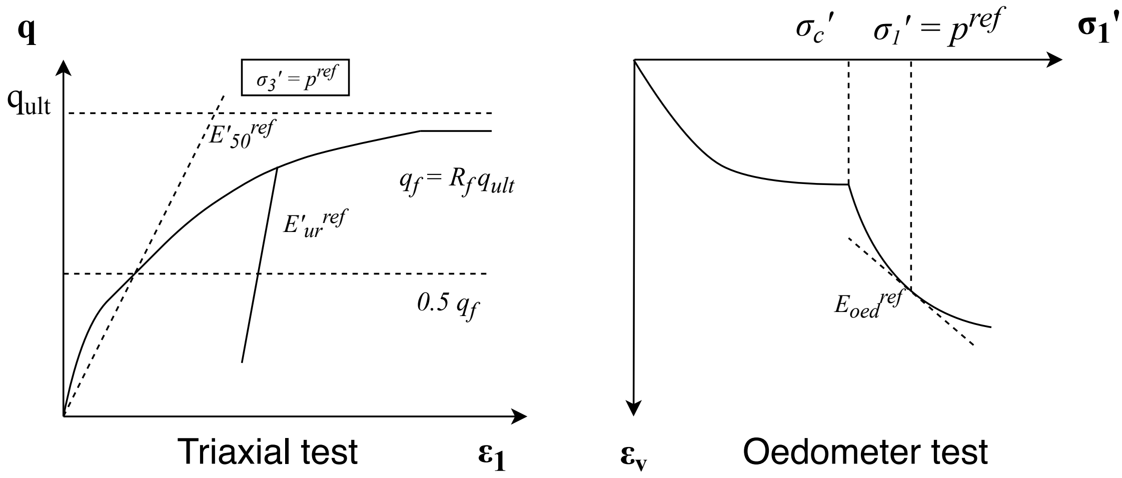

Figure 2.20: The plotted HS-model stiffness parameters retrieved from the results of triaxial and oedometer tests. Adapted from (Karstunen, 2016)

The failure criterion parameters and the dilatancy angle used in the MC-model is also used in the HS-model:

c	Cohesion	kN/m^2
ϕ	Friction angle	$^\circ$
ψ	Angle of dilatancy	$^\circ$

The main parameters for soil stiffness in the HS-model:

E_{50}^{ref}	Secant stiffness in standard drained triaxial test	kN/m^2
E_{oed}^{ref}	Tangent stiffness for primary oedometer loading	kN/m^2
E_{ur}^{ref}	Unloading/reloading stiffness	kN/m^2
m	Power of stress-level dependency of stiffness	$-$

The parameter m represent the stress dependency in the stiffness parameters. When observing soft clays, it should be considered equal to 1 (Brinkgreve, 2017*b*). As mentioned in section Laboratory tests, the cohesion c' for soft clays can be assumed equal to 0. The stiffness moduli E_{50}^{ref}, E_{oed}^{ref} and E_{ur}^{ref} are calculated and simplified in the following Equations 2.10, 2.11 and 2.12:

$$E_{50} = E_{50}^{ref}\left(\frac{c\cdot cos\phi - \sigma_3'\cdot sin\phi}{c\cdot cos\phi + p^{ref}\cdot sin\phi}\right)^m \Rightarrow E_{50} = E_{50}^{ref}\left(\frac{-\sigma_3'}{p^{ref}}\right) \tag{2.10}$$

$$E_{ur} = E_{ur}^{ref}\left(\frac{c\cdot cos\phi - \sigma_3'\cdot sin\phi}{c\cdot cos\phi + p^{ref}\cdot sin\phi}\right)^m \Rightarrow E_{ur} = E_{ur}^{ref}\left(\frac{-\sigma_3'}{p^{ref}}\right) \tag{2.11}$$

$$E_{oed} = E_{oed}^{ref}\left(\frac{c\cdot cos\phi - \frac{\sigma_3'}{K_0^{nc}}\cdot sin\phi}{c\cdot cos\phi + p^{ref}\cdot sin\phi}\right)^m \Rightarrow E_{oed} = E_{oed}^{ref}\left(\frac{-\sigma_3'}{p^{ref}}\right) \tag{2.12}$$

Additional advanced parameters for HS-model:

ν_{ur}	Poisson's ratio for unloading-reloading	$-$
p^{ref}	Reference stress for stiffness	kN/m^2
K_0^{nc}	K_0-value for normal consolidation	$-$
R_f	Failure ratio q_f/q_ult (default R_f= 0.9)	$-$

The value of ν_{ur} is usually about 0.2 and in the HS-model it is a pure elastic parameter. The usual default value of stiffness reference stress p^{ref} is 100 kN/m^2. While using the HS-model in PLAXIS the K_0^{nc} is a independent input parameter and defined by $K_0^{nc} = 1 - sin\phi$. The value can be changed, but then it becomes depended on other values such as E_{50}^{ref}, E_{oed}^{ref}, E_{ur}^{ref} and ν_{ur}. All inputs are not possible and if it is manually changed, it can only have a certain range of valid K_0^{nc}-values (Brinkgreve, 2017*b*).

As described in the MC-model, dilatancy angle ψ can have a considerable impact on the soil behavior due to the current state of the density. But eventually, after extensive shearing, the dilatancy come to an end. This behavior can be included in the HS-model as "Dilatancy cut-off" and shown in Figure 2.21.

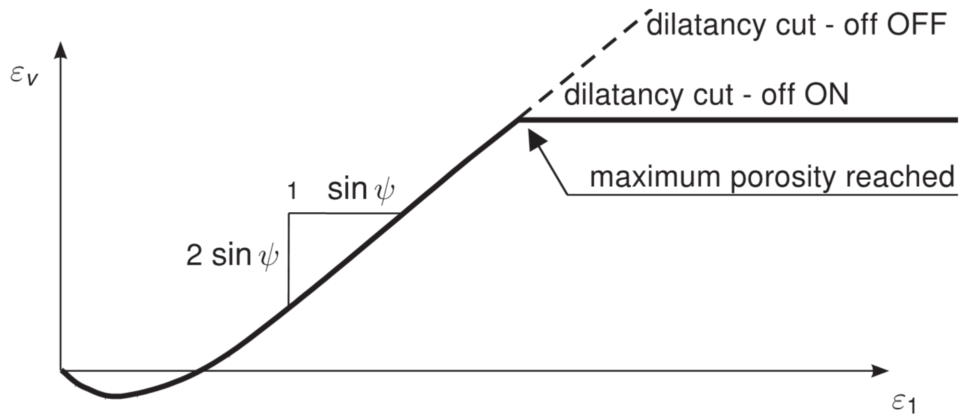

Figure 2.21: The effect off dilatancy cut off in a strain curve from a standard triaxial test, retrieved from (Brinkgreve, 2017*b*).

The HS-model also introduce a cap yield surface because the shear hardening, in a p'-q plot, do not capture the plastic volume strain often observed in soft clays. Fig 2.22 illustrate the yield lines and the elastic region within them Brinkgreve (2017*b*).

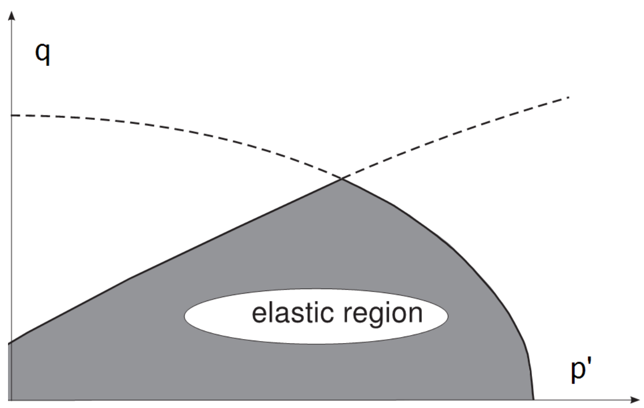

Figure 2.22: Cap yield surfaces in a HS-model(Brinkgreve, 2017*b*).

The shear yield locus can expand up to the Mohr-Coulomb failure line and within the cap yield surface defined by a function of the pre-consolidation stress σ_p retrieved from OCR and POP.

The cap enables the possibility to formulate a model with independent input parameter of both E_{50}^{ref} and E_{oed}^{ref}. For more details, see PLAXIS manual for material manuals (Brinkgreve, 2017*b*).

2.5.4 Hardening Soil model with small-strain stiffness (HSs)

The HSs-model add some more details about the soil behavior since it consider more accurate effects of unloading and reloading compared to the plain HS-model.

The reason for this is mainly due to the strong stiffness variation with increasing shear strain amplitude in the regime of small strains shown in Figure 2.23 (Brinkgreve, 2017*b*). The shear modulus G plays a crucial role for modeling deep excavations and soil-structure interaction problems.

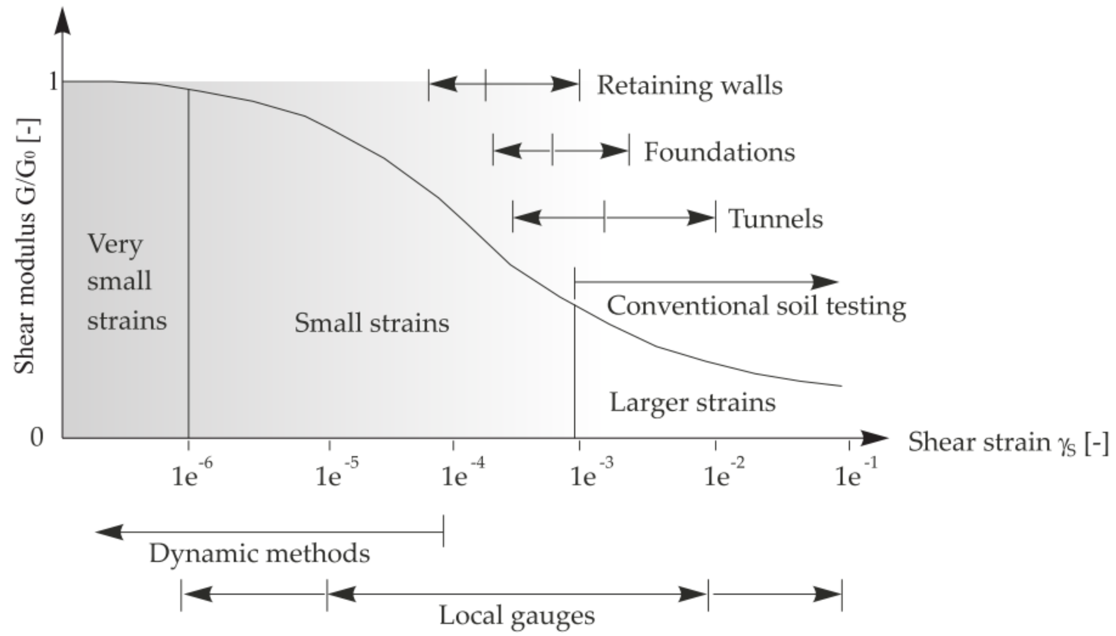

Figure 2.23: Characteristic stiffness-strain behaviour

The HSs-model use the same parameters as the HS-model:

E_{50}^{ref}	Secant stiffness in standard drained triaxial test	kN/m^2
E_{oed}^{ref}	Tangent stiffness for primary oedometer loading	kN/m^2
E_{ur}^{ref}	Unloading/reloading stiffness	kN/m^2
m	Power of stress-level dependency of stiffness	$-$
ν_{ur}	Poisson's ratio for unloading-reloading	$-$

And the additional HSs-model parameters are the initial or very small strain shear modulus G_0 and the threshold shear strain $\gamma_{0.7}$:

G_0^{ref}	Reference shear modulus at very small strains, $\epsilon < 10^{-6}$	$[-]$
$\gamma_{0.7}$	The shear strain level at which the secant shear modulus G is reduced to about 70% of G_0	$[-]$

The Young's modules of very small strains E_0 can be calculated by $E_0 = 2G_0(1+\nu_{ur})$ and illustrated in a drained triaxial test shown in Figure 2.24.

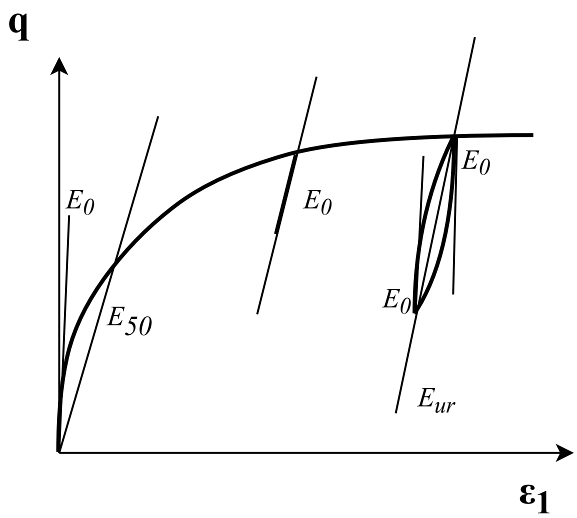

Figure 2.24: Stiffness parameters E_{50}, E_{ur} and E_0 in a drained triaxial test. Adapted from Brinkgreve (2017*b*).

The shear modulus G_0 can be calculated by Equation 2.13, and just as in the HS-model c can be set as 0 and m to 1.

$$G_0 = G_0^{ref}\left(\frac{c \cdot cos\phi - \sigma_3' \cdot sin\phi}{c \cdot cos\phi + p^{ref} \cdot sin\phi}\right)^m \Rightarrow G_0 = G_0^{ref}\left(\frac{-\sigma_3'}{p^{ref}}\right) \tag{2.13}$$

Figure 2.25 illustrate the shear modulus of G_0 and G_{ur} during a cyclic shear test.

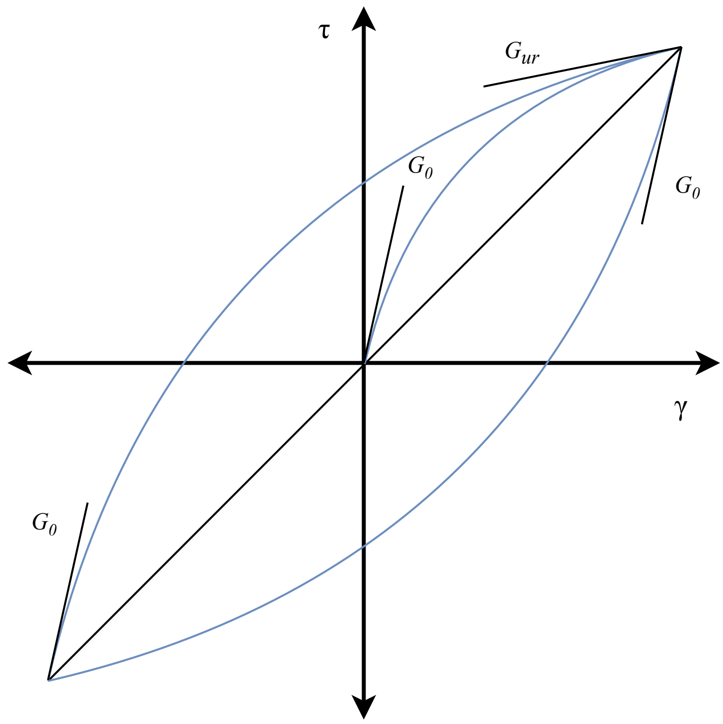

Figure 2.25: Stiffness parameters in cyclic shear test, adapted from Brinkgreve (2017*b*)

The shape of the curve of stiffness-strain behavior in Figure 2.23 is described as a log function of $G/G_0(\gamma)$. It is common to specify the shear strain $\gamma_{0.7}$ at which ratio $G/G_0 = 0.7$, see Figure 2.26.

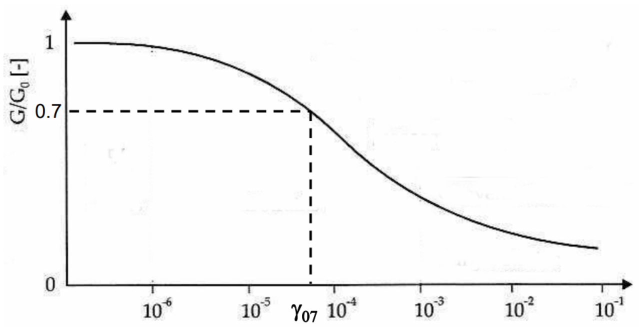

Figure 2.26: The shear strain level at which the G is reduced to about 70 % of G_0, adapted from Brinkgreve (2017*b*).

2.5.5 NGI-ADP: Anisotropic shear strength model for clay (ADP)

The NGI-ADP model is an anisotropic total stress undrained shear strength model. The soil shear strength S_u is defined for active, passive and direct simple shear stress paths. Therefore, the results are according to the data given from lab and/or field tests (Brinkgreve, 2017*b*).

The characteristics of this material model are:

- Input parameters for undrained shear strength for three different stress paths: active, direct simple shear and passive.
- A yield criterion based on a translated approximated Tresca criterion.
- Elliptical interpolation functions for plastic failure strains and for strengths in arbitary stress paths.
- Isotropic elasticity, retrieved from the unloading/reloading shear modulus G_{ur}.

For clay the ADP-model especially consider the deformations and soil-structure interactions for undrained loading.

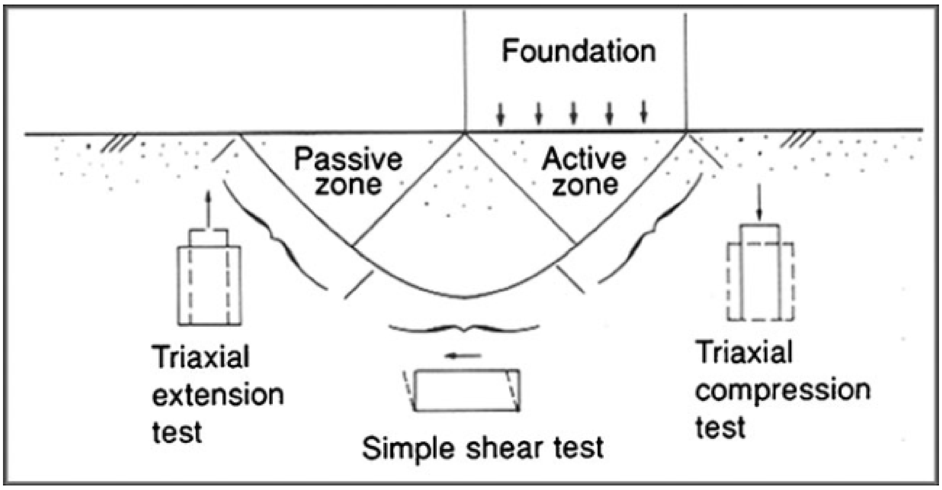

Figure 2.27: ADP stress-path illustration (Grimstad et al., 2012).

The ADP-model is a total stress undrained shear strength model suitable for modelling undrained conditions. Effective stress analysis can not be performed with this model, and therefore time effects are not considered. Also note that this model do not account for a tension cut-off or softening after failure (Brinkgreve, 2017*b*).

Stiffness parameters used for the ADP-model:

G_{ur}/s_u^A	Ratio un-/reloading shear modules over active shear strength	-
γ_f^C	Shear strain at failure in triaxial compression	%
γ_f^E	Shear strain at failure in triaxial extension	%
γ_f^{DSS}	Shear strain at failure in direct simple shear	%

The shear modulus ratio of G_{ur}/s_u^A is typically between the values of 150-250. If the shear strength is increasing with depth, the constant ratio G_{ur}/s_u^A gives a shear stiffness increasing linearly with depth. The shear strains at failure γ_f^C and γ_f^E can be seen in Figure 2.28.

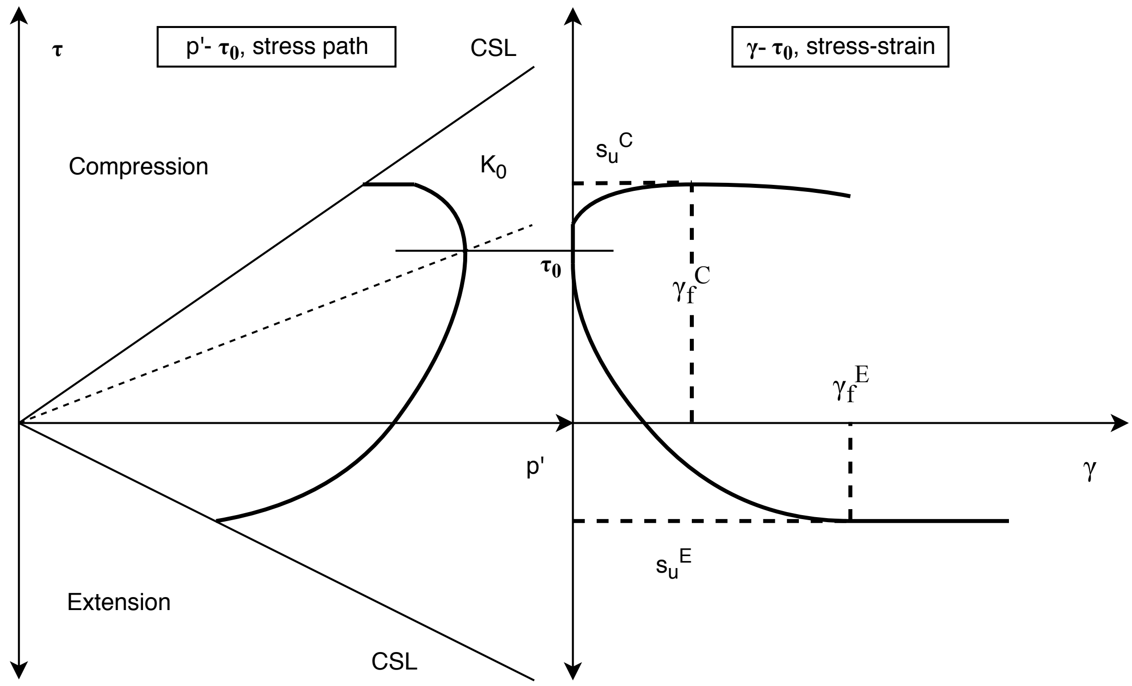

Figure 2.28: Examples of typical stress-paths and stress-strain curves for triaxial compression and extension, adapted from Grimstad et al. (2012).

The values for shear strain in normally consolidated and slightly over-consolidated clays are usually in the order ; $\gamma_f^C < \gamma_f^{DSS} < \gamma_f^E$. Typical ranges according to Brinkgreve (2017*b*); γ_f^C = 3 - 8 %, γ_f^{DSS} = 2 - 8 %, γ_f^E= 0,5 - 4 %.

From field tests (Wood, 2017), the ranges for Gothenburg clay can be assumed as; γ_f^C = 2 - 3 %, γ_f^{DSS} = 6 - 8 %, γ_f^E= 4 - 5 %.

Strength parameters of the ADP-model:

$s^A_{u\,ref}$	Reference active shear strength	$kN/m^2/m$
$s_u^{C,TX}/s_u^A$	Ratio triaxial compressive shear strentgth over active shear strength	-
y_{ref}	Reference depth	m
$s^A_{u\,,inc}$	Increase of shear strentgh with depth	$kN/m^2/m$
s_u^P/s_u^A	Ratio of passive shear strength over active shear strength	-
τ_0/s_u^A	Initial mobilization	-
s_u^{DSS}/s_u^A	Ratio of direct simple shear strength over active shear strength	-

The reference shear strength $s^A_{u\,ref}$ is retrieved from undrained active stress paths for the reference depth of y_{ref}. Below this depth the shear strength and stiffness may increase linearly with increasing depth and above the strength is set to $s^A_{u\,ref}$.

The strength parameters of ADP can be illustrated in Figure 2.29. Further details about each parameter can be found in Brinkgreve (2017*b*).

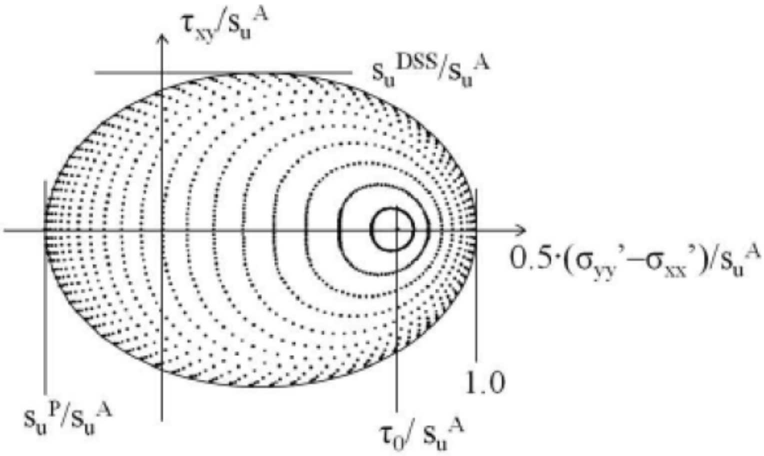

Figure 2.29: Strength parmeters in a typical deviatoric plane strain plot of equal shear strain contours, (Grimstad et al., 2012).

2.5.6 Comparison of HS and ADP

The PLAXIS manual explaining the material models, rates their differences in terms of soil type, applications and type of loading.

HS and HSs

Considering soil types:

- The most suitable material model for over-consolidated clay and fair for normally consolidated clay.

Considering different types of applications:

- HSs is suitable for all types of applications, e.g. good for excavation.

Considering different types of loading and soils:

- The best standard for primary compression, un-/re-loading, shear/deviatoric loading, and compression/extension shear, however not all loading combination can be used in the same time due to limitation in the input parameters. It is also reasonable for modelling undrained and cyclic loading.

ADP

Considering soil types:

- The ADP-model is most suitable for normally consolidated clay in short-term analysis, in case only undrained strength is known.

Considering different types of applications:

- Only fair modelling for excavation. Better for embankment, slope and offshore.

Considering different types of loading and soils:

- The best standard for undrained shear type of loading. Only reasonable for primary compression and un-/re-loading.

3

Case Study

In order to conduct a numerical modeling for a deep excavation using diaphragm wall and cross-walls in soft soil conditions a real and already constructed project with similar characteristics was chosen. A typical and simplified cross-section based on the selected project is set to be the base for the comparison between the outcome from the numerical calculations using different material models. The soil parameters used in the calculations are obtained from other researches (Wood, 2017), where extensive soil data was used and calibrated using FE.

3.1 The Lilla Bommen Tunnel (LBT)

The previous experiences of the Göta tunnel project showed to be compatible to fulfill the aim of this thesis. Therefore the tunnel section of Lilla Bommen (LBT) have been chosen to be the base for the case study.

The location of LBT lies within the central parts of Gothenburg close to existing buildings, in soft clay deposit and close to the construction of the new Central Station in the West Link project. The support structure of LBT used diaphragm walls with cross-walls and were calculated with numerical models (Karlsrud et al., 2006). However, the material model used for the modelling of LBT were a MC-model which have some limitations compared to the material models of HSs and ADP.

Figure 3.1: Location of LBT (red) and central station in the West Link (yellow), adapted from (MetroArkitekter, 2018)

3.1.1 Location

The modelled cross-section of LBT was purposely located a bit away from other previous studies, which showed some unfavorable circumstances therefore could be avoided. However, this made it hard to find real relevant survey data to validate the study. The red line in Figure 3.2 represents the cross-section, at the longitudinal section 2/840 in Appendix A "Drawings of Lilla Bommen tunnel". The Torsten Henriksson pedestrian bridge can also be used as an approximate location reference.

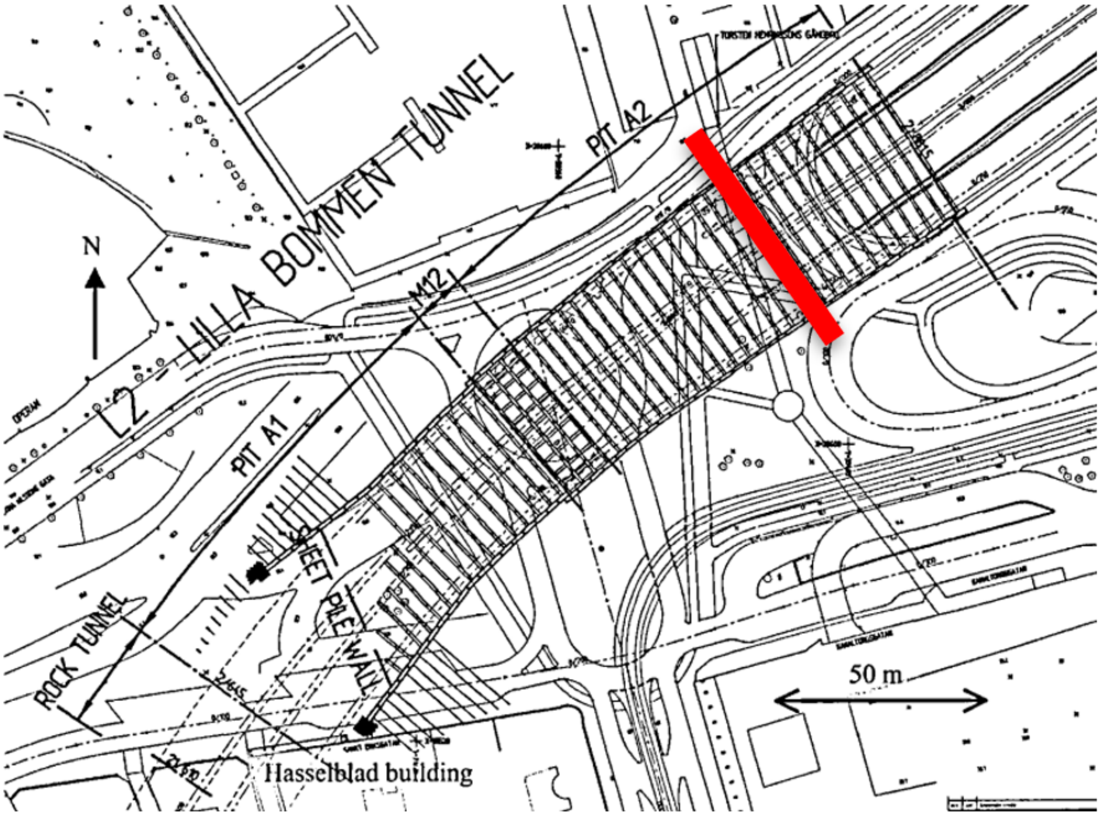

Figure 3.2: Location of LBT cross-section, adapted from (Karlsrud, 1983).

3.1.2 Geometry

The geometry for the structure used in the model is based on the section view E-E at 2/800 in Appendix A "Drawings of LBT". In Figure 3.3 the excavation appear to be about 8 m deep and 40 meter wide.

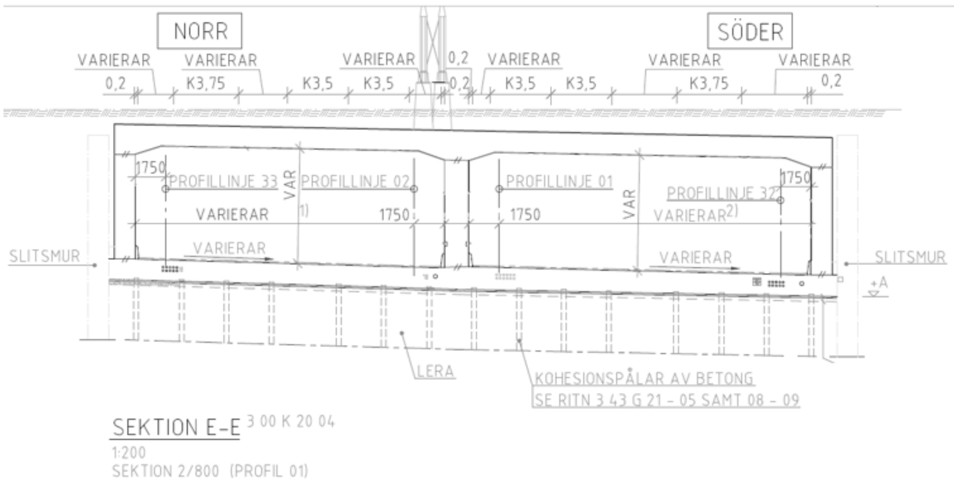

Figure 3.3: LBT drawings, section view E-E (2/800).

3.1.3 Excavation sequence of LBT

As mentioned in the literature review the LBT used the Cut-and-cover method. Initially the diaphragm wall and cross-walls are were installed. The excavation were executed partly in different steps, in plateaus with a length of 10-12 meters and depth of 3-4 m along the diaphragm wall. Struts were installed along the excavation at the top and cross walls in the bottom. See illustration in Figure 3.4.

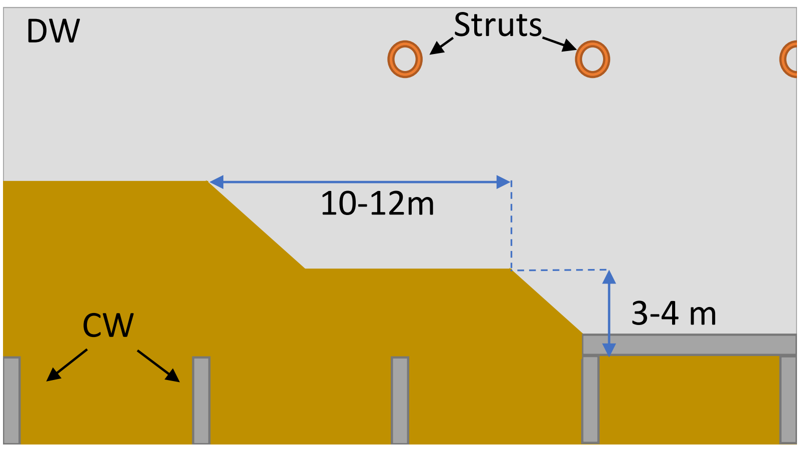

Figure 3.4: LBT excavation sequence.

3.2 Implementation

The LBT is modelled in PLAXIS 2D and calculated by the two different material models, HSs and ADP, for the different soil layers. In order to compare the material models a base model is established as reference, with as much as equal parameters as possible. Following sections will present the model input parameters and adaptations.

3.2.1 Modelling assumptions

Some necessary assumptions in order to enable the modelling and reduce the computing process in PLAXIS.

Assumptions:

- Horizontal soil layers.
- Each layer considered homogeneous within its borders.
- Groundwater considered hydrostatic and undrained conditions.

3.2.2 Structure geometry

The dimensions for the diaphragm wall and cross-wall in the model for this case study is adopted from the drawings of LBT and shown in figure 3.5 from Appendix A. The excavation depth is 7.5 m, depth of diaphragm wall 11.5 m, width of cross-wall 40 m divided by 2. Only one half of the excavation support structure is needed to be modeled since it can be assumed to be symmetric. The thickness of the diaphragm wall is set to be 1.2 m and 0.8 m for the cross-walls.

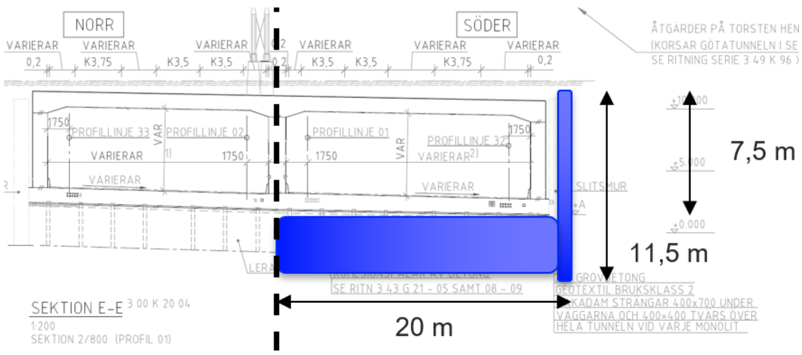

Figure 3.5: Dimensions of LBT support structure and excavation.

Figure 3.6 is a cross-section from the PLAXIS-model. The following list below explain some of the details shown in the figure.

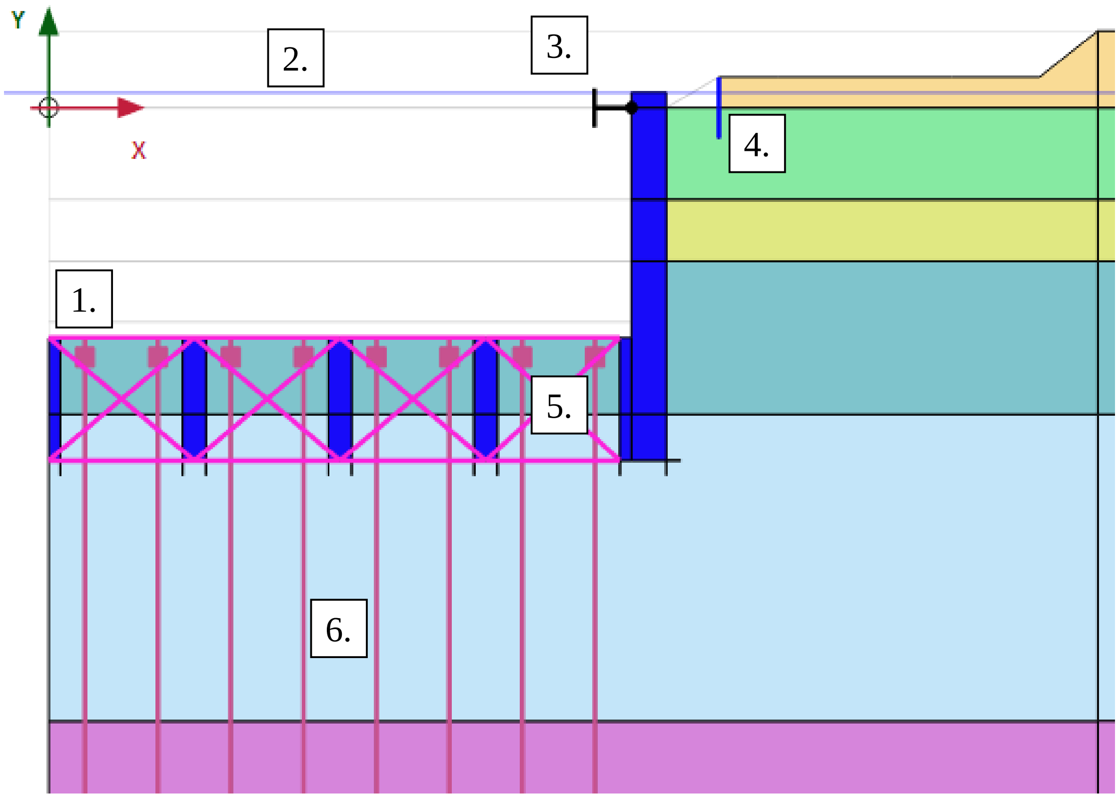

Figure 3.6: Section example from PLAXIS-model (Phase 7).

1. Final excavation step, at phase 7 and the most critical.
2. Water level is set to be at +0.5 m.
3. The strut is placed 0.5 m below the top of the diaphragm wall and -2.5 m below initial surface.
4. A sheet pile wall, installed to handle a pseudo soil failure problem in the fill layer of the model.
5. A truss representing the cross-wall, see 3D-2D adaption in section 3.2.3.
6. Piles installed at excavation bottom, according to drawings in Appendix A, A-A section.

3.2.3 3D-2D converting method

The model for LBT is modeled in PLAXIS 2D, while the effects of using cross-walls is in 3D. In 2D it is possible to capture the lateral support of the CW, but it does not consider the friction that occur between the CW and adjacent soil. This friction counteract the effect of bottom heave (Karlsrud et al., 2006).

This can be solved by converting the lateral force support into a imaginary steel truss and turn the CW parallel to the DW, see illustration in Figure 3.7. The CW is placed with the same distance from each other as earlier between and connected to the DW. The truss will simulate the lateral force and the CW will simulate the effects caused by the friction in the interface between CW/soil and CW/DW.

For a full converting calculation, go to Appendix B, "Converting stiffness of cross-wall to truss".

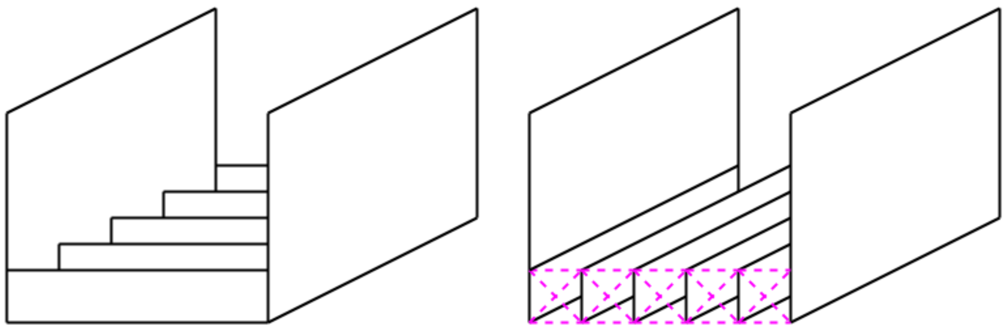

Figure 3.7: Illustration of the 3D-2D converting method. Shifting the CW from perpendicular to parallel to the DW.

3.2.4 Phases

In order to simulate the construction stages of the LBT, the PLAXIS-model consist of different phases, shown in Table 3.1 with comments for each step.

Table 3.1: Settings for the modelled phases.

	EL [m]	Calc type	Reset disp.	Loading type	Pore pressure	Comment
Initial Phase	2,5	K0 proc.		Staged constr.	Phreatic	
Phase 1	0	Plastic	Yes	Staged constr.	Phreatic	Excavation of fill and dry crust
Phase 2	0	Plastic	No	Staged constr.	Phreatic	Installation of DW, CW and piles
Phase 3	0	Plastic	Yes	Staged constr.	Phreatic	Reset displacements
Phase 4	-3	Plastic	No	Staged constr.	Phreatic	Installation of strut
Phase 5	-3	Plastic	No	Staged constr.	Phreatic	Excavation
Phase 6	-5	Plastic	No	Staged constr.	Phreatic	Excavation
Phase 7	-7,5	Plastic	No	Staged constr.	Phreatic	Excavation, most critical phase
Phase 8	-7,5	Plastic	No	Staged constr.	Phreatic	Installation of bottom plate
Phase 9	-7,5	Consol.	No	Staged constr.	Phreatic	Consolidation for 180 days
Phase 10	-7,5	Safety	No			Calculated on phase 7

3.2.5 Flow conditions

The water flow during the excavation is also modelled in the PLAXIS application "Flow conditions". Each excavation step is set as dry clusters and interpolation of pore water pressure for each bottom. Figure 3.8 display the phase 7 as example, with grey as dry cluster and orange as interpolated pore pressure.

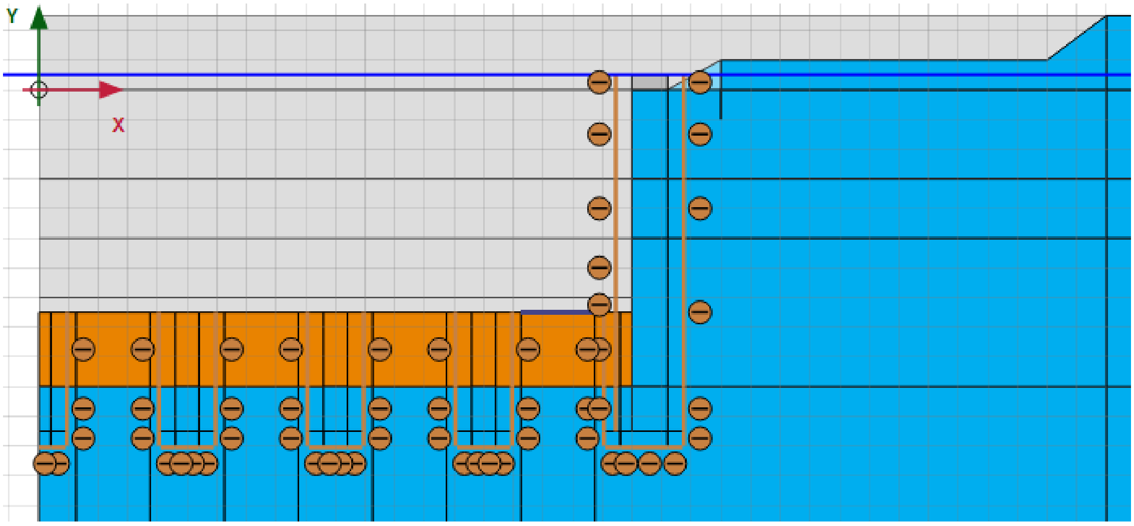

Figure 3.8: Water flow and interpolation in phase 7.

3.2.5.1 Bottom heave and Safety Analysis

In the final excavation step of phase 7 there is risk for bottom heave, since it is before the installation of the bottom plate. It is therefore important to ensure if the soil goes to failure or not. The basic mechanism bottom heave is illustrated in Figure 4.5.

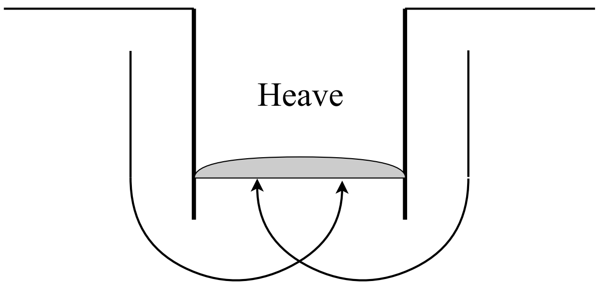

Figure 3.9: Basic mechanism of bottom heave.

A formula to calculate the stability of the bottom heave is presented in Equation 3.1 by (Sällfors, 2013). Full calculation of the stability factor for the LBT-model, see Appendix C "Calculation of Basal heave stability".

$$F_c = N_c * \frac{\tau_{fu}}{\gamma * H + q - p} \tag{3.1}$$

$$\text{If } F_c >= 1,5 \quad \rightarrow \quad \text{Stability OK!}$$

The stability factor value was calculated as $1,04$, which does not fulfill the required value of $1,5$ to discard the risk of bottom heave. However, this simplified calculation does not regard the friction that originate between the soil and the cross-walls, which would have created a higher stability factor. Further calculations of the model, to account for the friction, was conducted by using the PLAXIS Safety Analysis tool. It was calculated for the most critical situation, phase 10, and did not go to failure. Failure by hydraulic heave is not relevant since it is only layers of clay.

3.2.6 Interfaces

The interfaces are separated into three different areas, as can be shown of the three different colours in Figure 3.10:

- The purple interface represents the surface between DW or CW and the soil.
- The white serve as the specific surface between the DW and the CW.
- The brown interface is a extension at the bottom of the DW and CW to prevent calculation errors.

The reason to separate the purple and white interfaces is to investigate if the specific interface at the contact surface between the DW and CW have different impact on the model then the other interfaces.

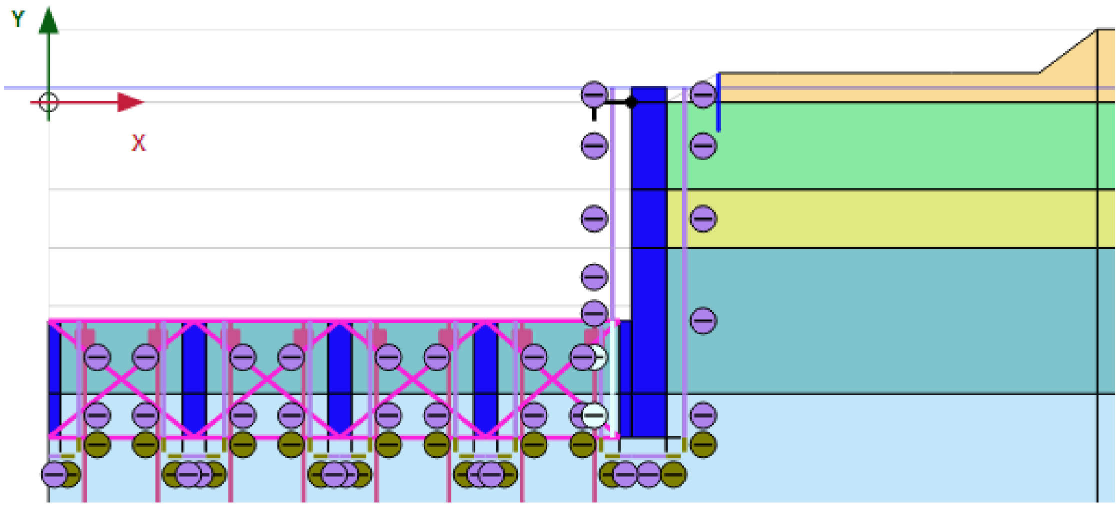

Figure 3.10: Interfaces in the PLAXIS-model.

In order to distinguish small displacements and permanent slip in the interfaces, the MC-model is used to simulate these with its elastic and plastic behaviour. The interface strength R_{inter} properties can be calculated from the cohesion c and friction angle φ in the soil and interface:

$$R_{Inter} = \frac{c_{interface}}{c_{soil}} = \frac{tan\varphi_{interface}}{tan\varphi_{soil}}$$

In the tab-sheet for interfaces the value of R_{Inter} can be entered manually, otherwise it is set as rigid with the default value of 1. For real soil and structure interaction the interface is often weaker then 1, often assumed to be around 0,7. If the R_{Inter} value is reduced, both interface strength and stiffness is reduced as well (Brinkgreve, 2017*a*).

Table 3.2 presents the parameters values for both the interfaces between DW/Soil and DW/CW with the only difference in R_{Inter}.

Table 3.2: Parameters for the interfaces between DW/Soil and DW/CW.

	Parameters	Values	Units
Material set	Material model	MC	-
	Drain type	Undrained A	-
General properties	y_{unsat}	16	kN/m^3
	y_{sat}	16	kN/m^3
Advanced	Dilatancy cut-off	No	-
	e_{init}	0,5	-
	e_{min}	Auto	-
	e_{max}	Auto	-
Stiffness	E'	7,00E+03	kN/m^2
	ν'	0,2	-
Strength	c'_{ref}	1	-
	ϕ'	33	$\circ$
	ψ'	0	$\circ$
Advanced	Default values	Yes	-
GW model	Data set	Std	-
Soil	Type	Very fine	-
	< 2 microm	Auto	%
	2-50	Auto	%
	50-2 millim	Auto	%
Flow parameters	Default values	No	-
	k_x	0,001	m/day
	k_y	0,001	m/day
	dilatancy_{unsat}	0	m
	e_{init}	0,5	-
	S_s	Auto	1/m
Change of permeab	c_k	1,00E+15	-
Interface	Strength	Manual	-
	R_{inter}	0,6* or 0,8**	-
	Con. gap closure	Yes	-
Real interface thickness	δ_{inter}	0	-
GW	Cross perm.	Imp.	-
	Drainage conductivity	0	$m^3/day/m$
K0 settings	K_0 determ.	Auto	-
	$K_{0,x} = K_{0,z}$	Auto	-
	$K_{0,x}$	0,53	-
	$K_{0,z}$	Auto	-

* Interface of the interaction between DW/soil.
** Interface of the interaction between DW/CW.

3.2.7 Input data for structures

The following subsections present the input data used for the structures in the PLAXIS-model. Some of them are estimations or set to standard values, some are retrieved from other models adapted for similar conditions in the nearby area of Region City (Wood, 2014) while others are calculated.

3.2.7.1 Diaphragm wall and cross-wall

Table 3.3 presents the material set used for both the diaphragm wall and the cross-walls.

Table 3.3: Input data for the diaphragm wall and cross-wall.

	Parameters	Values	Units
Material set	Material model	Linear elastic	-
	Drain type	Non-porpous	-
General	y_{unsat}	25	kN/m^3
properties	y_{sat}	25	kN/m^3
Advanced	Dilat cut-off	No	-
	e_{init}	0,5	-
	e_{min}	Auto	-
	e_{max}	Auto	-
Stiffness	E	3.10E+07	-
	ν	0.2	-
Flow parameters	Default values		-
	k_x	0	m/day
	k_y	0	m/day
	dilatancy$_{unsat}$	1.00E+04	m
	e_{init}	0.5	-
Change of permeab	c_k	1.00E+15	-
Interface	$Strength$	Rigid	-
	R_{inter}*	1*	-
	$Con.gapclosure$	Yes	-
Real interface thick	delta$_{inter}$	0	-
GW	$Crossperm.$	Imp.	-
	$Drainageconduct.$	0	$m^3/day/m$
K0 settings	K_0 $determ.$	Auto	-
	$K_{0,x} = K_{0,z}$	Auto	-
	$K_{0,x}$	Auto	-
	$K_{0,z}$	Auto	-

* R_{inter} does not matter since we use specific interfaces.

3.2.7.2 Temporary sheet pile wall

In order to conduct the model, without soil failure above the diaphragm wall, a sheet pile wall (SPW) were installed. Table 3.4 present the specific input data.

Table 3.4: Input data for the SPW.

	Identification	Value	Units
Material set	Material type	Elastic	-
Properties	Isotropic	Yes	-
	End bearing	No	-
	EA_1	3,00E+06	kN/m
	EA_2	Auto	kN/m
	EI	6,84E+04	kNm^2/m
	d	Auto	m
	w	0	$kN/m/m$
	ν	0,3	-
	Rayleigh α	0	-
	Rayleigh β	0	-

3.2.7.3 Piles

The piles used in the PLAXIS-model use the input data for a standard pile of 270x270 mm and are presented in Table 3.5. Figure 3.11 below display a standard pre-cast concrete pile, with mechanical joint and rock tip (Axelsson, 2016).

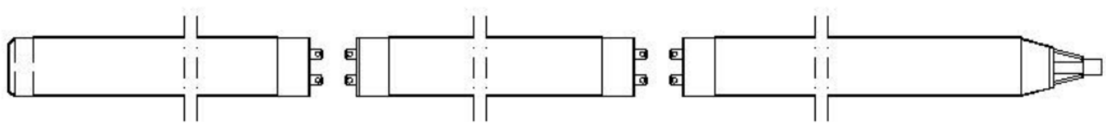

Figure 3.11: Typical standard pile, (Axelsson, 2016).

Table 3.5: Input data for the piles.

	Identification	Values	Units
Material set	Material type	Elastic	-
Properties	E	3,00E+07	kN/m^2
	y	10	kN/m^3
	Pile type	Predefined	-
	Predefined pile type	Massive square	-
	Width	0,275	m
	A	Auto	m^2
	I	Auto	m^4
	Lspacing	4,5	m
	Rayleigh α	0	-
	Rayleigh β	0	-
Axial skin resistance	Axial skin resistance	Linear	-
	$T_{skin,start,max}$	17*	kN/m
	$T_{skin,end,max}$	42*	kN/m
Lateral skin resistance	Lateral skin resistance	Unlimited	-
Base resistance	F_{max}	36**	kN
Interface stiffness factor	Default values	No	-
	Axial stiffness factor	0,1***	-
	Lateral stiffness factor	0,1***	-
	Base stiffness factor	1***	-

*Calculation of Axial skin resistance, see Appendix C.

**Calculation of Base resistance, see Appendix C.

***Interface stiffness factor. Axial, lateral and base stiffness factor retrieved from other research (Wood and Karstunen, 2017).

3.2.7.4 Struts

Input data for the struts, which is assumed to have a standard diameter of 750 mm.

Table 3.6: Input data for the struts.

	Identification	Value	Units
Material set		Elastic	-
Properties	EA_{strut}	9.639*	kN
	$L_{spacing}$	5	m

*Calculation strut EA_{strut}, see appendix C

3.2.7.5 Truss

Table 3.7 presents the parameters used for the truss representing the cross wall. For calculation and more about the conversion, see Section 3.7 "3D-2D converting method" mentioned earlier.

Table 3.7: Input data for the trusses.

	Identification	Value	Units
Material set		Elastic	-
Properties	EA	2.17E+07*	kN
	$L_{spacing}$	5	m

* See calculation in Appendix B.

3.3 Selected models and parameters

The selected models in this case study is the Hardening Soil small strain model (HSs) and NGI-ADP model (ADP) that have been presented in previous chapter 2 Literature Review section 2.5 Material models.

The soil parameters used for modelling the base model of LBT and the material models have been retrieved from two different investigations in the nearby area. Most of the data used for the HSs parameters have been evaluated from triaxial tests conducted for Jernhusen in Region City (Wood, 2014). The ADP parameters have been retrieved from preliminary design for the West Link project (Trafikverket, 2013).

Many other reports have also used this data, for have been summarized in a PM from Trafikverket named "Design Base Geoteknik" (Wood, 2017).

The conditions for the data used for modelling LBT were merged from these two the best way possible to minimize any unnecessary differences in the sensitivity analysis.

Figure 3.12 presents the adjustment of the soil layers for the fictional model of LBT from the two different soil parameters. They are defined the same way in both material models but generally adapts to the data from the HSs-model. For more detailed in formation, see the referred literature.

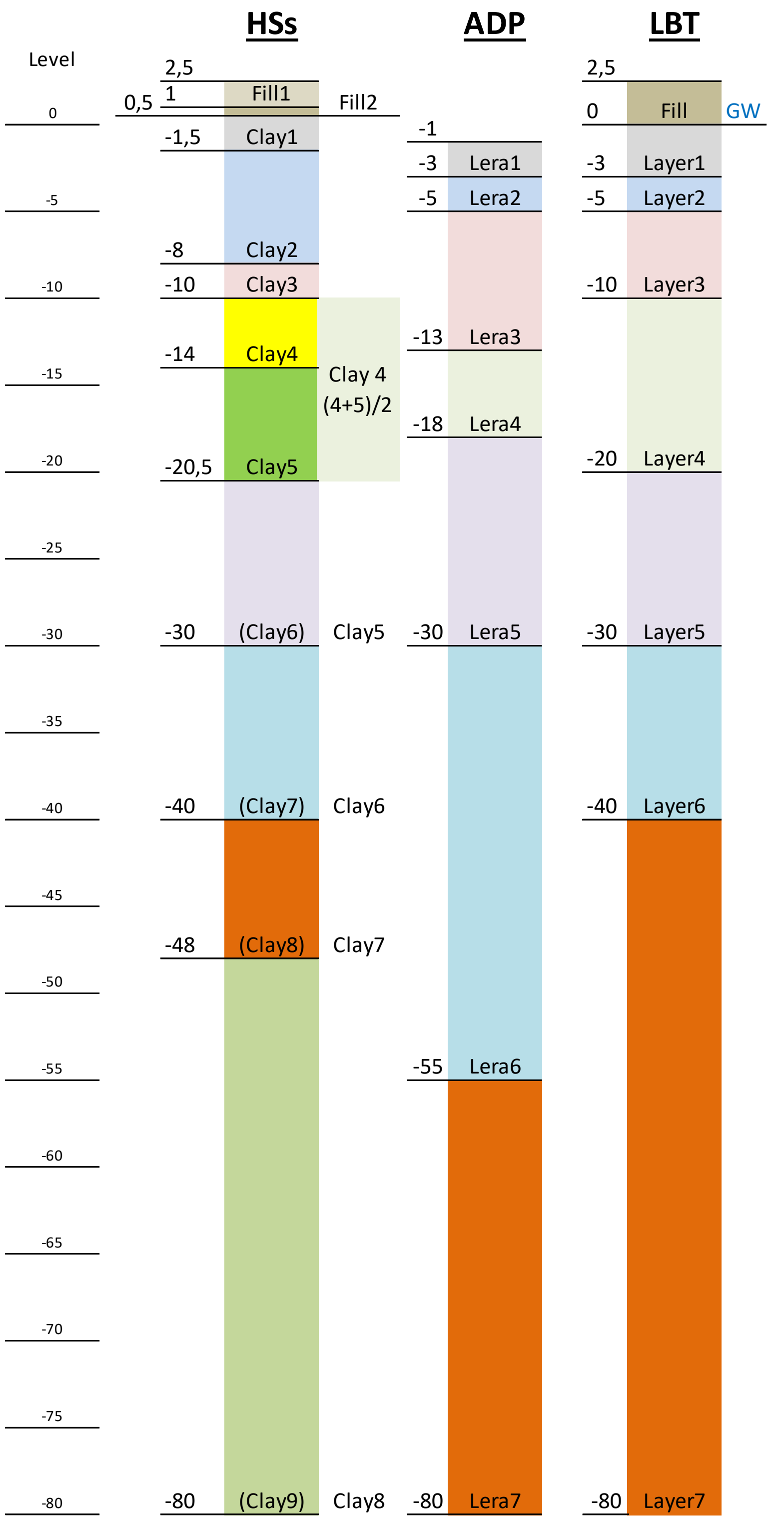

Figure 3.12: Soil layers adaption. HSs & ADP from RegionCity adapeted for LBT.

3.4 Soil parameters

In pursuance of better visualise the soil parameters, they will be plotted in different diagrams with data from given data simulated in test and compared with field tests. The following Tables present input data and parameters for the material models, more details can be found in Appendix D.

Table 3.8: General input parameters to both material models.

Soil	Top [m]	Bot [m]	Δz [m]	γ $[kN/m^3]$	γ_w $[kN/m^3]$	OCR [-]	POP [-]	$K0$ [-]	$K0_{nc}$ [-]	ϕ' [°]
Fill*	2,5	0	2,5	18	10	-	-	0,5	Auto	35
Clay1	0	-3	3	16	10	2,00	0	0,7	0,47	32
Clay2	-3	-5	2	16,5	10	1,65	0	0,7	0,47	32
Clay3	-5	-10	5	15,5	10	1,38	32	0,63	0,47	32
Clay4	-10	-20	10	15,7	10	1,25	32	0,61	0,47	32
Clay5	-20	-30	10	16,3	10	1,17	32	0,58	0,49	30,5
Clay6	-30	-40	10	16,2	10	1,14	0	0,57	0,49	30,5
Clay7	-40	-80	40	16,4	10	1,14	0	0,56	0,49	30,5

* The Fill layer use the MC-model.

Table 3.9: Specific parameters to HSs-model.

Soil	c_{ref} [kPa]	E_{50}^{ref} [kPa]	E_{oed}^{ref} [kPa]	E_{5ur}^{ref} [kPa]	G_0^{ref} [kPa]	G_{ur} [kPa]
Clay1	1	7000	3002	27000	77480	6800
Clay2	1	7000	3400	33700	39700	8800
Clay3	1	7000	3068	24250	40210	10800
Clay4	1	15400	8300	30800	39230	15200
Clay5	0	13100	6600	26200	40960	20800
Clay6	0	13100	6600	26200	36060	27200
Clay7	0	10500	5285	21000	37460	44400

Table 3.10: Specific parameters to the ADP-model.

Soil	y_{ref} [m]	$s^A_{u,inc}$ $[kN/m^2]$	$s^A_{u,ref}$ [kPa]	s^P_u/s^A_u [-]	T_0/s^A_u [-]
Clay1	0	0	23	0,565	0,4
Clay2	-3	2,3	23	0,569	0,45
Clay3	-3	2,3	23	0,582	0,47
Clay4	-3	2,3	23	0,589	0,5
Clay5	-3	2,3	23	0,595	0,55
Clay6	-3	2,3	23	0,6	0,57
Clay7	-3	2,3	23	0,603	0,55

Table 3.11: Specific parameters to the ADP-model.

Soil	y_{ref} [m]	T_0/s^A_u [-]	G_{ur}/s^A_u [-]	γ^C_f [-]	γ^E_f [-]	γ^{DSS}_f [-]
Clay1	0	0,652	400	2	6	4
Clay2	-3	0,656	400	2	6	4
Clay3	-3	0,668	400	2	6	4
Clay4	-3	0,676	400	2	6	4
Clay5	-3	0,682	400	2	6	4
Clay6	-3	0,687	400	2	6	4
Clay7	-3	0,69	400	2	6	4

3.4.1 Initial In-situ

The plot in Figure 3.13 presents the in-situ stresses and pore water pressure for the modelled case study. The soil showed to be slightly over-consolidated.

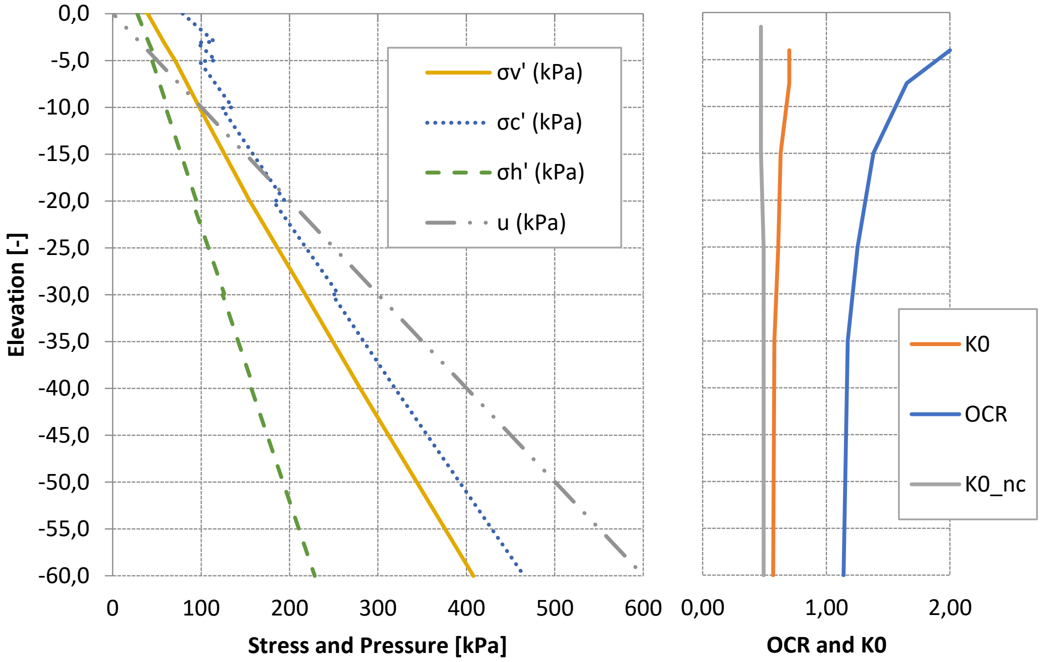

Figure 3.13: In-situ stresses, pore water pressure, OCR and K0.

3.4.2 Numerical model parameters

Following subsections illustrate the stiffness and strength parameters used in HSs- and ADP-model. For more details about calculations of parameters presented, see Equations described in 2.5 Material models.

Stiffness

Figure 3.14 presents the stiffness parameters E_{50}, E_{oed} and E_{ur} with depth, used in the HSs material model. The E_{50} and E_{oed} are quite similar while E_{ur} is about the double. In the transition between the different layers the stiffness reduces a bit.

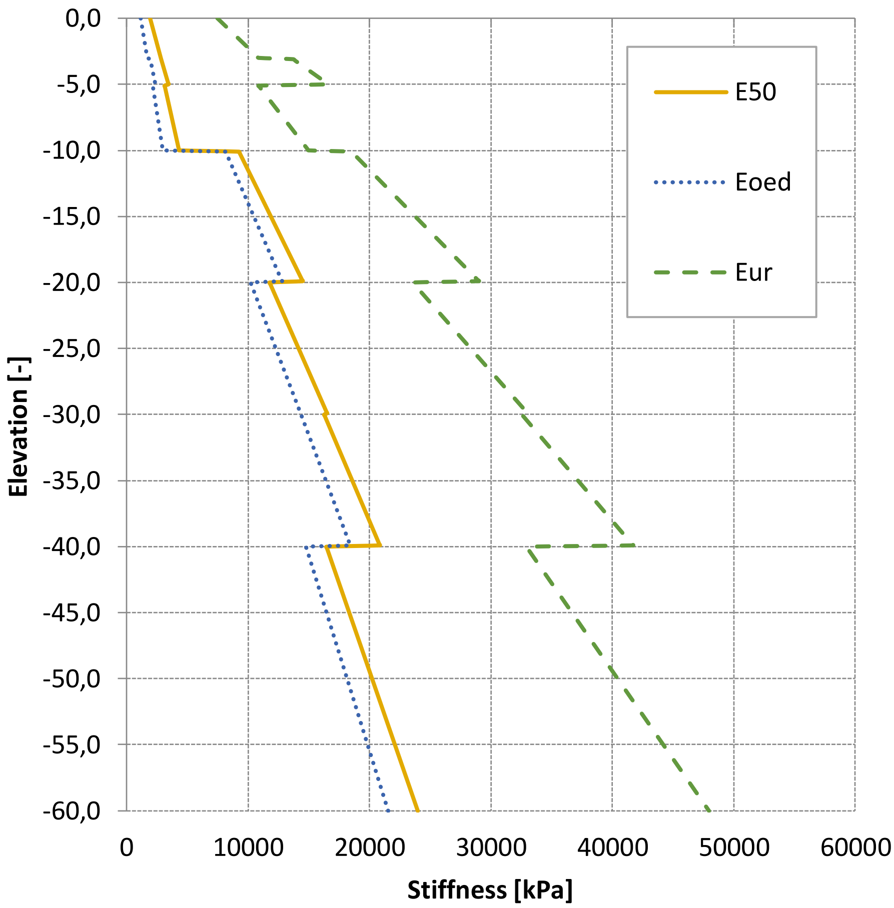

Figure 3.14: Young's modules E_{50}, E_{oed} and E_{ur}.

Figure 3.15 represents shear modules at very small strains G_0 used in HSs-model compared to un-/reloading shear modules G_{ur} used in the ADP-model. G_0 is constant since the reference value in ADP-model of $G_{ur}/S_u^A = 400$. G_0 is calculated from the HSs-model parameter G_0^{ref} with Equation 2.13.

The initial shear modulus G_0 is higher then the constant G_{ur}. Therefore, the HSs-model have higher shear stiffness than the ADP-model which results in smaller deformations and strains, however G_0 will also be degraded but still higher than ADP-model.

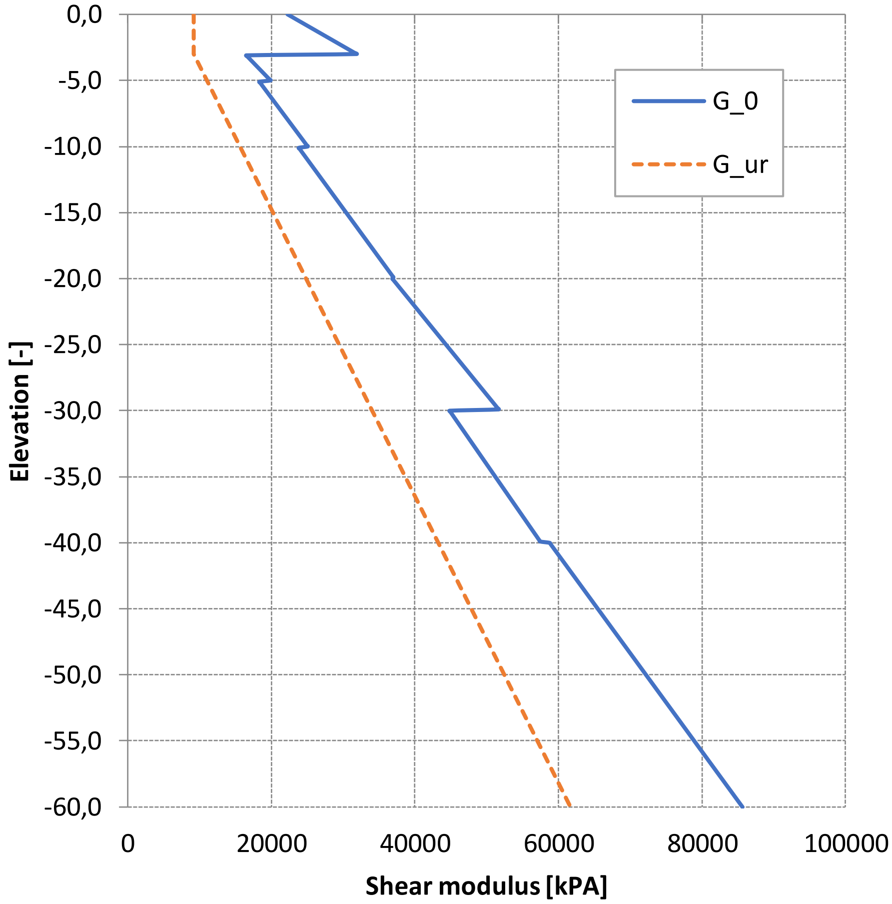

Figure 3.15: Shear modules, initial G_0 and un-/reloading G_{ur}.

Strength

The strength parameter of the initial mobilization τ_0/s_u^A is compared in Table 3.16 between the simulated in-situ value and field test values retrieved from Region City (Wood, 2014). The simulated shear strength and field test converge quite well. For more details, see 2.5 Material models and Brinkgreve (2017*b*).

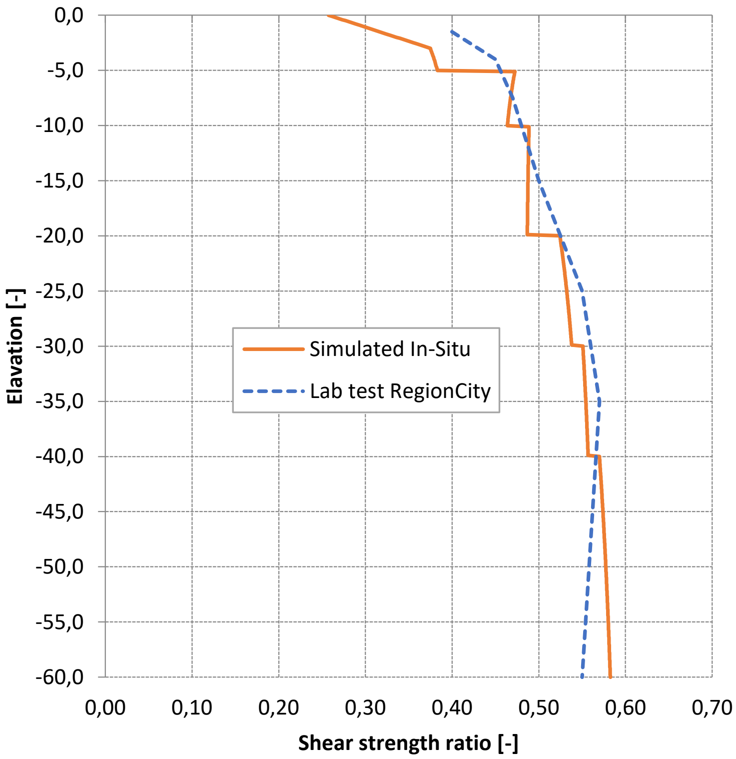

Figure 3.16: Initial mobilisation ratio of τ_0/s_u^A, a comparison between simulation and lab test values.

3.5 Simulation of soil parameters

PLAXIS have a feature called Soil-Test which simulate theoretical laboratory tests for different material sets defined by the user. The available simulation options are triaxial, CRS, oedometer, DSS and General. In the last option, any random stress path can be simulated by presenting the right boundary conditions.

3.5.1 CRS test

Figure 3.17 shows the simulated stress-strain curve of the HSs clays 1 to 7 conducted in PLAXIS Soil Test, according to the settings in Table 3.12, compared to real tests of field samples from Region City (Wood, 2014). Comments on the CRS test simulation:

- This set of parameters are not able to capture the real soil behaviour under CRS conditions.
- Only the initial part before the pre-consolidation pressure is captured to some extend.

Table 3.12: Input data CRS SoilTest.

Type of test	Input	Mob.Rel. Shear Strength	Initial	kN/m^2	Phase 1	Incre.	%
Drained	σ_c'	No	σ_{xx}	-5	Duration: 1 day	$\delta\epsilon_{xx}$	0
			σ_{yy}	-5	Steps: 500	$\delta\epsilon_{yy}$	-10
			σ_{zz}	-5		$\delta\epsilon_{zz}$	0
			τ_{xy}	0		$\delta\gamma_{xy}$	0

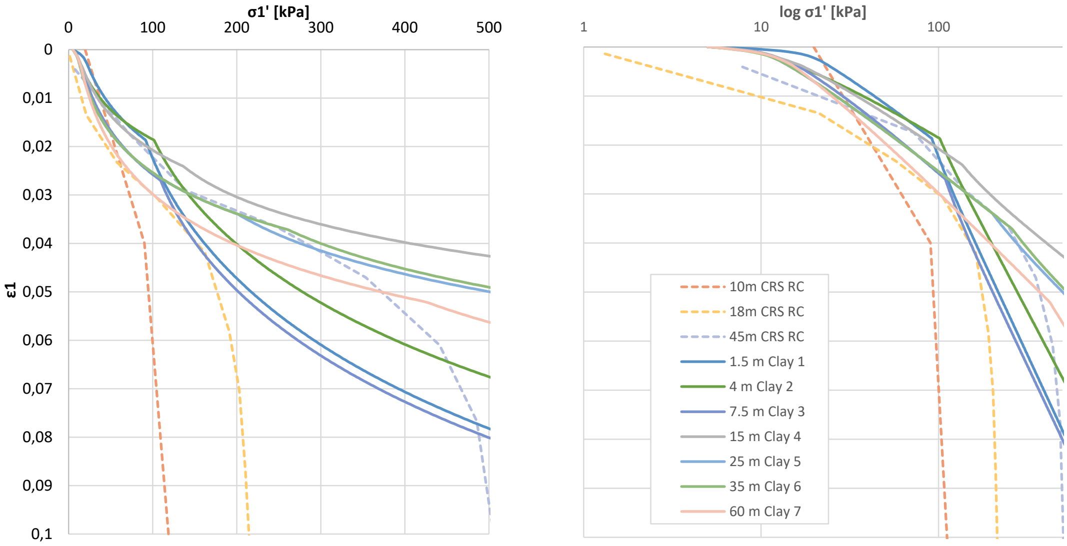

Figure 3.17: CRS plots of stress-strain and logarithmic stress-strain in the HSs-model.

3.5.2 Triaxial test

Figure 3.18 presents p'-q stress space of simulated test using HSs. Table 3.13 presents the input paramters for clay 1 to 7 simulated in PLAXIS SoilTest and compared with lab tests from Region City (Wood, 2014). The lab test are retrieved from a effective stress path plot in triaxial space s'-t and converted to p'-q using equations in 3.2. Comments on $p'q$-plot in Figure 3.18:

- The presented MC-failure line is plotted with $\phi = 32°$, sample clay 5 to 7 have $\phi = 30.5°$ and therefore do not intercept with the line.
- Partial aniosotropy using the MC failure in HSs. However still same friction angle in compression and extension, where the path exceeds.

$$q = 2t, \quad p = \frac{3s' - t}{3} \tag{3.2}$$

Table 3.13: Input data Triaxial SoilTest.

Type	Direction	Consolid.	Input	Units
Undrained	Comp. & Ext.	$K0 = 0.7$	Initial eff. stress, σ_v'	kN/m^2
			Maximum strain, σ_{yy}	%
			Steps: 500	-
			Vertical precons. stress, σ_c'	kN/m^2
			Mob. Rel. Shear strength: No	-

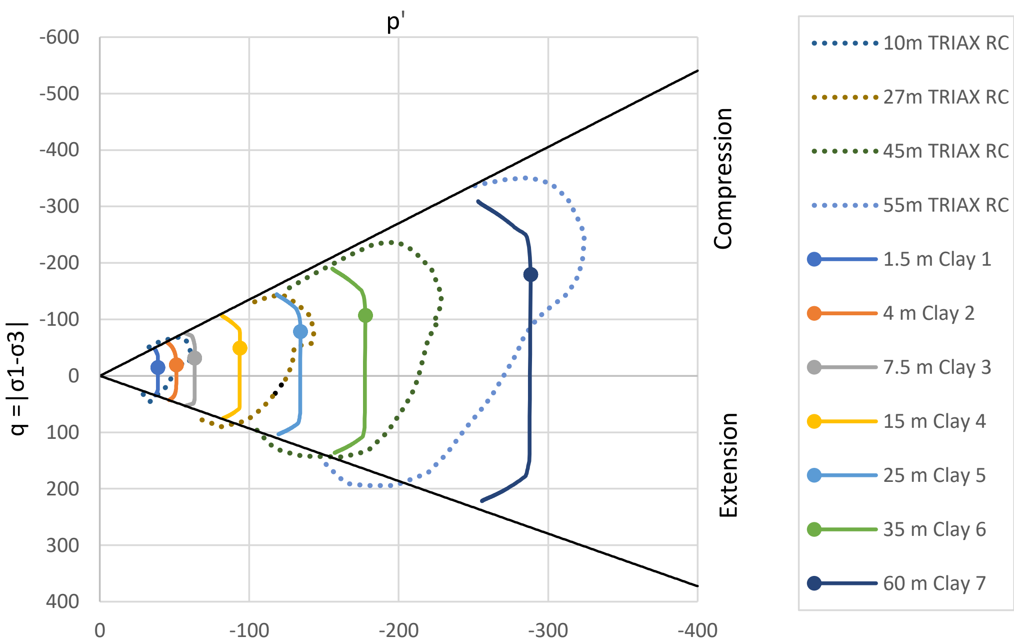

Figure 3.18: Comparison of $p' - q$ stress space in a triaxial test in the HSs-model.

The simulated major principal strain and deviatoric shear compered to Region City lab test is presented in Figure 3.19. Comments on the HSs-model strength parameters:

- The lab test from Region City only presents strain and deviatoric shear in compression.
- The HSs-model simulation appears to be stiffer at small strain.
- The simulation from HSs-model do not capture the clay softening behavior.

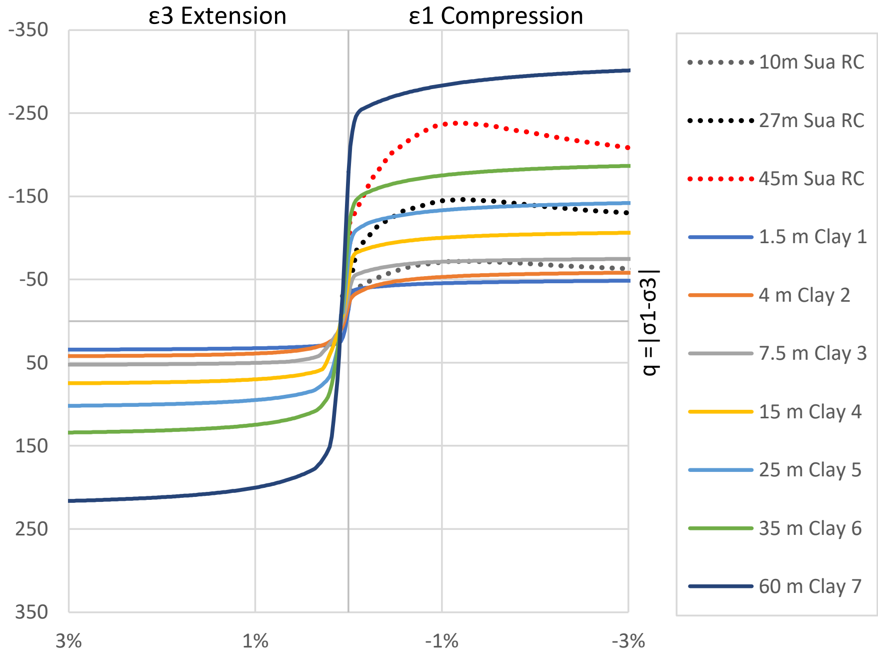

Figure 3.19: Comparison of major principal strain and deviatoric shear between simulation and lab test values in the HSs-model.

Figure 3.20 presents the shear strength s_u comparison between the ADP-model simulation and lab test values from Region City. Comments on the ADP-model strength parameters:

- The simulated values for shear strength i compression S_u^A fits very well, whilst extension S_u^P indicate a small overestimation in the HSs-model.

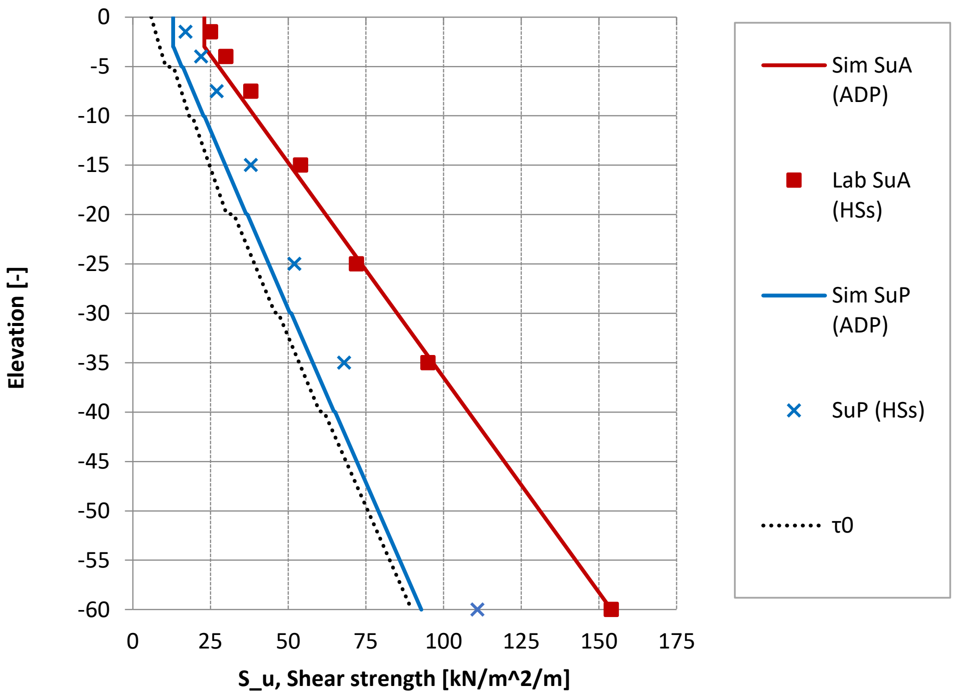

Figure 3.20: Comparison of shear strength S_u between simulation and lab test values in the ADP-model.

4

Results

This chapter presents the results from 38 individual PLAXIS-calculations conducted for the material model comparison and parameter study. To investigate the result for the vast amount of data, only a few output variables have been chosen to visualize the effects.

4.1 Parameters

A total number of 18 variations combining the two material models and different parameters were chosen to be alternated for a sensitivity analysis, in order to investigate the effect on the LBT boundary value problem. These can be divided in 3 categories:

- Interface parameters for both material models.
- Stiffness parameters of the HSs-model.
- Stiffness and strength parameters of ADP-model.

For further information about the parameters, go back to the Literature Review chapter or see PLAXIS manual (Brinkgreve, 2017*b*).

4.1.1 Interface parameters

R_{inter}: Interface reduction factor.

E': Interface stiffness.

The elasto-plastic MC-model with undrained (A) is used to describe the behavior of interfaces for modelling the soil-structure interaction. The Coulomb shear stress criterion is used to separate elastic behaviour, where small displacements can occur within the interface, and plastic interface behaviour when permanent slip may occur (Brinkgreve, 2017*a*).

Note that a value of R_{inter} less then 1 reduces the strength c', ψ and ϕ as well as the stiffness E' of the interface. Suggestions for R_{inter} interaction between clay and concrete is 0.7-1 (Karstunen, 2016).

The parameter study investigates the effects of changing R_{inter} and E' between the diaphragm wall/adjacent soil (DW/Soil) and diaphragm wall/cross-wall (DW/CW), for both the HSs and ADP-models.

4.1.2 HSs stiffness parameters

E_{50}^{ref}: Secant reference stiffness in standard drained triaxial test.
E_{oed}^{ref}: Tangent reference stiffness for primary oedometer loading.
E_{ur}^{ref}: Un-/reloading reference stiffness.

Due to limits in altering the parameters of the HSs-model in PLAXIS, some alternations had to be made in order to be able to conduct a parameter study. These are presented in the Sensitivity analysis. Note that it is the reference value at $p_{ref} = 100kPa$ that is varied.

4.1.3 ADP stiffness and strength parameters

Stiffness
G_{ur}/s_u^A: Ratio un-/reloading shear modules over undrained active shear strength.
γ_f^C: Shear strain at failure in triaxial compression.
γ_f^{DSS}: Shear strain at failure in direct simple shear.
γ_f^E: Shear strain at failure in triaxial extension.

If the shear strength is increasing with depth the constant ratio for G_{ur}/s_u^A gives a shear stiffness increasing linearly with depth.

Strength
s_u^P/s_u^A: Ratio of plain strain passive shear strength over plane strain active shear strength.
s_u^{DSS}/s_u^A Ratio of direct simple shear strength over active shear strength.

4.2 Output variables

This section present the chosen output variables for comparison and evaluation of the parameter study. Appendix D presents more details about the extraction of the variables. All output variables are taken from phase 7, at full excavation before the bottom plate is constructed, since it is the most critical phase.

Deformation, u_x

Plotting all the horizontal displacements in the diaphragm wall. This type of displacements is often monitored during the construction by surveyors or by installed inclinometers.

Bending moment, M

The bending moment effecting the diaphragm wall.

Axial forces of strut and cross-wall truss, N

The axial forces acting on the diaphragm wall from the strut and cross-wall. Calculation for these output variables have been presented in previous chapter Case Study and Appendix B and C.

Total normal stress due to earth pressure, σ_N

Some abnormalities were observed in this output parameter, mostly on the passive side, which probably is due to the truss model for the CW at this zone.

Heave at the excavation bottom, u_y

There is a zigzag pattern of the heave deformation, a model effect due to the cross-walls and the piles. The peak values represents the heave at the soil between the cross-walls. The friction on the cross-wall reduces the heave in the soil.

Settlements, u_y

Settlements behind the diaphragm wall at ground surface.

4.3 Base-model comparison and evaluation

This section illustrates and comment the differences found in comparing the results of the material models HSs and ADP. Step by step the input parameters have been evaluated by observations of the differences in the material models and other modelling consequences. The iteration of the base-model using the material models HSs and ADP is presented below as an example for the sensitivity analysis and present the major differences between the material models before altering the parameters. The whole comparison of the base-model is presented in Appendix E Complete Sensitivity Analysis.

Horizontal deformations in the diaphragm wall, u_x

- The ADP-model shows a relatively higher clockwise rotation of the wall compared to the HSs-model.
- The strut have greater counteracting effect on the diaphragm wall then the cross-wall. An error in equivalent length in the modelling might have contributed to this. It is normal that the wall tend to rotate at the bottom.

Direction	u_x		u_y	
Material model	HSs	ADP	HSs	ADP
Strut position	2 mm	4 mm	10 mm	20 mm

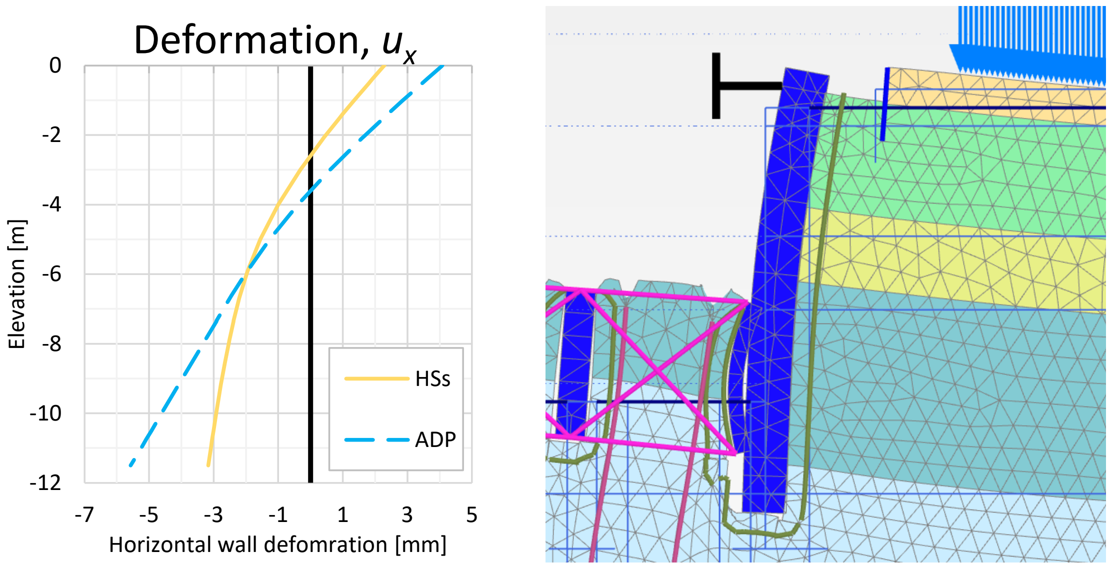

Figure 4.1: HSs/ADP comparison. Plot of u_x deformation and deformed mesh view scaled up 50 times.

Bending moment in the diaphragm wall, M

- Truss acting more like a point-load rather then a distributed-load which can be seen in both M-diagram and deformed mesh view.
- Cross-wall slightly bent resulting in less contact in the interface to diaphragm wall.
- Bending moment approximately equal to 0 [kNm/m] in the middle of cross-wall.
- Maximum bending moment difference between HSs and ADP, ΔM = 100 [kN-m/m].

Material model	HSs	ADP
Maximum bending moment	520 [kNm/m]	600 [kNm/m]

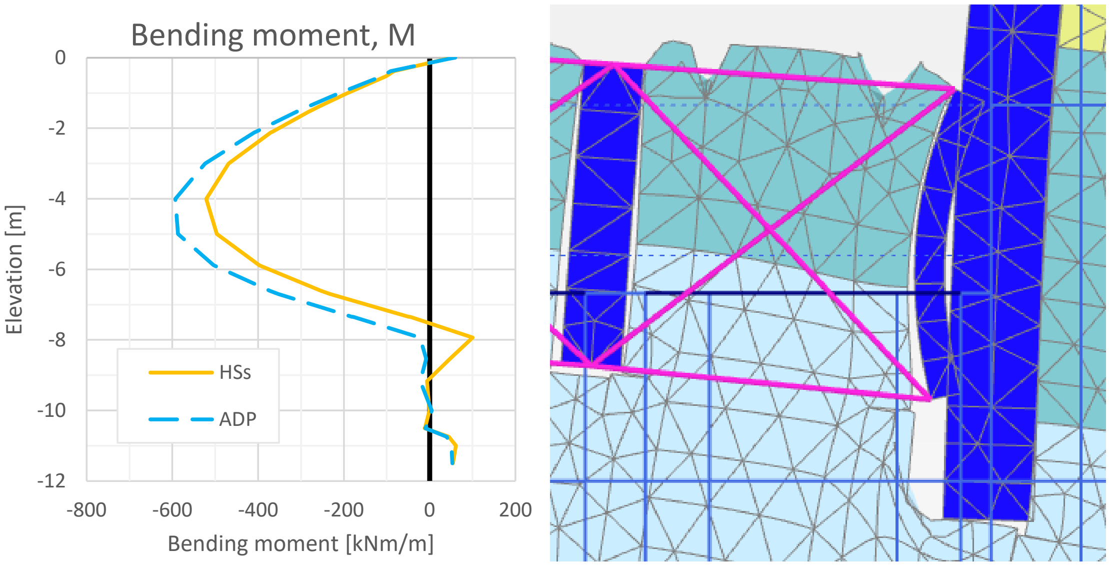

Figure 4.2: HSs/ADP comparison. M-diagram and deformed mesh scaled up 50 times.

Axial normal forces acting on strut and truss, N

- The axial normal force of the truss is the sum of the resulting horizontal force of each individual bar. Significantly higher axial normal force in truss compared to strut.
- Due to wrong input value for the equivalent length of the strut, it most certainly have affected the axial force of the strut and truss in both the HSs and ADP.
- The axial normal force for HSs is slightly higher in the strut and significantly less in truss.

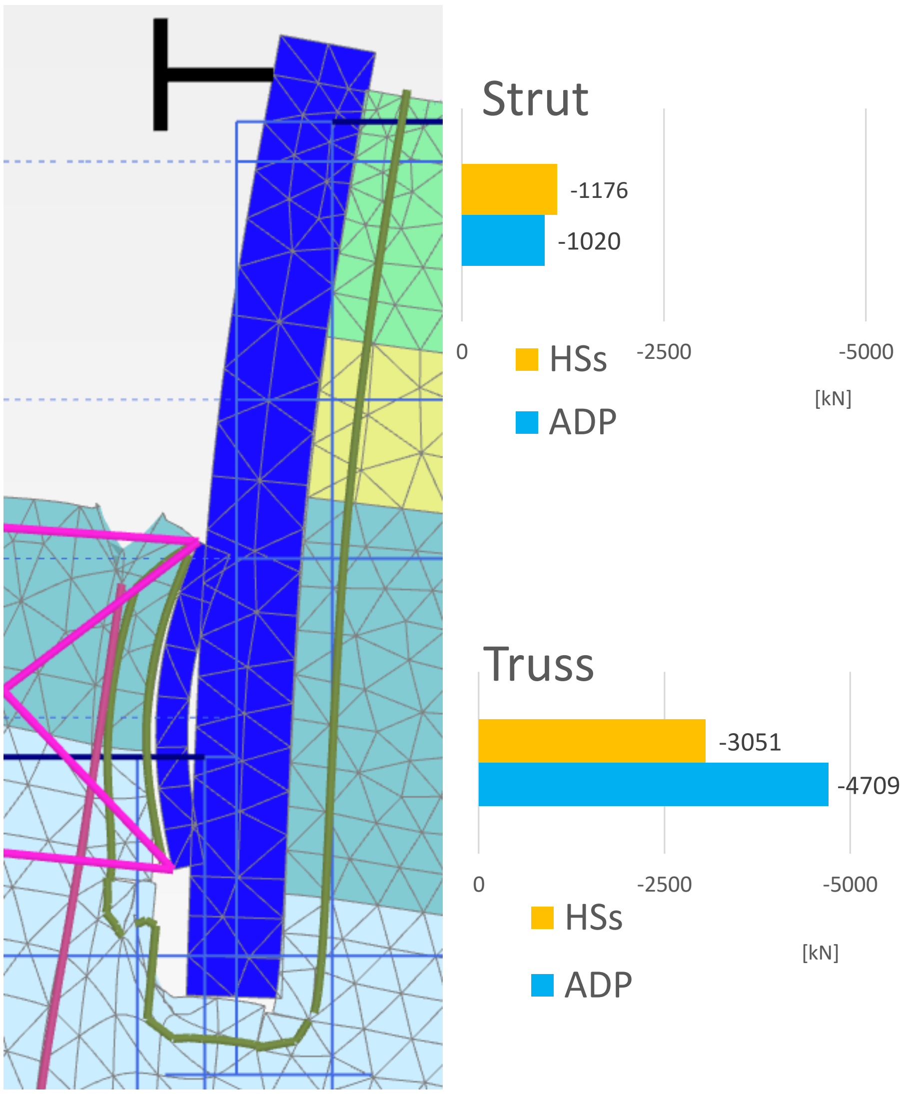

Figure 4.3: HSs/ADP comparison. Axial normal forces acting on strut and truss.

Active/Passive earth pressure, σ

- HSs: A minor change in pressure between the clay layers.
- The earth pressure in the ADP-model initially decreases and during the first clay layer have at a lower value but then surpasses the HSs with a constant increase with depth.
- Most likely, the effects of the cross-wall implementation, shows some disruptions in pressure in the marked areas in the figure and is considered deceptive and therefore neglected.

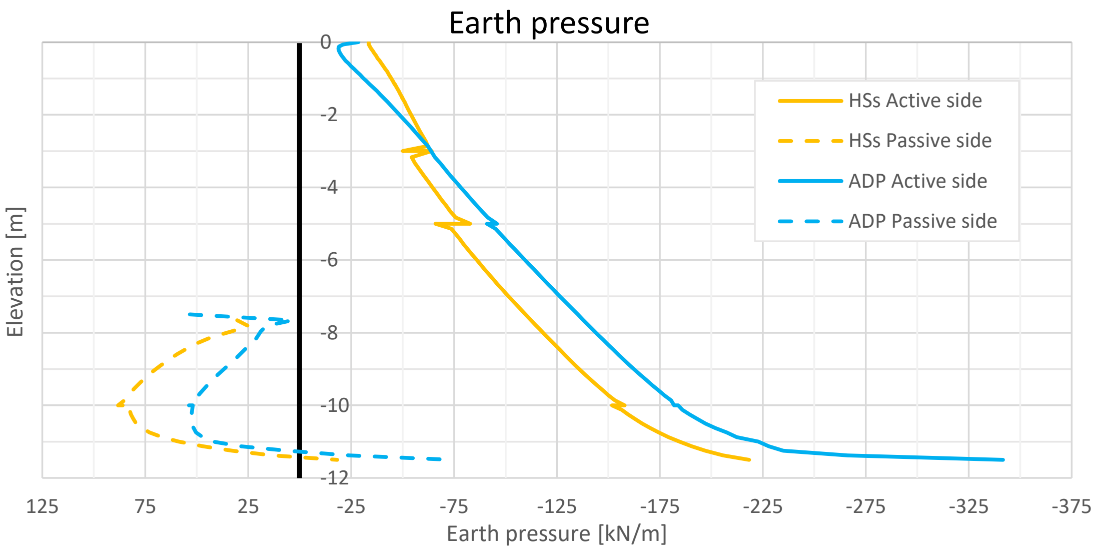

Figure 4.4: HSs/ADP comparison. Active/Passive earth pressure σ.

Heave at excavation bottom, u_y

- The heave is higher in the middle of the excavation compared to the joint of DW/CW, especially in the ADP-model.

Material model	HSs	ADP
Maximum heave	6 cm	2 cm

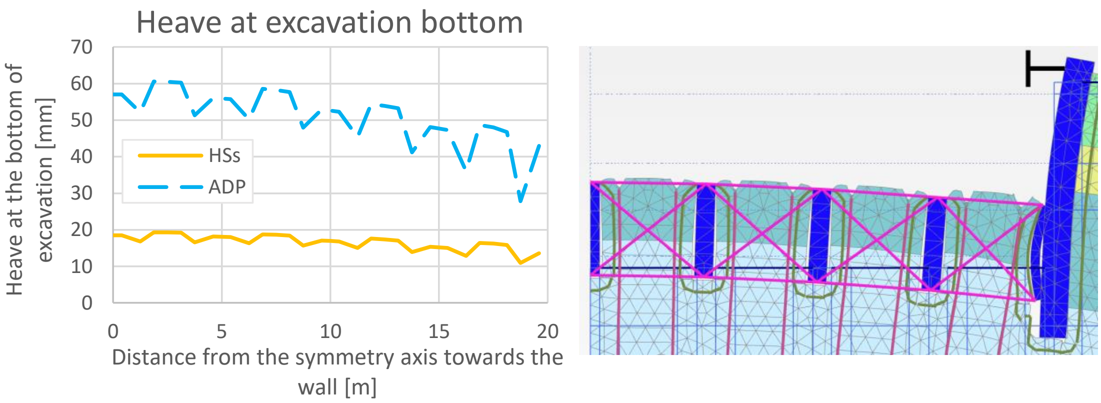

Figure 4.5: HSs/ADP comparison. Heave at excavation bottom.

Settlements behind the diaphragm wall, u_y

- Notice that the measurements start at $x = 20m$ and therefore include the displacements of the diaphragm wall as well.
- The first 15 m behind the diaphragm wall is most likely effected by the excavation of the fill and the PLAXIS-model adaptation of the temporary sheet pile wall.
- Initially heave within the excavated fill layer and the cross over to settlements occur at the same place for both material models.
- ADP shows significant more heave and settlement than HSs.

Material model	HSs	(u_x)	ADP	(u_x)
Maximum settlement	5 mm	(< 70 m)	19 mm	(peak at 60 m)

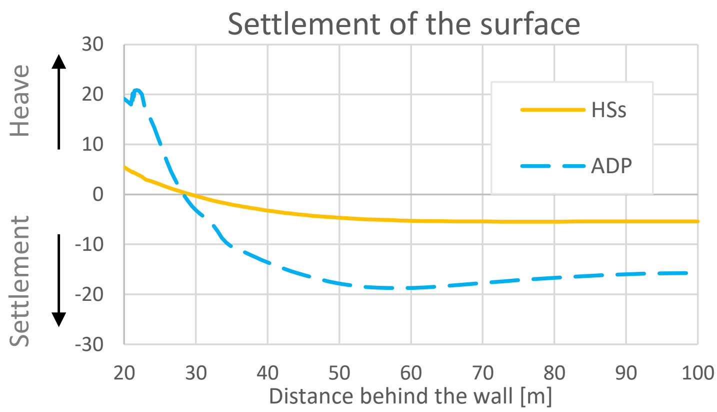

Figure 4.6: HSs/ADP comparison. Settlements u_y behind the diaphragm wall.

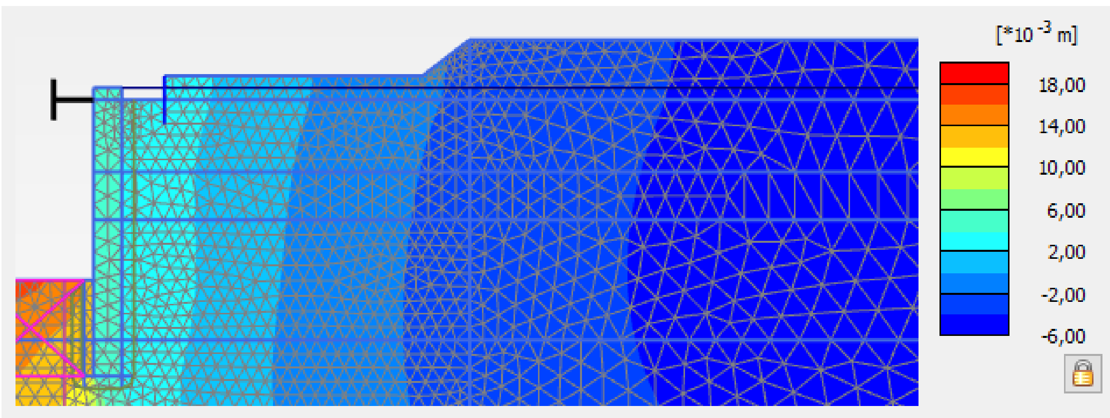

Figure 4.7: Settlements shown in PLAXIS of the HSs-model.

Summary of HSs/ADP base-model comparison

In almost all of the cases the ADP-model showed higher difference from the reference value than in the HSs-model, especially in heave at the excavation bottom.

The distribution of the axial load between the truss and strut is effected by the modelling mistake of the equivalent length of the strut. However, this mistake was present in all models which still make the analysis valid as the same error applies in all cases.

The truss is a good approximation to transfer the horizontal forces from the diaphragm wall. However the concentration effect at the truss joint between DW/CW is not realistic and need to be improved.

4.4 Parameter study and Sensitivity analysis

In order to get a comprehensive overview of all the output data of the parameter study, a matrix of the sensitivity analysis is presented in Figure 4.8. In general the differences shown from the parameter study are quite small, but the changes still indicate how the single parameter affects the output. The short for Min and Max, in Figure 4.8, indicate if the parameter have a reduced or increased value compared to the reference value. In order to get a better understanding of the influence of the parameter a percentage of the alternation is also presented, calculated as the difference of Min/Max compared to Ref divided by Ref. More details about the alternations of the parameters can be found in Appendix D "Full input and output data".

The colour grading of insignificant, minor and notable differences are a assessment of the parameters impact in relation to the reference and the other alternations. The complete sensitivity analysis is presented in Appendix E. From the notable differences displaced in Figure 4.8, a number of six calculated combinations of parameters and material models have been chosen for further investigations:

- 6: Interface between diaphragm wall and cross-wall R_{inter} (ADP).
- 7: Interface stiffness between diaphragm wall and cross-wall, E' (HSs).
- 8: Interface stiffness between diaphragm wall and cross-wall, E' (ADP).
- 12: New reference: $E_{50} \cdot MIN/MAX$, $E_{ur} = 6 \cdot E_{50}$.
  (See 4.4.1 for further explanation)
- 13: G_{ur}/s_u^A Ratio un-/reloading shear modulus over undrained active shear strength.
- 16: y_f^{DSS} Shear strain at failure in direct simple shear.

4.4.1 Parameters adaption for the HSs stiffness parameters

As mentioned in the Literature Review about the HSs material model, the stiffness parameters E_{50}^{ref} E_{oed}^{ref} and E_{ur}^{ref} are dependent on each other and can not be altered separately. Therefore, the stiffness parameters in all clay layers of calculations number 9 to 12 had to be altered in stiffness sets with relation to each other. New start values had to be set as "New reference", where $E_{ur}^{ref} = 2 \cdot E_{50}^{ref}$ and E_{oed} set to fulfill the $K0_{nc}$-value. In order to observe the impact of the stiffness parameters, the E_{ur}^{ref} in the new reference value were increased by multiplying with 2, 4 and 6. The new references set where then multiplied with a Min and Max value as done with other parameters. See Appendix D "Full HSs input data" where the reference value is marked green and then multiplied by 0,8 and 1,2.

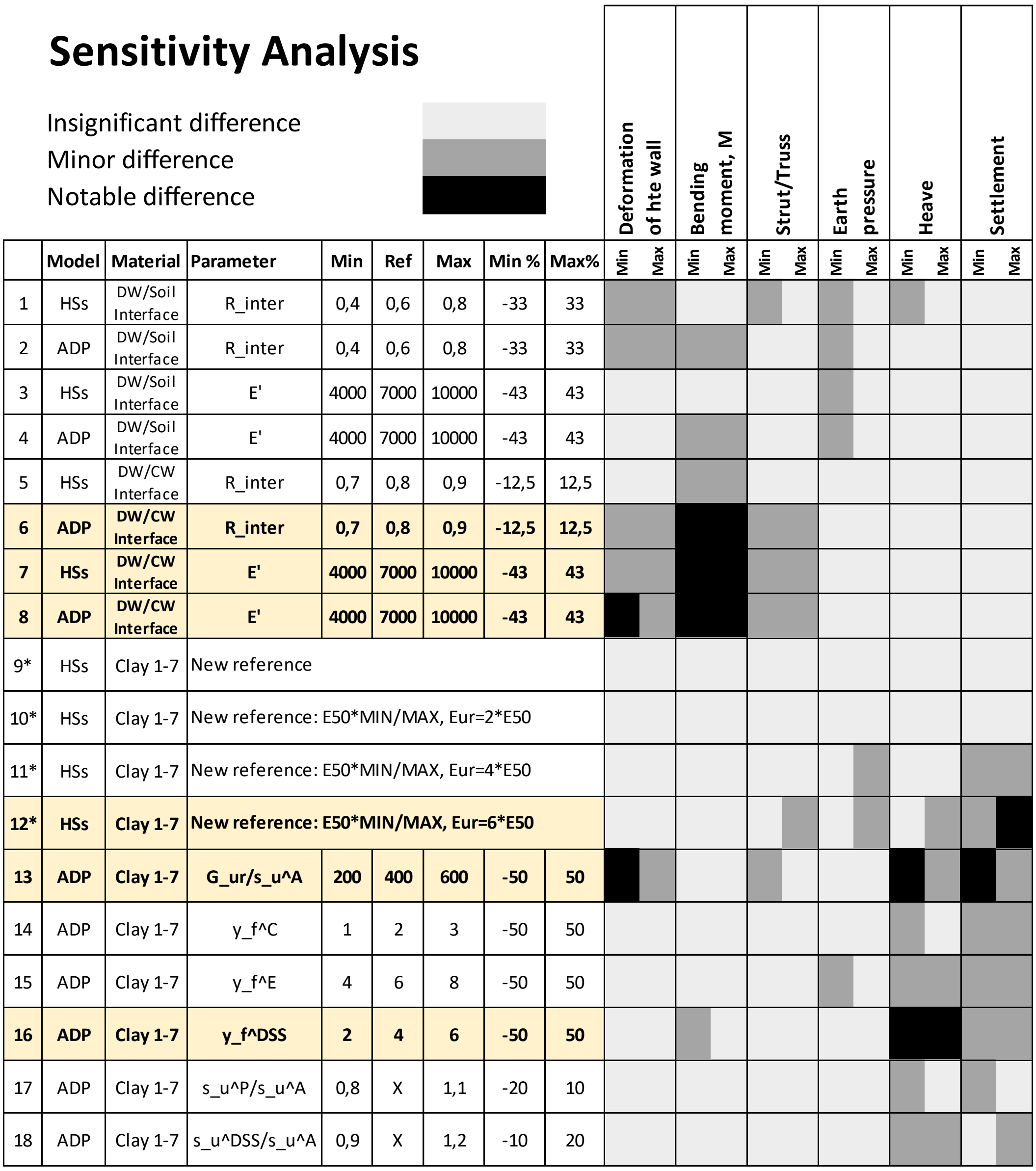

	Model	Material	Parameter	Min	Ref	Max	Min %	Max%
1	HSs	DW/Soil Interface	R_inter	0,4	0,6	0,8	-33	33
2	ADP	DW/Soil Interface	R_inter	0,4	0,6	0,8	-33	33
3	HSs	DW/Soil Interface	E'	4000	7000	10000	-43	43
4	ADP	DW/Soil Interface	E'	4000	7000	10000	-43	43
5	HSs	DW/CW Interface	R_inter	0,7	0,8	0,9	-12,5	12,5
6	**ADP**	**DW/CW Interface**	**R_inter**	**0,7**	**0,8**	**0,9**	**-12,5**	**12,5**
7	**HSs**	**DW/CW Interface**	**E'**	**4000**	**7000**	**10000**	**-43**	**43**
8	**ADP**	**DW/CW Interface**	**E'**	**4000**	**7000**	**10000**	**-43**	**43**
9*	HSs	Clay 1-7	New reference					
10*	HSs	Clay 1-7	New reference: E50*MIN/MAX, Eur=2*E50					
11*	HSs	Clay 1-7	New reference: E50*MIN/MAX, Eur=4*E50					
12*	**HSs**	**Clay 1-7**	**New reference: E50*MIN/MAX, Eur=6*E50**					
13	**ADP**	**Clay 1-7**	**G_ur/s_u^A**	**200**	**400**	**600**	**-50**	**50**
14	ADP	Clay 1-7	y_f^C	1	2	3	-50	50
15	ADP	Clay 1-7	y_f^E	4	6	8	-50	50
16	**ADP**	**Clay 1-7**	**y_f^DSS**	**2**	**4**	**6**	**-50**	**50**
17	ADP	Clay 1-7	s_u^P/s_u^A	0,8	X	1,1	-20	10
18	ADP	Clay 1-7	s_u^DSS/s_u^A	0,9	X	1,2	-10	20

Figure 4.8: Matrix of the Sensitivity Analysis.

* See previous explanation in subsection 4.4.1 and Appendix D for specific values.

4.4.2 Further investigations of parameters

Following sections present the outputs from the highlighted calculations shown in Figure 4.8.

6: Interface between diaphragm wall and cross-wall R_{inter} (ADP)

Table 4.1 show the parameter alternations and Figure 4.9 display the selected results. The following observations are made:

- A small alternation of max/min 12 %) in the reference value R_{inter} have a relatively high influence to the deformation and bending moment in comparison to the other observed relations between Max/min and Ref values.
- The effect of altering R_{inter} increase with depth in the horizontal deformations u_x, even though it is very small.
- Lowering the interface increase the bending moment and vice versa with a maximum difference of +/- 70 [kNm/m].

Table 4.1: Parameter settings for calculation number 6.

Model	Material	Parameter	Min	Ref	Max	Min %	Max %
ADP	DW/CW	R_{inter}	0,7	0,8	0,9	-12	12

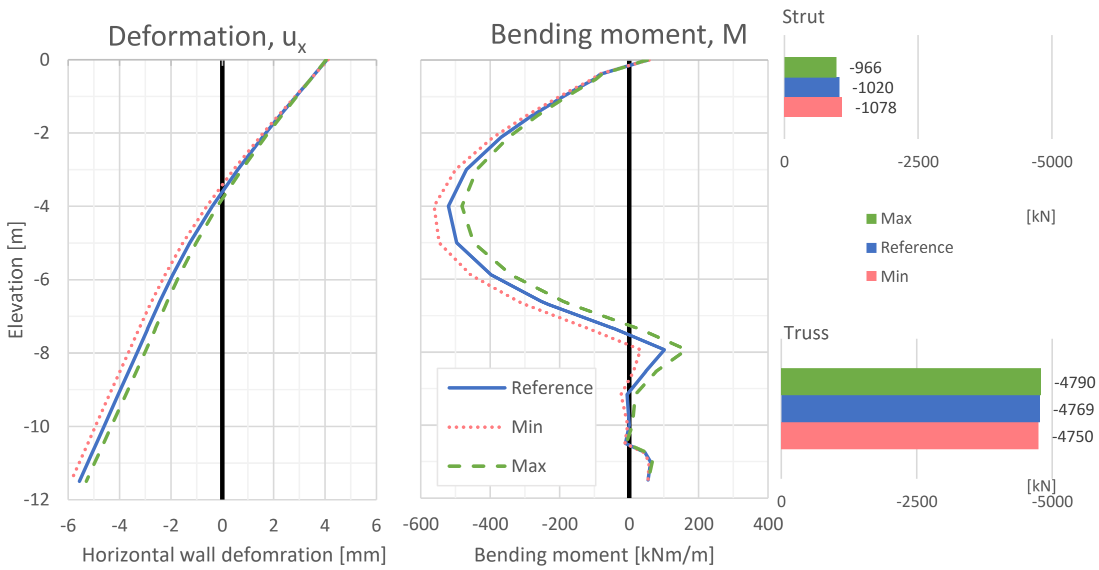

Figure 4.9: Output parameters for calculation number 6. Presenting deformation, bending moment and axial forces.

7: Interface stiffness between diaphragm wall and cross-wall, E' (HSs)

Table 4.2 show the parameter alternations and Figure 4.10 display the selected results. The following observations are made:

- Deviation from the reference value in horizontal deformations u_x increase with depth.
- Maximum difference in horizontal deformations u_x while decreasing $E' \rightarrow 0{,}4$ mm.
- Maximum difference in horizontal deformations u_x while increasing $E' \rightarrow 0{,}2$ mm.
- Deviation from the reference value in bending moment M increase until it reach the excavation bottom.
- Maximum difference in bending moment M while decreasing $E' \rightarrow 29\ kNm/m$.
- Maximum difference in bending moment M while increasing $E' \rightarrow 21\ kNm/m$.

Table 4.2: Parameter settings for calculation number 7.

Model	Material	Parameter	Min	Ref	Max	Min %	Max %
HSs	DW/CW	E'	4000	7000	10000	-43	43

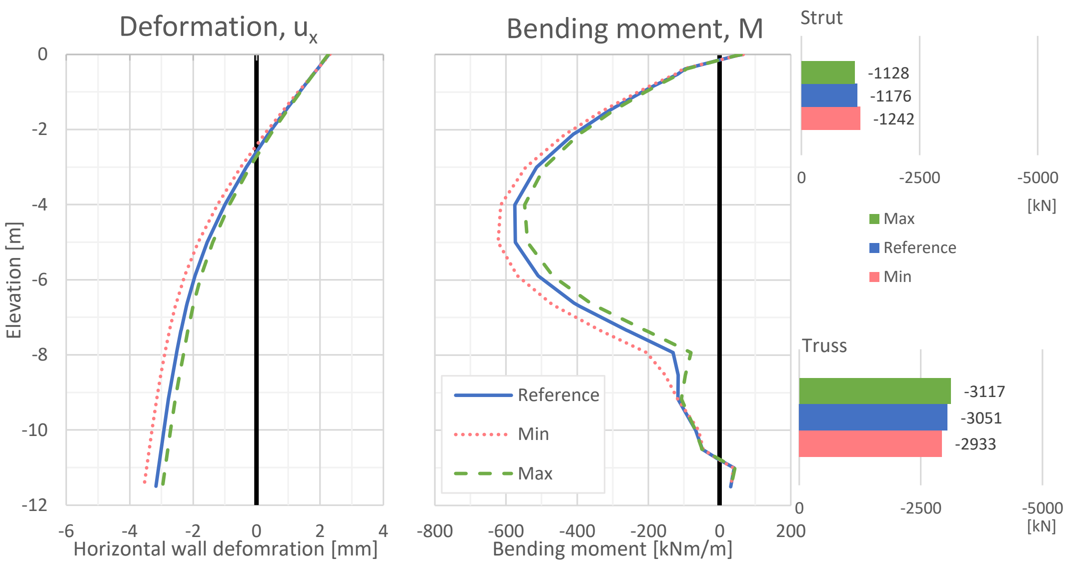

Figure 4.10: Output parameters for calculation number 7. Presenting deformation, bending moment and axial forces.

8: Interface stiffness between diaphragm wall and cross-wall, *E*' (ADP)

Table 4.3 show the parameter alternations and Figure 4.11 display the selected results. The following observations are made:

- Very similar to calculation number 7, even though the material model is changed.
- Deviation from the reference value in horizontal deformations u_x increase with depth.

Table 4.3: Parameter settings for calculation number 8.

Model	Material	Parameter	Min	Ref	Max	Min %	Max %
ADP	DW/CW	E'	4000	7000	10000	-43	43

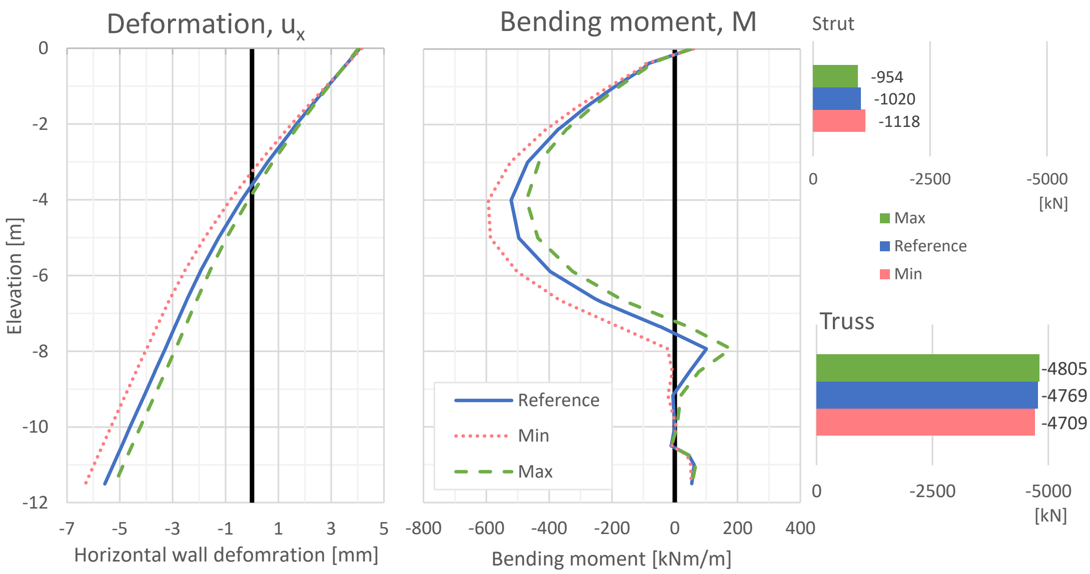

Figure 4.11: Output parameters for calculation number 8. Presenting deformation, bending moment and axial forces.

12: New reference: $E_{50} \cdot MIN/MAX$, $E_{ur} = 6 \cdot E_{50}$

Table 4.4 show the parameter alternations and Figure 4.12 display the selected results. The following observations are made:

- Notice that this calculation use a new reference parameters in the base-model due to limitations in altering the stiffness parameters in the HSs, see explanation in 4.4.1 in initial part of this section.
- Intersection from heave to settlement changes.
- Relatively small impact even though being the most affect parameter of the HSs stiffness model.

Table 4.4: Parameter settings for calculation number 12. (Calculated with new reference values).

Model	Material	Set of parameters	Min/Max	$K0_{nc}$-limit	Factor
HSs	Clay 1-7	E_{50}^{ref}, E_{oed}^{ref}, E_{ur}^{ref}	$E_{50}^{ref} \cdot 0,8/1,2$	$E_{oed}^{ref} \cdot K0_{nc}$	$E_{ur}^{ref} \cdot 6$

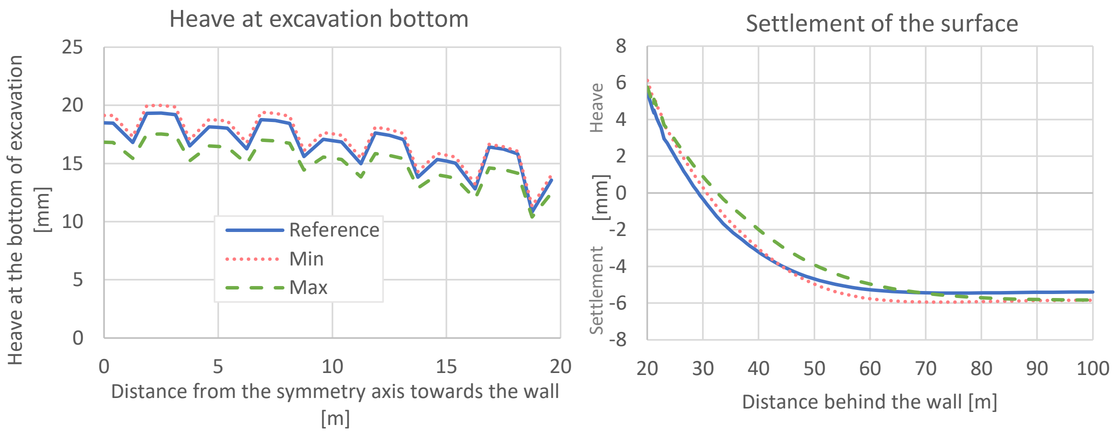

Figure 4.12: Output parameters for calculation number 12. Presenting heave at excavation and settlement behind the wall.

13: G_{ur}/s_u^A Ratio un-/reloading shear modulus over undrained active shear strength

Table 4.5 show the parameter alternations and Figure 4.13 display the selected results. The following observations are made:

- Deviation from the reference value in horizontal deformations u_x decrease with depth. Cross-wall dominant below excavation level.
- G_{ur}/s_u^A (200): Max difference in u_x = 2,3 mm at top of the diaphragm wall and strut.
- G_{ur}/s_u^A (600): Max difference in u_x = 0,8 mm at top of the diaphragm wall and strut.
- The effect on heave at excavation bottom is significant higher in reducing the parameter compared to increasing. Heave u_y compared to reference value is +18 mm respectively -5 mm.
- The effect on settlement of the surface is notable higher in reducing the parameter compared to increasing. u_y = +1,5 mm respectively -6 mm. Settlement peak at x = 60 m.

Table 4.5: Parameter settings for calculation number 13.

Model	Material	Parameter	Min	Ref	Max	Min %	Max %
ADP	Clay 1-7	G_{ur}/s_u^A	200	400	600	-50	50

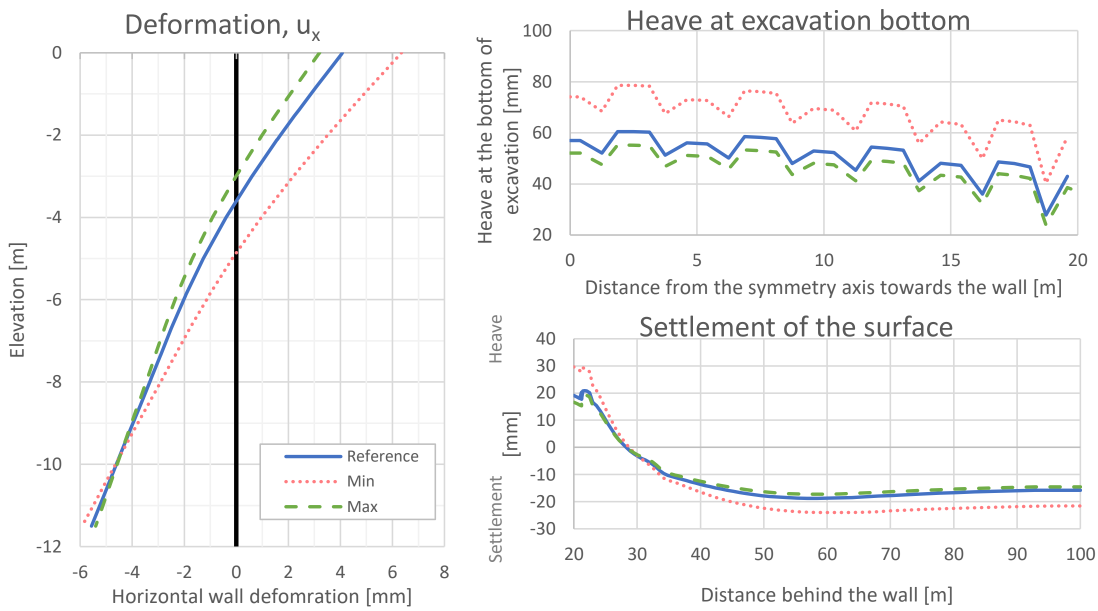

Figure 4.13: Output parameters for calculation number 13. Presenting deformation, heave at excavation and settlement behind the wall.

16: y_f^{DSS} Shear strain at failure in direct simple shear

Table 4.6 show the parameter alternations and Figure 4.14 display the selected results. The following observations are made:

- For heave, reducing the ratio of s_u^{DSS}/s_u^A by only -10 % have greater impact than increasing it by 20 %.

Model	Material	Parameter	Min	Ref	Max	Min %	Max %
ADP	Clay 1-7	γ_f^{DSS}	2	4	6	-50	50

Table 4.6: Parameter settings for calculation number 16.

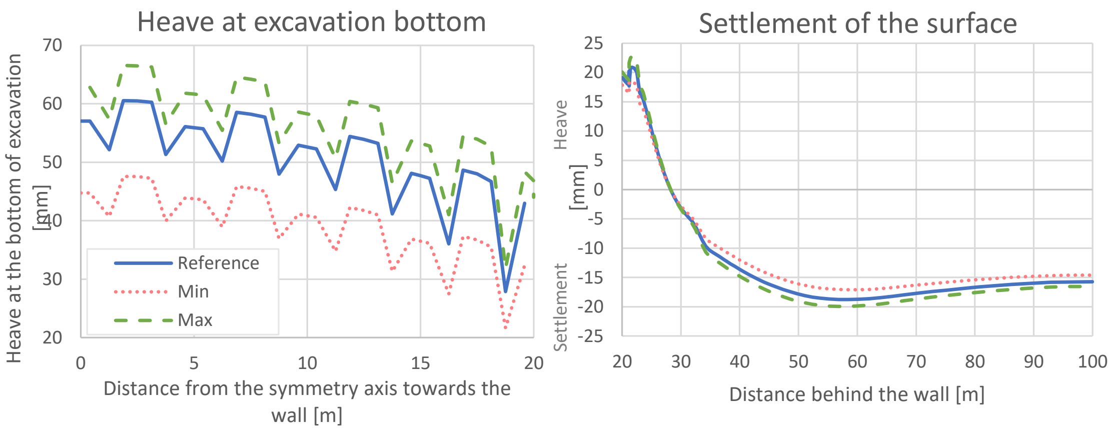

Figure 4.14: Output parameters for calculation number 16. Presenting heave at excavation and settlement behind the wall.

Summary of results for parameter study

The impact of the parameter alternations showed to be considerable smaller than expected.

Interfaces

The results regarding the interfaces only showed relevant changes in deformations and bending moment for the interaction between the diaphragm walls and the cross-walls.

Calculating with different material models showed to have very little effect. The ADP-models showed a significantly larger effect due to the fact it has a larger impact in general, stated in the comparisons of HSs and ADP.

E' had a larger impact than R_{inter} since it was possible for a bigger deviation from the reference value. Changing R_{inter} also effects E' but not as much.

HSs

Since it was hard to alter the stiffness parameters E_{50}^{ref}, E_{oed}^{ref} and E_{ur}^{ref} separately in PLAXIS the result needed to be interpreted considering the change in the base-model.

The increase of stiffness in this parameter study showed considerable small changes in general, only a minor influence of heave and settlement could be noticed for the highest alteration.

ADP

The shear strain in direct shear γ_u^{DSS} had the biggest influence of the shear strain parameters, remarkably mainly in heave and settlements and almost nothing in the other outputs.

The parameters with greatest impact in the ADP model were the ratio between un-/reloading shear modulus over undrained active shear strength G_{ur}/s_u^A. Reducing this parameter showed a notable deformation by rotating the diaphragm wall, the top outwards and the bottom inwards from the excavation, increasing settlements and heave within the excavation.

5

Discussion

General

Writing a master thesis is very much a living process where the purpose and focus often changes along the way as the initial circumstances shift. The aim for this master thesis eventually became to model the Lilla Bommen tunnel in order to do a back calculation since it already have been built and supposedly would have a lot of measurement data from the construction phase. However, it showed to be quite hard and time consuming to find relevant data to validate the modelled section and therefore the thesis once again had to shift into comparing the material models with a sensitivity analysis and validate them the best way possible.

Diaphragm and cross-walls

As mentioned in the introduction, the construction method with diaphragm an cross-walls is widely used and well tested internationally; also with similar circumstances in soft clays. In Sweden this construction method have not been commonly used since there have been quite few deep excavations in urban environments, and also due to high economical costs as a consequence of high demanding regulations. Today the regulations have adapted and this method will probably be more commonly used in the future, given the growth of urban areas.

Soil parameters

In order to retrieve sufficient input data for the two different material models, two other investigations of soil parameters were merged from nearby locations. This is not considered to have any significant impact on the result since the conditions are more or less the same within this small area. The data used to validate the simulated soil test is only retrieved from one of these areas.

Modelling

The location for the modelled section, near Thorsten Henriksson pedestrian bridge, was not located in the same area as in previously reports. The reason for this was to avoid some unfavorable circumstances such as old foundations from harbour docks and nearby bedrocks, however this made it hard to find relevant data for back calculation and validation.

Another important issue to address is the fact that a model is often just a set of simplifications used to describe a complex reality in the best way possible. In this case, modelling a 3-dimensional solution of using a cross-wall in a 2-dimensional model, have significant effect on the result and must be considered. The connection between the truss bars and the cross-wall seems to have a bending effect of the cross-wall adjacent to the diaphragm wall. The friction between these two may therefore be reduced due to less slip-surface, which probably results in a increased upward movement of the cross-walls. The bending moment diagram also indicate less contact between the diaphragm and the cross-wall since it acts like point loads rather than distributed. Furthermore, proper calibration of the DW-CW is necessary in order to account for the separation distance in the out-of-plane.

The strut may also have a bit misleading effect on the lateral deformation since a small error was discovered in the base-model. The equivalent length was set as 1 m instead of 20 m which is the width of the modelled half of the whole section and therefore not able to deform properly (i.e. stiffer behaviour).

The use of different material models in the clay showed no distinction in the model for the interface simulations since these were modelled using Mohr-coulomb and did not needed to be calculated separately.

Due to limitations in PLAXIS a few alternations had to be made for some of the calculations to be successful. Initially the base-models had to add a small sheet pile wall, instead of a slope, to handle an unrealistic soil collapse in the fill layer. The stiffness parameters E_{50}^{ref}, E_{eod}^{ref} and E_{ur}^{ref} in the HSs-model also encountered some limitations in the parameter study since the PLAXIS-program did not allow them to differ within certain span (related to K_0 and each other) and were adjusted according the recommendations from the PLAXIS-program.

Sensitivity analysis

As expected the biggest differences were found between the material models since they are fundamental different in several ways. Nevertheless, based on the excavation size the deformations were very small. The alternations of the material model parameters showed small changes in magnitude but interesting changes in trend.

The HSs-model showed smaller influence than the ADP-model in almost all cases, except for the earth pressure on the passive side at the cross-wall. This is probably due to the fact that the axial force from the truss is higher in ADP and therefore have an easing effect on the earth pressure.

A combination of the lateral deformation, settlement and heave illustrated in Figure 5.1 clearly indicates a higher rotational deformation from active to passive side in ADP compared to HSs. This is most likely due to the consideration of the small-strain shear modulus and higher stiffness in the passive zone in the HSs model.

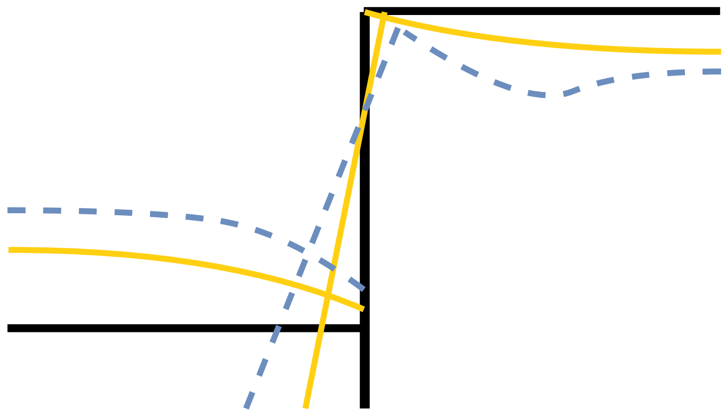

Figure 5.1: The trend of the displacements in HSs (yellow) and ADP (blue)

Generally R_{inter} is very hard to estimate in reality and should be a critical parameter to study. For the interfaces, altering the stiffness parameter E' showed greater influence than R_{inter}, mostly in the bending moment and the lateral deformation for the lower part of the diaphragm wall. Changing R_{inter} affects E' as well but could not be altered as much in the parameter study since the changes were based on a specific ratio.

The result from the HSs parameters of E_{50}^{ref}, E_{eod}^{ref} and E_{ur}^{ref} were difficult to evaluate separably in the parameter study. After the adjustment to fit PLAXIS they did not show any significant difference, even though the reference value were increased by 600 %. The change noticed however were a small reducing effect on the heave and settlement.

Regarding the parameters of ADP the ratio of un-/reloading shear modules over undrained active shear strength G_{ur}/s_u^A and the shear strain at failure in direct simple shear γ_f^{DSS} showed some interesting observations. Reducing G_{ur}/s_u^A tended to increase the lateral displacements behind the DW as well as for the settlement and heave. This is similar with the overall displacements previously mentioned and illustrated in figure 5.1, but instead the lateral movement takes place in the upper part of the diaphragm wall. Reducing γ_f^{DSS} also showed more displacements, mainly in heave but no laterally, which is interesting considering it was reduced by 10% and increased with 20%.

6
Conclusion

The use of numerical models for deep excavation in soft soils proves to be very beneficial and useful in order to comprehend the complex challenges in modelling the reality. However, numerical models required proper calibration and understanding of the used soil models and boundary conditions.

The combination of diaphragm and cross-walls are internationally used with a lot of positive experiences, especially in reducing the heave and ground settlement for deep excavations. In the case of Lilla Bommen, the same results were observed in the models herein and the real construction. The complexities of this solution can be simplified and modelled in a 2D and catch the effect of both the counteracting force by lateral cross-wall and friction between them and the heaving soil. However, further investigations needed to look at the interface between the cross-walls and diaphragm walls.

The ADP-model showed larger displacements than in the HSs- model. However, both showed very small movements in relation to the excavation width and depth. ADP is easy to implement for analyzing undrained shear strength in clay while HSs can be more accurate in excavations since it consider the small strain behavior but requires more thorough calibration. It was hard to perform a sensitivity analysis on the stiffness parameters of the HSs-model since there is a limit in PLAXIS to vary them separately. Nevertheless, the current study of these parameters did not show any significant changes in the results.

For the HSs-model, the parameters that had the most impact in the sensitivity analysis were E_{50} and E_{ur}, specially for the settlement behind the diaphragm wall. It is important to highlight that the HSs-model overestimate the passive stiffness and strength of the clay with the current parameters compared to the ADP-model.

For the ADP model the ratio of un-/reloading shear modules over active shear strength G_{ur}/s_u^A and the direct shear strain γ_f^{DSS} showed most notable effect of the evaluated parameters, specially for the heave at the excavation bottom.

In addition to the soil model parameters, the interface parameters between the diaphragm wall and cross-wall showed significant effect in the results. The most important parameter in this case was E'.

Limitations and recommended further investigations

In relation to the limited time of a master thesis it was considered to be enough to compare the material models and do a parameter study. The focus was to investigate the material models behaviour in a deep excavation in soft clay case rather than a specific location in Lilla Bommen. Furthermore the model was based on the blueprints and soil conditions of a existing object which were successfully constructed and therefore considered to be realistic.

The following list presents some interesting aspects and parameters recommended for further studies:

- Interface between diaphragm and cross-wall. Using other material models more refined than the Mohr-Coulomb model.
- Times effects (e.g. creep). This thesis was only based on the construction phase (short-term) with the diaphragm walls as temporary elements.
- A parameter study of the small strain part of the HSs-model, G_0 and $\gamma_{0.7}$ and the G_{ur} in the ADP-model.
- Compare the conversion of the 3D-problem to a 2D-model with a model using PLAXIS 3D.

Bibliography

Alén, C., Lindvall, A., Johansson, M., Magnusson, J. and Norén, C. (2006), Slitsmurar som permanenta konstruktioner, Technical report, Svenska Byggbranschens utvecklingsfond (SBUF), Stockholm.

Axelsson, G. (2016), 'Design of piles - swedish practice', *ISSMGE - ETC 3International Symposium on Design of Piles in Europe, Leuven, Belgium, 28-29 April* pp. 1–17. International Society for Soil Mechanics and Geotechnical Engineering.

Brinkgreve, R. (2017*a*), *PLAXIS 2D Reference Manual 2016*, PLAXIS Company, Plaxis bv P.O. Box 572, 2600 AN DELFT, Netherlands.

Brinkgreve, R. (2017*b*), *PLAXIS Material Models Manual 2016*, PLAXIS Company, Plaxis bv P.O. Box 572, 2600 AN DELFT, Netherlands.

Ergun, M. U. (2008), 'Deep excavations', *Electronic Journal of Geotechnical Engineering* pp. 1–34. Middle East Technical University.

Eriksson, P., Jendeby, L., Olsson, T. and Svensson, T. (2004), 'Kohesionspålar', *Pålkommissionen Rapport 100* . Linköping, Sweden.

Grimstad, G., Andresen, L. and Jostad, H. P. (2012), 'Ngi-adp: Anisotropic shear strength model for clay', *International journal for numerical and analytical methods in geomechanics* **36**(4), 483–497.

Hsieh, H.-S., Lu, Y.-C. and Lin, T.-M. (2008), 'Effects of joint details on the behavior of cross walls', *Journal of GeoEngineering* **3**(2), 55–60.

Karlsrud, K. (1983), 'Performance and design of slurry walls in soft clay', *Norwegian Geotechnical Institute Publication* . 149.

Karlsrud, K. and Andresen, L. (2008), 'Design and performance of deep excavations in soft clays', *6th International Conference on Case Histories in Geotechnical Engineering, Arlington, VA, August 11-16 2008* pp. 1–26. Missouri University of Science and Technology.

Karlsrud, K., Engelstad, Ø., Wunsch, R. and Svärd, D. (2006), 'Diaphragm walls with cross-walls used to prevent bottom heave in soft clay for lot 2 of lilla bommen tunnel in gothenburg', *Geotechnical Aspects of Underground in Soft Ground - Bakker et al (eds)* . Taylor and Francis Group.

Karstunen, M. (2016), 'Numerical modelling: Parameters for hsmodel and hssmall model', Lecture slides. Course BMT041 Infrastructural Geo-Engineering 2016, Chalmers Technical University, Göteborg.

Keller (2017), 'Diaphragm walls and barrettes', digital image.
URL: *http://kellergrundlaggning.se/documents/Files/26-01E.pdf*

Knappett, J. and Craig, R. (2012), *Craigs soil mechanics, 8th ed*, Spon Press Taylor and Francis, Abingdon, Oxon.

Kullingsjö, A. (2007), *Effects of deep excavations in soft clay on the immediate surroundings-Analysis of the possibility to predict deformations and reactions against the retaining system*, Doktorsavhandlingar vid Chalmers tekniska högskola. Ny serie, no: 2683, Institutionen för bygg- och miljöteknik, Geologi och geoteknik, Chalmers tekniska högskola,, Göteborg.

Lager, T. and Persson, T. (2005), Omgivningspåverkan vid installation av slitsmurar - jämförelse mellan beräknade och uppmätta markrörelser, Master's thesis, Institutionen för bygg- och miljöteknik, Geologi och geoteknik, Chalmers tekniska högskola, Göteborg.

Li, M.-G., Chen, J.-J., Xu, A.-J., Xia, X.-H. and Wang, J.-H. (2014), 'Case study of innovative top-down construction method with channel-type excavation', *Journal of Construction Engineering and Management* **140**(5), 05014003. American Society of Civil Engineers.

Long, M. (2001), 'Database for retaining wall and ground movements due to deep excavations', *Journal of Geotechnical and Geoenvironmental Engineering* **127**(3), 203–224. American Society of Civil Engineers.

MetroArkitekter (2018), 'Flygfoto över området kring station centralen. bilden visar stationens läge och placering av plattformar och entréer.', digital image.
URL: *https://bit.ly/2VljuDZ*

OpenStreetMaps (2015), 'Maps of central gothenburg in sweden, including layer of västlänken train tunnel', digital image.
URL: *https://bit.ly/2XgCYXP*

Ou, C.-Y., Hsieh, P.-G. and Lin, Y.-L. (2010), 'Performance of excavations with cross walls', *Journal of Geotechnical and Geoenvironmental Engineering* **137**(1), 94–104.

Puller, M. (2003), *Deep excavations: a practical manual*, 2 edn, Thomas Telford publishing, London.

RailSystem (2015), 'Cut and cover', digital image.
URL: *http://www.railsystem.net/cut-and-cover/*

Rude, A. (1972), 'Anleggsarbeid, eidsvolls plass', digital image.
URL: *https://bit.ly/2V2HQCj*

Rude, A. (1975), 'Fellestunnelen bygges under studenterlunden', digital image.
URL: *https://bit.ly/2VMdvFk*

Sällfors, G. (2013), *Geoteknik, Jordmateriallära och Jordmekanik*, Cremona, Göteborg.

Trafikverket (2013), Pm f 05-009, geotekniska materialparametrar station centralen, Technical Report TRV 2013/92336, Trafikverket, Kruthusgatan 17 40533, Göteborg.

Trafikverket (2016), Ansökan om tillstånd enligt miljöbalken för anläggandet av västlänken och olskroken planskildhet, teknisk beskrivning, Technical Report TRV 2016/3151, Trafikverket, Kruthusgatan 17 40533, Göteborg.

Wood, D. M. (2004), *Geotechnical modelling*, Spon Press, London.

Wood, T. (2014), Regioncity, phase 3 - site characterization and sensitivity analysis, Technical Report 5023021, Chalmers Technical University, Göteborg.

Wood, T. (2017), Design base geoteknik, Technical Report TRV 2015/74805, Trafikverket Västlänken E02 Centralen, Göteborg.

Wood, T. and Karstunen, M. (2017), 'Modelling the creep of deep foundations in soft gothenburg clays', *European Journal of Environmental and Civil Engineering* pp. 1–19.

Wu, S.-H., Ching, J. and Ou, C.-Y. (2014), 'Probabilistic observational method for estimating wall displacements in excavations', *Canadian Geotechnical Journal* **51**(10), 1111–1122.

Appendices

A

Drawings of Lilla Bommen tunnel

Väg 45, Götatunneln Lilla Bommen, L2

Sammanställning I

Sammanställning II

Sammanställning III

Sammanställning IV

Slitsmur, N och S väggen, mått

ALLMÄNNA ANVISNINGAR

VÄG 45, GÖTATUNNELN, SKEDE 1,
SEKTION 2/615 – 2/881,5 I PROFIL 1.

BESTÄMMELSER
ARBETET UTFÖRS ENLIGT FÖLJANDE BESTÄMMELSER:

TUNNEL 99	PUBL 1999:138, VÄGVERKET 1999
BRO 94, DEL 1-9	PUBL 1994:2-4, 6-8, 1999:18-20 VÄGVERKET 1994, 1999
SUPPLEMENT 4	PUBL 1999:21 VÄGVERKET 1999
VÄG 94	PUBL 1994:21, VÄGVERKET 1994
BKR 99	KONSTRUKTIONSREGLER BOVERKET 1999
BBK 94	BETONGKONSTRUKTIONER BAND 1 OCH 2 BOVERKET 1994 (BFS 1993:58 MED ÄNDRINGAR T.O.M. BFS 1998:38)
SUPPLEMENT 1	BBK 94 BOVERKET 1996
BSK 99	STÅLKONSTRUKTIONER BOVERKET 1999
TBt301 L2	TEKNISK BESKRIVNING TUNNELARBETEN, PM 04 UTGÅVA 6 DATERAD 2000-10-25
TBt/geo301 L2	TEKNISK BESKRIVNING TUNNEL/GEOTEKNIK, PM 03 UTGÅVA 3 DATERAD 2000-09-29
TBt/berg308 L2	TEKNISK BESKRIVNING TUNNEL/BERG PM 03 UTGÅVA 3 DATERAD 2000-09-29

BELASTNINGAR
ENLIGT TUNNEL 99 PUBL 1999:138 OCH TBt301 L2 SAMT TBt/geo301 L2.
TUNNELN ÄR ÄVEN DIMENSIONERAD FÖR EN FRAMTIDA BELASTNING AV CENTRUMTUNNELN ENLIGT PM 04, DATERAT 2000-10-25.

LIVSLÄNGDSKLASS, MILJÖKLASS OCH TÄCKANDE BETONGSKIKT (TB).

KONSTRUKTIONSDEL	LK	MK	TB
TUNNEL:	L2		
BOTTENPLATTA			
UK (MOT GROVBETONG)		B4/A3	50
PÅLAD UK (MOT GROVBETONG)		B4/A3	150
ÖK (ISOLERAD)		B4/A3	35
YTTERVÄGGAR			
UTSIDA		B4/A3	35
INSIDA (VÄGMILJÖ)		B4/A4	55
INNERVÄGGAR			
BAKSIDA		B4/A3	35
INSIDA (VÄGMILJÖ)		B4/A4	55
TAK			
ÖK		B4/A3	35
UK		B4/A4	55
TVÄRTUNNELVÄGGAR OCH ÄNDVÄGG VID SEKTION 2/653		B4/A3	35
BERGPÅSLAG 2/650-2/653	L2		
BOTTENPLATTA			
UK (MOT GROVBETONG)		B4/A3	50
ÖK (ISOLERAD)		B4/A3	35
VÄGGAR OCH TAK		B4/A4	55
BERGPÅSLAG 2/645-2/650	L2		
BOTTENPLATTA			
UK		B4/A4	55
ÖK (ISOLERAD)		B4/A3	35
VÄGGAR OCH TAK		B4/A4	55
DU 5	L2	B4/A3	35

SÄKERHETSKLASS
SK2 FÖR DU 5. I ÖVRIGT SK3.

GRUNDFÖRHÅLLANDEN
SE AV VÄGVERKET UPRÄTTAD TEKNISK BESKRIVNING TUNNEL/GEOTEKNIK (TBt/geo301 L2) DATERAD 2000-09-29.

ARBETENA SKER I ÖPPEN SCHAKT MELLAN SLITSMURAR, SE RITNINGAR UPPRÄTTADE AV LBT DESIGN TEAM OCH NORDCONSULT.

GRUNDLÄGGNING
GRUNDLÄGGNING SKER FÖR DELEN 2/653-2/748,2 I PROFIL 01 PÅ PACKAD SPRÄNGSTEN PÅ PACKAD SPRÄNGBOTTEN SAMT PÅ GRÄVPÅLAR MED STÅLKÄRNEPÅLAR I SPETSEN.
DELAR AV TUNNELN ÄR FÖRANKRAD MED STÅLKÄRNEPÅLAR.
ANVISNINGAR FÖR STÅLKÄRNEPÅLAR SE RITNING 3 00 G 21 15.
DELEN 2/748,2-2/882,5 I PROFIL 01 ÄR DELS GRUNDLAGD PÅ 400 mm SPRÄNGSTEN PÅ LERA DELS PÅ KOHESIONSPÅLAR (KOMPENSATIONSGRUNDLÄGGNING) – SE RITNING 3 43 G 21 01 OCH FÖLJANDE.

SENAST 5 DAGAR FÖRE PLANERAD GJUTNING AV BOTTENPLATTA SKA BESTÄLLAREN UNDERRÄTTAS SÅ ATT BESIKTNING KAN UTFÖRAS.

DU 5 BYGGS DIREKT PÅ TUNNELTAKET OCH FÖRANKRAS I DETTA MOT UPPLYFT ENLIGT RITNING 3 42 K 23 03.

BETONG
MILJÖKLASS: B4

======= BETECKNAR DILATATIONSFOG.
-//-//-//- BETECKNAR GJUTFOG, ENDAST MARKERADE GJUTFOGAR FÅR UTFÖRAS.
-//-//-//- BETECKNAR SKYMD DITO.

BETONG K45 ANVÄNDS ENLIGT BRO 94 43.3 MED UTFÖRANDE ENLIGT 44.4. BTG I, T, VATTENTÄT, VIBRERAS, VCT≤ 0.40. ANLÄGGNINGSCEMENT TYP STD P DEGERHAMN ELLER LIKVÄRDIGT SKALL ANVÄNDAS, SE BRO 94, 43.22 .
BETONGEN SKALL PROPORTIONERAS FÖR MAXIMAL STENSTORLEK 16 mm.
BETONGEN SKALL VARA FROSTBESTÄNDIG ENL. BRO 94, 43.32 SAMT UPPNÅ "GOD FROSTBESTÄNDIGHET" VID PROVNING ENL. SS 137244 FÖRFARANDE I RESP IV, METOD A. LUFTHALT ENLIGT BBK 94, 7.3.2.
BLANDNINGSTID FÖR BETONGEN MIN. 3 MINUTER.
KONTROLL AV BETONGEN SKALL UTFÖRAS ENL. BRO 94, 45.
GJUTBLÅSOR STÖRRE ÄN 8 mm (STÖRSTA MÅTTET VID UPPRENSAT HÅL) SKALL ÅTGÄRDAS PÅ AV BESTÄLLAREN GODTAGBART SÄTT.
(BETONGEN EFTERBEHANDLAS ENL. BRO 94, 44.43.) DOCK SKALL VATTENHÄRDNING PÅGÅ KONTINUERLIGT I MINST 5 DYGN.

DÄR SJÄLVKOMPAKTERANDE BETONG ANVÄNDS SKA DEN UTFÖRAS I K60 MED VCT≤ 0.4. PROVGJUTNING SKA UTFÖRAS ENLIGT TBt301 L2, 4.33.

GJUTFOGAR
GJUTFOGAR UTFÖRS ENLIGT TUNNEL 99, 3.5.6.7 OCH TBt301 L2.
SE RITNING 3 42 K 23 03 – 07. GJUTFOGAR SOM ÄR ÅTKOMLIGA FÖRE ÅTERFYLLNING FÖRSEGLAS ENLIGT BRO 94 62.389.
BETRÄFFANDE BESIKTNING AV GJUTFOGAR SE TBb 301 l2, 6.42.

DILATATIONSFOGAR
DILATATIONSFOGAR UTFÖRS VINKELRÄTT VÄGENS LUTNING MHT ATT KLINKERPLATTORNA PLACERAS I VÄGENS LUTNING. SE RITN. 3 42 K 23 19
FOGBAND SKA UPPFYLLA KRAVEN ENLIGT BRO 94, 43.71.

ARMERING
MILJÖKLASS: A3, A4.
ANVÄND ARMERINGSKVALITET B500B ENLIGT AV VÄGVERKET GODTAGET FABRIKAT.

TÄCKANDE BETONGSKIKT (TB) ENLIGT TABELL. GÄLLER ÄVEN TILL EVENTUELLA MONTERINGSJÄRN MED Ømax=16mm UK PLATTA, I ÖVRIGT Ø=12 mm.

LITTERERING ENL. SVENSK ARMERINGSANVISNING 1A 1979 (BASTA).
BOCKNINGSTYPER ENL. TYPBLAD 2A 1979. RAK STÅNG BETECKNAS DOCK MED A. LAGERLÄNGDER BETECKNAS MED LL.
HÖGST VARANNAN STÅNG SKARVAS I SAMMA SNITT. MINSTA STÅNGLÄNGD 4 m.
SKARVLÄNGDER DÄR EJ ANNAT ANGES: 50Ø FÖR B500B.
MEKANISKA SKARVAR FÅR ANVÄNDAS UTOM I RAMHÖRN. SKARVARNA SKALL UPPFYLLA KRAVEN I BRO 94,43.61 OCH VARA CERTIFIERADE ENLIGT 10. 81.

BOCKNINGSRADIER DÄR EJ ANNAT ANGES (mm):

KVALITET	B500B		BYGLAR B500B
BOCKNINGSVINKEL	≤90°	>90°	
DIMENSION			
10 mm	64	64	24
12 mm	64	100	32
16 mm	100	125	64
20 mm	125	160	64
32 mm	200	250	–
25 mm	160	200	–

SVETSNING AV ARMERING
SVETSKLASS WC
SVETSELEKTRODER ENLIGT BRO 94, 55.22.
SVETSNING FÅR ENDAST UTFÖRAS AV SVETSARE SOM AVLAGT GODKÄNDA PROV ENLIGT SS06520 ALTERNATIVT EN287-1:1992.
SVETSNING UTFÖRS ENLIGT BRO 94, 55.2 OCH BSK 99, 8:43.

FORMSÄTTNING
SYNLIGA BETONGYTOR FORMSÄTTS MED SLÄT FORM OCH SÅ ATT KRAVEN I SIS 81 20 02, TABELL 1-3, KLASS 2A UPPFYLLS.
FORMSLÄPPMEDEL SKA VARA MILJÖVÄNLIGT OCH AV VEGETABILISK ART.
DEN FÄRDIGA BETONGYTAN SKA VISA JÄMNHET I FÄRG OCH STRUKTUR OAVSETT NÄR OCH HUR GJUTNINGEN HAR SKETT.
VID SKARVNING MELLAN FORMSKIVOR BORTSLIPAS GJUTSKÄGG OCH OJÄMNHETER EFTER FORMRIVNING. OTÄTA FORMSKARVAR FÅR INTE FÖREKOMMA. ANTALET SKARVAR SKALL MINIMERAS.
ICKE SYNLIGA BETONGYTOR FORMSÄTTS MED VALFRITT MATERIAL. VAL AV FORM SKA INTE GE OTÄTA SKARVAR.
TILL ICKE SYNLIGA YTOR RÄKNAS YTOR SOM BEKLÄDS MED KLINKERS ELLER SOM DÖLJS PÅ ANNAT SÄTT T EX GENOM BRANDSKYDD.
DISTANSKLOSSAR SKA TILLVERKAS ENLIGT BRO 94, 43.74 OCH VARA TILLVERKADE AV SAMMA CEMENTTYP SOM OMGIVANDE BETONG.

BEKLÄDNAD AV TUNNELVÄGGAR
TUNNELVÄGGAR BEKLÄDS MED KLINKERPLATTOR FRÅN ÖVERKANT SOCKELELEMENT ENLIGT RITNINGARNA 3 42 K 23 04 OCH 3 42 K 23 05.
KLINKERPLATTORNA MONTERAS I VÄGENS LUTNING.
MÖNSTERSÄTTNING VID TVÄRTUNNEL SE RITNING 342 K 23 16.
GENOMFÖRINGAR FÅR EJ GÖRAS I KLINKERPLATTORNA.

ISOLERING OCH BELÄGGNING
ISOLERING : 35 mm PGJA
5 mm ISOLERINGSMATTA.
FÖRE UTLÄGGNING AV ISOLERINGSMATTA YTBEHANDLAS BOTTENPLATTA MED EPOXI, MED AVSTEG FRÅN BRO 94,62.24. KRAV ENLIGT TBt301 L2, 6.23.
BELÄGGNING UTFÖRS ENLIGT TBv301 L2 OCH TBv/bel.- GÖTATUNNELN.

TUNNELTAK, UTOM UNDER DU 5, SAMT TAK PÅ DU 5 ISOLERAS MED 5mm HELKLISTRAD ISOLERINGSMATTA ENLIGT BRO 94, 62.241 SAMT 35 mm SKYDDSLAGER AV POLYMERMODIFIERAD GJUTASFALT ENLIGT BRO 94, 63.312 NEDDRAGES 300mm ENLIGT BRO 94, 62.436. KANTFÖRSEGLING MED EPOXI SE RITNING 3 42 K 23 06.
TEMPORÄR BELÄGGNING UNDER BYGGNADSTID ENLIGT TBb 301 L2, 6.33.

BRANDISOLERING
BRANDISOLERING UTFÖRS MED 30mm TJOCK SKIVA DICON TU, TILLVERKAD AV AESTUVER. ARBETSBESKRIVNING FÖR MONTERING REDOVISAS PÅ RITNING 3 42 K 23 06, FASTSÄTTNING ENLIGT LEVERANTÖRENS ANVISNINGAR (I MONOLITH OCH TAKPLATTA UTFÖRANDE EFTER GJUTNING)
DILATATIONSFOGAR BRANDSKYDDAS ENLIGT DETALJ PÅ RITNING 3 42 K 23 19.

YTBEHANDLING
ALLA SYNLIGA (EJ BEKLÄDDA) YTOR I TUNNELN YTBEHANDLAS ENLIGT BRO 94, 44.541.
ENLIGT BRO 94,43.722 SKA YTBEHANDLINGSPREPARAT VARA SILAN UTAN LÖSNINGSMEDEL, SOM UPPFYLLER KRAVEN I BRO 94,43.722 OCH ÄR VERIFIERAT ENLIGT BRO 94, 45.42. INTRÄNGNINGSDJUPET SKA VARA MINST 5 mm (DJUPIMPREGNERING SE TBt301 L2 BILAGA1), VILKET PÅVISAS GENOM PROVTAGNING ENLIGT TBt301 L2, 4.523.

ELEKTROKEMISK POTENTIALMÄTNING
ANSLUTNING FÖR ELEKTROKEMISK POTENTIALMÄTNING UTFÖRS PÅ UNDERSIDA VOT VID YTTER- OCH INNERVÄGG I VARDERA TUNNELRÖRET.
ANSLUTNINGARNA UTFÖRS ENLIGT BRO 94, SUPPLEMENT 4, 41.129 OCH BILAGA 9-26.

STÅLKONSTRUKTIONER
STÅLKVALITET I STÅLKÄRNEPÅLAR SE RITNING 3 00 G 21 15.
INFÄSTNINGSDETALJER UTFÖRS I KVALITET EN 1.4436.
ROSTFRITT OCH SYRAFAST MATERIAL FÅR EJ HA METALLISK KONTAKT MED ARMERINGEN.

ÅTER- OCH MOTFYLLNING
UTRYMME MELLAN TUNNELVÄGGAR OCH SLITSMURAR FYLLS MED BETONG ENLIGT ARBETSBESKRIVNING 3 G 34 00 17.
ÅTERFYLLNING I ÖVRIGT UTFÖRS ENLIGT TBb/geo301 L2, PUNKT 7.3.
VID FYLLNING TILLSES ATT BETONGYTORNA EJ SKADAS.
VID ÖVERFYLLNAD PÅ TUNNELTAK MED SPRÄNGSTEN LÄGGS ETT 0.2 m TJOCKT SKYDDANDE LAGER AV SAMKROSS 0-18 mm NÄRMAST SKYDDSLAGRET. PACKNING UTFÖRS ENLIGT VÄG 94, 4.10.
UTRYMMET MELLAN YTTERVÄGGARNA VID BERGPÅSLAG FYLLS MED PACKAD SPRÄNGSTEN.

TRYCKUTJÄMNING
FÖR TRYCKUTJÄMNING VID AVSCHAKTNING INSTALLERAS I MONOLIT 1-16 RÖR Ø50 I VÄGGARNA, SE RITNING 3 42 K 23 07.

DRÄNERING
BOTTENPLATTA I MONOLIT 16-19 FÖRSES MED DRÄNERINGSKANALER 20×80 mm I GJUTASFALT

LAGER
DILATATIONSFOGARNA I SEKTION 2/748,2 OCH 2/776,0 FÖRSES MED ALLSIDIGT RÖRLIGA NEOTOPFLAGER SE RITNING 3 43 K 23 91-94, TYP MAGEBA.
TJOCKLEK PÅ ÖVRE LAGERPLATTA VARIERAR,
VID LAGERBYTE SE PÄRM 22 I SLUTDOKUMENTATION.

MÄTDUBBAR
UTRUSTNING FÖR AVVÄGNING (REGISTRERING AV HORISONTAL -OCH VERTIKALRÖRELSER): PRISMA MED MÄTARM LEICA GPH1 GÄNGA M10.
DON INSTALLERAS PÅ BÅDA SIDOR SE RITNING 3 00 K 20 04.
PRECISIONSMÄTNING UTFÖRS 1 GÅNG/MÅNAD.
MÄT- OCH KONTROLLPROGRAM UPPRÄTTAS AV ENTREPRENÖREN.

HÄNVISNINGAR
INGJUTNINGSDETALJER:
RÖR FÖR VATTEN OCH AVLOPP SAMT EL OCH SIGNAL FRAMGÖR AV MÅTTRITNINGARNA.
INFÄSTNINGSDETALJER, SE RITNING 3 42 K 21 07.

ÖVERGÅNGSKONSTRUKTIONER
DILATATIONSFOGAR UTFÖRS MED ÖVERGÅNGSKONSTRUKTIONER VID TRAFIKERADE YTOR, SE RITNING 3 42 K 23 20.

UTSÄTTNINGSDATA

KOORDINATSYSTEM:	GÖTEBORGS LOKALA KOORDINATSYSTEM
HÖJDSYSTEM:	GÖTEBORGS LOKALA HÖJDSYSTEM GH 88 = RH70 + 10,07 m
FIX NR:	90550 +16.199

DOKUMENTFÖRTECKNING
SE RITNING 3 00 K 20 14.

SITUATIONSPLAN 1:5000

O 1561:01 jc / O 1561:02 jå Rev D
GODTAGEN AV VÄGVERKET, SEKTION BRO- OCH TUNNELTEKNIK, ENLIGT BREV DATERAT 2004-03-03 MED DIARIENUMMER O 1561 2004:175

O 1561:01 jc / O 1561:02 jå Rev C
GODTAGEN AV VÄGVERKET, SEKTION BRO- OCH TUNNELTEKNIK, ENLIGT BREV DATERAT 2003-12-19 MED DIARIENUMMER O 1561 2003:1453

O 1561:01 jc / O 1561:02 jå
GODTAGEN AV VÄGVERKET, SEKTION BRO- OCH TUNNELTEKNIK, ENLIGT BREV DATERAT 2003-03-17 MED DIARIENUMMER O 1561 2003:228

REV	ANT	ÄNDRINGEN AVSER	GODKÄND	DATUM
E	6	ALLMÄN REVIDERING	LC	04-09-10
D	1	BETONGKVALITET	LC	04-02-20
C	5	DOKUMENTFÖRTECKNING FLYTTAD TILL RITN. 3 00 K 20 07 + TEXT	LC	03-12-12
B	4	AVVÄGNINGSDON+DOKUMENTFÖRTECKNING	LC	03-08-08
A	1	TEXT	LC	03-06-13

HANDLINGEN ÄR UPPRÄTTAD ENLIGT KVALITETSSYSTEM FÖR REINERTSEN AB, UTGÅVA 5 DATERAT 2002-03-01.

1:100 0 1 2 3 4 5 6 7 8 9 10 m

RELATIONSHANDLING | FÖRVALTNINGSHANDLING

Vägverket Region Väst
GÖTATUNNELN Ett projekt i Göteborgsöverenskommelsen
BILFINGER+BERGER BAUAKTIENGESELLSCHAFT
AF Spesialprosjekt AS
REINERTSEN

VÄG 45, GÖTATUNNELN
LILLA BOMMEN, L2
300 GEMENSAMT
SKEDE 1
SEKTION 2/615,0 – 2/881,5 I PROFIL 01
ALLMÄNNA ANVISNINGAR

SAMMANSTÄLLNING I

UPPDRAG NR	RITARE	KONSTR	GRANSK	KONSTBYGGNADSNR	FORMAT	SKALA
2001-0290	EE/ DW	LENNART CLAESON	LENNART CLAESON	O 1561	A1	1:100

GODKÄND AV LBT KB ENLIGT BREV DATERAT: 2002-03-20

GÖTEBORG 02-07-26
LENNART CLAESON

OBJEKT NR	RITNINGSNR	REV
429011	3 00 K 20 02	E

XREF:Q:\01\20010290_GT\RELATIONSHANDLINGAR_A2\3\K\MODELL\K3002052 06-02-02 15:56
PLOTTAD:06 02 02 15:57 Fil: Q:\01\20010290_GT\Relationshandligar_A2\3\K\Ritdef\300K2002.dwg

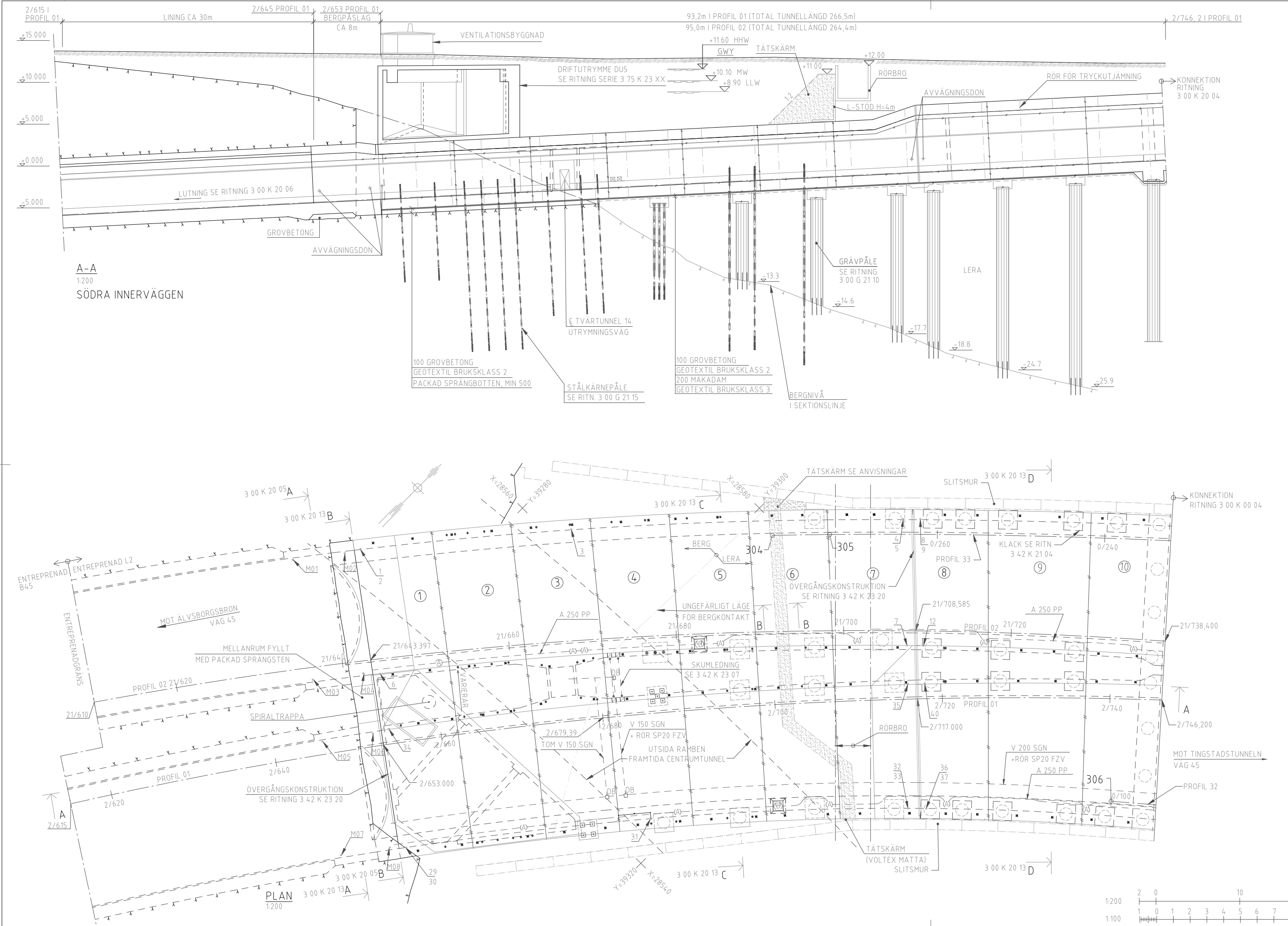

ANVISNINGAR

KONSTRUKTIONSTYP: 910 TUNNEL
MATERIAL: 120 ARMERAD BETONG
ALLMÄNNA ANVISNINGAR SAMT FÖRTECKNING ÖVER RITNINGAR, ARBETSBESKRIVNINGAR OCH KONTROLLPLANER SE RITNING 3 00 K 20 02 RESP 3 00 K 20 14.

UTSÄTTNINGSDATA

KOORDINATSYSTEM: GÖTEBORGS LOKALA KOORDINATSYSTEM
HÖJDSYSTEM: GÖTEBORGS LOKALA HÖJDSYSTEM GH 88=RH 70 +10.07m.
FIX NR: 90550 +16.199

BELASTNINGAR

TUNNELN ÄR BERÄKNAD FÖR LASTER ENLIGT TUNNEL 99, PUBL. 1999:138, SAMT TEKNISK BESKRIVNING TUNNEL (TBt 301 L2) DATERAD 2000-10-25 OCH PM 4 "LASTFÖRUTSÄTTNINGAR MED HÄNSYN TILL CENTRUMTUNNELN" DATERAD 2000-10-25.
TUNNELN ÄR RÄKNAD FÖR EN AVSCHAKTNING PÅ EN GODTYCKLIGT PLACERAD 15m LÅNG STRÄCKA. TUNNELN ÄR DIMENSIONERAD FÖR EN FRAMTIDA EXTRA UPPFYLLNAD PÅ 0.5m.

TRAFIKBELASTNING EG A/B 250/310 KN PÅ TUNNELTAKET
TRAFIKLAST I TUNNELN ÄR EG A/B 270/310
MILITÄRA FORDON FÅR FRAMFÖRAS

OM CENTRUMTUNNELN BYGGS SKALL INSIDA VÄGGAR UNDER DENSAMMA FÖRSES MED BRANDSKYDDSISOLERING. DENNA SKALL KUNNNA KLARA KURVA III (RWS) ENLIGT TUNNEL 99, 3.3.4.4 MED 120 min ANGREPPSTID SAMT AVSVALNING ENLIGT TUNNEL 99, 4.2.1.

BESTÄMMELSER

ARBETET UTFÖRS ENLIGT FÖLJANDE BESTÄMMELSER:

TUNNEL 99	PUBL 1999:138, VÄGVERKET 1999
BRO 94, DEL 1-9	PUBL 1994:2-4, 6-8, 1999:18-20 VÄGVERKET 1994, 1999
SUPPLEMENT 4	PUBL 1999:21, VÄGVERKET 1999
VÄG 94	PUBL 1994:21, VÄGVERKET 1994
BKR 99	KONSTRUKTIONSREGLER, BOVERKET 1999
BBK 94	BETONGKONSTRUKTIONER BAND 1 OCH 2 BOVERKET 1994 (BFS 1993:58 MED ÄNDRINGAR T.O.M. BFS 1998:38)
SUPPLEMENT 1	BBK 94, BOVERKET 1996
BSK 99	STÅLKONSTRUKTIONER, BOVERKET 1999
TBt301 L2	TEKNISK BESKRIVNING TUNNELARBETEN, PM 04 UTGÅVA 6 DATERAD 2000-10-25
TBt/geo301 L2	TEKNISK BESKRIVNING TUNNEL/GEOTEKNIK, PM 03 UTGÅVA 3 DATERAD 2000-09-29
TBt/berg308 L2	TEKNISK BESKRIVNING TUNNEL/BERG PM 03 UTGÅVA 3 DATERAD 2000-09-29

DOKUMENTFÖRTECKNING

RITNINGAR, KONTROLLPLANER OCH ARBETSBESKRIVNINGAR
SE DOKUMENT 3 00 K 20 14

MÄTDUBBAR

AVVÄGNINGSDON ENL. RITN. 3 00K 20 02 OCH DENNA RITNING.
HÖJDER AVVÄGS TILL RELATIONSRITN. SE TABELL RITN. 3 00 K 20 04.

ÅTERFYLLNING

MOTFYLLNING MOT TUNNELVÄGGAR UTFÖRS MED KROSSMATERIAL 0-4mm, DÄR FINJORDSHALTEN d<0.063mm EJ FÅR ÖVERSTIGA 10%.

FYLLNING PÅ TUNNELTAKET SKER MED PACKNINGSBARA JORDMASSOR, FRIKTIONSJORD ELLER BERGMASSOR ENLIGT VÄG 94, kap. 4.5.

TÄTSKÄRM

MELLAN km 2/700 OCH 2/705 UTFÖRS EN TÄTSKÄRM MELLAN TUNNELVÄGGAR OCH SLITSMURAR UPP TILL ÖVERKANT TUNNELTAK BESTÅENDE AV FYLLNING MED SAND ELLER KROSSMATERIAL 0-4mm MED 13% INBLANDNING AV BENTONIT TYP VOLCLAY SG 40. ÅTERFYLLNING PÅ TUNNELTAK SKER MED UPPSCHAKTAD PLASTISK LERA UPP TILL NIVÅ +11.0.

LAGER

SE RITNING 3 42 K 23 91-94

BETECKNINGAR

- RÖR FÖR TRYCKUTJÄMNING ø50
- STÅLKÄRNEPÅLE ø120
- (XX) MONOLIT (GJUTETAPP) XX
- BETONGPÅLE 275x275
- (B) (A) AVLOPPSLEDNING FÖR BRAND OCH SPOLVATTEN MED NEDSTIGNINGS-, TILLSYNS- OCH DAGVATTENBRUNN. LEDNINGSLÄGE FÅR LOKALT ANPASSAS TILL ARMERING VID GRÄVPÅLAR.
- (A) DAGVATTENBRUNN ø400 UTAN SANDFÅNG, UTAN VATTENLÅS.
- (B) NEDSTIGNINGSBRUNN ø1000 MED SANDFÅNG OCH VATTENLÅS.
- DB DRAGBRUNN
- AVVÄGNINGSDON
- PLANERAD MARKNIVÅ
- XX PLANGEOMETRI PUNKT

BELÄGGNINGAR
SE RITNING 3 00 K 20 02

RÄCKE
SE RITNING 3 00 K 20 13

DILATATIONSFOG

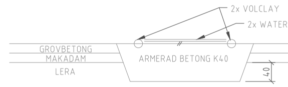

B-B
TÄTSKÄRM UNDER BOTTENPLATTA

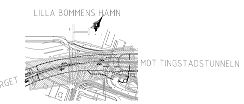

SITUATIONSPLAN 1:5000

O 1561:01 xl/O 1561:02 xx
GODTAGEN AV VÄGVERKET, SEKTION BRO-OCH TUNNELTEKNIK, ENLIGT BREV DATERAT 2004-04-13 MED DIARIENUMMER O 1561 2004:328

HANDLINGEN ÄR UPPRÄTTAD ENLIGT KVALITETSSYSTEM FÖR REINERTSEN AB, UTGÅVA 6 DATERAT 2003-03-31.

GODKÄND AV LBT KB ENLIGT BREV DATERAT: 2004-03-22

REV	ANT	ÄNDRINGEN AVSER	GODKÄND	DATUM
A	-	ALLMÄN REVIDERING	LC	04-09-10

RELATIONSHANDLING — FÖRVALTNINGSHANDLING

Vägverket Region Väst
GÖTATUNNELN — Ett projekt i Göteborgsöverenskommelsen
BILFINGER+BERGER · AF Spesialprosjekt AS · Skanska/Anjobygg · REINERTSEN

VÄG 45, GÖTATUNNELN
LILLA BOMMEN, L2
300 GEMENSAMT

SEKTION 2/615 – 2/746.2 I PROFIL 01
PLAN OCH LÄNGSSEKTION

SAMMANSTÄLLNING II

UPPDRAG NR	RITARE	KONSTR	GRANSK	KONSTBYGGNADSNR	FORMAT	SKALA
2001-0290	JENNY LEJON	LARS HANSSON	LENNART CLAESON	O 1561	A1F	1:200
		GÖTEBORG	2004-03-26	OBJEKT NR: 429011	RITNINGSNR: 3 00 K 20 03	REV: A
		LENNART CLAESON				

Plottad: 06 05 03 11:05 Fil: Q:\01\20010290_GT\Relationshandligar_A2\3\K\Ritdef\300K2003.dwg

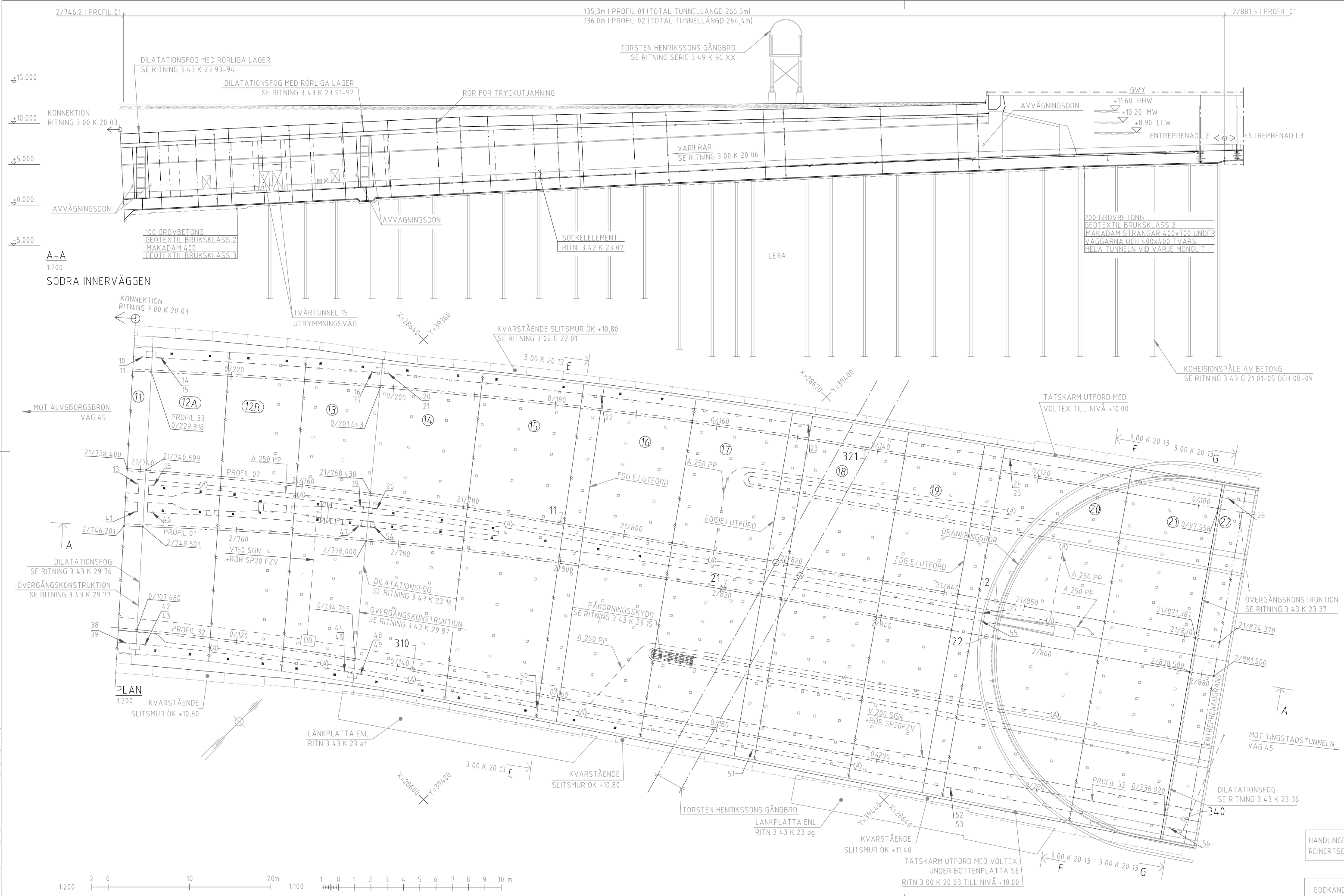

AVVÄGNINGSDON

Don	X	Y	HÖJD
1	28 542,774	39 270,061	-2,206
2	28 542,663	39 269,999	0,760
3	28 562,147	39 286,161	1,979
4	28 590,937	39 313,230	3,888
5	28 591,077	39 313,369	0,922
6	28 534,183	39 281,781	-2,566
7	28 581,042	39 323,881	0,534
8	28 592,476	39 314,785	0,997
9	28 592,374	39 314,699	3,988
10	28 613,780	39 337,209	5,531
11	28 613,875	39 337,310	2,541
12	28 582,425	39 325,297	0,640
13	28 602,715	39 347,411	2,110
14	28 615,334	39 338,925	2,680
15	28 615,253	39 338,826	5,628
16	28 632,413	39 358,488	6,923
17	28 632,508	39 358,600	3,946
18	28 604,010	39 348,936	2,236
19	28 620,190	39 368,837	3,541
20	28 633,825	39 360,175	4,050
21	28 633,730	39 360,069	7,017
22	28 650,279	39 380,533	8,312
23	28 665,751	39 401,046	9,366
24	28 680,395	39 421,528	7,067
25	28 680,327	39 421,426	9,976
26	28 621,467	39 370,498	3,595
27	28 665,015	39 432,225	7,196
28	28 696,440	39 443,535	8,507
29	28 521,706	39 298,683	-2,811
30	28 521,612	39 298,603	0,117
31	28 544,766	39 316,885	1,629
32	28 567,415	39 337,761	0,313
33	28 567,321	39 337,660	3,207
34	28 529,884	39 287,618	-2,509
35	28 577,477	39 327,594	0,601
36	28 568,962	39 339,327	0,375
37	28 568,860	39 339,216	3,334
38	28 587,973	39 360,348	1,778
39	28 587,904	39 360,257	4,728
40	28 578,935	39 328,986	0,693
41	28 599,744	39 350,062	2,189
42	28 589,513	39 362,204	1,882
43	28 589,448	39 362,134	4,832
44	28 604,527	39 381,909	3,128
45	28 604,428	39 381,769	6,074
46	28 601,110	39 351,544	2,277
47	28 617,885	39 370,707	3,539
48	28 605,688	39 383,541	3,231
49	28 605,584	39 383,413	6,174
50	28 618,068	39 401,767	7,338
51	28 633,133	39 424,101	8,896
52	28 647,059	39 444,715	7,566
53	28 646,989	39 444,610	10,400
54	28 619,222	39 372,284	3,634
55	28 663,775	39 433,090	7,203
56	28 662,025	39 467,548	9,102
M01	28 536,214	39 265,017	-2,601
M02	28 541,187	39 268,835	-2,334
M03	28 527,796	39 276,820	-2,869
M04	28 532,608	39 280,542	-2,615
M05	28 523,373	39 282,855	-2,958
M06	28 528,310	39 286,445	-2,612
M07	28 515,350	39 294,016	-3,264
M08	28 520,126	39 297,489	-2,872

MÄTNING UTFÖRD:

ANVISNINGAR

ALLMÄNNA ANVISNINGAR SE RITNING 3 00 K 20 02
ANVISNINGAR I ÖVRIGT SE RITNING 3 00 K 20 03

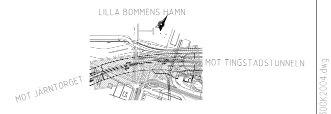

SITUATIONSPLAN 1:5000

O 1561:01 xm/O 1561:02 xy

GODTAGEN AV VÄGVERKET, SEKTION BRO-OCH TUNNELTEKNIK,
ENLIGT BREV DATERAT 2004-04-13 MED DIARIENUMMER O 1561 2004:328

HANDLINGEN ÄR UPPRÄTTAD ENLIGT KVALITETSSYSTEM FÖR REINERTSEN AB, UTGÅVA 6 DATERAT 2003-03-31.

REV	ANT	ÄNDRINGEN AVSER	GODKÄND	DATUM
A	-	ALLMÄN REVIDERING	LC	04-09-10

RELATIONSHANDLING | FÖRVALTNINGSHANDLING

Vägverket Region Väst
GÖTATUNNELN — Ett projekt i Göteborgsöverenskommelsen
BILFINGER+BERGER — AF Spesialprosjekt AS — Anjobygg — REINERTSEN

VÄG 45, GÖTATUNNELN
LILLA BOMMEN, L2

300 GEMENSAMT

SEKTION 2/746.2 – 2/881.5 I PROFIL 01
PLAN OCH LÄNGSSEKTION

SAMMANSTÄLLNING III

UPPDRAG NR	RITARE	KONSTR	GRANSK	KONSTBYGGNADSNR	FORMAT	SKALA
2001-02-90	JENNY LEJON	LARS HANSSON	LENNART CLAESON	O 1561	A1F	1:200

GÖTEBORG 2004-03-26
LENNART CLAESON

GODKÄND AV LBT KB ENLIGT BREV DATERAT: 2004-03-22

OBJEKT NR	RITNINGSNR	REV
429011	3 00 K 20 04	A

Plottad: 06 04 19 11:25 Fil: Q:\01\20010290_GT\Relationshandlingar_A2\L1\K\Ritdef\300K2004.dwg

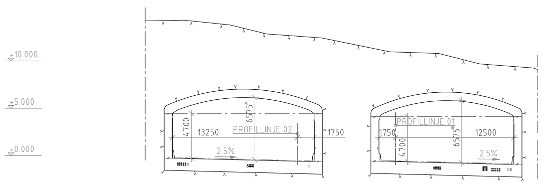

SEKTION A-A
1:200
SEKTION 2/648.8 (PROFIL 01)
*) ÖK BTG BOTTENPLATTA TILL UK BTG TAKPLATTA I ℄ TUNNEL

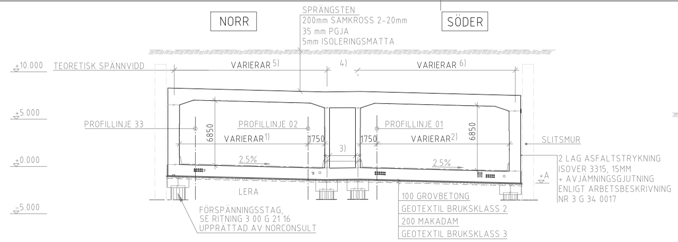

SEKTION D-D 3 00 K 20 03
1:200
SEKTION 2/733 (PROFIL 01)
KÖRFÄLTSINDELNING ENLIGT SEKTION C-C

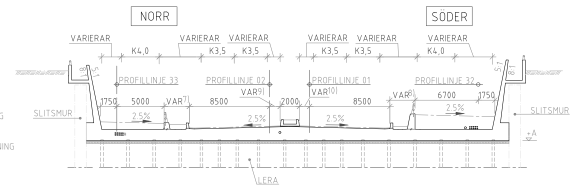

SEKTION G-G 3 00 K 20 04
1:200
SEKTION 2/879.5 (PROFIL 01)

ANVISNINGAR

ALLMÄNNA ANVISNINGAR SE RITNING 3 00 K 20 02.
ANVISNINGAR I ÖVRIGT SE RITNING 3 00 K 20 03.
TABELL FÖR HÖJD +A SE RITN 3 00 K 20 06
KANALISATION SE MÅTTRITNINGAR.

ANGIVNA FRIA MÅTT GÄLLER MELLAN VÄGGKAKEL
RESP. MELLAN ÖK BELÄGGNING OCH UK BRANDISOLERING.

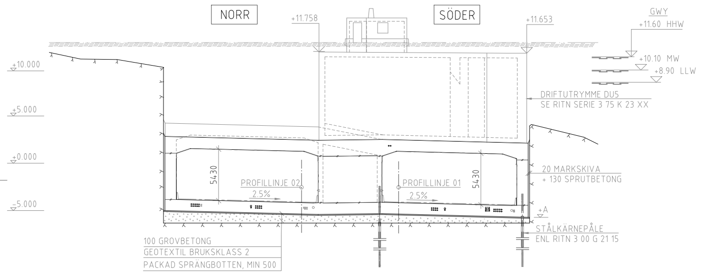

SEKTION B-B 3 00 K 20 03
1:200
SEKTION 2/653 (PROFIL 01)

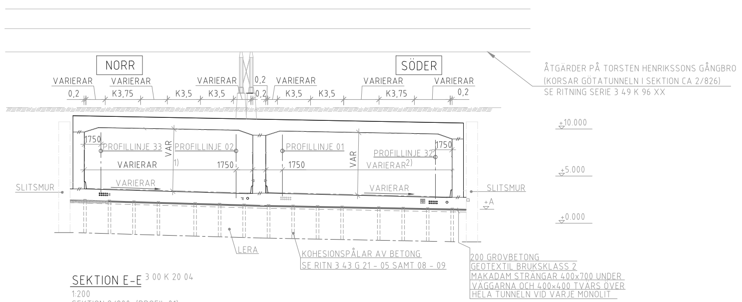

SEKTION E-E 3 00 K 20 04
1:200
SEKTION 2/800 (PROFIL 01)

ÅTGÄRDER PÅ TORSTEN HENRIKSSONS GÅNGBRO
(KORSAR GÖTATUNNELN I SEKTION CA 2/826)
SE RITNING SERIE 3 49 K 96 XX

FOTNOT	MELLAN SEKTIONER (PROFIL 01)	HORISONTALMÅTT LÄNGDER CA MÅTT I mm DÄR EJ ANNAT ANGES
1)	2/653,000 - 2/746,200	13250 - 13760
1)	2/746,200 - 2/860,500	13760 - 15610
2)	2/653,000 - 2/746,200	12500 - 14300
2)	2/746,200 - 2/860,500	14300 - 17545
3)	2/653,000 - 2/746,200	5735 - 1145
3)	2/746,200 - 2/792,000	2080-535
4)	2/653,000 - 2/746,200	6,23 - 3,26m
4)	2/746,200 - 2/792,000	2,95 - 1,14m
5)	2/653,000 - 2/746,200	15,89 - 16,51m
5)	2/746,200 - 2/860,500	16,51 - 18,26m
6)	2/653,000 - 2/746,200	15,14 - 16,95m
6)	2/746,200 - 2/860,500	16,95 - 20,13m
7)	2/820,356 - 2/881,500	0 - 2705
8)	2/812,532 - 2/881,500	0 - 2705
9)	2/860,500 - 2/881,500	1216 - 1216
10)	2/860,500 - 2/881,500	1200 - 1105

SITUATIONSPLAN 1:5000

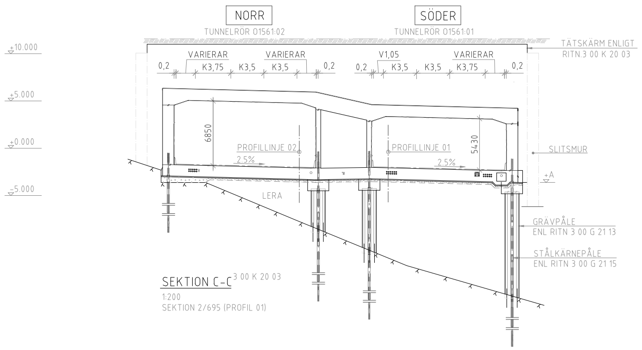

SEKTION C-C 3 00 K 20 03
1:200
SEKTION 2/695 (PROFIL 01)

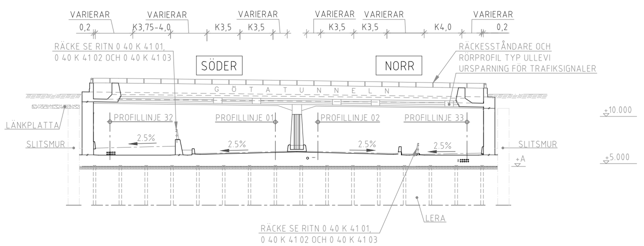

SEKTION F-F 3 00 K 20 04
1:200
SEKTION 2/864.6 (PROFIL 01)

0 1561:01 xn/0 1561:02 xz
GODTAGEN AV VÄGVERKET, SEKTION BRO-OCH TUNNELTEKNIK,
ENLIGT BREV DATERAT 2004-04-13 MED DIARIENUMMER 0 1561 2004:328

HANDLINGEN ÄR UPPRÄTTAD ENLIGT KVALITETSSYSTEM FÖR REINERTSEN AB, UTGÅVA 6 DATERAT 2003-03-31.

REV	ANT	ÄNDRINGEN AVSER	GODKÄND	DATUM
B	-	ÄNDRAT RITNINGSNUMMER	LC	04-12-21
A	-	ALLMÄN REVIDERING	LC	04-09-10

RELATIONSHANDLING — FÖRVALTNINGSHANDLING

Vägverket Region Väst
GÖTATUNNELN — Ett projekt i Göteborgsöverenskommelsen
BILFINGER+BERGER; AF Spesialprosjekt AS; Hanjobygg; REINERTSEN

VÄG 45, GÖTATUNNELN
LILLA BOMMEN, L2
300 GEMENSAMT
SEKTION 2/615,0 - 2/881,5 I PROFIL 01
TVÄRSEKTIONER
SAMMANSTÄLLNING IV

UPPDRAG NR	RITARE	KONSTR	GRANSK	KONSTBYGGNADSNR	FORMAT	SKALA
2001-0290	UO	LARS HANSSON	LENNART CLAESON	0 1561	A1F	1:200

GÖTEBORG 2004-03-26
LENNART CLAESON
OBJEKT NR 429011 — RITNINGSNR 3 00 K 20 13 — REV B

GODKÄND AV LBT KB ENLIGT BREV DATERAT: 2004-03-22

1:200 0 10 20m
1:100 0 1 2 3 4 5 6 7 8 9 10 m

Plottad: 06 01 09 17:57 Fil: Q:\01\20010290_GT\Relationshandlingar_A2\3\K\Ritder\300K2013.dwg

ALLMÄNNA ANVISNINGAR

PANELNUMRERING ENL RITNING NR 302 G 22 03

MOTFYLLNING FÅR HÖGST SKE TILL NIVÅN +12.60

HÄNVISNINGAR

SEKTIONER SE RITNING NR 301 G 22 55

BETR ÖVRIG TEXT SE RITNING NR 302G2201 OCH 302G2202

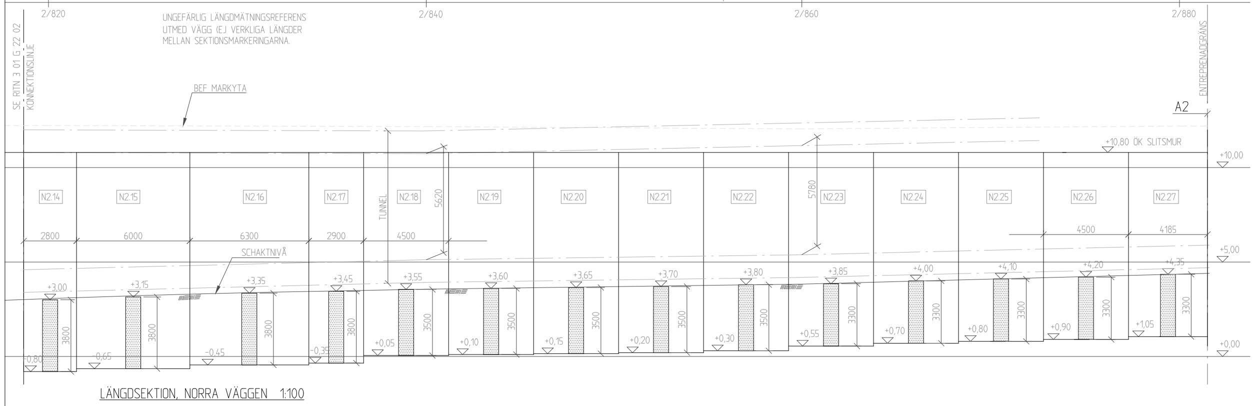

LÄNGDSEKTION, NORRA VÄGGEN 1:100

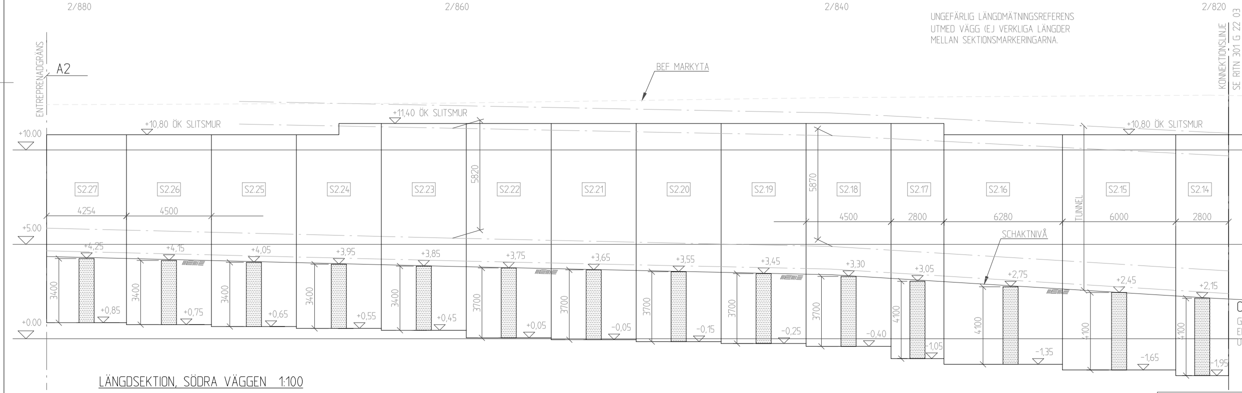

LÄNGDSEKTION, SÖDRA VÄGGEN 1:100

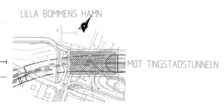

SITUATIONSPLAN 1:2500

Ö 1561:16 cl
GODTAGEN AV VÄGVERKET, SEKTION BRO- OCH TUNNELTEKNIK, ENLIGT BREV DATERAT 2003-06-02 MED DIARIENUMMER Ö 1561 2003:565.

UTFÖRD ENLIGT RITNING:

RELATIONSHANDLING | FÖRVALTNINGSHANDLING

Vägverket Region Väst
GÖTATUNNELN
Ett projekt i Göteborgsöverenskommelsen
BILFINGER+BERGER
AF Spesialprosjekt AS
REINERTSEN

VÄG 45, GÖTATUNNELN
LILLA BOMMEN, L2
STÖDKONSTRUKTION
DEL A2, 2/820-2/880

LÄNGDSEKTION
SLITSMUR, N & S VÄGGEN, MÅTT

STOCKHOLM	2003-05-16
GODKÄND GK3/UTLÅTANDE	
GÖTEBORG	2003-02-04
GODKÄND LBT/MK/UTLÅTANDE	

2001-0290	CG/DS/KK	Ö1561	A1	1:100
GÖTEBORG	2003-03-26			
429011		3 01 G 22 51		

1:100   1 0 1 2 3 4 5 6 7 8 9 10 m

XREF:L:\20010290\PROJ\3\G\MODELL\G3002205 05-11-30 10:30
L:\20010290\PROJ\3\G\MODELL\G3002204 05-11-30 10:36

PLOTTAD 05 12 14 17:52 Fil: L:\20010290\Proj\3\G\Ritn\301G2251.dwg

B

Converting stiffness of cross-wall to truss

The following equations are only valid for obtaining an equivalent axial stiffness for the cross-walls without any bending moment considered. This is an ideal case for a first order estimation of the truss. However, in reality the cross-walls will experience bending moments and the factor needs to be calibrated with a structural analysis.

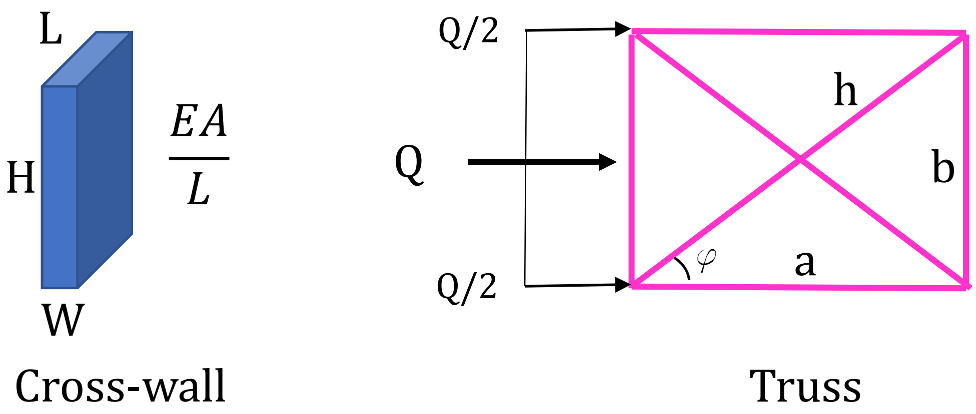

Truss

a	Adjacent cathetus	5	m
b	Opposite cathetus	4	m
h	Hypotenuse	6,4	m
φ	Angle		
Q	Force		

Cross-wall

E_c	Young's modulus fro concrete	$3,10 \cdot 10^7$	kN
H	Height of cross-wall	$0,8$	m
W	Width of cross-wall	4	m

Equilibrium:

$$\frac{EA_1}{L_1} = \frac{EA_2}{L_2}$$

$$L_2 = \frac{L_1}{cos\varphi}$$

$$\frac{EA_1}{L_1} = cos\varphi \frac{EA_2}{L_1}$$

$$A_1 = cos\varphi A_2$$

The inner elements are therefore equal to:

$$\frac{EA_1}{L_1} = \frac{E_s A_2}{cos\varphi}$$

Equilibrium to make the 4 steel bars in the truss equal to the cross-wall:

$$\frac{E_c A}{L_1} = 2\left(\frac{E_s A_1}{L_1}\right) + 2\left(\frac{E_s A_1}{cos\varphi L_1}\right)$$

$$E_c A = 2E_s A_1 \left(1 + \frac{1}{cos\varphi}\right)$$

Insert variables and sort out steel truss $E_s A_1$:

$$cos\varphi = cos\frac{a}{b} = 0.78 \quad \rightarrow \quad \varphi = 38.7°$$

$$A = W \cdot H = 3,2m^2$$

$$E_c A = 3,10 \cdot 10^7 \cdot 3,2 = 9,92 \cdot 10^7 kN$$

$$E_s A_1 = \frac{9,92 \cdot 10^7}{2 \cdot (1 + \frac{1}{cos38,7°})} = \underline{2,17 \cdot 10^7 kN}$$

C

Calculations

Calculation of Basal heave stability

Calculation of Basal heave stability F_c according to Eq C.1, adapted from (Sällfors, 2013):

$$\boxed{F_c = N_c \cdot \frac{c_u}{\gamma \cdot H + q - p}} \tag{C.1}$$

N_c	Stability factor
c_u	Undrained shear strength
γ	Unit weight of soil
H	Distance from surface to excavation bottom
q	External load
p	Load at excavation bottom

Which shear strength c_u should be used?
The shear strength c_u is a mean value of the shear strength at the excavation bottom $c_u(H)$ and the shear strength at a distance of $d + \frac{2 \cdot B}{3}$ from the excavation bottom $c_u(H + d)$. If $\frac{2 \cdot B}{3} > d$, the mean value is calculated between $c_u(H)$ and the shear strength at $2d$ from excavation bottom $c_u(H + 2d)$. See explanation of variables in Figure C.1.

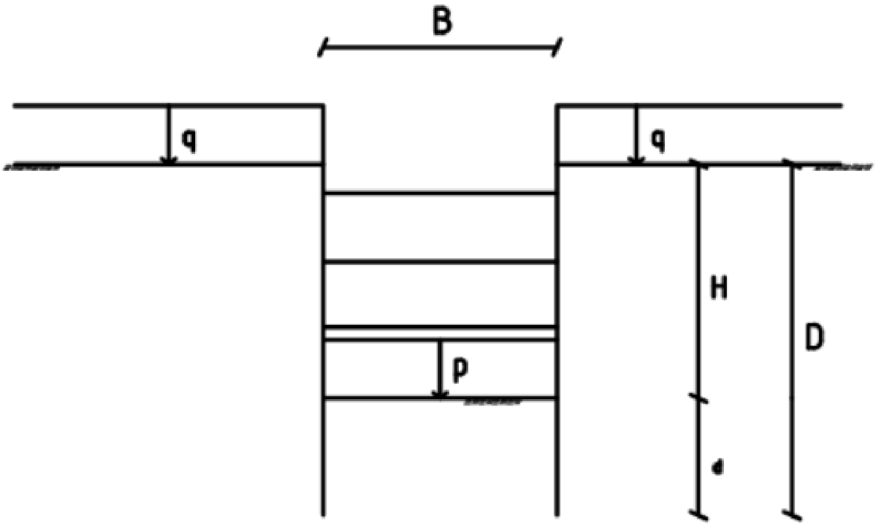

Figure C.1: Illustration of variables for calculation of basal heave stability, adapted from (Sällfors, 2013).

B	Width of excavation	40 m
H	Distance from surface to excavation bottom	7,5 m
d	Distance from excavation bottom to toe of support structure	4 m

$$\frac{2 \cdot B}{3} > d \rightarrow 2d$$

$$\frac{2 \cdot 40}{3} = 26,7 > 4 \rightarrow 8m$$

$$c_u = \frac{c_u(H) + c_u(H + 2d)}{2} = \frac{c_u(-7,5m) + c_u(-15,5m)}{2} = \frac{18,1 + 31,1}{2} = 24,6kN/m^2$$

Stability factor N_c?
N_c is determined by diagram in Figure C.2.

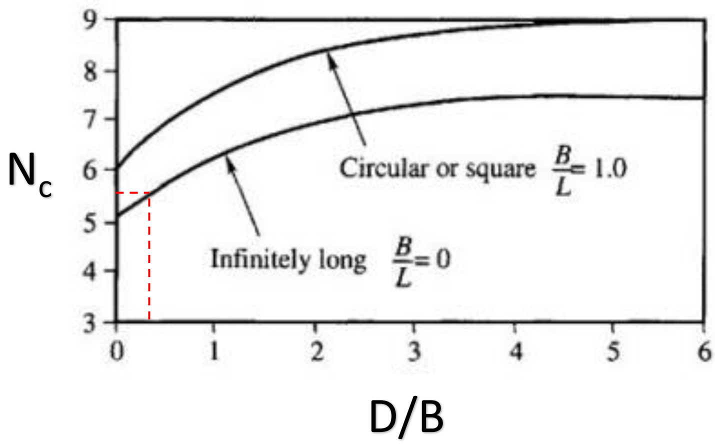

Figure C.2: Stability factor for braced excavations, adapted from (Kullingsjö, 2007).

L	Length of excavation, 0 if its elongated	0
D	Length of support structure	12 m

$$\frac{B}{L} = \frac{40}{0} = 0 \rightarrow Infinitely\ long$$

$$\frac{D}{B} = \frac{12}{40} = 0,3$$

$$N_c \rightarrow 5,5$$

γ	Unit weight of soil	16 kN/m^2
H	Distance from surface to excavation bottom	7,5 m
q	External load	10 kPa
p	Load at excavation bottom	0 kPa

$$F_c = N_c \cdot \frac{c_u}{\gamma \cdot H + q - p} = 5,5 \cdot \frac{24,6}{16 \cdot 7,5 + 10 - 0} = \underline{1,04}$$

Calculation of Axial skin friction

Calculation of skin according to Eq C.2 (Eriksson et al., 2004):

$$\boxed{T_{skin} = A_{Mantelsurface} \cdot c_u \cdot Factor} \tag{C.2}$$

W	Width of pile	0,275 m
A	Mantle surface/m for square = $4 \cdot W$	1,1 m^2/m
$c_{u,top}$	Undrained shear strength at -7,5 m	22 kN/m^2
$c_{u,bottom}$	Undrained shear strength at -27,5 m	54 kN/m^2
$Factor$	Retrieved from Eriksson et al. (2004)	0.7

$$T_{skin,start,max} = \underline{17 \quad kN/m} \quad T_{skin,end,max} = \underline{42 \quad kN/m}$$

Calculation of Base resistance

$c_u(z)$	Shear strength at -27,5 m	54 kN/m^2
A_{base}	Area at the base	$0,27^2$ m^2
L	Length of pile	9 m

$$F_{max} = c_u(z) \cdot L \cdot {A_{base}}^2 = 54 \cdot 9 \cdot 0,27^2 = \underline{36 \quad kN}$$

Calculation Strut stiffness

E_{strut}	E-modulus for steel	$2,10 \cdot 10^8$ kN/m^2
D	Diameter strut	0,75 m
t	Thickness of steel	0,02 m
A_{strut}	$D \cdot \pi \cdot t$	0,0459 m^2

$$EA_{strut} = E_{strut} * A_{strut} = \underline{9,639 \cdot 10^6 \quad kN}$$

D

Input and output data for material models

Full HSs input data

Hardening Soil small									
Retrived from:	*Triax, Region City, Tara Wood*								
	Identification:	**Clay 1**	**Clay 2**	**Clay 3**	**Clay 4**	**Clay 5**	**Clay 6**	**Clay 7**	**Units**
Material set	Material model	HSs	HSs	HSs	HSs	HSs	HSs	HSs	-
	Drain type	Undr(A)	Undr(A)	Undr(A)	Undr(A)	Undr(A)	Undr(A)	Undr(A)	-
General properties	y_unsat	16,5	15,5	15,7	16,3	16,2	16,4	16,5	kN/m^3
	y_sat	16,5	15,5	15,7	16,3	16,2	16,4	16,5	kN/m^3
Advanced	Dilat cut-off	No	No	No	No	No	No	No	-
	e_init	0,5	0,5	0,5	0,5	0,5	0,5	0,5	-
	e_min	Auto	Auto	Auto	Auto	Auto	Auto	Auto	-
	e_max	Auto	Auto	Auto	Auto	Auto	Auto	Auto	-
Stiffness									
Orgin	E_50^ref	7000	7000	7000	15400	13100	13100	10500	kN/m^2
	E_oed^ref	3002	3400	3068	8300	6600	6600	5285	kN/m^2
	E_ur^ref	27000	33700	24250	30800	26200	26200	21000	kN/m^2
Eoed = E50, Eur=2*E50, E50	E_50^ref	7000	7000	7000	15400	13100	13100	10500	kN/m^2
"Reference"	E_oed^ref	3781	2718	3781	8319	6593	6593	5285	kN/m^2
	E_ur^ref	14000	14000	14000	30800	26200	26200	21000	kN/m^2
		0,540	0,388	0,540	0,540	0,503	0,503	0,503	
Eoed = E50, Eur=2*E50, min(E50x0.8)	E_50^ref	5600	5600	5600	12320	10480	10480	8400	kN/m^2
"Eur=2*E50_MIN"	E_oed^ref	3025	2175	3025	6655	5275	5275	4228	kN/m^2
	E_ur^ref	11200	11200	11200	24640	20960	20960	16800	kN/m^2
		0,540	0,388	0,540	0,540	0,503	0,503	0,503	
Eoed = E50, Eur=2*E50, max(E50x1.2)	E_50^ref	8400	8400	8400	18480	15720	15720	12600	kN/m^2
"Eur=2*E50_MAX"	E_oed^ref	4538	3263	4538	9983	7913	7913	6342	kN/m^2
	E_ur^ref	16800	16800	16800	36960	31440	31440	25200	kN/m^2
		0,540	0,388	0,540	0,540	0,503	0,503	0,503	
Eoed = E50, Eur=4*E50, min(E50x0.8)	E_50^ref	5600	5600	5600	12320	10480	10480	8400	kN/m^2
"Eur=4*E50_MIN"	E_oed^ref	3025	2175	3025	6655	5275	5275	4228	kN/m^2
	E_ur^ref	22400	22400	22400	49280	41920	41920	33600	kN/m^2
		0,540	0,388	0,540	0,540	0,503	0,503	0,503	
Eoed = E50, Eur=4*E50, max(E50x1.2)	E_50^ref	8400	8400	8400	18480	15720	15720	12600	kN/m^2
"Eur=4*E50_MAX"	E_oed^ref	4538	3263	4538	9983	7913	7913	6342	kN/m^2
	E_ur^ref	33600	33600	33600	73920	62880	62880	50400	kN/m^2
		0,540	0,388	0,540	0,540	0,503	0,503	0,503	
Eoed = E50, Eur=6*E50, min(E50x0.8)	E_50^ref	5600	5600	5600	12320	10480	10480	8400	kN/m^2
"Eur=6*E50_MIN"	E_oed^ref	3025	2175	3025	6655	5275	5275	4228	kN/m^2
	E_ur^ref	33600	33600	33600	73920	62880	62880	50400	kN/m^2
		0,540	0,388	0,540	0,540	0,503	0,503	0,503	
Eoed = E50, Eur=6*E50, max(E50x1.2)	E_50^ref		8400	8400	18480	15720	15720	12600	kN/m^2
"Eur=6*E50_MAX"	E_oed^ref	0	3263	4538	9983	7913	7913	6342	kN/m^2
	E_ur^ref	0	50400	50400	110880	94320	94320	75600	kN/m^2
		0,540	0,388	0,540	0,540	0,503	0,503	0,503	
	power (m)	1	1	1	1	1	1	1	

Alternatives	Use alt	No	No	No	No	No	No	No	
	C_c	Auto	Auto	Auto	Auto	Auto	Auto	Auto	
	C_s	Auto	Auto	Auto	Auto	Auto	Auto	Auto	
	e_init	Done	Done	Done	Done	Done	Done	Done	
Strength	c'_ref	1	1	1	1	0	0	0	kN/m^2
	phi'	32	32	32	32	30,5	30,5	30,5	º
	psi'	0	0	0	0	0	0	0	º
Small strain	y_0.7	0,0004	0,0004	0,0004	0,0004	0,0006	0,0008	0,0009	
	G_0^ref	77480	39700	40210	39230	40960	36060	37460	kN/m^2
Advanced	Default values	No	No	No	No	No	No	No	
Stiffnes	v'_ur	0,15	0,15	0,15	0,15	0,15	0,15	0,15	
	p_ref	100	100	100	100	100	100	100	
	K_0^nc	0,53	0,47	0,53	0,53	0,53	0,53	0,53	
Strength	c'_inc	0	0	0	0	0	0	0	
	y_ref	0	0	0	0	0	0	0	
	R_f	0,9	0,9	0,9	0,9	0,9	0,9	0,9	
	Tension cut-off	Yes	Yes	Yes	Yes	Yes	Yes	Yes	
	Tensile str	0	0	0	0	0	0	0	
GW model	Data set	Std	Std	Std	Std	Std	Std	Std	
Soil	Type	Very fine	Very fine	Very fine	Very fine	Very fine	Very fine	Very fine	
	< 2 microm	Auto	Auto	Auto	Auto	Auto	Auto	Auto	%
	2-50	Auto	Auto	Auto	Auto	Auto	Auto	Auto	%
	50-2 millim	Auto	Auto	Auto	Auto	Auto	Auto	Auto	%
Flow parameters	Default values	No	No	No	No	No	No	No	
	k_x	1	0,00004	0,00002	4,00E-05	3,00E-05	5,00E-05	7,00E-05	m/day
	k_y	1	0,00004	0,00002	4,00E-05	3,00E-05	5,00E-05	7,00E-05	m/day
	dilatancy_unsat	0	0	0	10000	10000	10000	10000	m
	e_init	Done	Done	Done	Done	Done	Done	Done	
	S_s	Auto	Auto	Auto	Auto	Auto	Auto	Auto	1/m
Change of permeab	c_k	1,00E+15	1,00E+15	1,00E+15	1,00E+15	1,00E+15	1,00E+15	1,00E+15	
Interface	Strength	Rigid	Rigid	Rigid	Rigid	Rigid	Rigid	Rigid	
	R_inter	Auto	Auto	Auto	Auto	Auto	Auto	Auto	
	Con. gap closure	Yes	Yes	Yes	Yes	Yes	Yes	Yes	
Real interface thickness	delta_inter	Auto	Auto	Auto	Auto	Auto	Auto	Auto	
K0 settings	K_0 determ.	Manual	Manual	Manual	Manual	Manual	Manual	Manual	
	K_0,x = K_0,z	Yes	Yes	Yes	Yes	Yes	Yes	Yes	
	K_0,x	0,7	0,7	0,63	0,61	0,58	0,57	0,56	
	K_0,z	Auto	Auto	Auto	Auto	Auto	Auto	Auto	
Over-consolidation	OCR	2	1,65	1	1	1	1,14	1,14	
	POP	0	0	32	32	32	0	0	

Full ADP input data

Hardening Soil small									
Retrived from:	*Triax, Region City, Tara Wood*								
	Identification:	**Clay 1**	**Clay 2**	**Clay 3**	**Clay 4**	**Clay 5**	**Clay 6**	**Clay 7**	**Units**
Material set	Material model	HSs	HSs	HSs	HSs	HSs	HSs	HSs	-
	Drain type	Undr(A)	Undr(A)	Undr(A)	Undr(A)	Undr(A)	Undr(A)	Undr(A)	-
General properties	y_unsat	16,5	15,5	15,7	16,3	16,2	16,4	16,5	kN/m^3
	y_sat	16,5	15,5	15,7	16,3	16,2	16,4	16,5	kN/m^3
Advanced	Dilat cut-off	No	No	No	No	No	No	No	-
	e_init	0,5	0,5	0,5	0,5	0,5	0,5	0,5	-
	e_min	Auto	Auto	Auto	Auto	Auto	Auto	Auto	-
	e_max	Auto	Auto	Auto	Auto	Auto	Auto	Auto	-
Stiffness									
Orgin	E_50^ref	7000	7000	7000	15400	13100	13100	10500	kN/m^2
	E_oed^ref	3002	3400	3068	8300	6600	6600	5285	kN/m^2
	E_ur^ref	27000	33700	24250	30800	26200	26200	21000	kN/m^2
Eoed = E50, Eur=2*E50, E50	E_50^ref	7000	7000	7000	15400	13100	13100	10500	kN/m^2
"Reference"	E_oed^ref	3781	2718	3781	8319	6593	6593	5285	kN/m^2
	E_ur^ref	14000	14000	14000	30800	26200	26200	21000	kN/m^2
		0,540	0,388	0,540	0,540	0,503	0,503	0,503	
Eoed = E50, Eur=2*E50, min(E50x0.8)	E_50^ref	5600	5600	5600	12320	10480	10480	8400	kN/m^2
"Eur=2*E50_MIN"	E_oed^ref	3025	2175	3025	6655	5275	5275	4228	kN/m^2
	E_ur^ref	11200	11200	11200	24640	20960	20960	16800	kN/m^2
		0,540	0,388	0,540	0,540	0,503	0,503	0,503	
Eoed = E50, Eur=2*E50, max(E50x1.2)	E_50^ref	8400	8400	8400	18480	15720	15720	12600	kN/m^2
"Eur=2*E50_MAX"	E_oed^ref	4538	3263	4538	9983	7913	7913	6342	kN/m^2
	E_ur^ref	16800	16800	16800	36960	31440	31440	25200	kN/m^2
		0,540	0,388	0,540	0,540	0,503	0,503	0,503	
Eoed = E50, Eur=4*E50, min(E50x0.8)	E_50^ref	5600	5600	5600	12320	10480	10480	8400	kN/m^2
"Eur=4*E50_MIN"	E_oed^ref	3025	2175	3025	6655	5275	5275	4228	kN/m^2
	E_ur^ref	22400	22400	22400	49280	41920	41920	33600	kN/m^2
		0,540	0,388	0,540	0,540	0,503	0,503	0,503	
Eoed = E50, Eur=4*E50, max(E50x1.2)	E_50^ref	8400	8400	8400	18480	15720	15720	12600	kN/m^2
"Eur=4*E50_MAX"	E_oed^ref	4538	3263	4538	9983	7913	7913	6342	kN/m^2
	E_ur^ref	33600	33600	33600	73920	62880	62880	50400	kN/m^2
		0,540	0,388	0,540	0,540	0,503	0,503	0,503	
Eoed = E50, Eur=6*E50, min(E50x0.8)	E_50^ref	5600	5600	5600	12320	10480	10480	8400	kN/m^2
"Eur=6*E50_MIN"	E_oed^ref	3025	2175	3025	6655	5275	5275	4228	kN/m^2
	E_ur^ref	33600	33600	33600	73920	62880	62880	50400	kN/m^2
		0,540	0,388	0,540	0,540	0,503	0,503	0,503	
Eoed = E50, Eur=6*E50, max(E50x1.2)	E_50^ref		8400	8400	18480	15720	15720	12600	kN/m^2
"Eur=6*E50_MAX"	E_oed^ref	0	3263	4538	9983	7913	7913	6342	kN/m^2
	E_ur^ref	0	50400	50400	110880	94320	94320	75600	kN/m^2
		0,540	0,388	0,540	0,540	0,503	0,503	0,503	
	power (m)	1	1	1	1	1	1	1	

Hardening Soil small									
Retrived from:	*Triax, Region City, Tara Wood*								
	Identification:	**Clay 1**	**Clay 2**	**Clay 3**	**Clay 4**	**Clay 5**	**Clay 6**	**Clay 7**	**Units**
Material set	Material model	HSs	HSs	HSs	HSs	HSs	HSs	HSs	-
	Drain type	Undr(A)	Undr(A)	Undr(A)	Undr(A)	Undr(A)	Undr(A)	Undr(A)	-
General properties	y_unsat	16,5	15,5	15,7	16,3	16,2	16,4	16,5	kN/m^3
	y_sat	16,5	15,5	15,7	16,3	16,2	16,4	16,5	kN/m^3
Advanced	Dilat cut-off	No	No	No	No	No	No	No	-
	e_init	0,5	0,5	0,5	0,5	0,5	0,5	0,5	-
	e_min	Auto	Auto	Auto	Auto	Auto	Auto	Auto	-
	e_max	Auto	Auto	Auto	Auto	Auto	Auto	Auto	-
Stiffness									
Orgin	E_50^ref	7000	7000	7000	15400	13100	13100	10500	kN/m^2
	E_oed^ref	3002	3400	3068	8300	6600	6600	5285	kN/m^2
	E_ur^ref	27000	33700	24250	30800	26200	26200	21000	kN/m^2
Eoed = E50, Eur=2*E50, E50	E_50^ref	7000	7000	7000	15400	13100	13100	10500	kN/m^2
"Reference"	E_oed^ref	3781	2718	3781	8319	6593	6593	5285	kN/m^2
	E_ur^ref	14000	14000	14000	30800	26200	26200	21000	kN/m^2
		0,540	0,388	0,540	0,540	0,503	0,503	0,503	
Eoed = E50, Eur=2*E50, min(E50x0.8)	E_50^ref	5600	5600	5600	12320	10480	10480	8400	kN/m^2
"Eur=2*E50_MIN"	E_oed^ref	3025	2175	3025	6655	5275	5275	4228	kN/m^2
	E_ur^ref	11200	11200	11200	24640	20960	20960	16800	kN/m^2
		0,540	0,388	0,540	0,540	0,503	0,503	0,503	
Eoed = E50, Eur=2*E50, max(E50x1.2)	E_50^ref	8400	8400	8400	18480	15720	15720	12600	kN/m^2
"Eur=2*E50_MAX"	E_oed^ref	4538	3263	4538	9983	7913	7913	6342	kN/m^2
	E_ur^ref	16800	16800	16800	36960	31440	31440	25200	kN/m^2
		0,540	0,388	0,540	0,540	0,503	0,503	0,503	
Eoed = E50, Eur=4*E50, min(E50x0.8)	E_50^ref	5600	5600	5600	12320	10480	10480	8400	kN/m^2
"Eur=4*E50_MIN"	E_oed^ref	3025	2175	3025	6655	5275	5275	4228	kN/m^2
	E_ur^ref	22400	22400	22400	49280	41920	41920	33600	kN/m^2
		0,540	0,388	0,540	0,540	0,503	0,503	0,503	
Eoed = E50, Eur=4*E50, max(E50x1.2)	E_50^ref	8400	8400	8400	18480	15720	15720	12600	kN/m^2
"Eur=4*E50_MAX"	E_oed^ref	4538	3263	4538	9983	7913	7913	6342	kN/m^2
	E_ur^ref	33600	33600	33600	73920	62880	62880	50400	kN/m^2
		0,540	0,388	0,540	0,540	0,503	0,503	0,503	
Eoed = E50, Eur=6*E50, min(E50x0.8)	E_50^ref	5600	5600	5600	12320	10480	10480	8400	kN/m^2
"Eur=6*E50_MIN"	E_oed^ref	3025	2175	3025	6655	5275	5275	4228	kN/m^2
	E_ur^ref	33600	33600	33600	73920	62880	62880	50400	kN/m^2
		0,540	0,388	0,540	0,540	0,503	0,503	0,503	
Eoed = E50, Eur=6*E50, max(E50x1.2)	E_50^ref		8400	8400	18480	15720	15720	12600	kN/m^2
"Eur=6*E50_MAX"	E_oed^ref	0	3263	4538	9983	7913	7913	6342	kN/m^2
	E_ur^ref	0	50400	50400	110880	94320	94320	75600	kN/m^2
		0,540	0,388	0,540	0,540	0,503	0,503	0,503	
	power (m)	1	1	1	1	1	1	1	

Output parameter

Extraction of output variables.

Diagram	Phase	Tool	Location	Output
Deformation of the wall	Exc (-7,5m)	Cross section	A (20.6, 0) B (20.6, -11.5)	Total disp u_x
Earth pressure	Exc (-7,5m)	Select interface	left/right side interface of DW	Total normal stresses
Bending moment	Exc (-7,5m)	Structural forces, Cross line	A (20.6, 0) B (20.6, -11.5)	Automatic bending moment
Heave of the bottom of excavation	Exc (-7,5m)	Cross section	A (0.0, -7.5) B (20.0, -7.5)	Total disp u_y
Settlement of the surface	Exc (-7,5m)	Cross section	A (20, 0) B (100, 0)	Total disp u_y
Truss/Strut	Exc (-7,5m)	Click on strut/truss	NodeToNode 1_1, 16_1, 8_1, 9_1	Sum of N, (negative=compression)

E

Complete Sensitivity Analysis

#0 Comparison
HSs and ADP

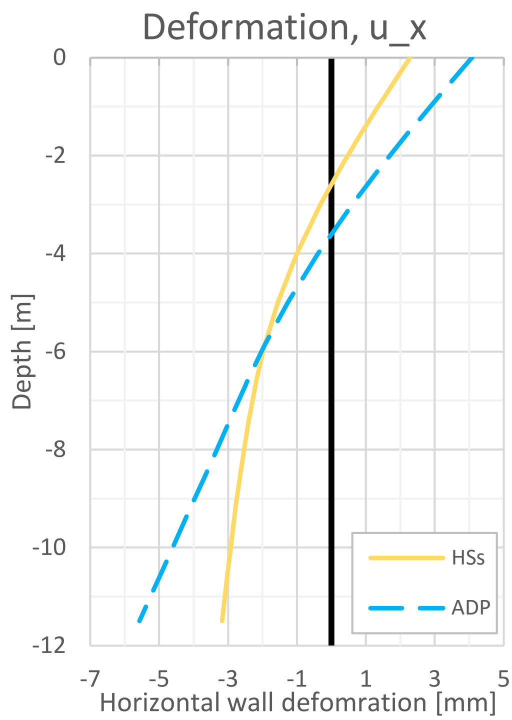

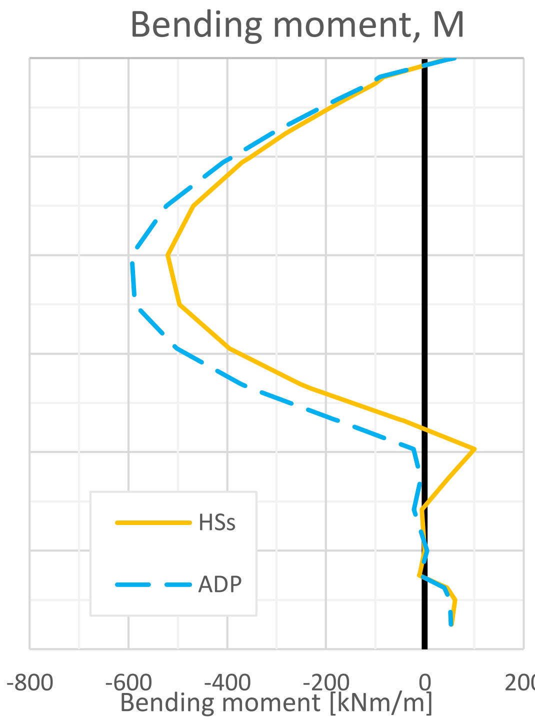

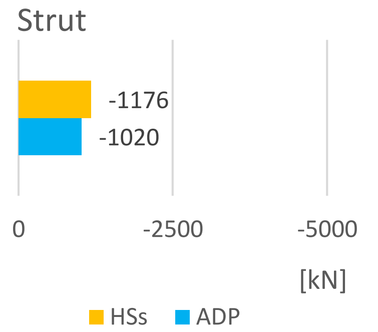

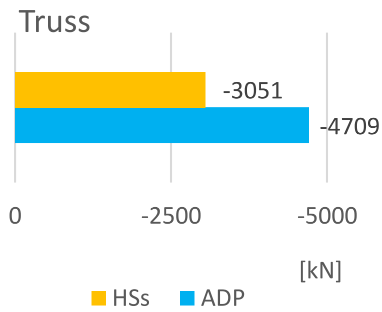

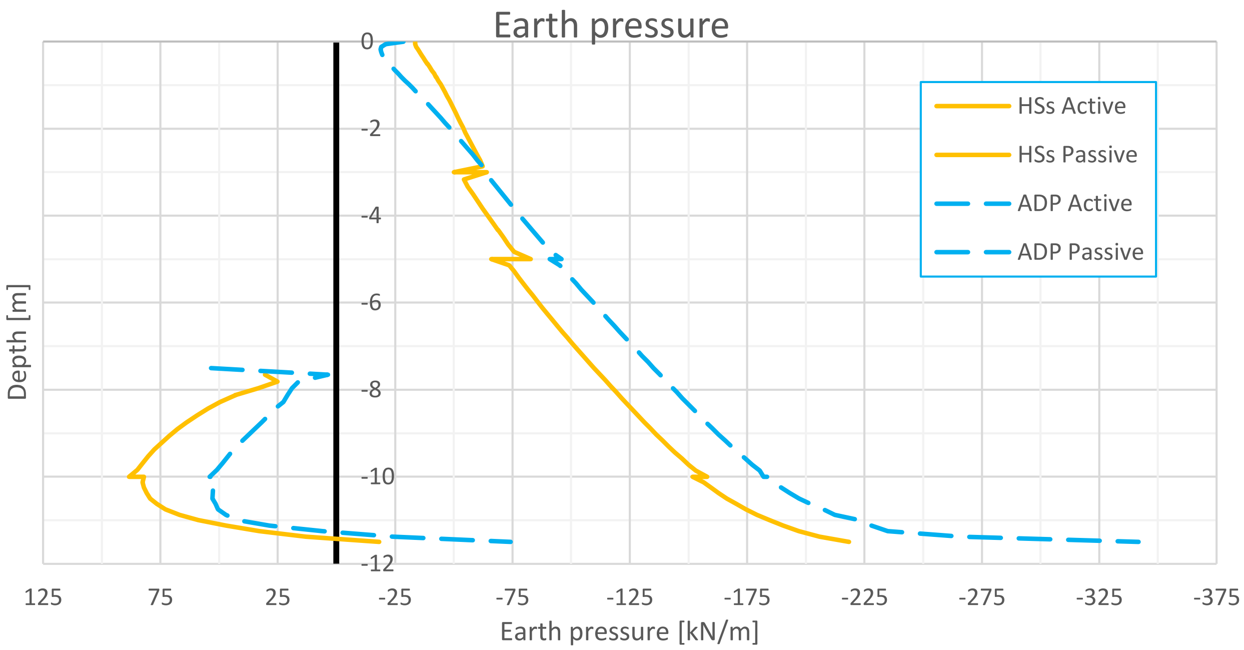

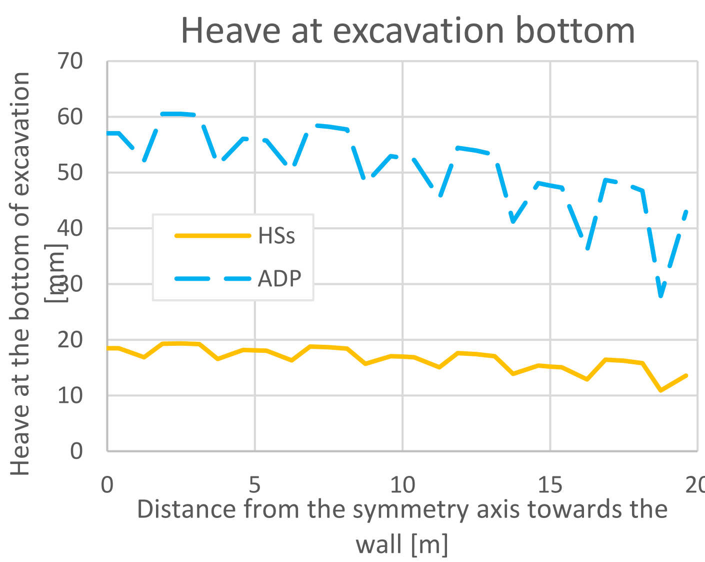

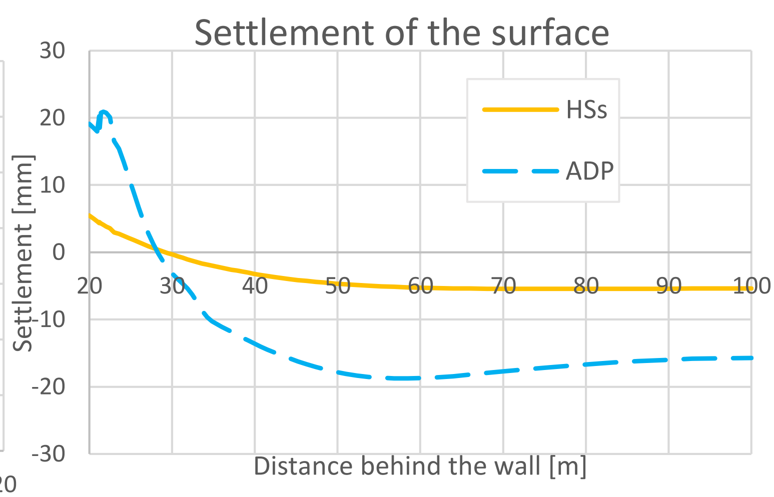

#1 Interface between diaphragm wall and adjacent soil, R_inter (HSs)

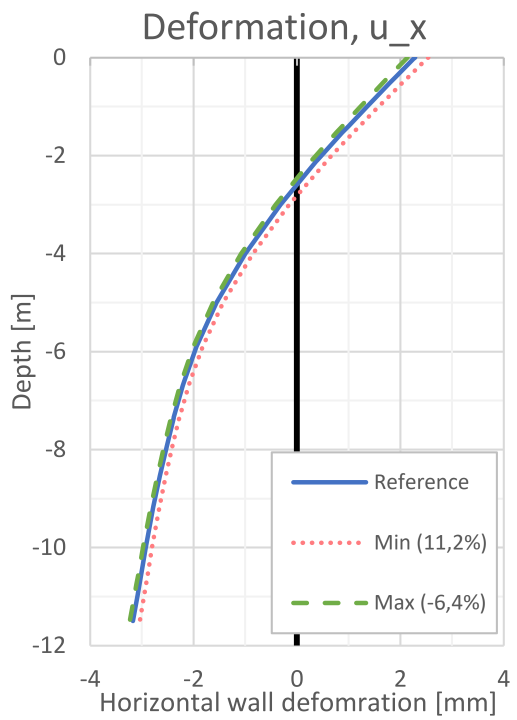

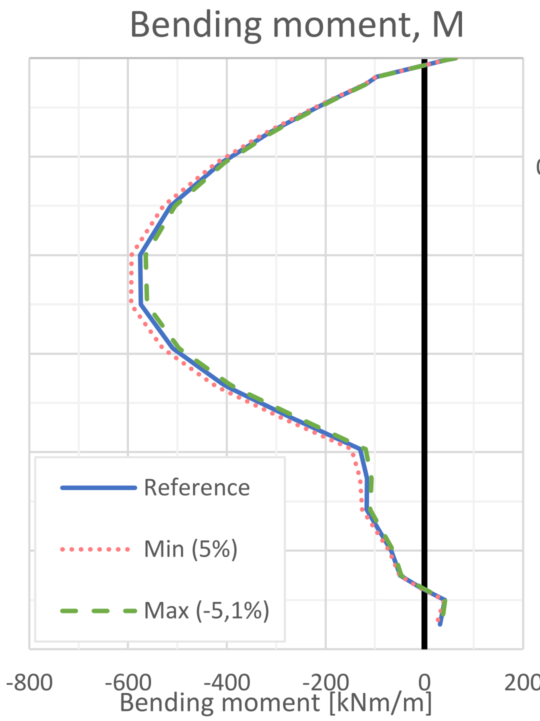

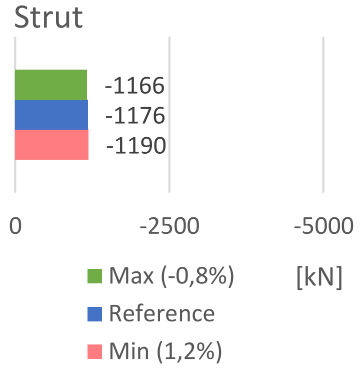

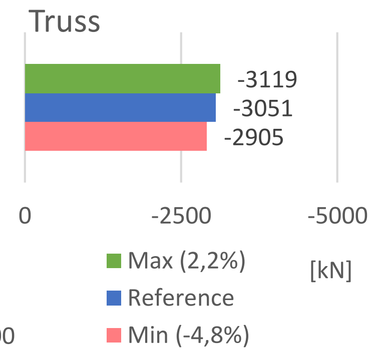

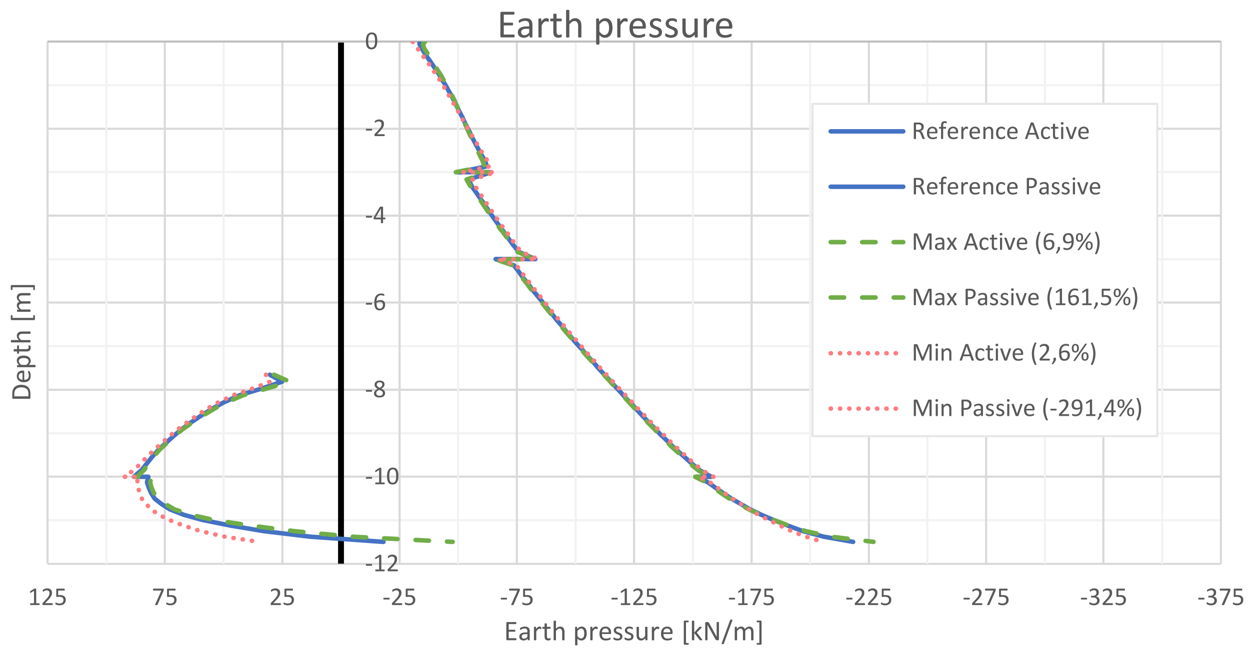

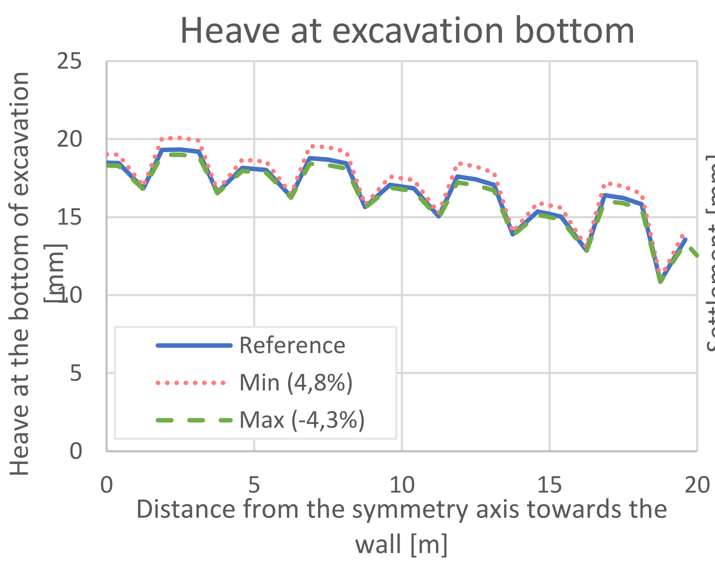

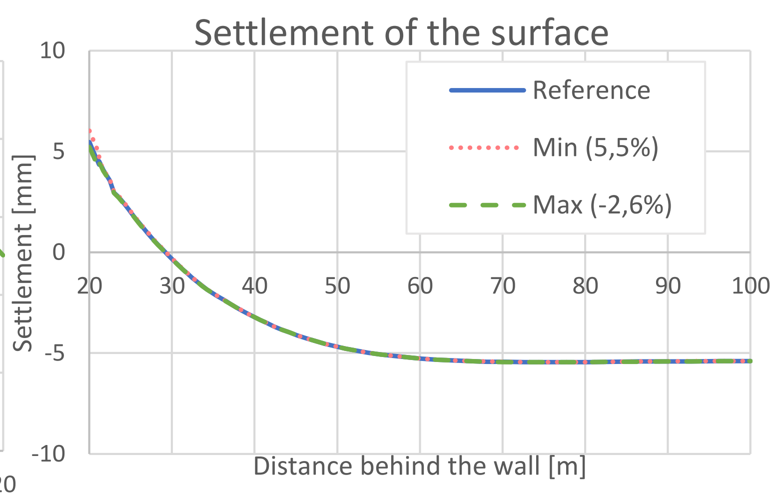

#2 Interface between diaphragm wall and adjacent soil, R_inter (ADP)

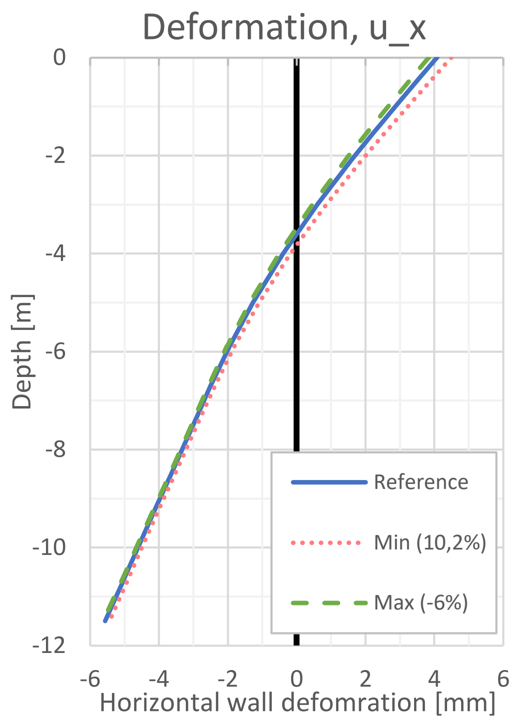

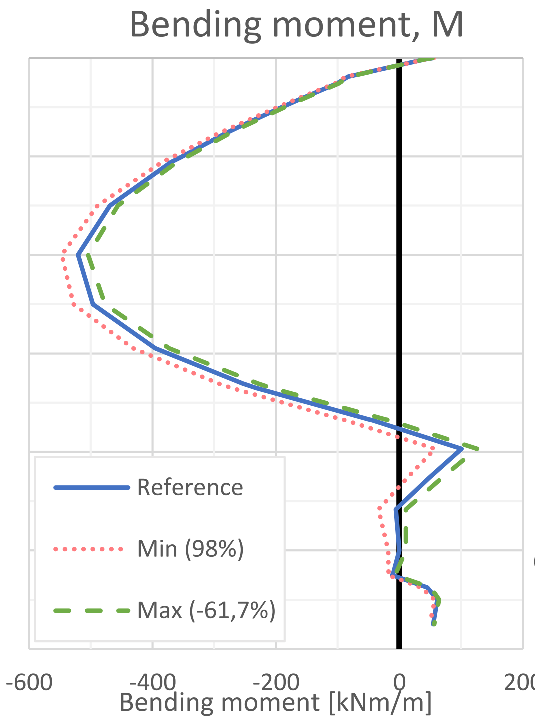

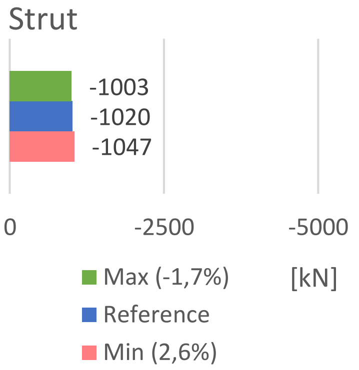

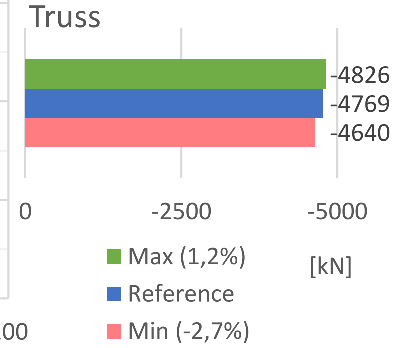

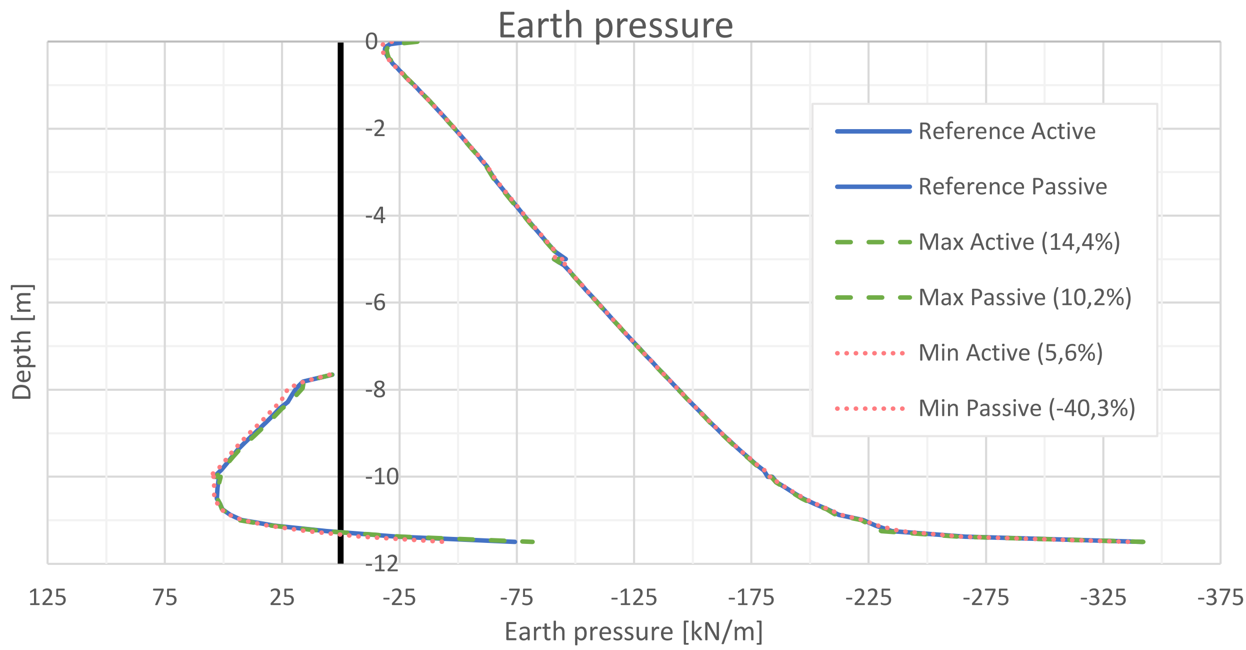

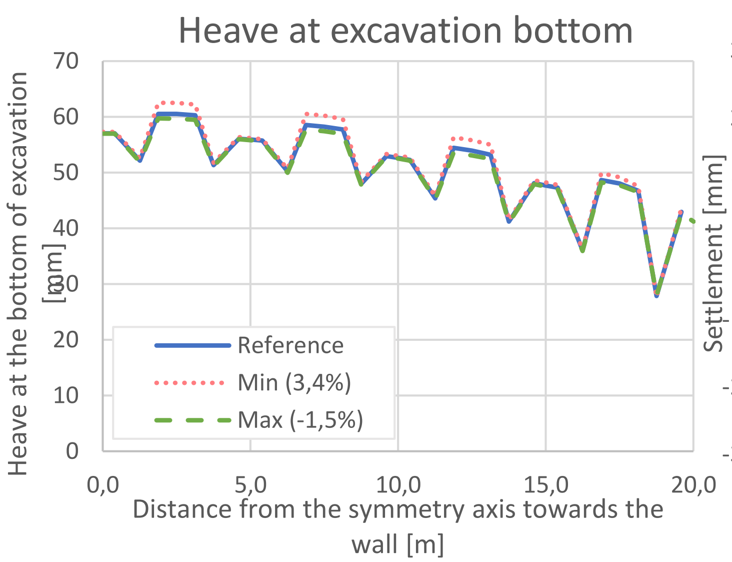

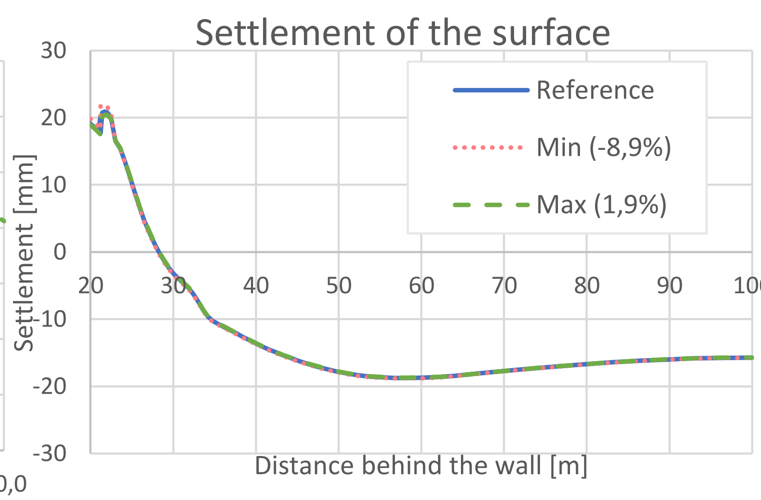

#3 Interface stiffness between diaphragm wall and adjacent soil, E’ (HSs)

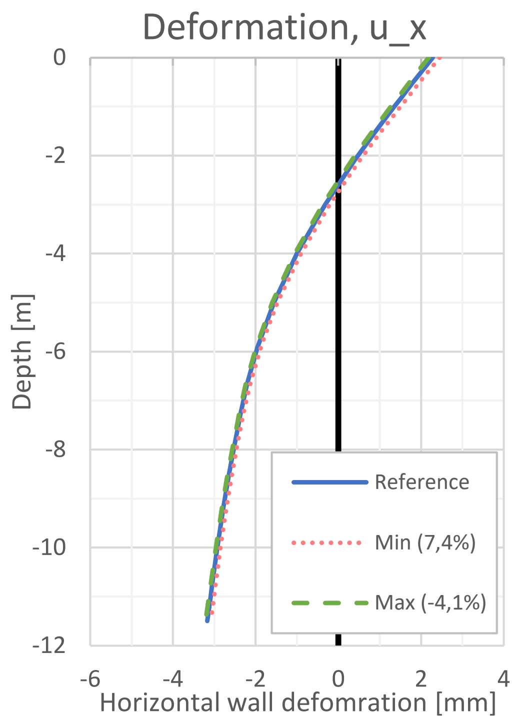

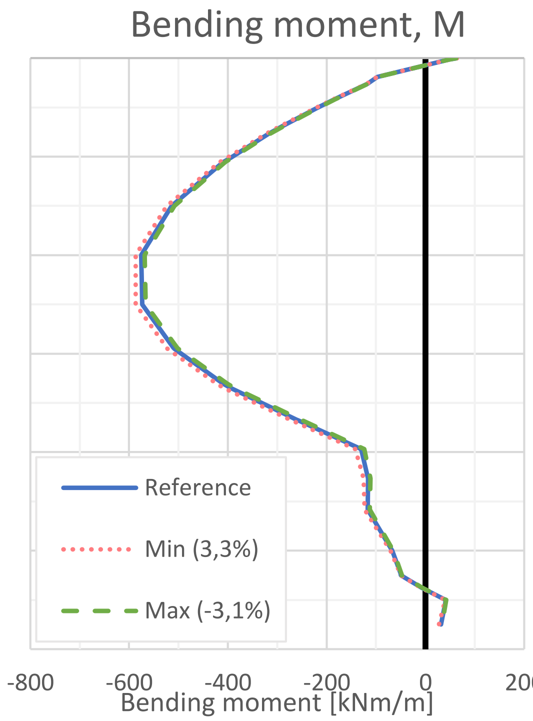

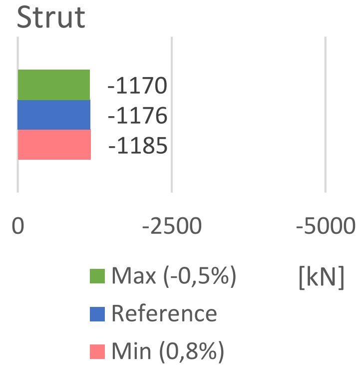

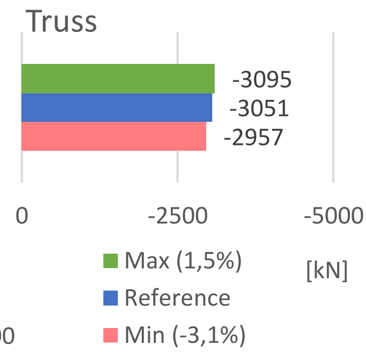

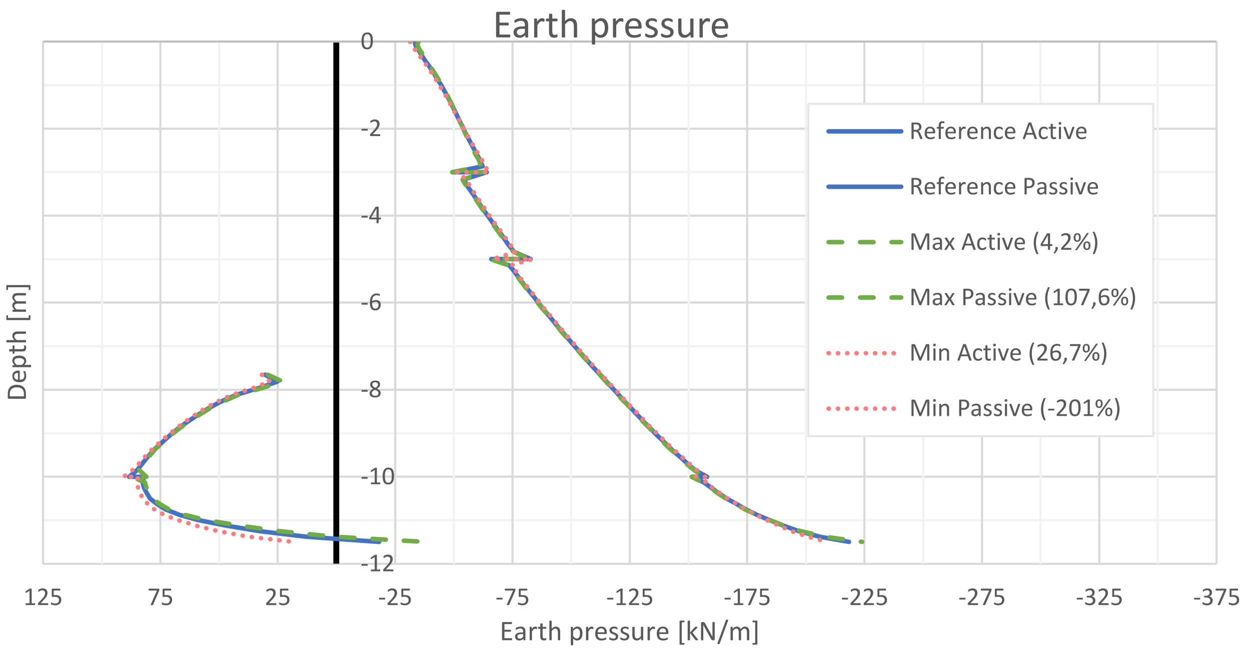

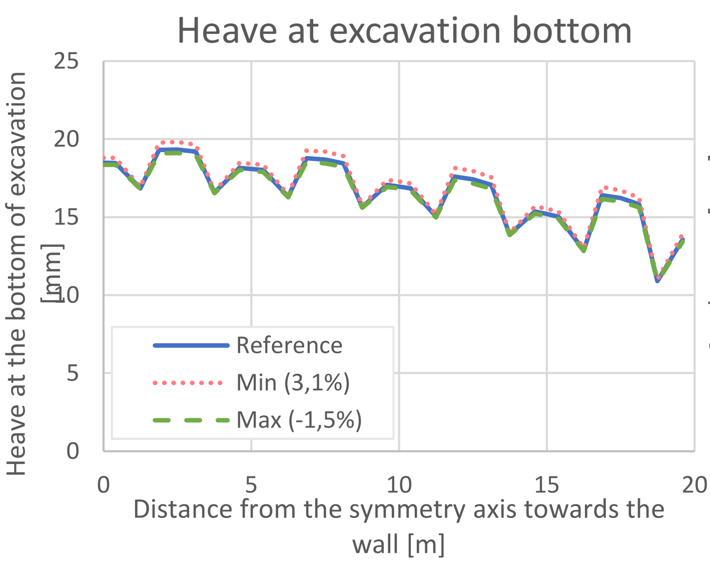

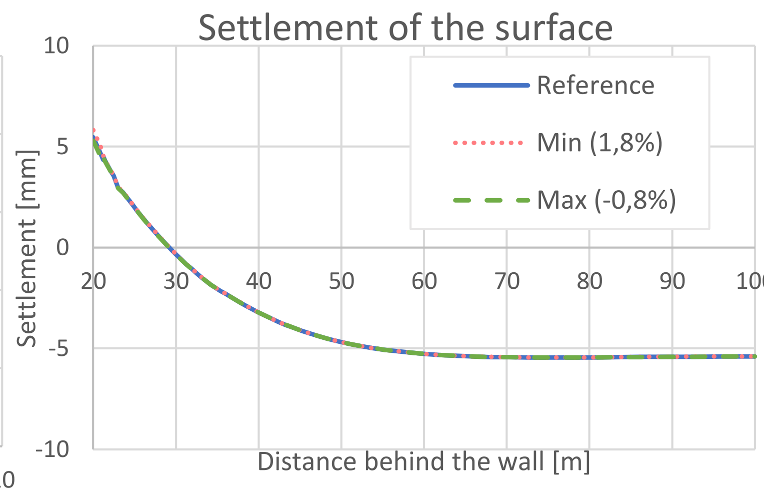

#4 Interface stiffness between diaphragm wall and adjacent soil, E' (ADP)

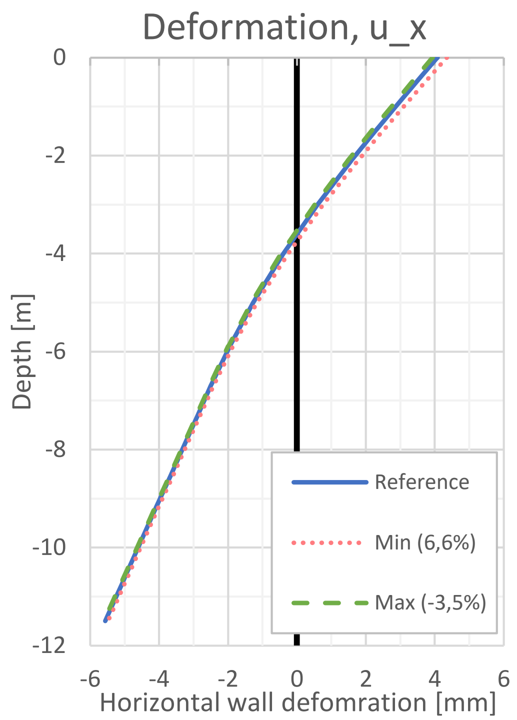

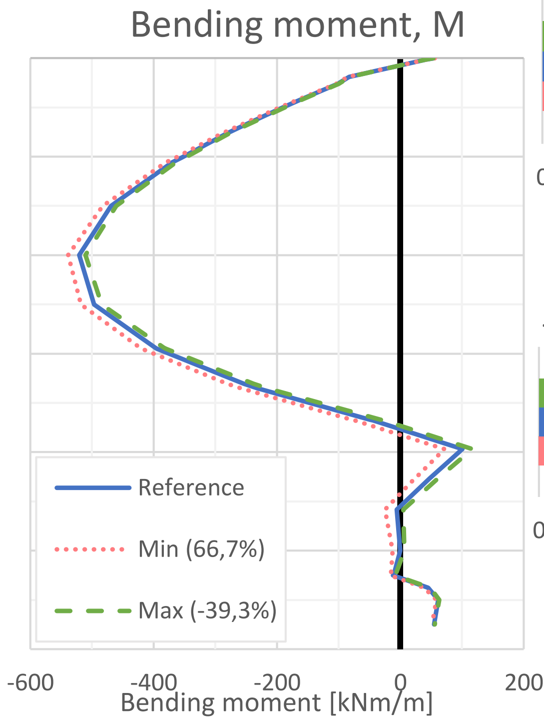

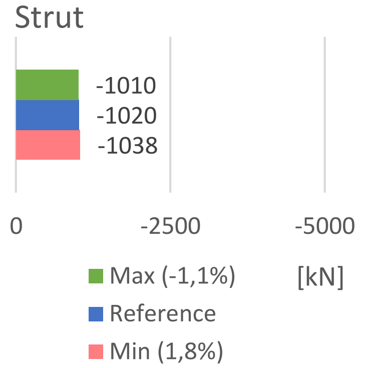

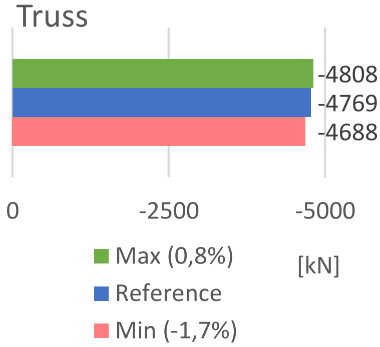

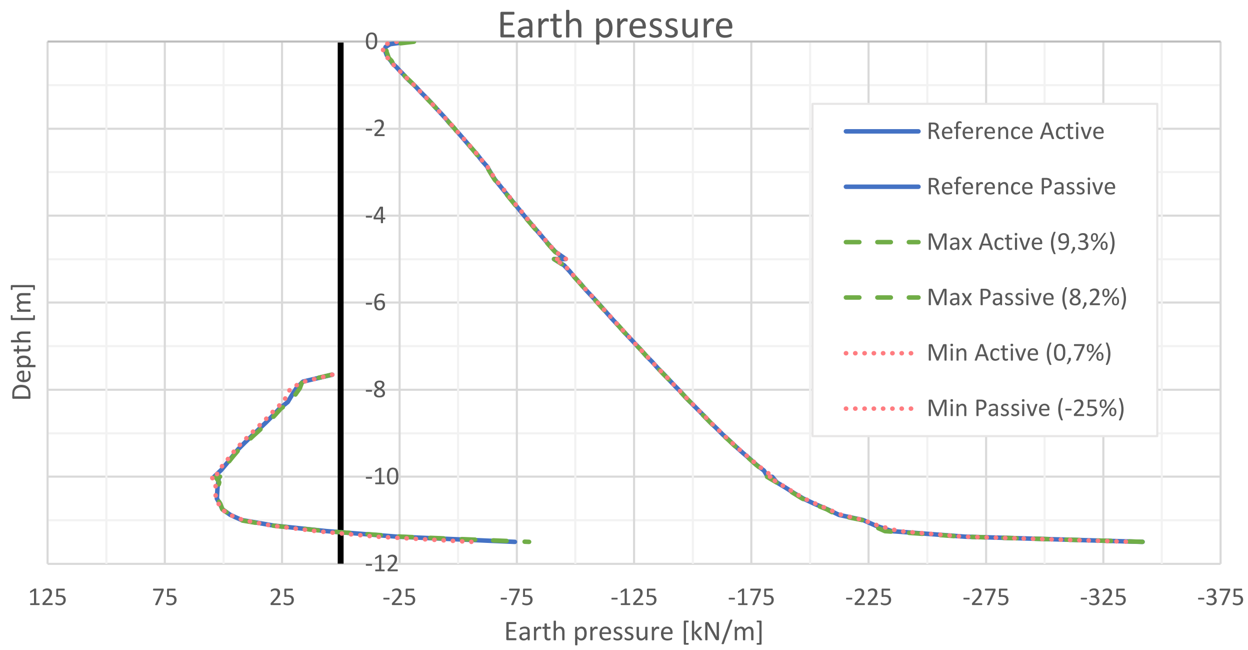

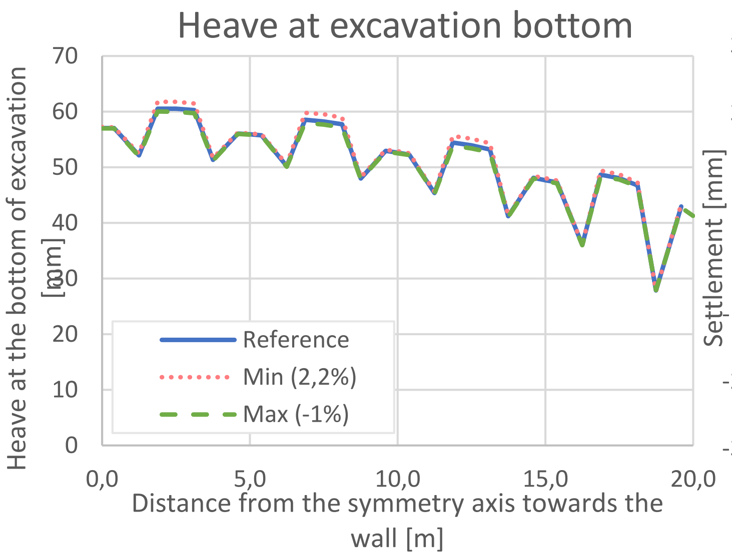

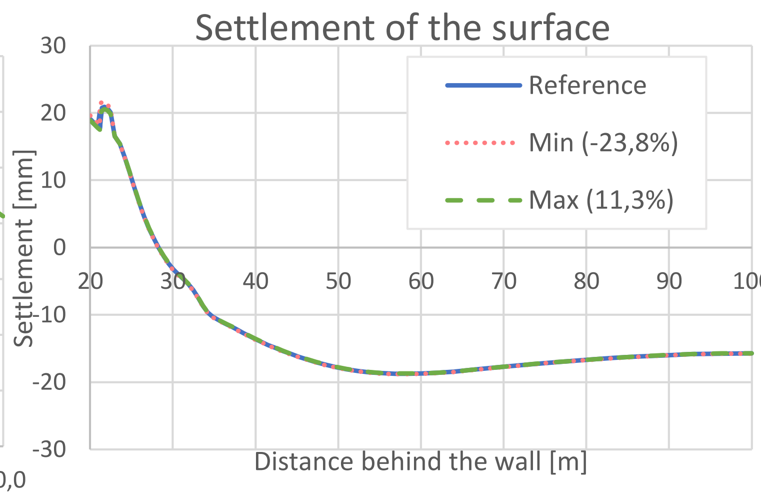

#5 Interface between diaphragm wall and cross-wall, R_inter (HSs)

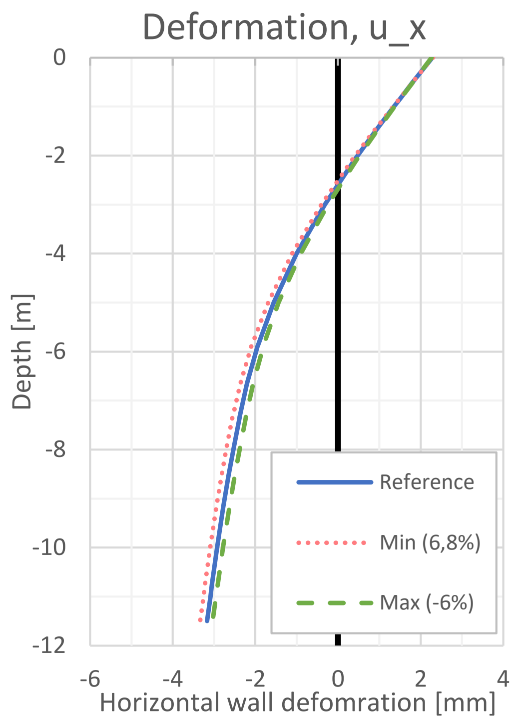

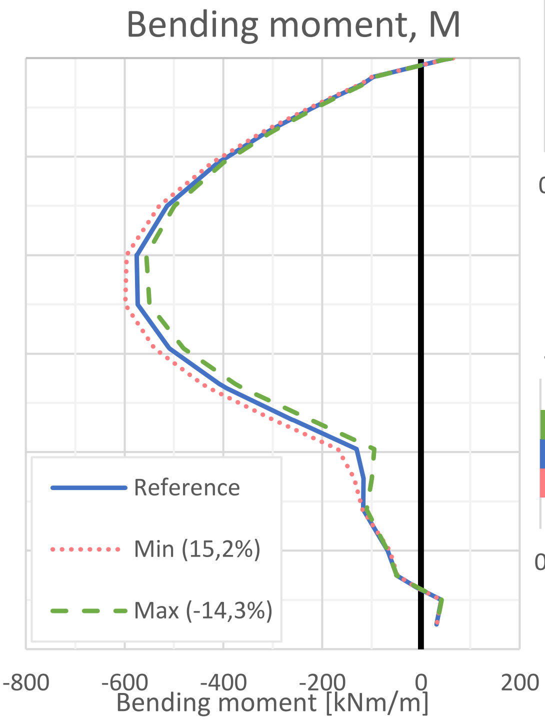

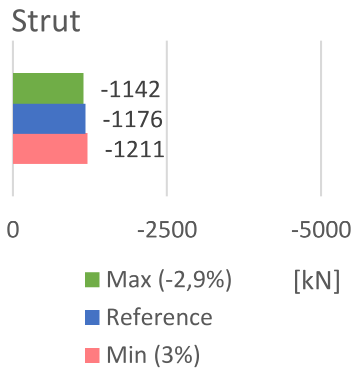

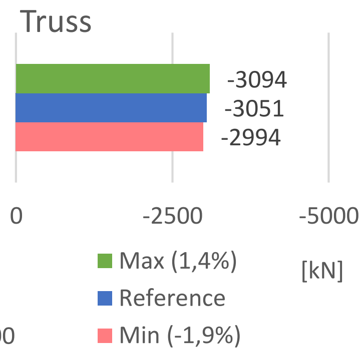

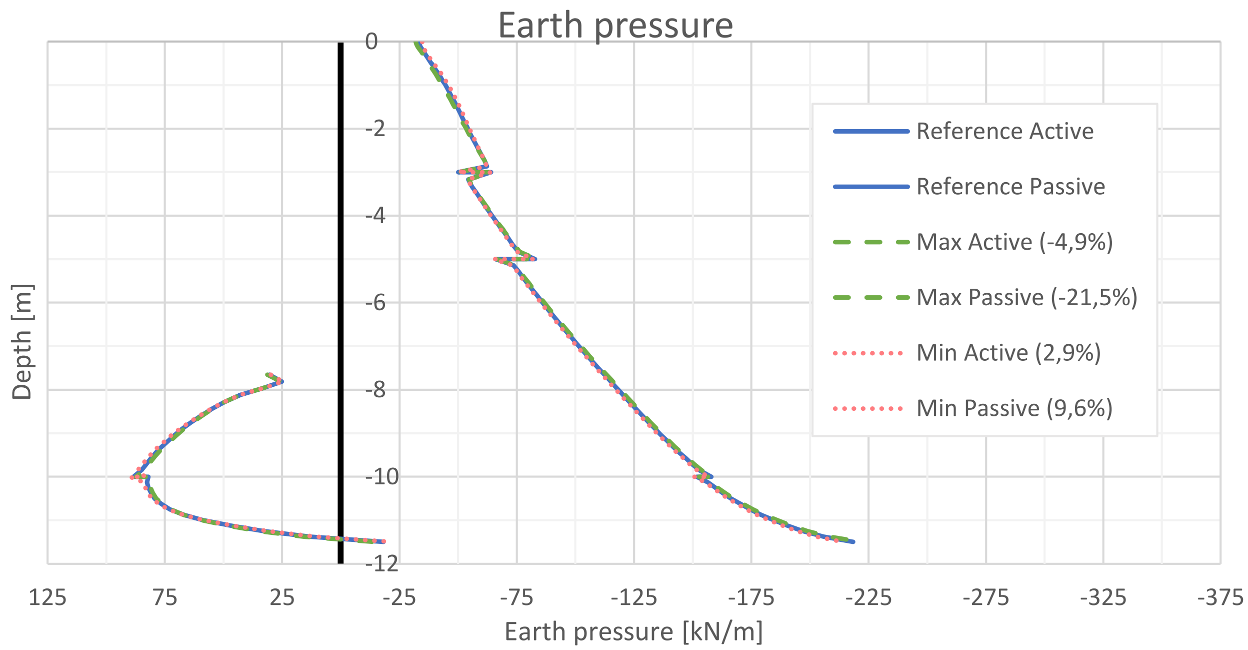

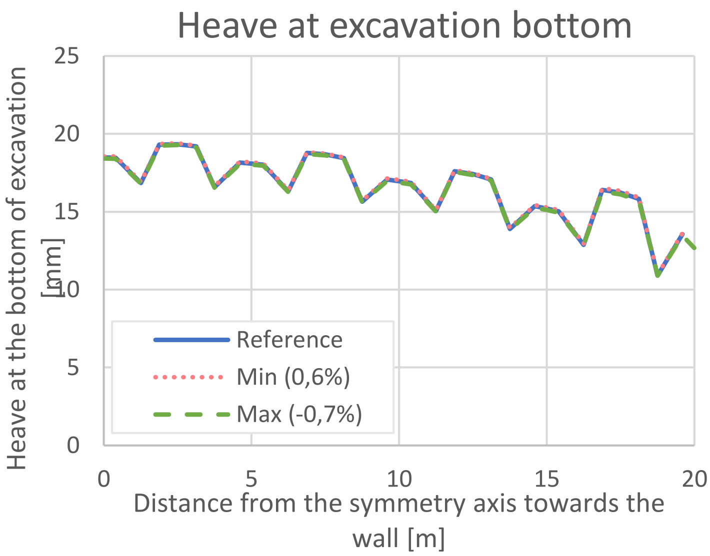

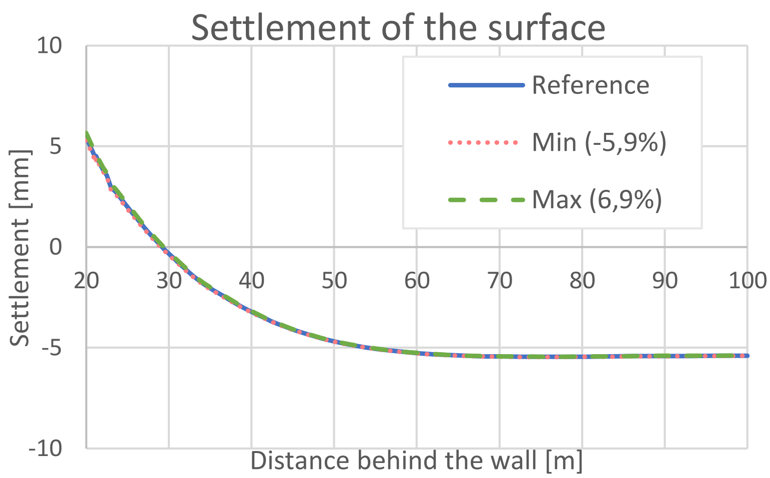

#6 Interface between diaphragm wall and cross-wall, R_inter (ADP)

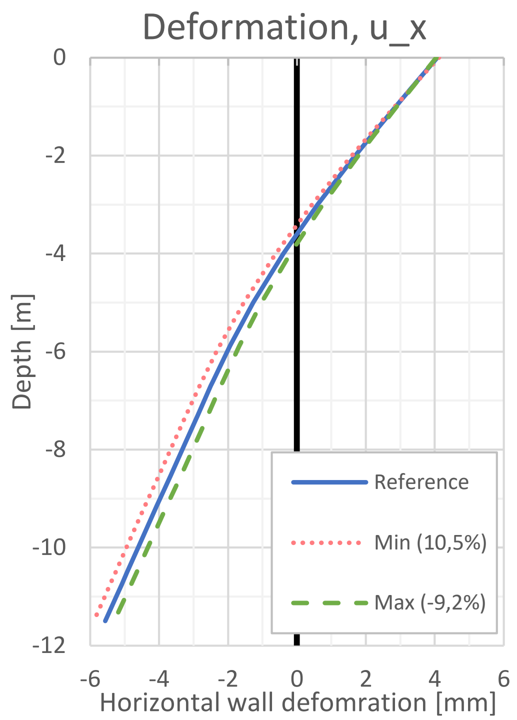

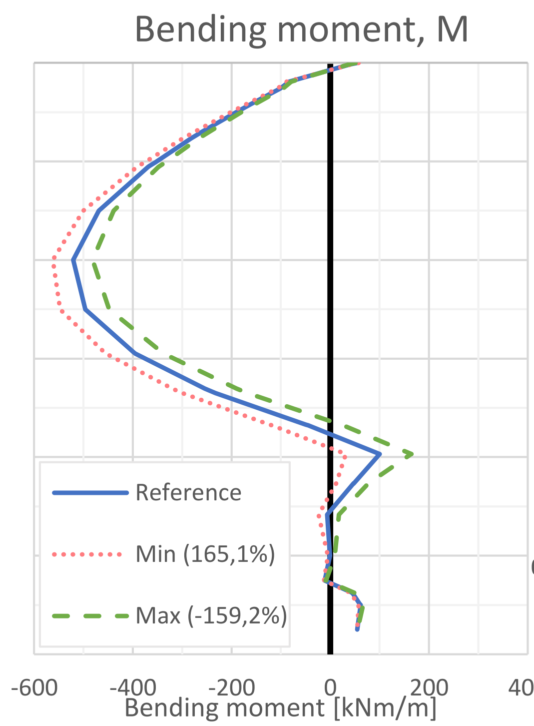

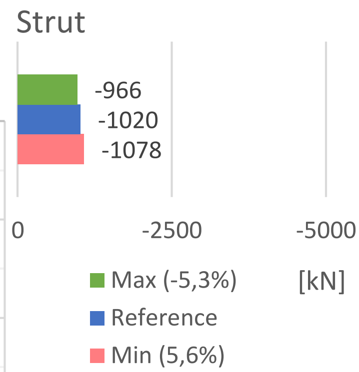

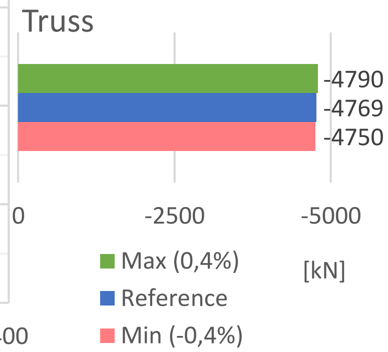

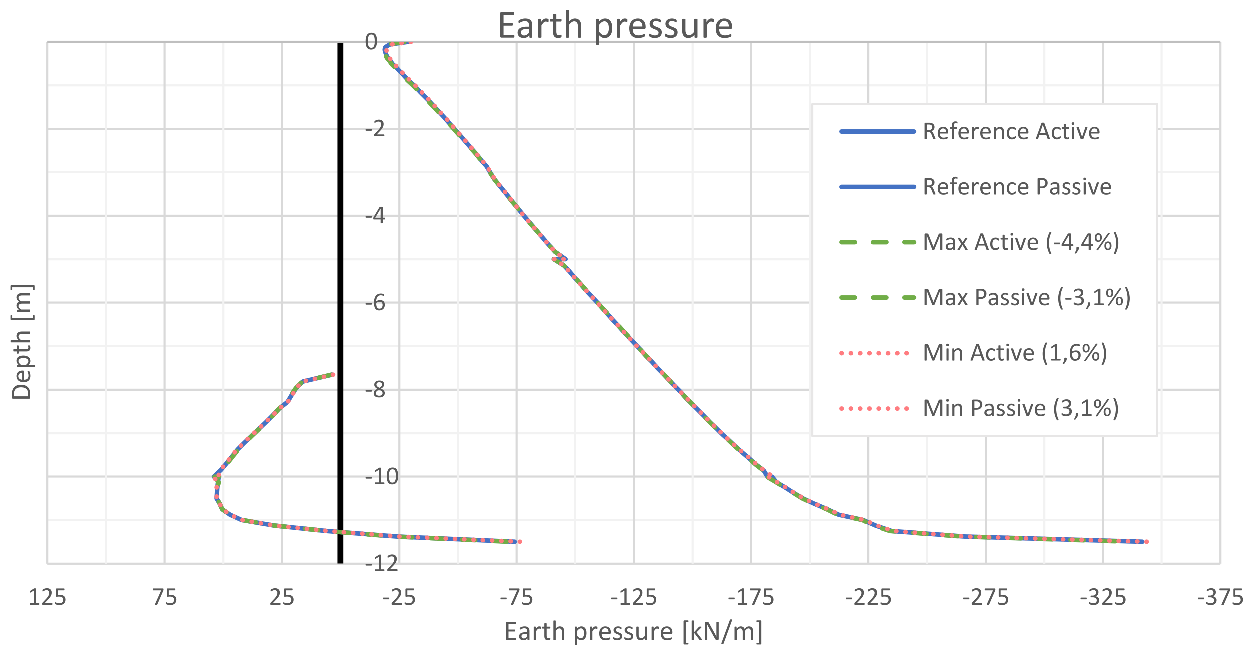

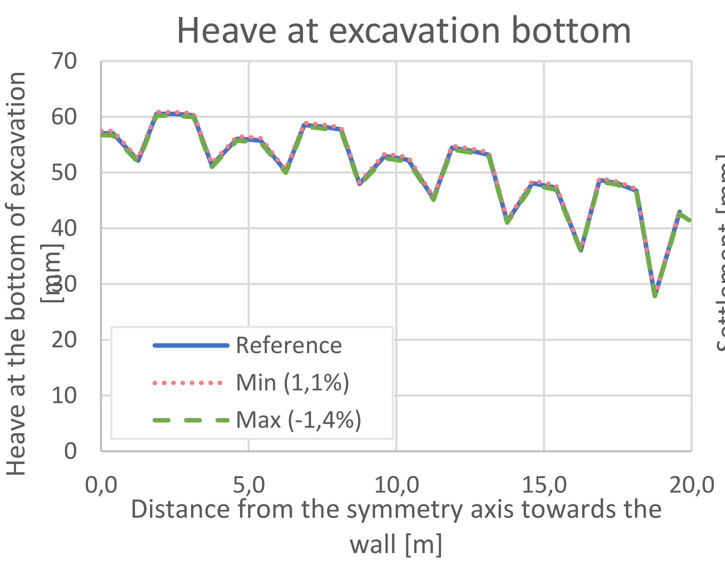

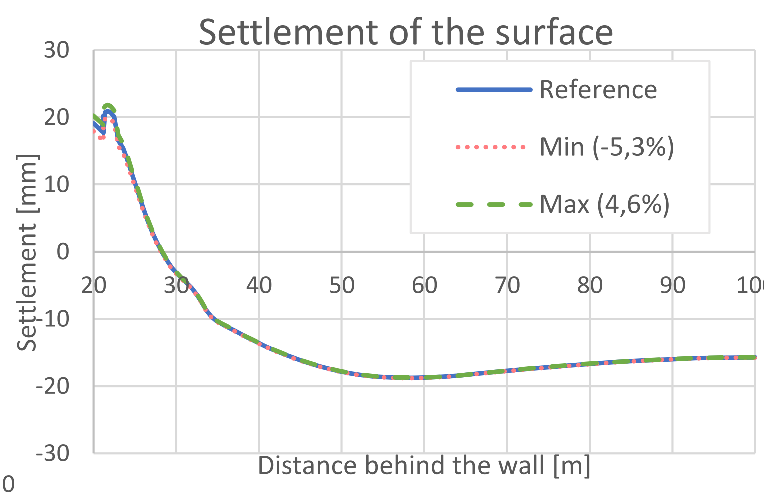

#7 Interface stiffness between diaphragm wall and cross-wall, E' (HSs)

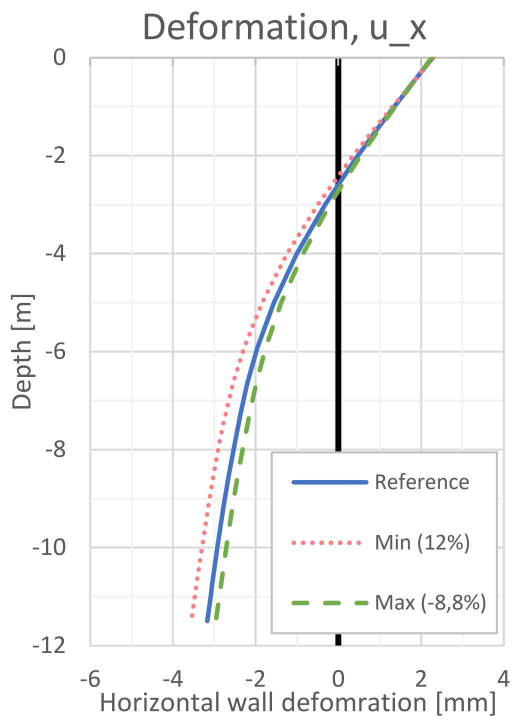

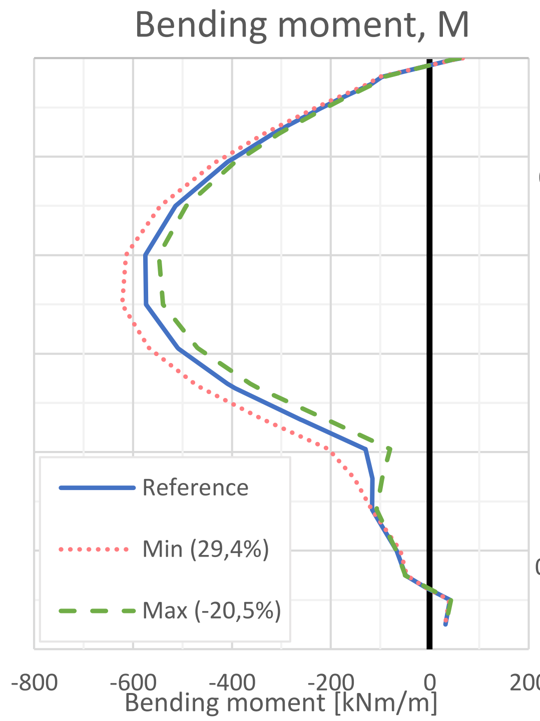

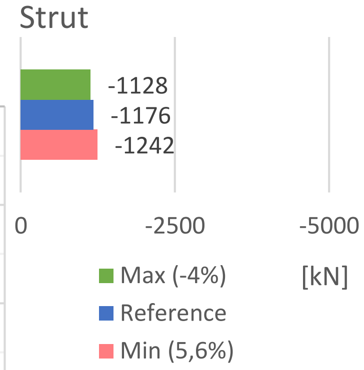

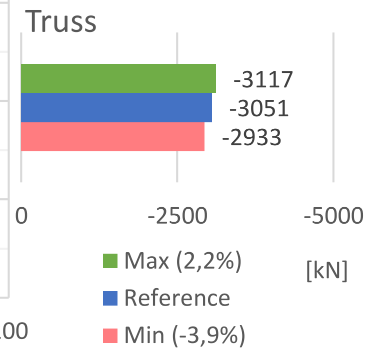

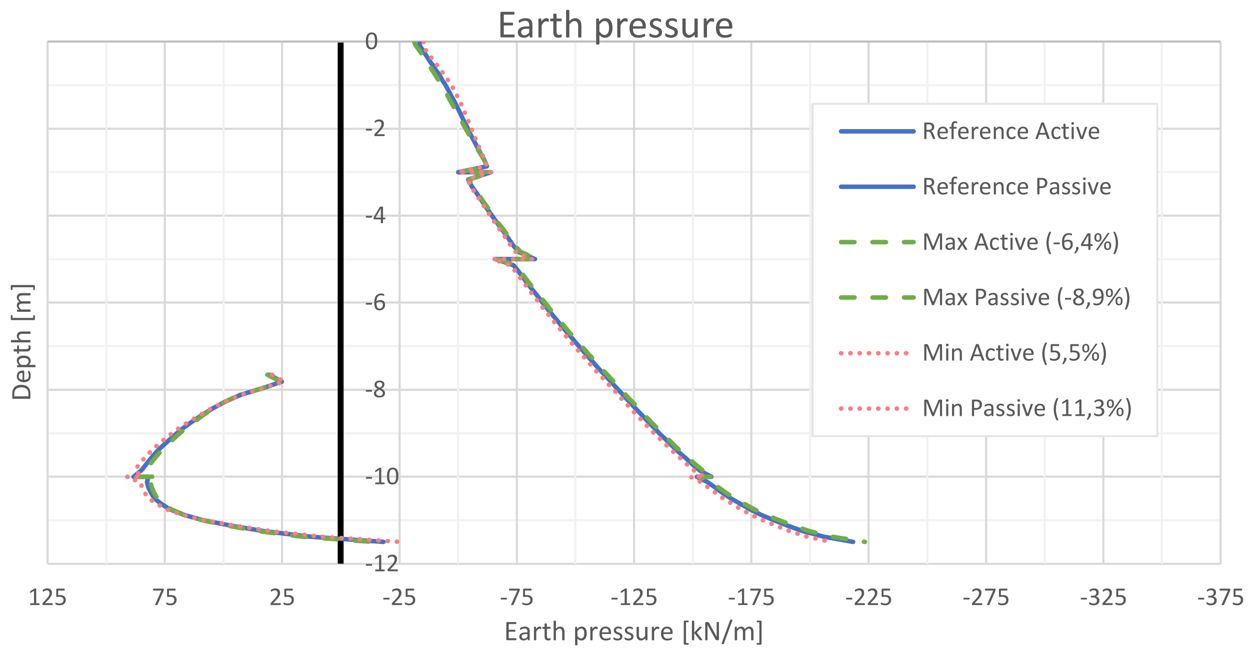

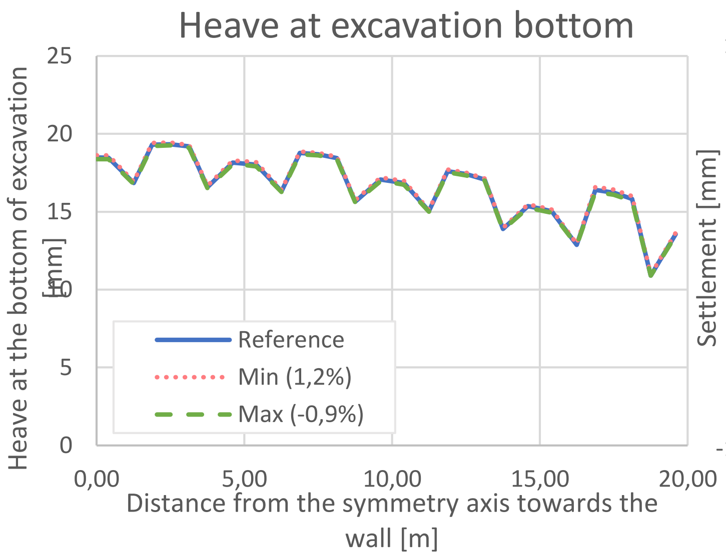

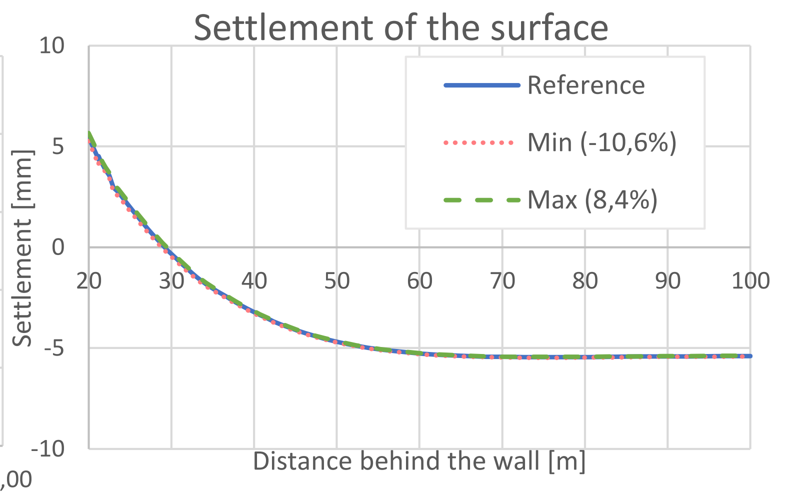

#8 Interface stiffness between diaphragm wall and cross-wall, E' (ADP)

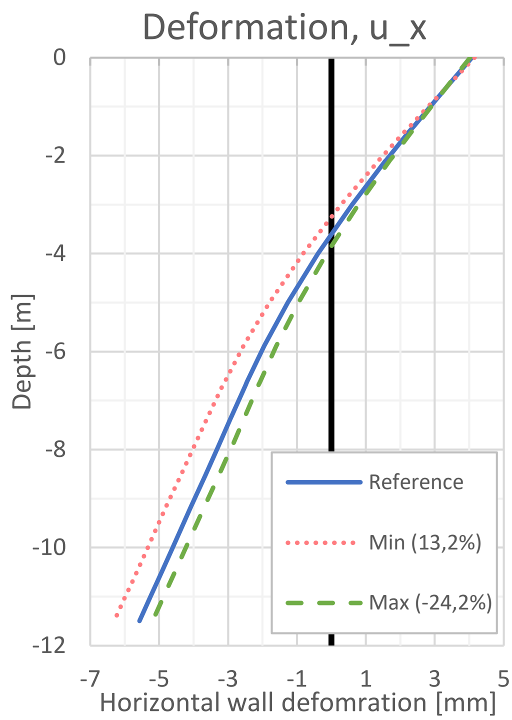

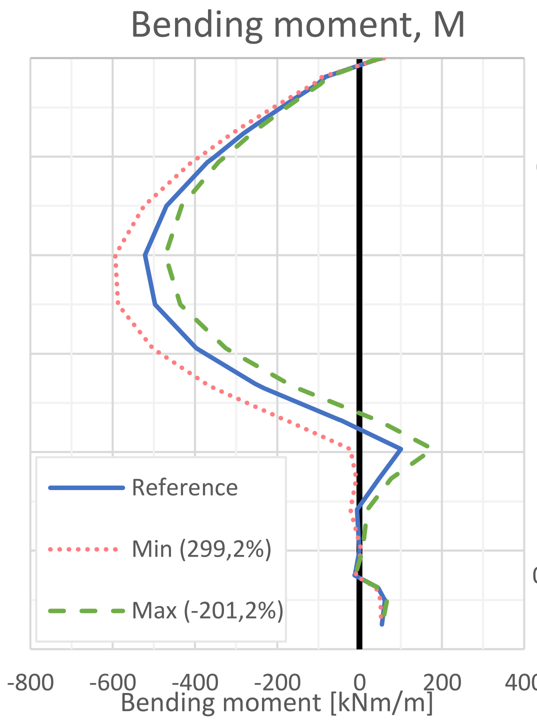

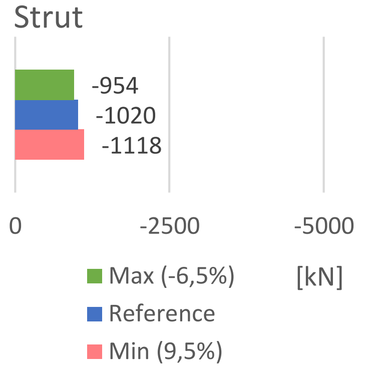

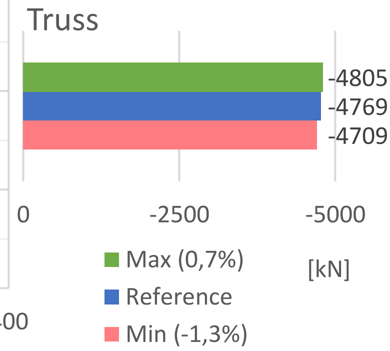

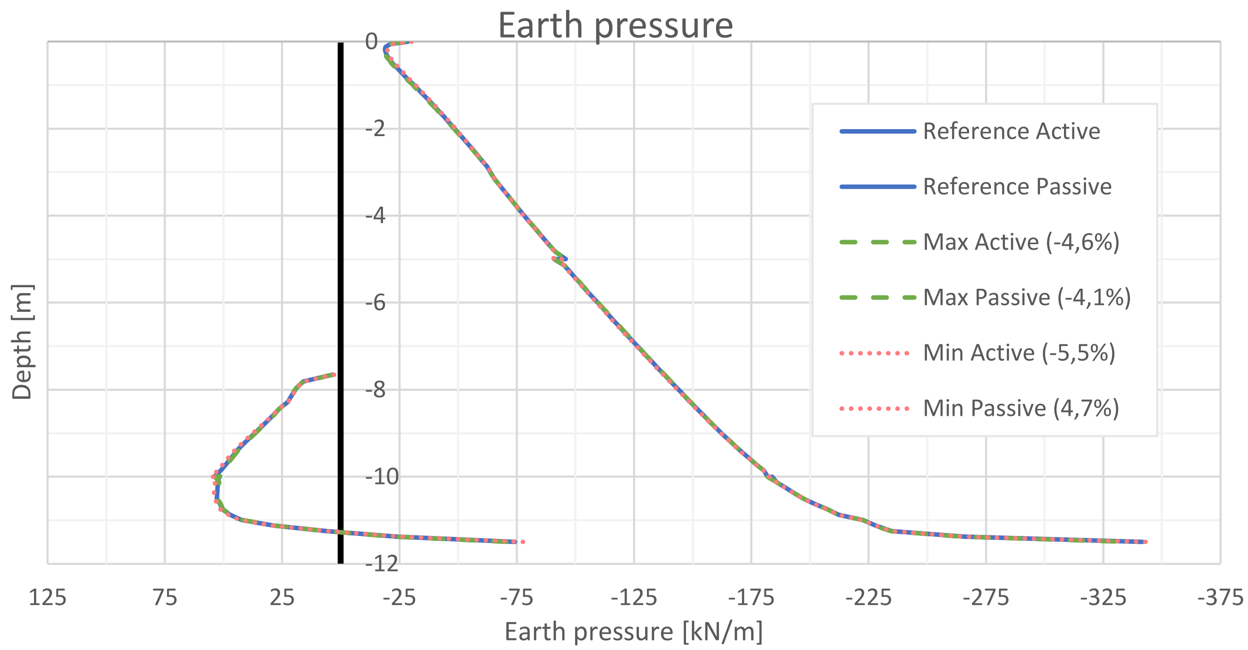

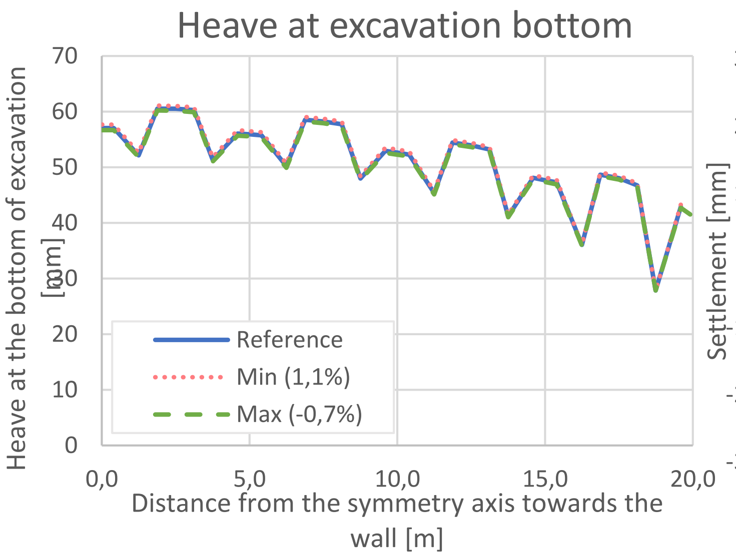

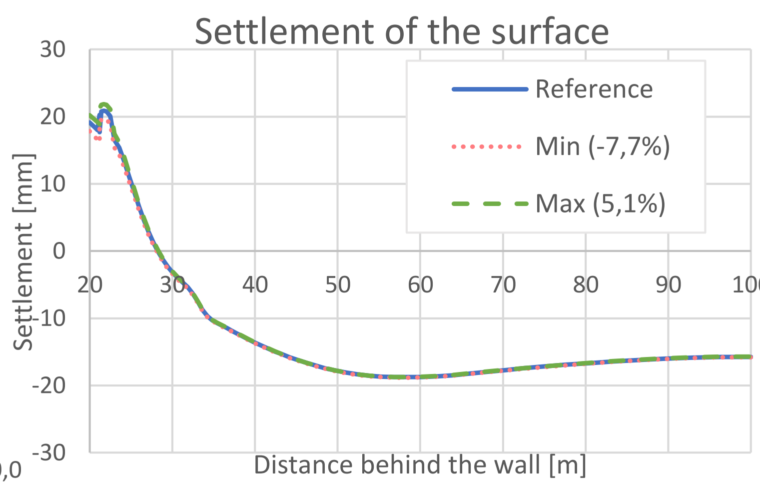

#9 Stiffness HSs (new reference)
E50, Eoed = 0,5*E50, Eur=2*E50

#10 Stiffness HSs
E50*MIN/MAX,Eoed = 0,5*E50, Eur=2*E50

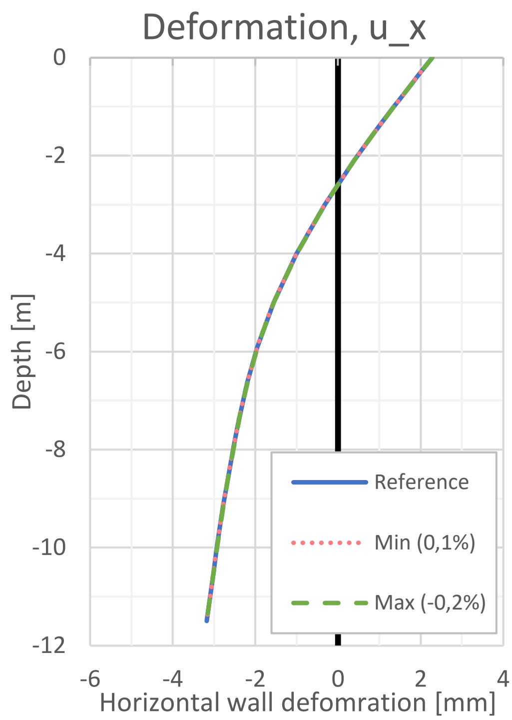

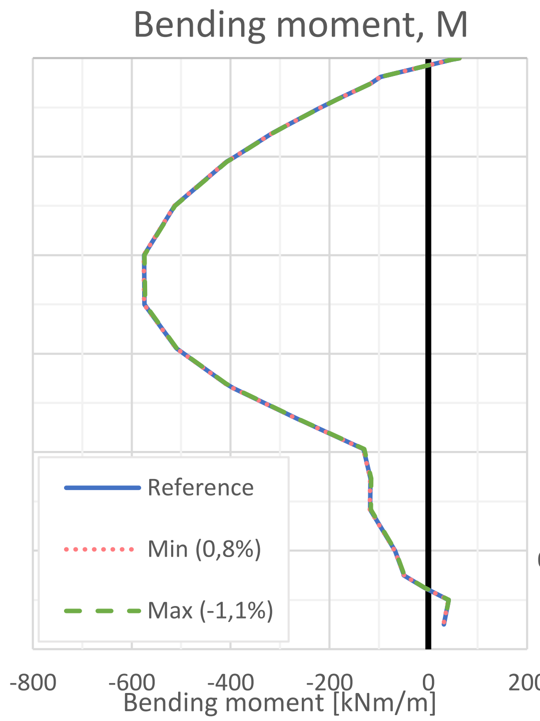

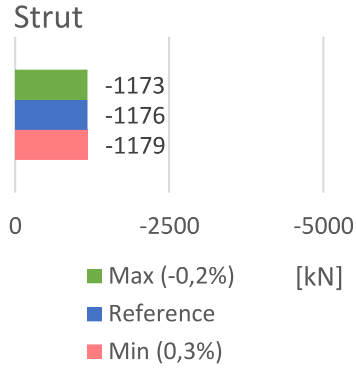

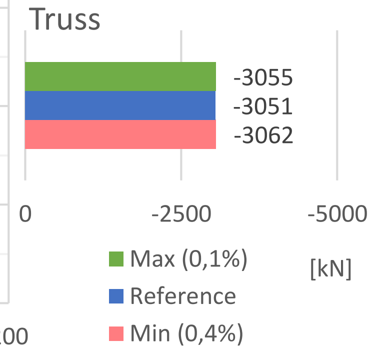

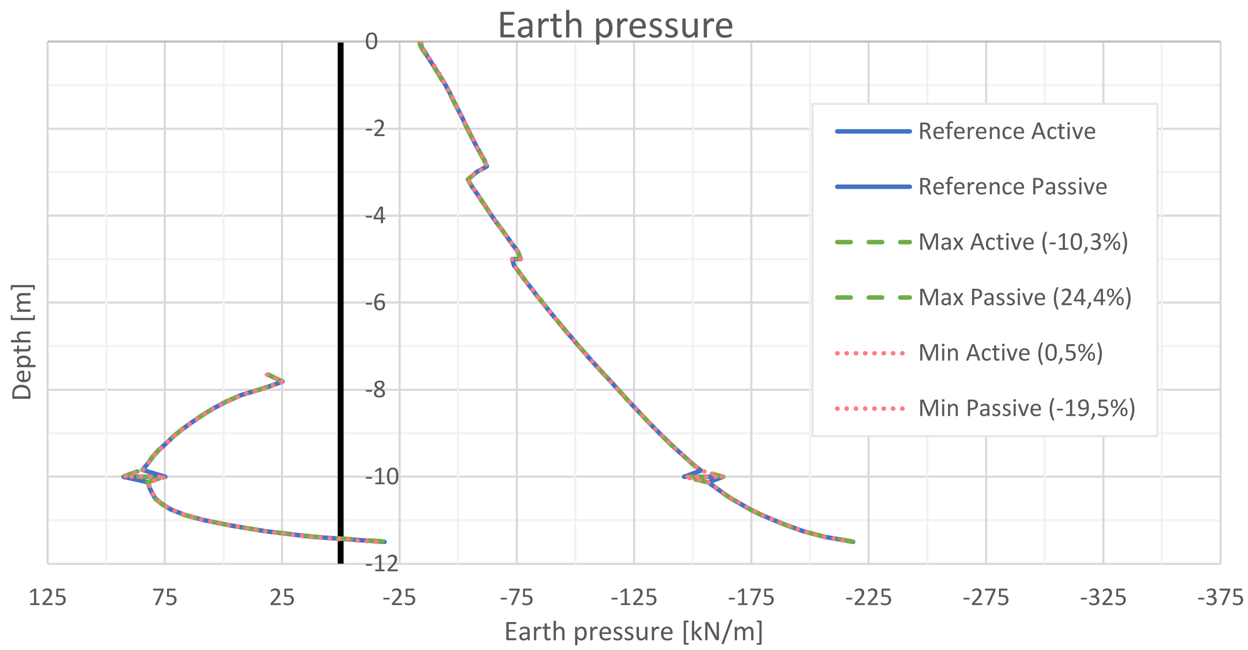

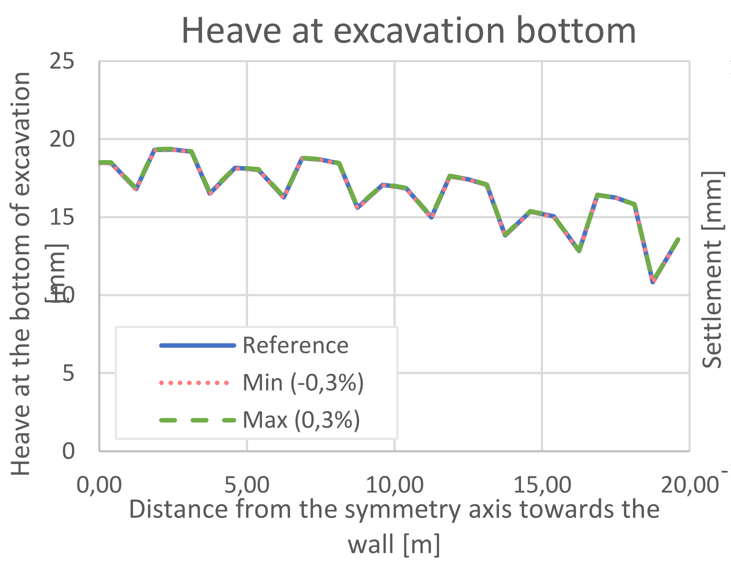

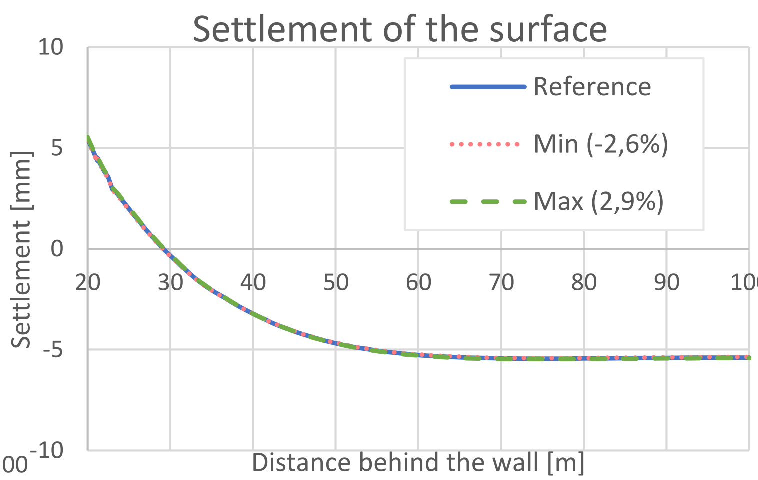

#11 Stiffness HSs
E50*MIN/MAX,Eoed = 0,5*E50, Eur=4*E50

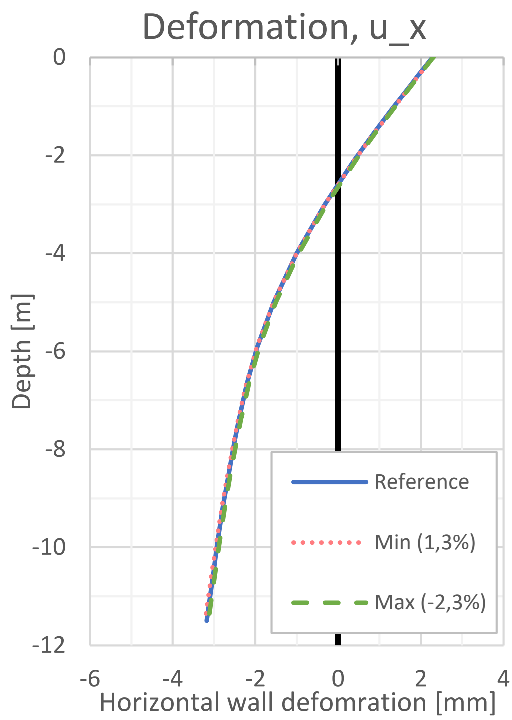

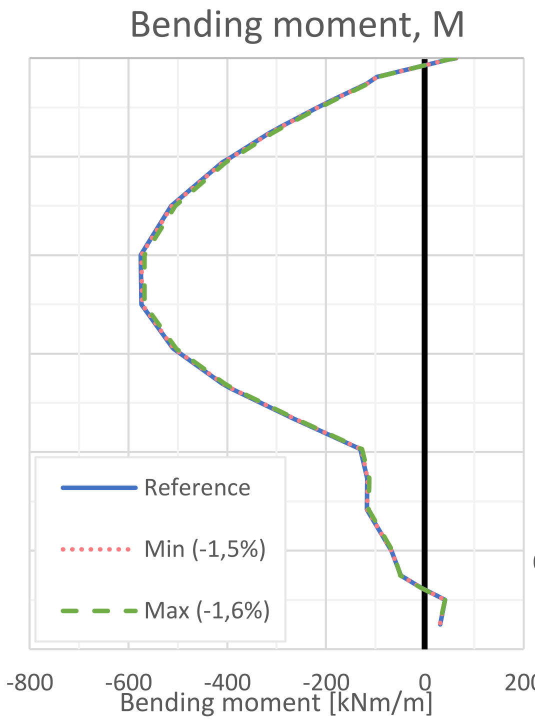

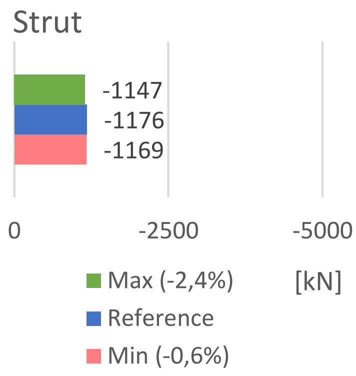

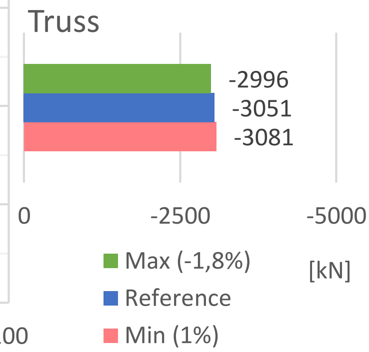

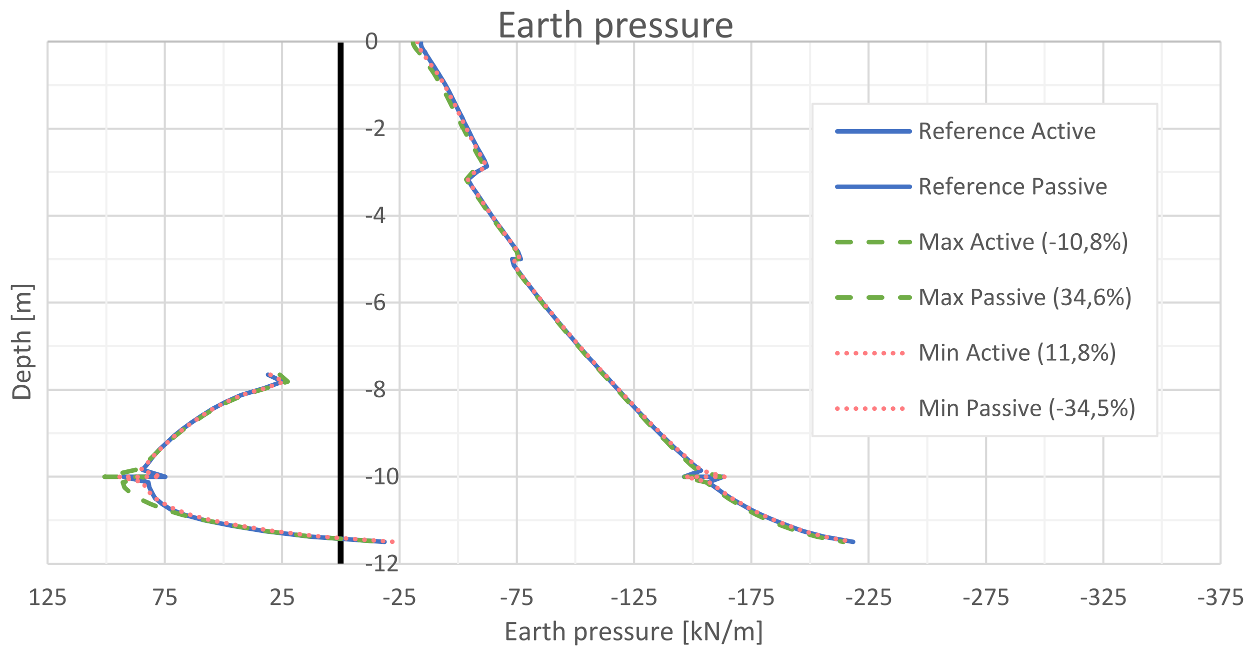

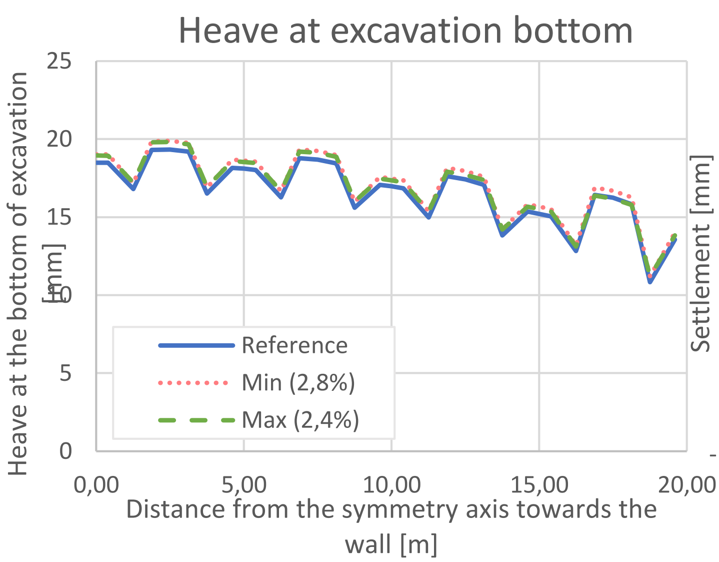

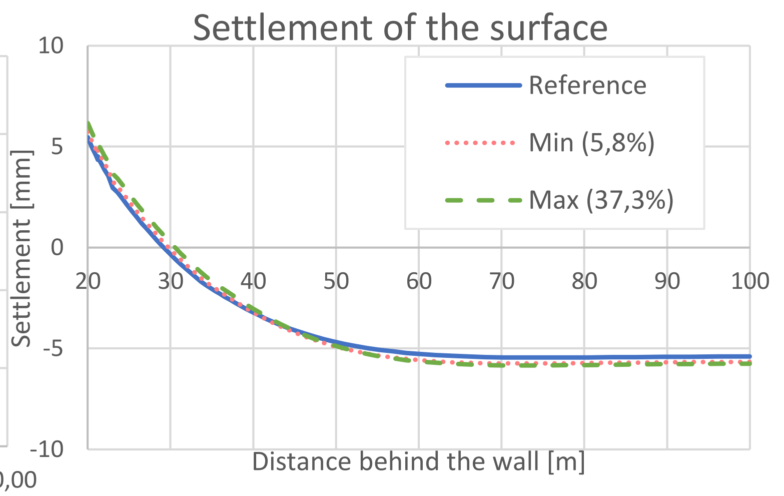

#12 Stiffness HSs
E50*MIN/MAX,Eoed = 0,5*E50, Eur=6*E50

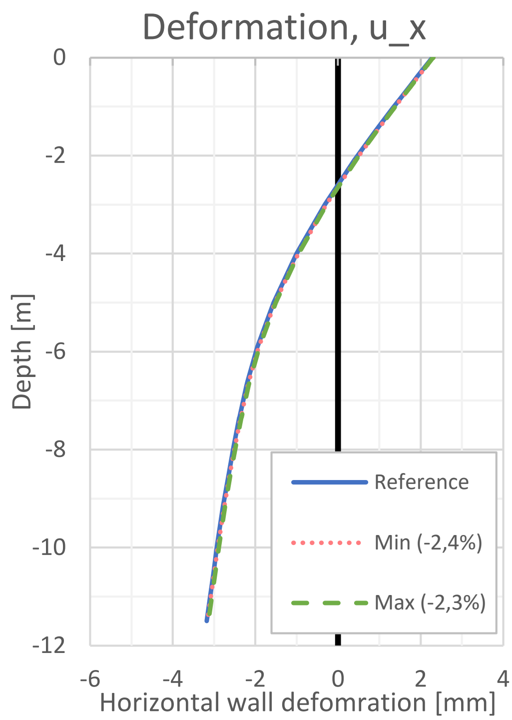

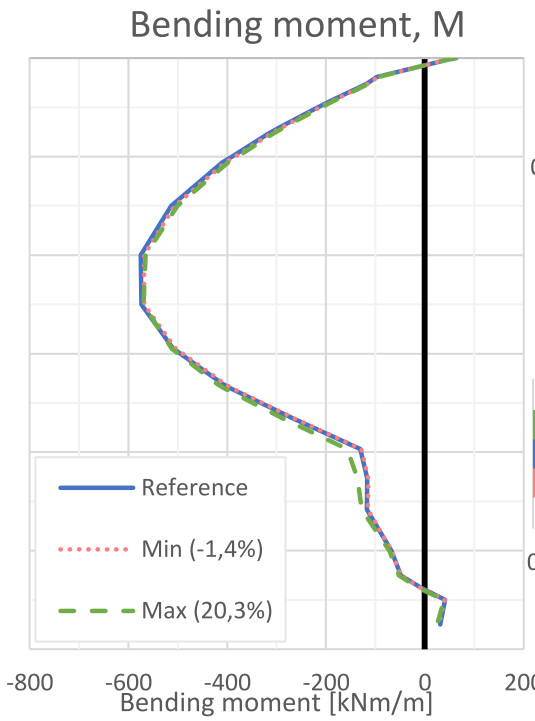

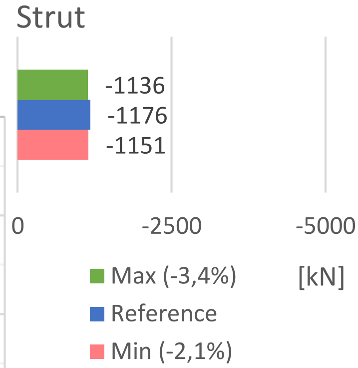

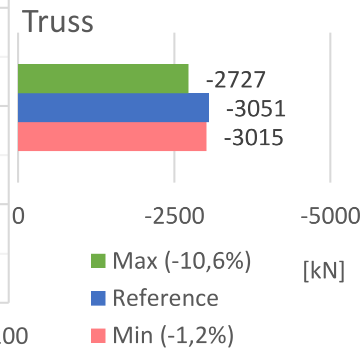

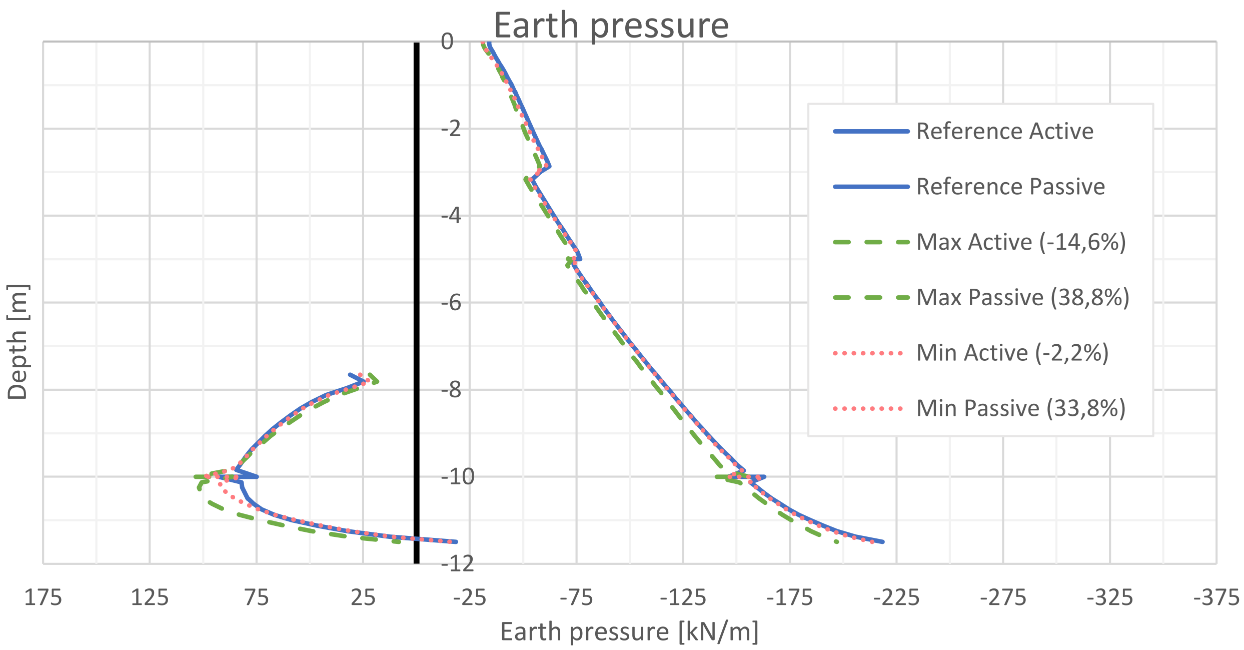

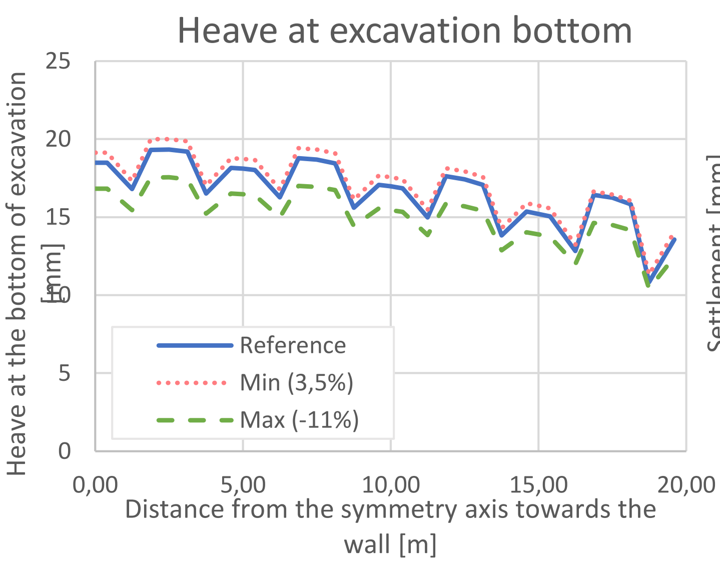

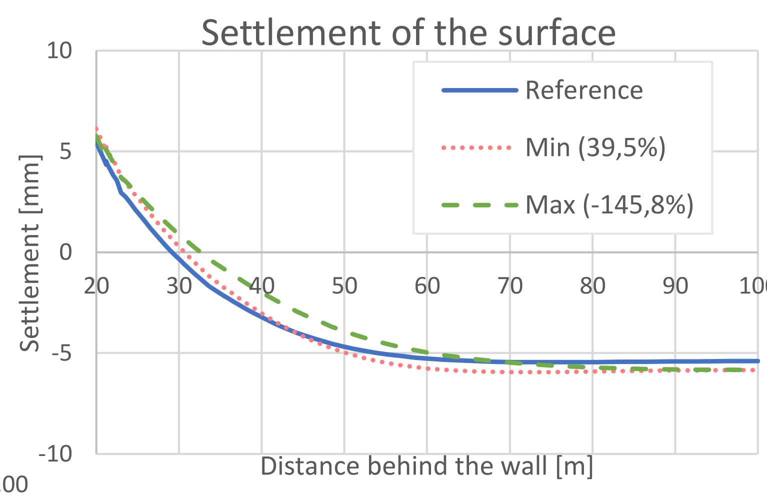

#13 Ratio un-/reloading shear modules over active shear strength, G_ur/s_u^A

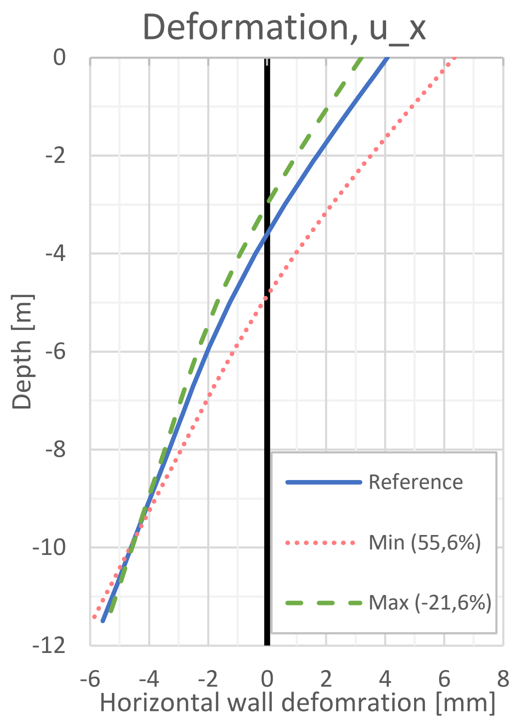

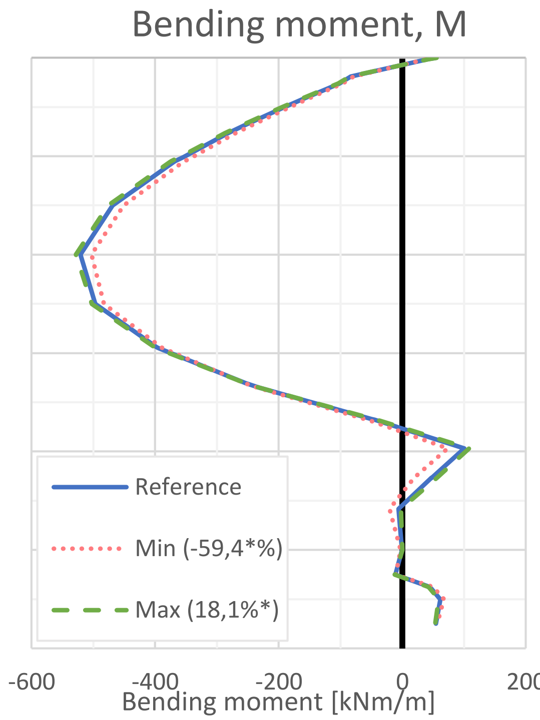

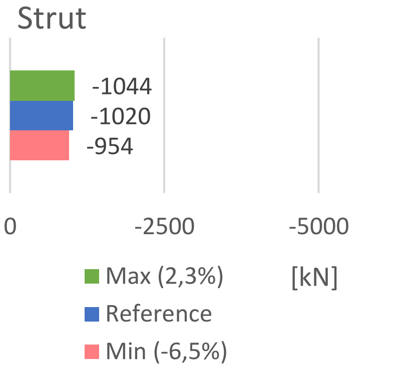

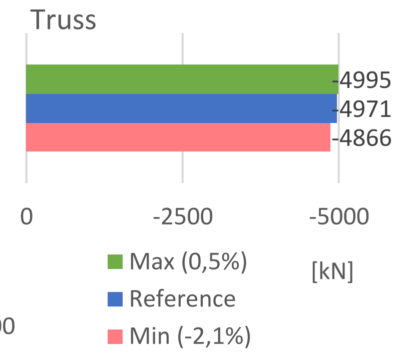

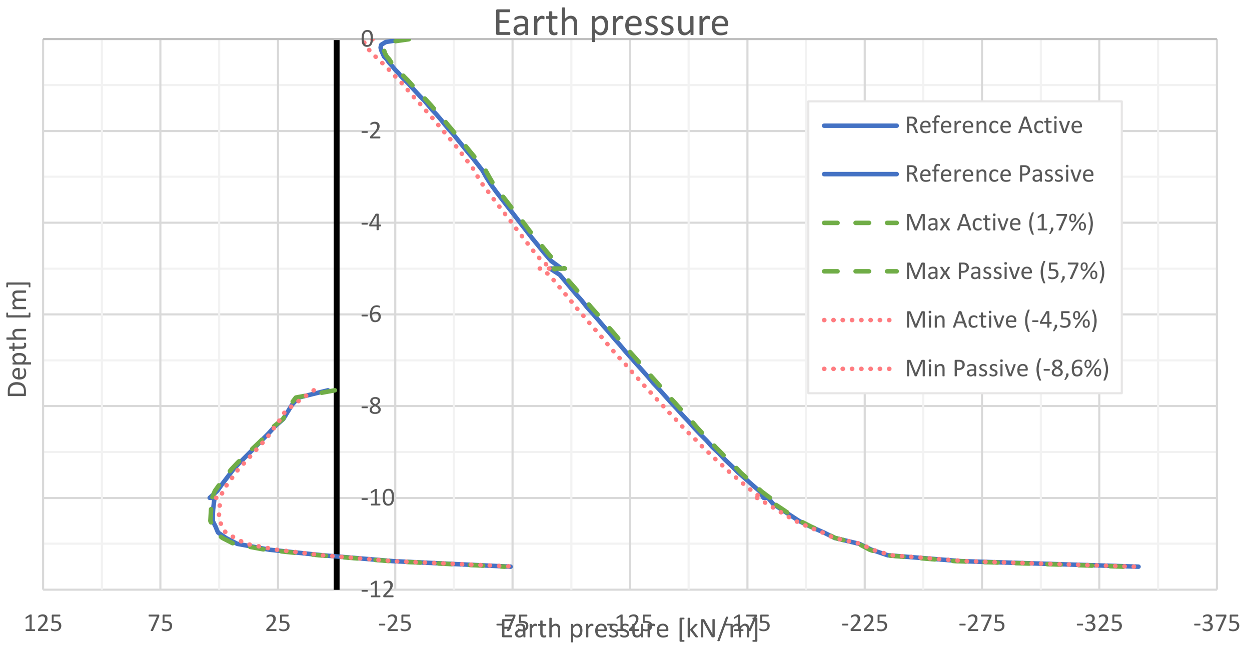

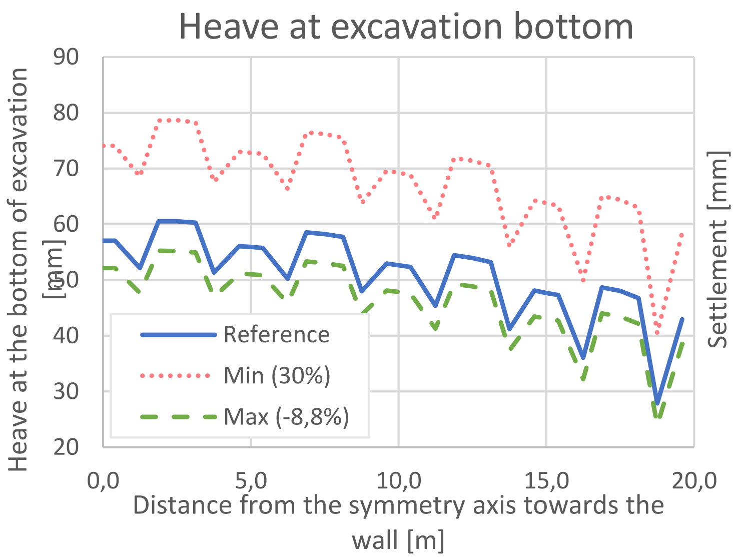

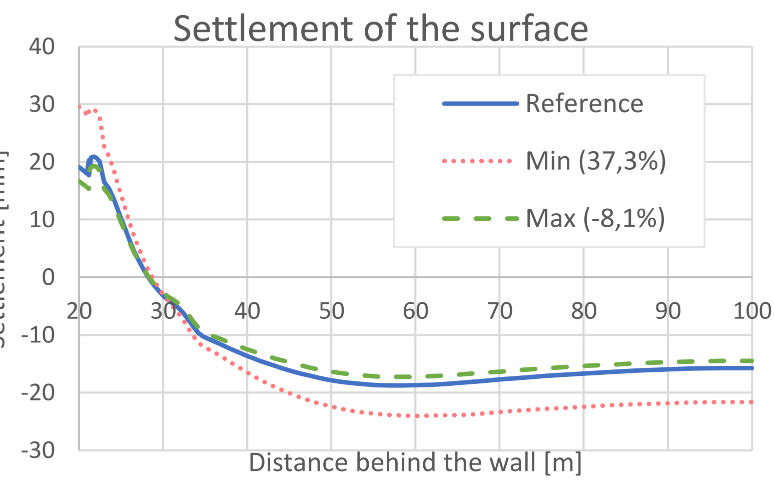

#14 Shear strain at failure in triaxial compression, gamma_f^C

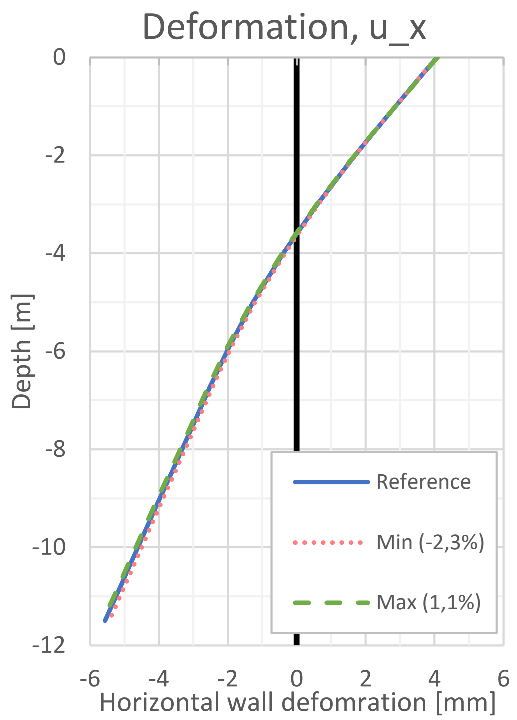

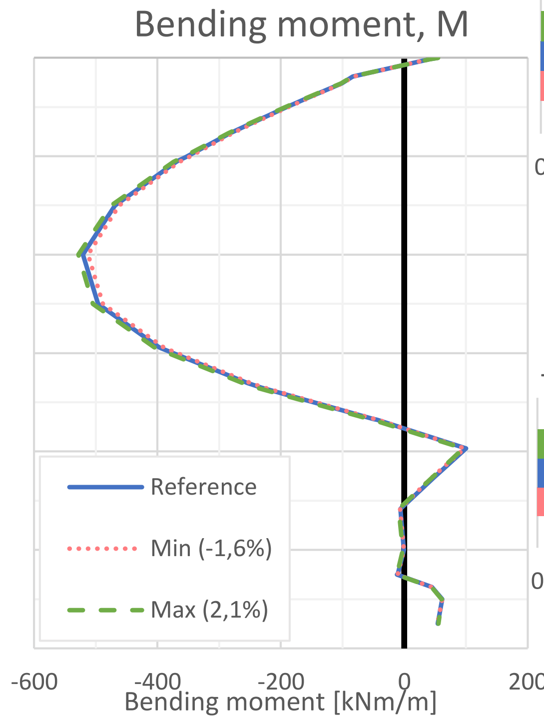

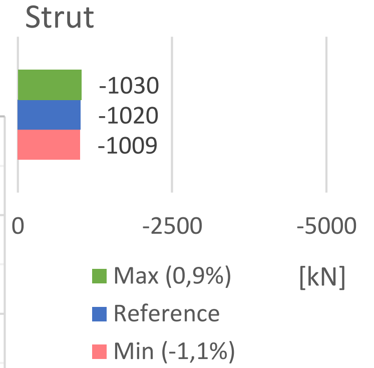

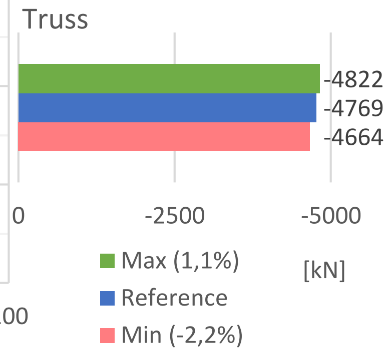

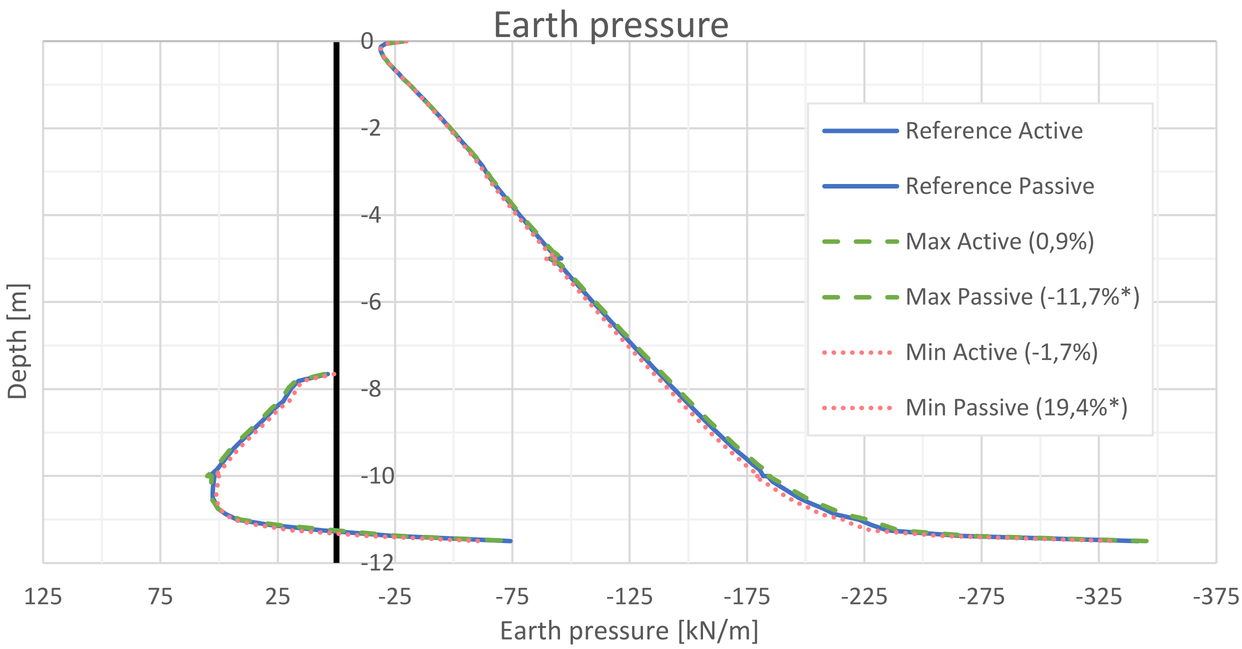

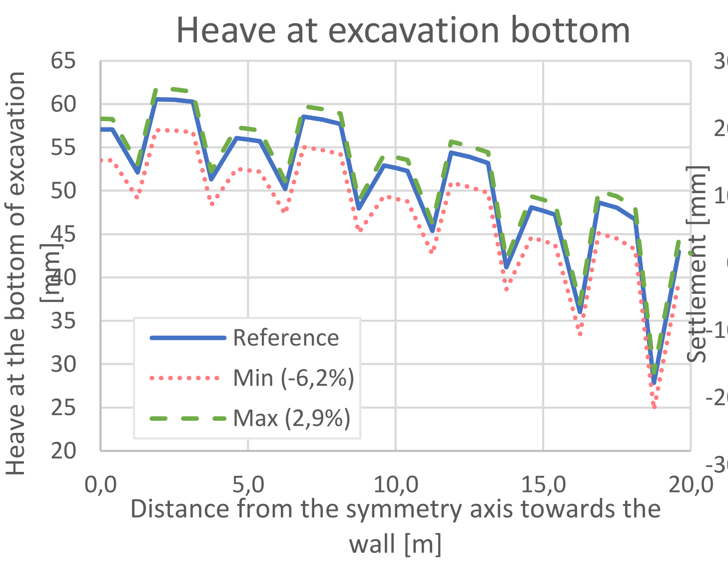

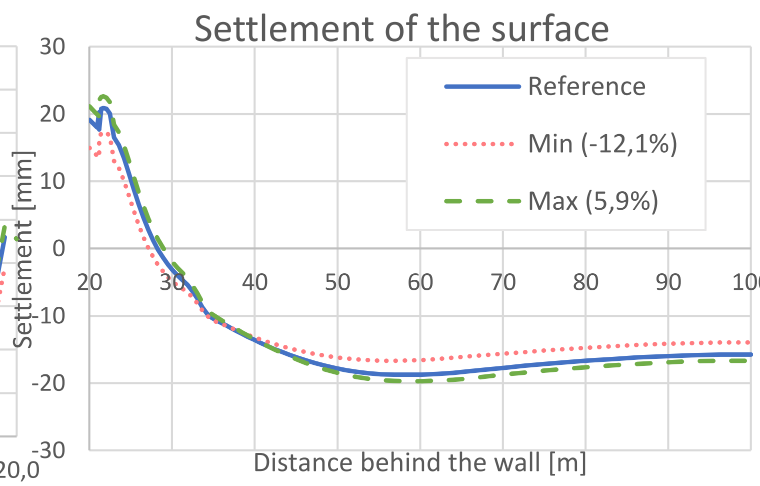

#15 Shear strain at failure in triaxial compression, gamma_f^E

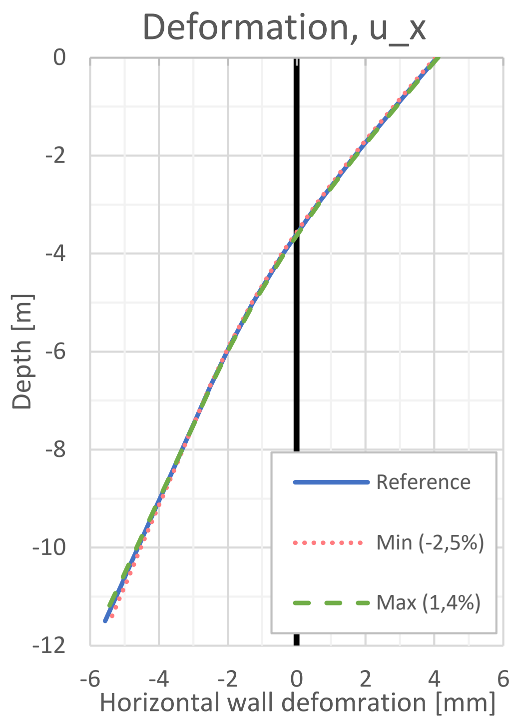

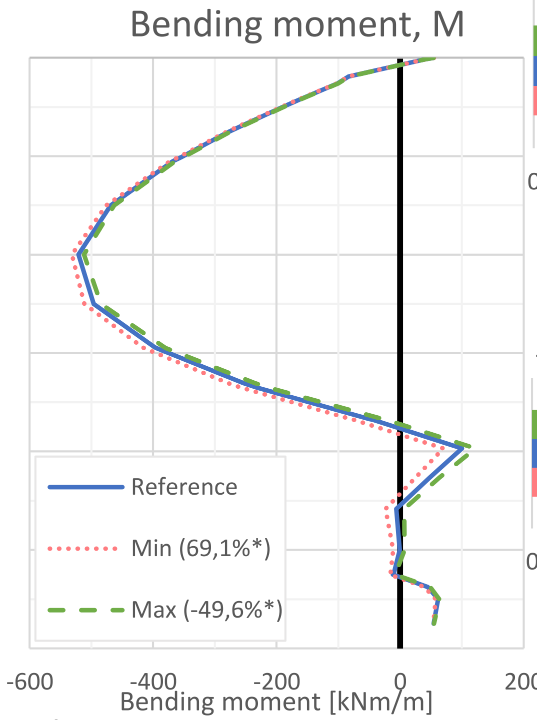

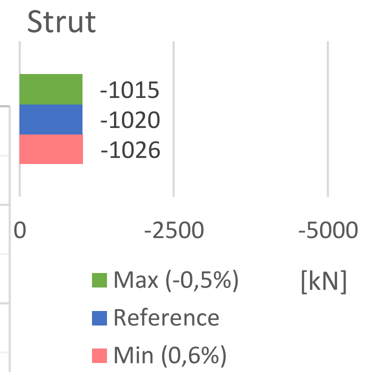

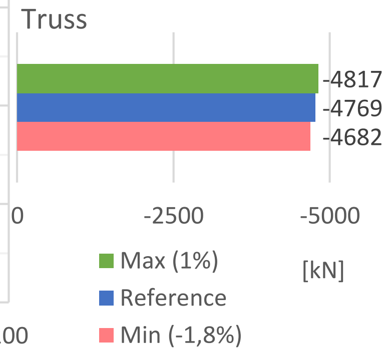

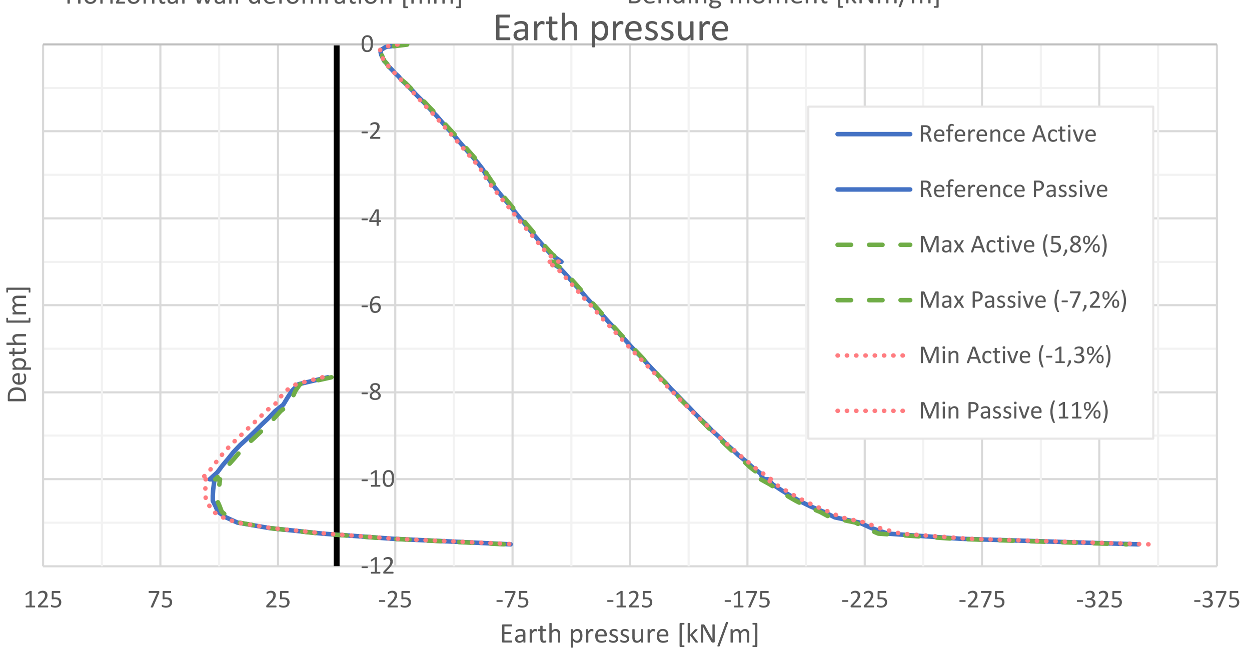

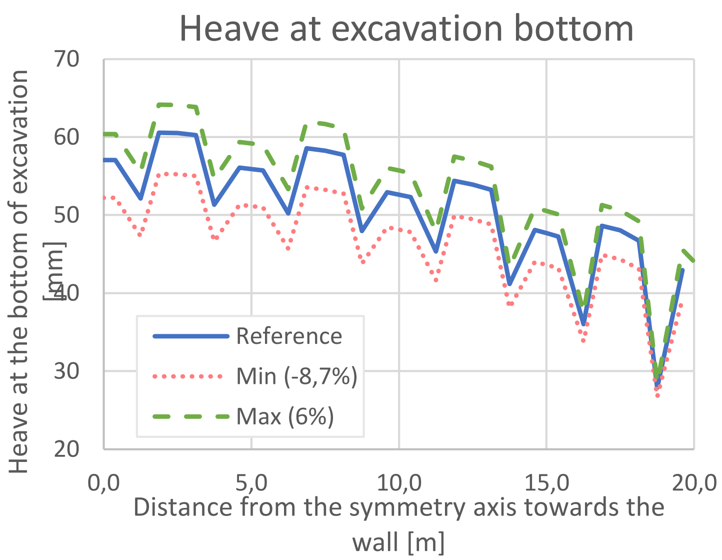

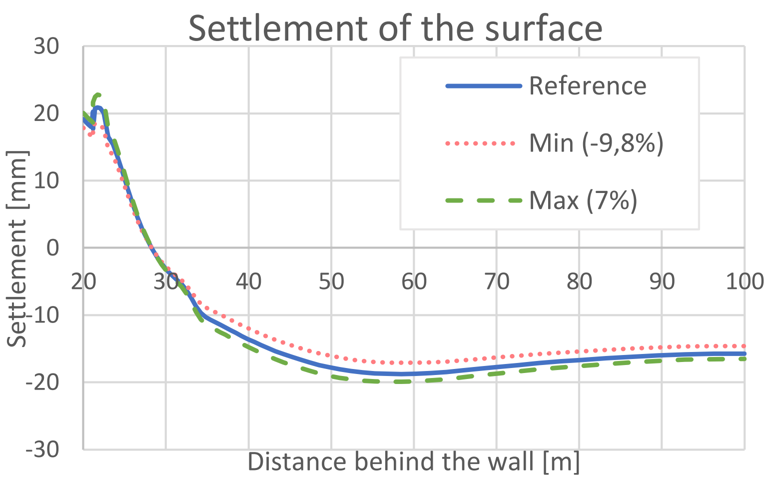

#16 Shear strain at failure in direct simple shear, y_f^DSS

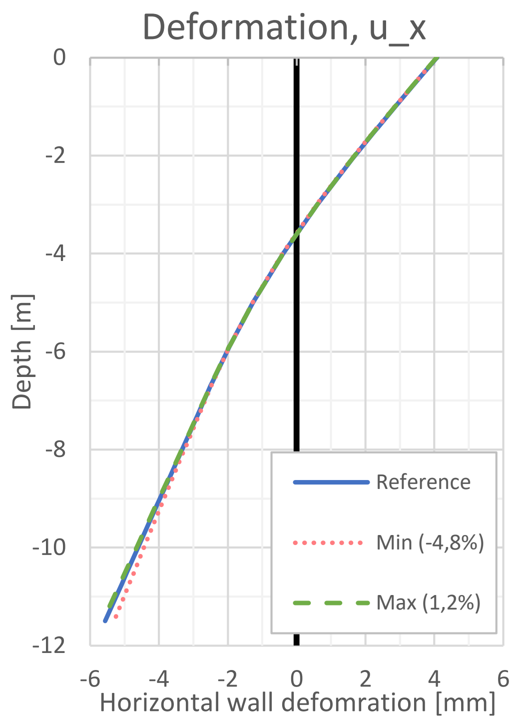

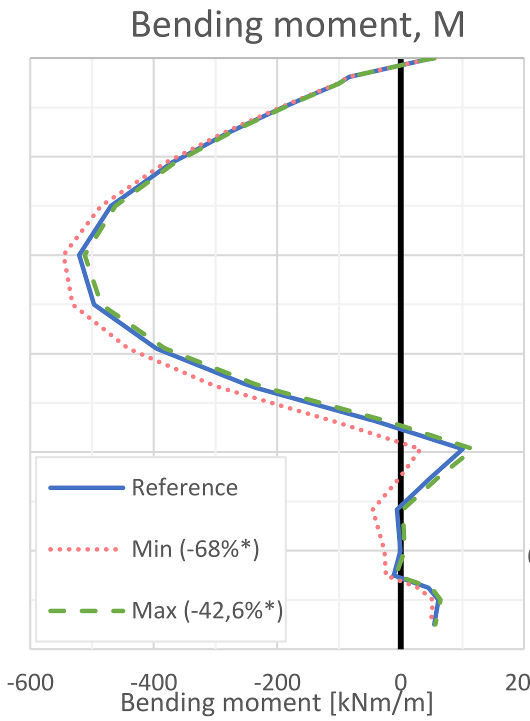

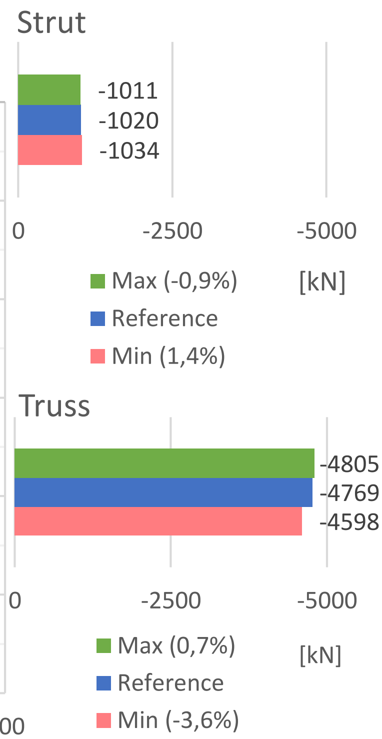

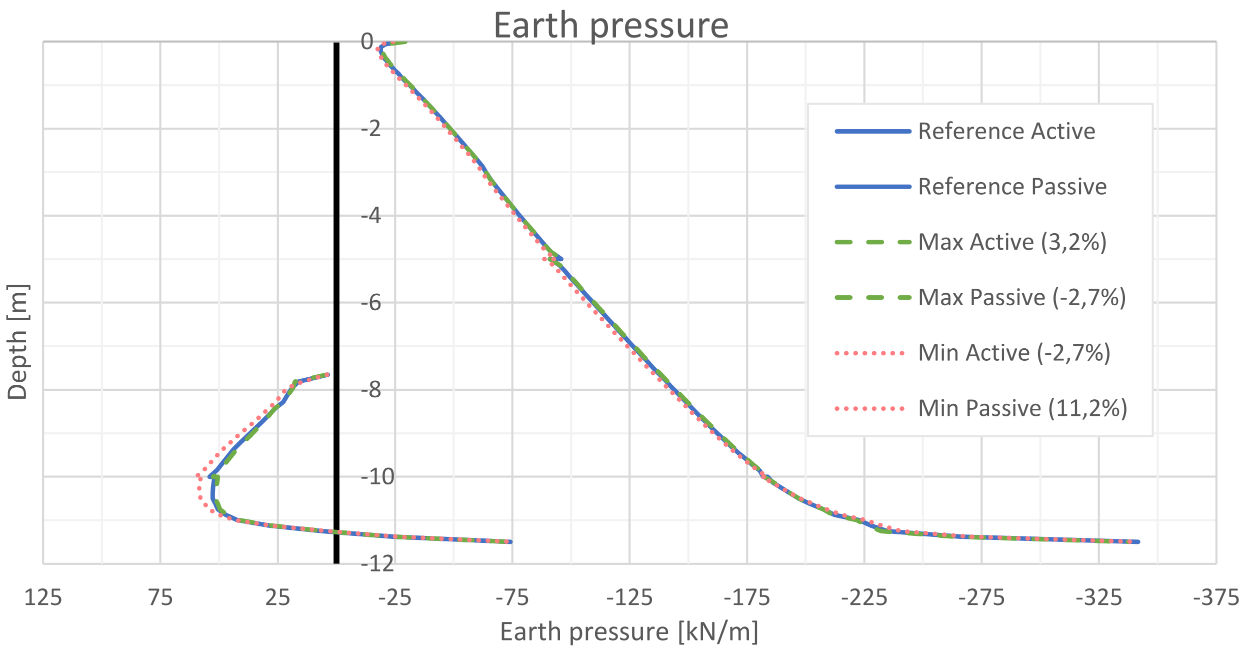

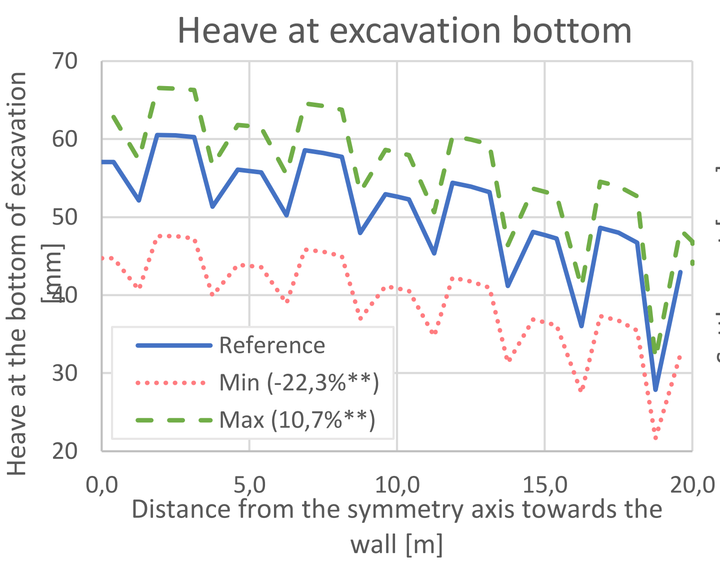

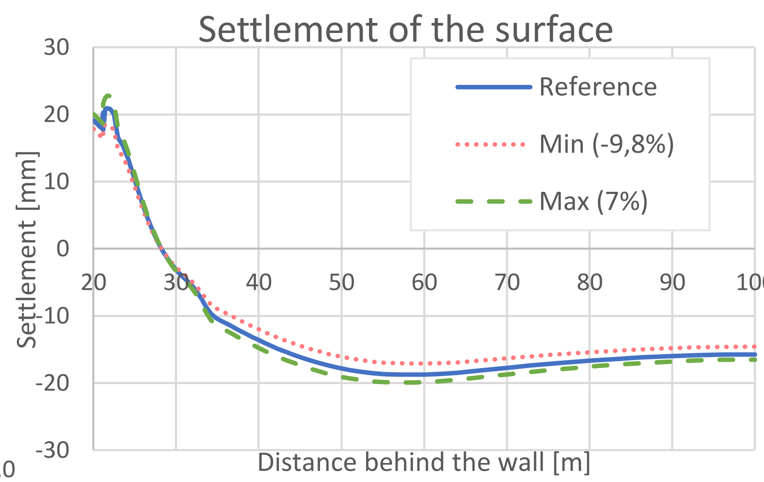

#17 Ratio of passive shear strength over active shear strength, s_u^P/s_u^A

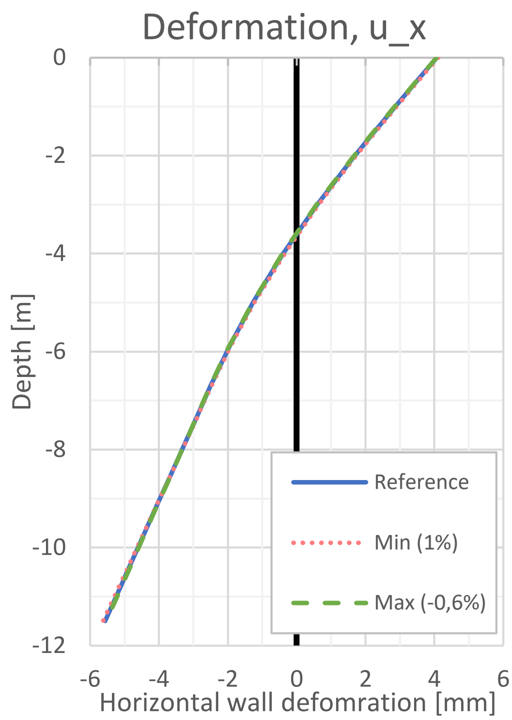

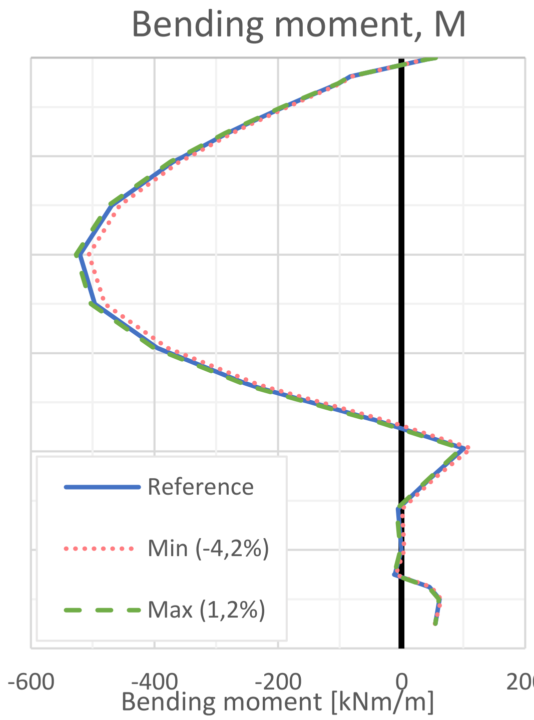

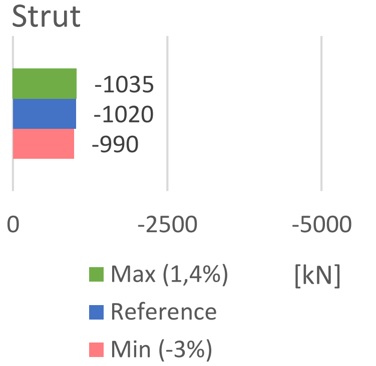

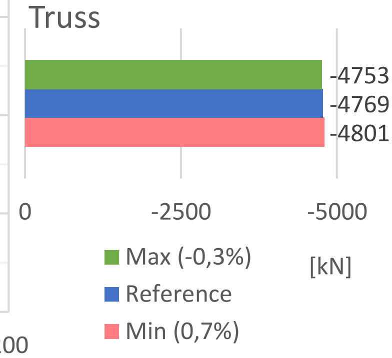

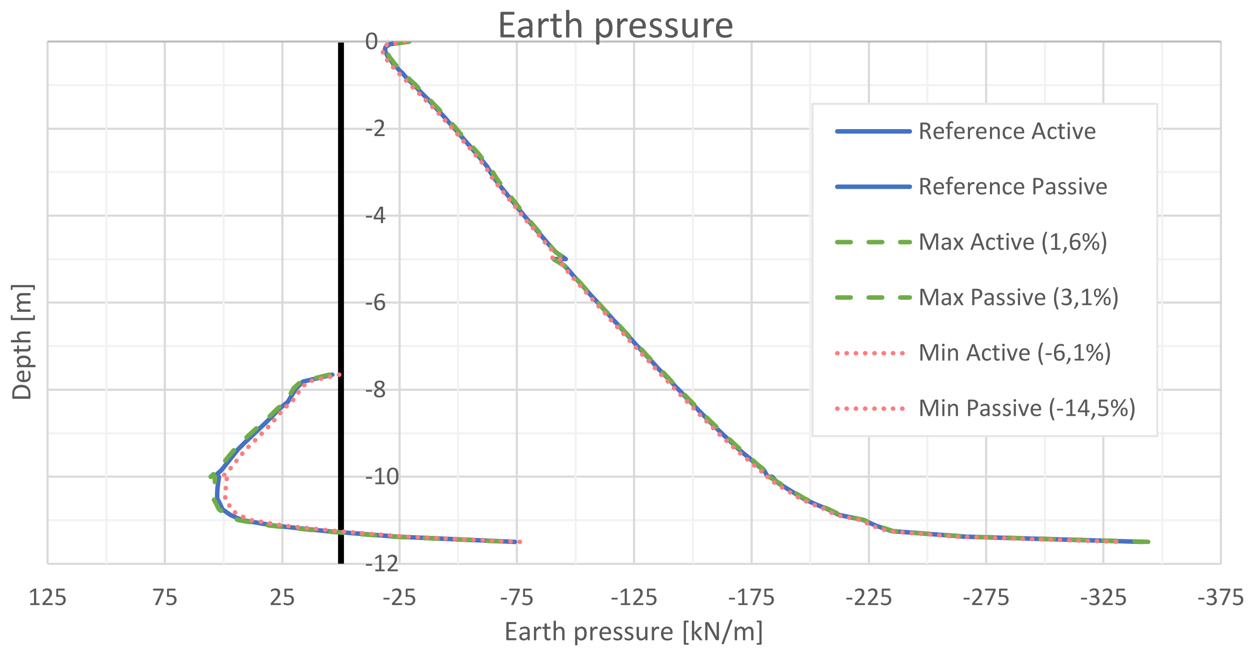

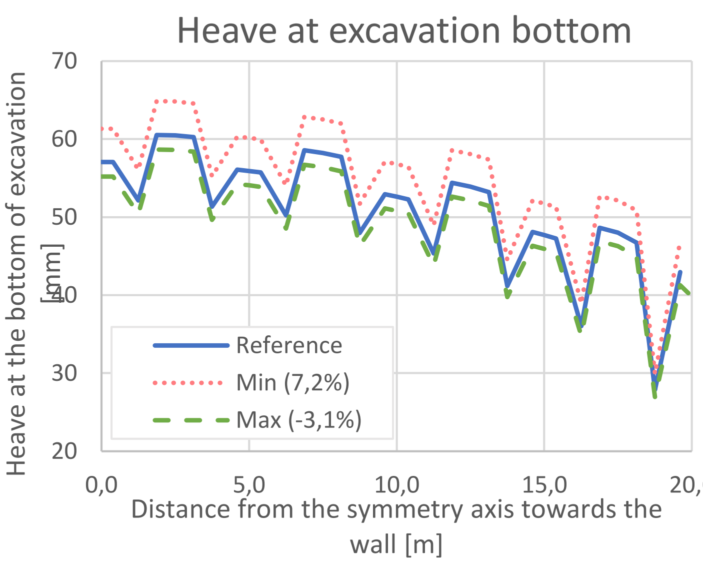

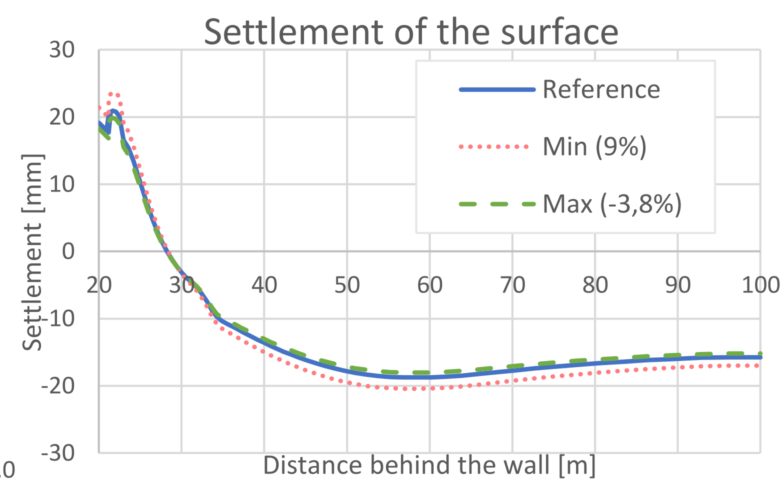

#18 Ratio of direct simple shear strength over active shear strength, s_u^DSS/s_u^A

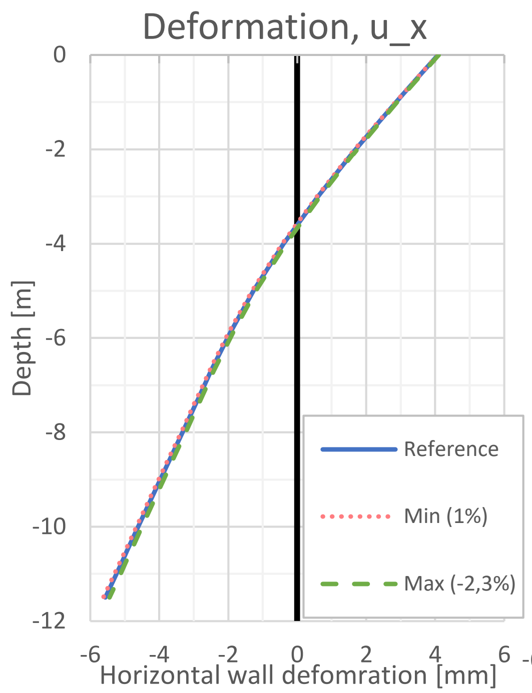

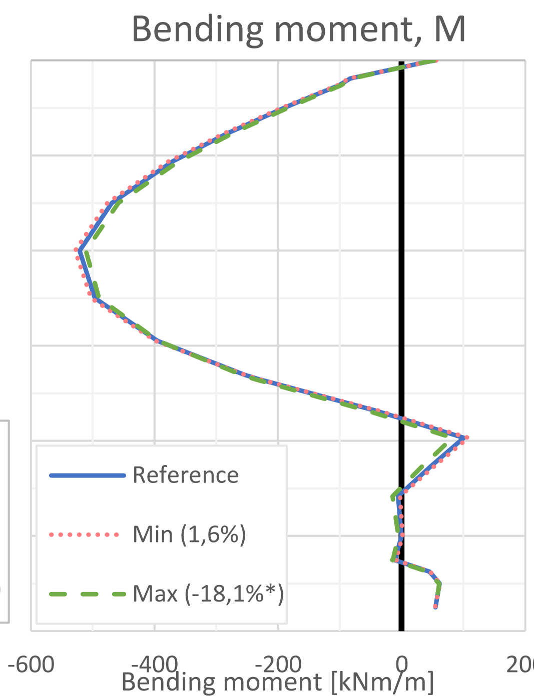

Strut

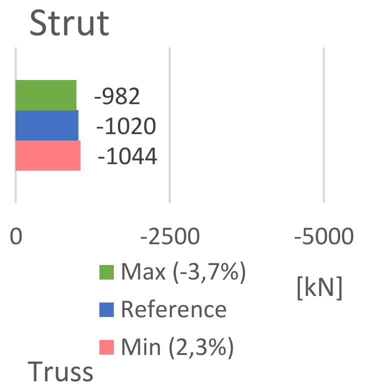

Truss